DIRECT EXTERIOR ORIENTATION DETERMINATION IN CLOSE-RANGE PHOTOGRAMMETRY FOR CULTURAL HERITAGE RECORDING.

by

Melanie Katharina Kirchhöfer

School of Civil and Building Engineering

A Doctoral Thesis

submitted in partial fulfilment of the requirements for the award of

Doctor of Philosophy

of Loughborough University

April 2012

Abstract

Keywords: close-range photogrammetry, cultural heritage recording, direct exterior orientation, offset calibration, low-cost system, consumer-grade camera, orientation sensor, data accessibility

In this thesis a low-cost approach for cultural heritage recording is developed. The necessity for comprehensive and accurate heritage recording derives from the constant threat of heritage being damaged or destroyed. Close-range photogrammetry utilising consumer-grade digital cameras has proven efficient in this area. Recognising the desirability to record data in a three-dimensional national coordinate system conventionally requires establishing coordinated target points for exterior orientation determination. This is time consuming, costly and can be objectionable on sensitive sites. In this study this problem was overcome by developing an image-based recording system that is capable of direct exterior orientation determination. The system comprises a consumer-grade digital camera, a small-size and low-cost orientation sensor, and a differential Global Positioning System (DGPS) receiver. The focus on low-cost and easy-to-use components enables utilisation by non-specialists for heritage recording.

In this research project methods for rotational and positional offset calibration between system components were devised and the practicability of the recording system was tested at Loughborough University and in case studies at two real heritage sites. Testing involved assessing offset calibration precision and stability as well as achievable absolute and relative accuracy. The results of these tests demonstrated that with sufficiently consistent calibration values, data for medium accuracy measurements (40 mm absolute and 12 mm relative accuracy) can be recorded without using any control.

This thesis also explores methods for enhancing usage and accessibility of data representing cultural heritage. It was demonstrated that storing image and corresponding exterior orientation information in a single file and visualising heritage data in Google Earth can provide several benefits for cultural heritage recording and conservation projects.

Acknowledgement

The time I conducted my PhD research at Loughborough University certainly was one of the most exciting and enjoyable periods of my life. The completion of this thesis would not have been possible without the help and support of many people.

First and foremost I would like to thank my supervisors Jim Chandler and Rene Wackrow for their excellent guidance during this research project, for their continuous encouragement, and for always being approachable and taking time to discuss problems, despite other responsibilities. Working with them was a real pleasure and I benefited greatly from this time, both on a professional and a personal level.

Further thanks are due to Paul Bryan of English Heritage for providing the TCM5 orientation sensor and for his support and advice concerning cultural heritage recording.

Thanks to Nick Rodgers and Mike Smeeton for their technical support in assembling and testing the recording system. Furthermore, I wish to thank Simona and Steve for helping to conduct the case studies at St. Catherine's Oratory and Roughting Linn. The permission to use these sites was kindly given by the National Trust and Edward Lambton, Earl of Durham, respectively.

I also thank the 'regulars' in the hot-desking area of the research hub and the researchers joining the Wednesday afternoon 'Tea and Biscuits', including Rory, Wang, Tom, Chris, Jon, Phil, Andrew, Louise, Jess, Koji, Adrien, and many more. They created a great sense of community and made working in the hub a pleasure.

My time in Loughborough was very enjoyable due to the great friends I made here, including Rene, Kasia, Rene, Steve, Simona, Rob, Daan, Sara, and many more. Thank you very much for the great time we spent travelling together and on nights out.

Last, but by no means least, I thank my family for their moral support and encouragement, especially when difficulties seemed overwhelming. Special thanks go to my parents as without their love and support I would have never got this far.

Thanks to the School of Civil and Building Engineering at Loughborough University for funding this PhD project.

Contents

List of Tables

List of Figures

Nomenclature

Greek symbols

$\Delta h, \Delta p, \Delta r$	Rotational offset calibration values
$\Delta x, \Delta y, \Delta z$	Positional-offset calibration values
$\Delta x', \Delta y', \Delta z'$	Corrections for image distortions
$\Delta x_{ai}, \Delta y_{ai}, \Delta z_{ai}$	Absolute positional offset calibration value for each image i
κ	Rotation about camera system z-axis
κ_{Ci}	Offset corrected κ for image i
κ_{D}	Directly determined κ
κ_{Di}	Directly determined κ for image i
κ_{P}	Photogrammetrically determined κ
κ_{Pi}	Photogrammetrically determined κ for image i
λ	Scale factor
φ	Rotation about camera system y-axis
φ_{Ci}	Offset corrected φ for image i
φ_{D}	Directly determined φ
φ_{Di}	Directly determined φ for image i
φ_{P}	Photogrammetrically determined φ
φ_{Pi}	Photogrammetrically determined φ for image i
ω	Rotation about camera system x-axis
ω_{Ci}	Offset corrected ω for image i
ω_{D}	Directly determined ω
ω_{Di}	Directly determined ω for image i

ω_P	Photogrammetrically determined ω
ω_{Pi}	Photogrammetrically determined ω for image i

Other symbols

a	Acceleration
$bottomFoV$	Angle defining bottom field of view in camera
c	Principal distance
F	Force
f	Camera focal length
h	Heading
h_{Ci}	Offset corrected h for image i
h_D	Directly determined h
h_{Di}	Directly determined h for image i
h_P	Photogrammetrically determined h
h_{Pi}	Photogrammetrically determined h for image i
hz	Length of the camera image sensor in horizontal direction
$\mathbf{i}$	Direction cosine vector x-axis
i	Index indicating image number
$\mathbf{j}$	Direction cosine vector y-axis
$\mathbf{k}$	Direction cosine vector z-axis
$leftFoV$	Angle defining left field of view in camera
m	Mass
N	Number of full carrier wave cycles between GPS receiver and satellite
O	Perspective centre
P	Principal point
p	Pitch
p_D	Directly determined p
p_{Di}	Directly determined p for image i
p_P	Photogrammetrically determined p
p_{Pi}	Photogrammetrically determined p for image i
p_{Ci}	Offset corrected pitch for image i

r	Roll
r_{Ci}	Offset corrected r for image i
r_D	Directly determined r
r_{Di}	Directly determined r for image i
r_P	Photogrammetrically determined r
r_{Pi}	Photogrammetrically determined r for image i
$\mathbf{R}_{\kappa\varphi\omega}$	Rotation matrix from source to target system (sequence XYZ)
$\mathbf{R}_{CN}$	Rotation matrix rotation orientation sensor coordinate system into camera system
$rightFoV$	Angle defining right field of view in camera
$s\Delta h$	Range of heading offsets
s_h, s_p, s_r	Standard deviation rotational offset calibration values
s_x, s_y, s_z	Standard deviation positional offset calibration values
$topFoV$	Angle defining top field of view in camera
vt	Length of the camera image sensor in vertical direction
X	x-coordinate in target system
x	x-coordinate in source system
x'	x-coordinate in image
X_0	Shift parameter in x-direction
$\mathbf{x}_0$	Non-rotated x-axis vector
X_{Ci}	Corrected x-position for image i
X_D	Directly determined x-position
X_{Di}	Directly determined x-position for image i
X_P	Photogrammetrically determined x-position
X_{Pi}	Photogrammetrically determined x-position for image i
X_{ri}	x-offset in non-rotated camera coordinate system for each image i
Y	y-coordinate in target system
y	y-coordinate in in source system
y'	y-coordinate in image
Y_0	Shift parameter in y-direction
$\mathbf{y}_0$	Non-rotated y-axis vector
Y_{Ci}	Corrected y-position for image i

Y_D	Directly determined y-position
Y_{Di}	Directly determined y-position for image i
Y_P	Photogrammetrically determined y-position
Y_{Pi}	Photogrammetrically determined y-position for image i
Y_{ri}	y-offset in non-rotated camera coordinate system for each image i
Z	z-coordinate in target system
z	z-coordinate in source system
Z_0	Shift parameter in z-direction
$\mathbf{z}_0$	Non-rotated z-axis vector
Z_{Ci}	Corrected z-position for image i
Z_D	Directly determined z-position
Z_{Di}	Directly determined z-position for image i
Z_P	Photogrammetrically determined z-position
Z_{Pi}	Photogrammetrically determined z-position for image i
Z_{ri}	z-offset in non-rotated camera coordinate system for each image i

Abbreviations and acronyms

1D	One-dimensional
2D	Two-dimensional
3D	Three-dimensional
ASCII	American Standard Code for Information Interchange
Arctan2	Four-quadrant inverse tangent
BSW	British Standard Whitworth
C#	C sharp
CAD	Computer-Aided Design
CIPA	International Committee for Documentation of Cultural Heritage
DEM	Digital Elevation Model
DGPS	Differential Global Positioning System
EDM	Electronic Distance Meter
EGM 96	Earth Gravitational Model 1996
ERA	England's Rock-Art
EU	European Union

Exif	Exchangeable Image File Format
GAP	General Adjustment Program
GIS	Geographic Information System
GPS	Global Positioning System
GRS 80	Geodetic Reference System 1980
GSM	Global System for Mobile Communications
ICOMOS	International Council on Monuments and Sites
ISPRS	International Society for Photogrammetry and Remote Sensing
JEITA	Japan Electronics and Information Technology Industries Association
JPEG	Joint Photographic Experts Group
KML	Keyhole Markup Language
KMZ	KML archive file
L1	GPS carrier wave
L2	GPS carrier wave
LPS	Leica Photogrammetric Suite
MatLab	MathWorks' Matrix Laboratory
MEMS	Micro-Electro-Mechanical System
MICHAEL	Multilingual Inventory of Cultural Heritage in Europe
NADRAP	Northumberland and Durham Rock Art Pilot
NET-HERITAGE	European Network on Research Programme Applied to the Protection of Tangible Cultural Heritage
NGA	National Geospatial-Intelligence Agency
NOAA	National Oceanic and Atmospheric Administration
OGC	Open Geospatial Consortium
OSGB36	Ordnance Survey Great Britain 1936 (British National Grid)
RGB	Red-Green-Blue
RL1	First recording section and data set at Roughting Linn
RL2	Second recording section and data set at Roughting Linn
RLA	First survey station established at Roughting Linn
RLB	Second survey station established at Roughting Linn
RMSE	Root Mean Square Error
SCO1	First data set collected at St. Catherine's Oratory

SCO2	Second data set collected at St. Catherine's Oratory
SCOA	First survey station established at St. Catherine's Oratory
SCOB	Second survey station established at St. Catherine's Oratory
SLR	Single Lens Reflex
SPS	Standard Position System
TLS	Terrestrial Laser Scanner
UNESCO	United Nations Educational, Scientific and Cultural Organisation
WGS 84	World Geodetic System 1984
WMS	Web Mapping Service

1 Introduction

This thesis is concerned with the application of close-range photogrammetry for recording of cultural heritage. Cultural heritage can be defined as "places [that] include historic buildings or monuments which bear the distinctive imprint of human history" (Herbert, 1995b). The necessity to record cultural heritage emanates from its importance for societies and from the constant risk of being damaged or even destroyed. The International Council on Monuments and Sites (ICOMOS) identifies recording as a means to attenuate the risk of losing cultural heritage, by providing data as basis for research, planning, conservation management, construction, and safekeeping (ICOMOS, 1996). Photogrammetry can be defined as encompassing "methods of image measurement and interpretation in order to derive the shape and location of an object from one or more photographs" (Luhmann et al., 2006). In close-range photogrammetry, the camera for image acquisition is generally placed on the ground and close to the object. Close-range photogrammetry has proven effective for heritage recording, because it provides the means to capture geometric and radiometric data rapidly and simultaneously.

However, the desirability to record within a three-dimensional (3D) national coordinate system normally requires establishing known coordinated control points on the heritage object for determining position and orientation (exterior orientation) of the camera during exposure. This remains time consuming, costly, requires surveying expertise, and attaching survey targets to heritage objects is rarely acceptable. In times of cost-cutting this cost can prevent cultural heritage being sufficiently recorded. As a result low-cost and more efficient and acceptable approaches for heritage data recording are required.

Expensive control point surveys could be avoided by direct determination of exterior orientation. This would also allow non-specialists to become involved, in particular when low-cost and easy-to-use devices are used. The term ‘low-cost’ in this study refers to commercial off-the-shelf products that are available at significantly lower-cost as their more specialised, high-grade counterparts. Therefore, the upper limit of what is perceived as low-cost differs for differing products. For the devices used in this research project, the upper limit of the low-cost range was £ 2,000. Consumer-grade cameras have already proven efficient for cultural heritage recording. Commercial survey-grade Inertial Measurement Units (IMU) are expensive but recently a range of cheaper orientation sensors have become available, which could have potential for direct determination of exterior orientation in close-range photogrammetry.

This thesis focuses on the development and testing of an image-based recording system that comprises a consumer-grade camera, low-cost orientation sensor, and survey-grade differential Global Positioning System (DGPS) receiver. This system is capable of direct exterior orientation determination and is designed to be usable by non-specialists for heritage recording. Furthermore, this thesis also explores the potential of further cost reduction in heritage recording by improving data usability and accessibility.

1.1 Aim and objectives

The aim of this research thesis was formulated as:

> *“Demonstrate the practicability of direct exterior orientation determination in close-range photogrammetry for reducing cost and enhancing and widening cultural heritage data recording, usage, and accessibility.”*

This aim was accomplished by achieving the following five main objectives:

1 *Critically review the usability of low-cost sensors that have potential to enhance cultural heritage recording.*

For achieving this objective an extensive literature review was conducted that investigated the benefits and drawbacks of consumer-grade digital cameras and low-cost sensors for orientation and position determination. Combining these sensors in a recording system enables direct exterior orientation determination, thus reducing cost in heritage recording by avoiding expensive control point surveys and enabling non-specialists to become involved. Based on the literature review and recording system tests conducted in this research project the performance of low-cost sensors for image capture and orientation and position determination was assessed. It was found that currently available consumer-grade digital cameras and low-cost orientation sensors have potential for enhancing cultural heritage recording by enabling direct exterior orientation determination in close-range photogrammetry. However, the accuracy of positioning using low-cost Global Positioning System (GPS) receivers is currently sufficient for enhancing cultural heritage recording.

2 *Design and develop an image-based recording system comprised of off-the-shelf sensors that is capable of direct exterior orientation determination and usable by non-specialists for heritage recording.*

A recording system comprising a consumer-grade digital single lens reflex (SLR) camera, a small-size orientation sensor, a survey-grade DGPS receiver, and an off-the-shelf laptop was assembled. Camera, orientation sensor and DGPS antenna were assembled in a rigid mounting frame that fixed these components in orientation and position and allowed offset calibration. With exception of the DGPS receiver, all components were low-cost. At the time of system assembly no low-cost positioning device was available that provided centimetre accuracy required in this project. This constraint will no doubt change and utilising a survey-grade DGPS allowed the principle of direct exterior orientation determination in close-range photogrammetry to be tested. The recording system was designed with a focus on ease-of-use and is expected to enable heritage recording by non-specialists.

3 Verify that the system can be sufficiently constrained to provide stable and accurate offset calibration values.

The aim of offset calibration is to estimate rotational and positional offsets between recording system components. Achieving stable and accurate offset calibration is crucial for accurate determination of the exterior orientation parameters of the camera directly from orientation sensor and DGPS measurements without using control points. Calibration stability was assessed by comparing the magnitude of calibration value changes to the expected accuracy of orientation sensor and DGPS measurements. During stability assessment it was demonstrated that consistent calibration values can generally be achieved if the camera is not detached from the mounting frame. It was also revealed that using inaccurate offset calibration values significantly decreases the achieved absolute accuracy.

4 Confirm that the recording system can provide data for medium accurate measurements in close range photogrammetry for cultural heritage recording.

The accuracy requirement in heritage recording depends upon the kind of object to be recorded and on the defined end product. This complicated the assessment of the accuracy achieved in recording system tests during this study, because boundaries between levels of accuracy (high, medium, low) are difficult to define. This problem was already discussed in Wackrow (2008). English Heritage's 'Metric Survey Specifications for Cultural Heritage' (English Heritage, 2009) defines accuracy requirements that are applicable to immovable objects with extents of approximately 5 m to 20 m that were recorded in this research project. For an end product with an output scale of 1:50 a photogrammetric processing accuracy of 9 mm in object space is required, while for 'Measured Building Surveys' at the same scale an accuracy level of 15 mm is acceptable. These values can certainly be considered high accuracy when recording buildings and other immovable heritage objects. Based on this, medium accuracy in this research project is defined as achieving measurements that deviate from their true values by 25 mm to 40 mm. Both, absolute and relative accuracy, were found to represent key measure of data quality. The absolute accuracy was determined through investigating the capability of the system to provide data for measurements that are accurate with respect to a 3D national coordinate system. The relative

accuracy was determined by assessing the capability of the system to provide measurements that are accurate with respect to each other. Achievable accuracy was quantified in initial recording system tests at Loughborough University and in case studies at real heritage objects. The results revealed suitability of the recording system for medium accuracy measurements (25 mm to 40 mm). The practicability of the system for real heritage recording projects was validated in two case studies. It was demonstrated that the system provides comprehensive and accurate data collection without attaching damaging targets to the heritage object and that it is suitable to be transported to heritage sites, which might be located in areas with limited access. However, it was also revealed that the type of heritage object to be recorded has to be considered when the recording system is assembled. Objects close to the ground that extend in horizontal direction require the DGPS antenna to be attached differently than objects that primarily extend vertically.

5 *Devise simple and low-cost methods for offset calibration and for enhancing cultural heritage data usability and accessibility and prove their practicability for medium accuracy heritage recording.*

This objective focuses on the potential for further cost reduction in heritage recording projects by using low-cost approaches and enhancing the involvement of non-specialists beyond heritage data acquisition. Achieving this objective included the critical review of simple methods that can be used for offset calibration and enhance heritage data usability and accessibility, respectively. Based on this, an offset calibration procedure was devised using algorithms that facilitate implementation without requiring specialised software and hardware. This procedure was applied throughout the project, proving that it is practical for medium accuracy heritage recording. Furthermore, the usability of cultural heritage data was enhanced by storing exterior orientation parameters in the same file as corresponding image data. This can improve data exchange and facilitate automation in data usage. During a case study the files containing image and exterior orientation parameters were visualised in Google Earth, demonstrating improved data usability and accessibility as well as the practicability of this approach for heritage recording projects.

1.2 Contribution to scientific knowledge

This thesis has contributed to knowledge in two areas:

- A recording system was developed that is capable of direct exterior orientation determination using a consumer-grade camera, a small-size and low-cost orientation sensor, and a survey-grade DGPS receiver. Similar systems have already been presented in the literature, but did not achieve accuracy sufficient for heritage recording (Section 2.8). Using the developed system, data for medium accuracy measurements can be recorded without using conventional control points. This demonstrates also, the usability of low-cost orientation sensors for direct exterior orientation determination, for some applications in close-range photogrammetry.

- This thesis investigated various approaches for reducing cost in cultural heritage data recording and processing. It has demonstrated that the recording system can help to avoid expensive control point surveys. Furthermore, the system is easy-to-use and portable, enabling the involvement of non-specialists in cultural heritage recording. Further potential for cost reduction was demonstrated by identifying approaches to data processing and usage that can also be utilised by non-specialists. It has proven that simple offset calibration methods that can be implemented without specialised software are sufficient for low-cost recording systems. Low-cost approaches to enhance data usability were also investigated. This has demonstrated that projects concerned with heritage recording and conservation can benefit from low-cost and easy-to-use methods for improving photogrammetric heritage data storage and accessibility.

1.3 Structure of thesis

The structure of this thesis is based on the logical progression of the research conducted. This thesis comprises seven chapters, a list of references, and two appendices.

- *Chapter 1: Introduction*

  This chapter introduces the topic of this research project, defines the aim and objectives, and identifies its contribution to knowledge

- *Chapter 2: Literature review*

  The findings of a review of literature relevant to this research are summarised. The main sections in this chapter focus on cultural heritage and the necessity for recording, photogrammetry, orientation and positioning sensors, and low-cost approaches for data acquisition and utilisation.

- *Chapter 3: Methodology*

  This chapter explains the construction of the recording system and the approaches used for offset calibration, data acquisition, and accuracy assessment. It also outlines approaches for enhancing heritage data usability and accessibility.

- *Chapter 4: Results*

  This chapter presents results of nine initial recording system tests conducted at Loughborough University. First, offset calibration precision and stability are assessed. This is followed by the evaluation of achieved absolute and relative accuracy.

- *Chapter 5: Case studies*

  This chapter describes two case studies that were conducted to verify the usability of the recording system for cultural heritage recording. Results obtained during offset calibration and accuracy assessment are presented. This chapter also includes findings of testing a low-cost approach for enhancing heritage data usability and accessibility.

- *Chapter 6: Discussion*

  This chapter reviews the findings that are presented in Chapters 4 and 5. Influences on offset calibration and achievable accuracy are identified. The practicability of the system for heritage recording is discussed and limitations and potential enhancements are identified. The recording system performance is compared to the performance of a system based upon a smartphone. This resulted in the assessment of the potential of smartphones as devices for low-cost heritage recording. This chapter also identifies the benefits and limitations of low-cost approaches to enhance data usability and accessibility.

- *Chapter 7: Conclusion*

  This chapter summarises the achievements of this research project and provides recommendation for future work.

- *Appendix A*

  This appendix contains MathWorks' Matrix Laboratory (MatLab) code that was developed for offset calibration. It consists of the main procedure that derives calibration values and applies them to direct measurements and sub-routines for converting photogrammetric angles into orientation sensor angles, and vice versa, and for creating rotation matrices.

- *Appendix B*

  This appendix contains a peer-reviewed conference paper presented at the symposium of the International Committee for Documentation of Cultural

Heritage (CIPA) 2011 in Prague, Czech Republic. It also contains a paper presented at the International Society for Photogrammetry and Remote Sensing (ISPRS) Working Group V/2 conference 2011 in York, United Kingdom.

2 Literature Review

This chapter summarises the findings of a review of literature relevant to this research project. First, an overview of cultural heritage and heritage recording methods is provided. Afterwards, the basic mathematical functions in photogrammetry and the characteristics of close-range photogrammetry are described. Sections that outline the usability of consumer-grade cameras in close-range photogrammetry are also included. Furthermore, this chapter reviews the working principles of currently available orientation and positioning sensors with special consideration of low-cost devices. The integration of position and orientation sensors for direct exterior orientation determination is explained and approaches to low-cost photogrammetric data recording are reviewed. The subsequent section is focused on the exploration of low-cost approaches for visualising and sharing image-based geographic data online. Finally, this chapter finishes in a short summary.

2.1 Cultural heritage

2.1.1 Definition

The term “heritage” can describe a wide variety of objects and concepts, and people comprehend different meanings of this term (Johnson and Thomas, 1995; Herbert, 1995b). Johnson and Thomas (1995) state that heritage often describes everything that is in some way connected to the past but that the more traditional meaning refers to

the natural world, buildings and monuments, the arts, and social customs and traditions.

According to Hewison (1989) the first "National Heritage" conference in the UK held in 1983, defined heritage as "that which a past generation has preserved and handed on to the present and which a significant group of the population wishes to hand on to the future".

If heritage is concerned only with objects created by humans and not nature, it is usually referred to as cultural heritage. The definition by Herbert (1995b) is "places [that] include historic buildings or monuments which bear the distinctive imprint of human history".

The most widely known body concerned with heritage is probably the United Nations Educational, Scientific and Cultural Organisation (UNESCO) formed in 1945. According to their "Convention concerning the protection of the world cultural and natural heritage" (UNESCO, 1972), cultural heritage comprises: man-made single monuments, groups of buildings and sites, which "are of outstanding universal value". This value can be of historical, artistic, scientific, aesthetic, ethnological or anthropological nature.

ICOMOS, which is the technical advisor to the UNESCO for World Heritage, defines cultural heritage in their Venice Charter 1964 (International Charter for the Conservation and Restoration of Monuments and Sites) as "urban or rural setting in which is found the evidence of a particular civilization, a significant development or a historic event" (ICOMOS, 1964). The definition in the Venice Charter comprises also "moderate works that gained a significant cultural value in the course of time", unlike the definition of the UNESCO for world heritage.

In the research agenda of English Heritage (2005) the term 'historic environment' is introduced and defined as "[that] what generations of people have made of the places in which they live". This very general view is narrowed by the requirement that it "has cultural value and significance worthy of sustainable management and conservation".

The previous definition mostly defines cultural heritage as some sort of physical object, generally man-made. The understanding of heritage can also include non-physical entities, or so-called intangible heritage, like: language, performing arts, and social practices (UNESCO, 2003). Due to the nature of this programme of PhD study, only tangible heritage is concerned in this thesis.

2.1.2 Importance

In 2000 a survey revealed that the majority of the English population regards heritage as important for education, the economy, and the cultural life of the country and consequently supports heritage conservation (Power of Place Office and English Heritage, 2000). Despite today's support, the concept of heritage protection is still recent. First attempts in England go back to the epoch of romanticism in the second half of the eighteenths century (Hunter, 1996; Aldridge, 1989). This can be attributed to a change in society accompanied by an increased interest in things connected to the past (Hunter, 1996). Over time, several values were attributed to heritage. The most frequently mentioned value is the forming of a cultural, national, local or even individual identity (Aldridge, 1989; Uzzell, 1989; Hewison, 1989; Yilmaz et al., 2007). In the "European Network on Research Programme Applied to the Protection of Tangible Cultural Heritage" (NET-HERITAGE) fact sheet, the cultural heritage found in the European Union (EU) is even seen as vital for establishing a collective European identity (European Communities, 2008). The valuation of heritage as guarantor for identity goes back to the nineteenth century (Hunter 1996). It is claimed that by understanding the past the present can be comprehended, which helps to build identity. Furthermore, the loss of cultural heritage is supposed to have a negative impact on the identity of a society (Laenen, 1989). Other values occurring in the literature include stewardship and scholarship. The concept of stewardship is based on the idea that heritage does not belong only to the present generation but to all generations, of both the past and the future (Hunter, 1996). It is the responsibility of people living today to preserve heritage as much as possible (ICOMOS, 1964; Hewison, 1989). Scholarship includes learning about the past and the heritage object itself (Hewison, 1989; Power of Place Office and English Heritage, 2000). In the aforementioned survey, more than 95% of the respondents agreed that the historic environment is essential for learning about the past and that schoolchildren should be given the opportunity to discover it (Power of Place Office and English Heritage, 2000). The economic value of heritage emerged more recently. Although some people see the danger that is posed on heritage by commercialisation (Hewison, 1989; Herbert, 1995a) it has to be considered that heritage can create jobs and support local economies (Herbert, 1995a).

2.1.3 Risk of losing heritage

Recognising that heritage is at risk is not a development of the last few decades. The earliest efforts to preserve heritage in Britain were initiated in the eighteenth century when people realised that a specific heritage object or site was threatened to be destroyed or lost (Hunter 1996). In modern times, the efforts to preserve heritage are still driven by the awareness of a constant, or even growing, threat (ICOMOS, 1996; UNESCO, 1972). Tangible cultural heritage can be threatened by neglect and decay, but also by deliberate destruction and damage due to social and economic progress (UNESCO, 1972; Power of Place Office and English Heritage, 2000; Ikeuchi et al., 2003; Palumba and Ogleby, 2004). Respective legislation has been established to protect heritage from being damaged or destructed. As a result neglect and decay is the greater threat for heritage in England today (English Heritage, 2008). But even heritage that is not neglected or threatened to be deliberately demolished can be lost. This can happen due to disasters (Andrews et al., 2005; Yilmaz et al., 2007) or armed conflict (UNESCO, 1954). Another threat is imposed on heritage by tourism (Palumba and Ogleby, 2004). The use for tourism can be considered as a value of heritage, but it also puts pressure on the objects themselves. Fawcett (1998) assert that mass tourism in the last five decades contributed more to wear and tear of historic floors than several centuries of regular use. Hewison (1989) even considers tourism the real threat to heritage, because it is forced to comply with consumer demands and market structures.

2.1.4 Heritage recording

The necessity of recording derives from the fact that heritage is subject to risk. Comprehensive and accurate documentation can attenuate the risk of losing heritage and in the worst case assist as a basis for reconstruction (Palumba and Ogleby, 2004). Miri and Varshosaz (2005) define recording for backup in case of damage or destruction, preparation for conservation, and monitoring changes as main reasons for heritage recording.

In literature, the term “documentation” is mostly used to describe the process of acquiring, processing, interpreting and storing data and information about cultural

heritage (ICOMOS, 1964; Yilmaz et al., 2007). Heritage "recording" can be defined as part of the documentation process (ICOMOS, 1996; Moullou and Mavromati, 2007), but in many cases no clear distinction is made between both terms and they are often used as synonyms (Leroy, 2005; Yilmaz et al., 2007). In this research project, everything concerning the collection of data that describes the physical properties of heritage at a given time will be referred to as "recording", analogous to the definition in ICOMOS (1996).

The requirements on what should be recorded and which techniques should be used depends on the type of heritage object, the reason for recording (ICOMOS, 1996; Haddad and Akasheh, 2005), and user needs (Ardissone et al., 2005; Agosto et al., 2005). There appears to be a general demand for detailed and highly accurate surveys derived using the best available techniques (ICOMOS, 1964; UNESCO, 1972; Moullou and Mavromati, 2007). The "Principle for the recording of monuments, groups of buildings and sites" (ICOMOS, 1996) demands sufficiently detailed records for presentation, promotion, and potential reconstruction of heritage. Furthermore, heritage recording has to comply with the type of heritage object, the purpose of recording, must not cause damage, and the storage medium must be durable over time.

2.1.5 Accessibility of cultural heritage data

Technical developments provide new ways of making cultural heritage data widely accessible to a diverse audience (Bonfigli et al., 2004; Masci et al., 2007; Mudge et al., 2007; Sharpe et al., 2008). In the literature a number of heritage related projects can be found that have online access to their data and results integrated in their project conception (Gabellone and Monte, 2005; Çayırezmez, 2007; Seto et al., 2009). Others are concerned with the technology of digital accessibility of cultural heritage data (Bonfigli et al., 2004; Masci et al., 2007; Pietroni and Forte, 2007). This highlights the increased importance of public accessibility to cultural heritage data, which is also acknowledged in Bonfigli et al. (2004), Buhagiar et al. (2006), and Sharpe et al. (2008). Digital access to data removes physical barriers and enables heritage to be promoted to a wider audience. This increases the public awareness of cultural heritage and improves education. Furthermore, it facilitates heritage protection, knowledge transfer, research, and communication between organisations and individuals

interested in cultural heritage (Buhagiar et al., 2006; Mudge et al., 2007; Pietroni and Forte, 2007; European Communities, 2008). According to Çayırezmez (2007) the possibility of making heritage data accessible to all stakeholders saves time and cost by avoiding repeated recording work. At the same time it helps to protect heritage by providing information to investigators of developing projects about cultural heritage objects in the project area.

The internet provides one means to make heritage data widely accessible (Bonfigli et al., 2004) and a number of websites can be found. CyArk is a non-profit organisation that collects and stores data of significant world heritage sites for digital preservation (CyArk, n.d.). For registered users the website offers access to data, such as high resolution photographs, 3D point clouds, Computer-Aided Design (CAD) drawings, and 3D models as well as textual information about the heritage sites. Furthermore, they have imbedded functionalities to view their recorded sites and 3D models in Google Earth.

The England's Rock Art (ERA) website was developed as part of the Northumberland and Durham Rock Art Pilot (NADRAP) project. It provides access to a database of images and information about rock-art panels in Northumberland and County Durham, England. On the website users are encouraged to contribute to the database by starting to record rock-art located in other parts of England themselves (Sharpe and Barnett, 2008).

Access to digital imagery of various heritage objects is offered by online archives such as Images of England, an image archive of listed buildings in England, or those accessible via the Multilingual Inventory of Cultural Heritage in Europe (MICHAEL) online portal (English Heritage, 2007a; MICHAEL, n.d.).

In Seto et al. (2009) the approach of making heritage data accessible online is different to the examples of purposely built websites described above. They achieved a low-cost display of data on the internet by using the possibility of uploading images to Google Earth and Google Maps. This approach is intuitive and widens the accessibility of cultural heritage data.

2.2 Methods of heritage recording

2.2.1 Measured drawings

Measured drawings represent a traditional method of heritage recording, which utilises simple equipment such as tape measure, plumbs, and manual laser distance measurements (Arias et al., 2005). Manually drawn sketches are annotated with manual measurements on site. This data is used to produce a scaled digital drawing in CAD or a scale analogue drawing on a drawing board (English Heritage, 2000). A draughtsperson can observe and interpret key features on site, note them down (Blake, 2007) and at the same time obtain a better understanding of the state of the object (Nishumura and Kimoto, 2009). That seems to be the major advantage and the reason why measured drawings are still regarded as an important recording method, despite the appearance of more effective digital methods (Andrews et al., 2007). Yilmaz et al. (2007) and Clowes (2002) state that two-dimensional (2D) drawings are inadequate for many aspects of heritage recording. Furthermore, Arias et al. (2005) note that unintentional loss of information can occur.

2.2.2 Total Station survey

A Total Station combines a theodolite and an Electromagnetic Distance Meter (EDM) in one single instrument. Using a Total Station requires two known survey stations. The theodolite is used to measure angles between the survey stations and points on objects. The EDM is used to measure slope distances from the Total Station to the object points. Using angle and distance observations the object can be accurately positioned relative to the survey station. Total Stations remain frequently used instruments for conducting topographic surveys in heritage recording projects (Achille et al., 2005; Campanella et al., 2005; Haddad and Akasheh, 2005; Grussenmeyer et al., 2008). An operator controlling the Total Station measures only distinctive points that represent features, including edges and corners (English Heritage, 2000; Achille et al., 2005). No information is captured within the areas between measured points.

Individual point measurements are very accurate, but data collection is time consuming and this method has become less attractive for heritage recording (Haddad and Akasheh, 2005; Boochs et al., 2007). Usually, topographic surveying is used to assign a geographic location to data derived from laser scanning and photogrammetry (georeferencing) or as basis for drawings (Ardissone et al., 2005; Campanella et al., 2005; Boochs et al., 2007; Grussenmeyer et al., 2008). Another application of the Total Station is to evaluate the accuracy of other recording methods.

2.2.3 Laser scanning

According to Böhler and Marbs (2004) and Lerma et al. (2010) terrestrial laser scanners (TLS) have been increasingly used in heritage recording projects. A laser scanner automatically captures a vast number of 3D points to represent an object in short time (Arias et al., 2005; Boochs et al., 2007). As a result, a Digital Elevation Model (DEM) can be produced efficiently (Agosto et al., 2005). Other products derived from laser scanner point clouds include 3D surface models and 3D drawings (Böhler and Marbs, 2004; Haddad and Akasheh, 2005). The increase in utilising TLS for cultural heritage recording required guidelines for ensuring the provision of products that meet the needs of the end user (Barber et al., 2003). Guidelines informing about how to successfully achieve appropriate and useful laser scan data and when to use this technique were developed in a project funded by English Heritage and conducted by the School of Civil Engineering and Geosciences at Newcastle University. These guidelines were published in English Heritage (2007b). Another outcome of this project is a website that provides information, guidance, and news concerning 3D heritage recording using TLS but also other techniques, such as photogrammetry (Heritage3D, n.d.).

The drawback of TLS is that measurements are not directed to specific features of the object, for example edges, but rather cover the whole area with a dense net of measured points (Boochs et al., 2007). These do not necessarily coincide with edges and point features representing the object. Nevertheless, it is suitable for recording of a wide range of objects, especially items of complex nature (Böhler and Marbs, 2004; Ardissone et al., 2005; Haddad and Akasheh, 2005). Another significant disadvantage of this method is the high equipment cost (Arias et al., 2005). Böhler and Marbs

(2004) state the cost for a terrestrial laser scanner being between € 50,000 and € 200,000 (approximately £ 42,500 to £ 174,000), although costs have reduced significantly more recently (cost up to £ 60,000) (Laefer and Lennon, 2008).
Often a digital camera is mounted on a laser scanner, either externally or internally, to aid the selection of the scan area and targets and to be able to assign Red-Green-Blue (RGB) colour information to each measured point (Agosto et al., 2005).

2.2.4 Photogrammetric heritage recording

In photogrammetry (Section 2.3) spectral information reflected from an object is recorded and stored within photographic images. Digital technology has improved the use of photogrammetry in heritage recording by speeding up data processing, providing cheaper equipment, and enable non-specialists to employ photogrammetric methods (Clowes, 2002; Girelli et al., 2005; Tack et al., 2005; Yilmaz et al., 2007).
Photogrammetry is well suited for heritage recording (Girelli et al., 2005; Chandler et al., 2007; Avşar et al., 2008; Lerma et al., 2010). Indeed, CIPA was established for exploring the potential of photogrammetry in heritage recording (CIPA, 2010). Advantages of close-range photogrammetry include fast data capture and high level of detail and consistency (Blake, 2007; Avşar et al., 2008; Grussenmeyer et al., 2008). Other significant advantages are the possibility to extract 3D data and record geometric and textural data simultaneously (Fryer et al., 2007).
Tack et al. (2005) describe occlusion as one of the major problems of close-range photogrammetry and Haddad and Akasheh (2005) do not see photogrammetry suitable for all types of heritage objects, especially if these are small and complex.
Captured images are usually not the end product but a medium to collect and store the required data. Products derived from images include: rectified photos and orthophotos, digital surface models, 2D models, 3D models and 2D as well as 3D line drawings (Clowes, 2002; Böhler and Marbs, 2004; Tack et al., 2005).

2.2.5 Comparison of methods

The literature provides a diverse range of opinions about which method is best suited for cultural heritage recording. The focus often is on laser scanning and

photogrammetry. Both laser scanning and photogrammetry can capture a high amount of data in short time and are considered to meet the requirements for cultural heritage recording (Böhler and Marbs, 2004; Girelli et al., 2005; Avşar et al., 2008). A noticeable number of authors (Böhler and Marbs, 2004; Ardissone et al., 2005; Haddad and Akasheh, 2005; Linsinger, 2005; Blake, 2007; Grussenmeyer et al., 2008) compared different recording methods and stated that the method to be used should depend on the type of object and the purpose of recording. No general recommendations can be made and often a combination of different methods is suggested. Day (2010) remarks that the question is how laser scanning and photogrammetry can complement each other and not which one is the better recording method. That is probably the reason why various combinations of photogrammetry and laser scanning have been used for cultural heritage recording in recent years (Lerma et al., 2010).

Previously mentioned heritage recording methods usually have to be accomplished by people trained in the respective method (Haddad and Akasheh, 2005; Andrews et al., 2007). The skill levels required for interpreting the data differs between recording methods. For non-specialists it is easier to extract information from a photographic image rather than from a laser scanner point cloud (Ardissone et al., 2005).

A further distinctive constraint associated with different recording methods is cost. Manual methods are labour intensive (Haddad and Akasheh, 2005) and laser scanning requires expensive and specialised hardware and software (Böhler and Marbs, 2004). Böhler and Marbs (2004) state that cameras ranging from low-cost to high-end products can be used for photogrammetry. However, to meet the required accuracy level, a camera must meet certain standards, such as providing stable interior orientation, small lens distortions, and sufficient resolution.

2.3 Photogrammetry

Luhmann et al. (2006) define photogrammetry as encompassing “methods of image measurement and interpretation in order to derive the shape and location of an object from one or more photographs of that object”. It follows that photogrammetry

basically can be employed in all circumstances where photographs can be used to record objects.

2.3.1 Brief history

First use of photogrammetry occurred shortly after the invention of photography. In the 1850s Laussedat used the concept of rays intersecting in space to develop a method to determine coordinates of an object in a pair of photographs. Contemporaneously, Meydenbauer successfully implemented photogrammetry to record buildings (Kraus, 1993). Due to the lack of reliable stable aerial platforms, the early photogrammetric applications had a terrestrial character (Fryer et al. 2007).

In the early twentieth century, Pulfrich and Fourcade independently developed stereocomparators (Figure 2.1) that allowed measurement of image coordinates simultaneously on two photographs, for subsequent numerical computations (Luhmann et al., 2006).

A few years later, the first analogue stereoplotters were developed to mechanically plot topography from terrestrial photographs (Kraus, 1993; Luhmann et al., 2006). Soon after, progress in aviation and global conflict triggered the rise of aerial photogrammetry and instruments for stereoplotting using aerial photographs (Alspaugh, 2004; Luhmann et al., 2006). In the mid twentieth century, developments in electronic computing facilitated the emergence of analytical photogrammetry.

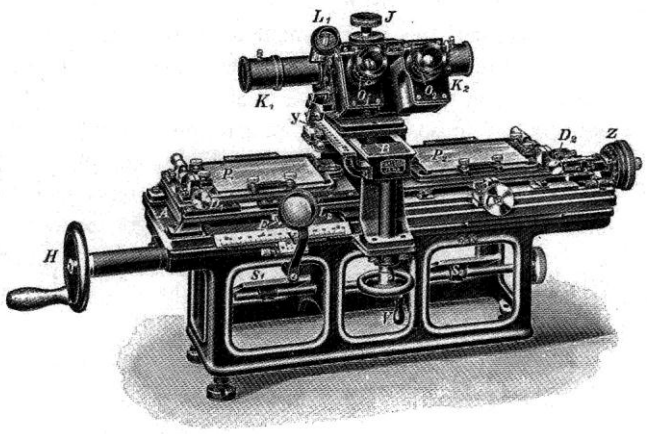

Figure 2.1: Stereocomparator developed by Pulfrich (from Luhmann et al., 2006).

Helava first published the basic concept of analytical plotters in 1958 and built the first prototypes in the early 1960s (Petrie et al., 2004). Computers were now built into stereoplotters. Their computational power made the removal of mechanical constraints possible. This resulted in the implementation of more flexible methods that improved precision, accuracy, and enabled gross error detection. One of these methods is the bundle adjustment method. Bundle adjustment utilised information about coordinated points in object space and their corresponding projections in image space to estimate the position and orientation of cameras in a triangulation process (Mikhail et al., 2001). Mikhail et al. (2001) consider it the most flexible and accurate triangulation method used in photogrammetry. In this method camera positions and orientations are not restricted. Also, the imaging system is not limited to central projection and interior orientation parameters of cameras can be included as unknowns to be estimated during the bundle adjustment. This makes the bundle adjustment method significant, in particular for close-range photogrammetry (Luhmann et al., 2006). Although the principles were already known in the first half of the twentieth century, the bundle adjustment could only be efficiently implemented in the 1970s, when computers with sufficient computational power evolved. This lifted the restrictions on orientation and position of the camera as well as on the type of camera to be used in photogrammetric applications (Luhmann et al., 2006).

Towards the end of the twentieth century, further technological developments, particularly the cost reduction of memory and storage, led to the emergence of digital photogrammetry. Digital cameras, which store all imagery in digital form, replaced the analogue cameras. In the same way stereoplotters were replaced by digital photogrammetric workstations. Although the working environment for photogrammetry has changed, the basic principles remain (Mikhail et al., 2001).

2.3.2 Mathematical models

2.3.2.1 Coordinate transformations

The location of a point in space often is defined in relation to an arbitrary 3D Cartesian coordinate system. This coordinate system is defined by an origin, three reference directions and a scale. Coordinates in one system can be transformed into coordinates in another system using the 3D Helmert Transformation. The Helmert

Transformation requires 7 parameters: 3 rotations, 3 shifts and 1 scale (Figure 2.2). The three rotation parameters represent the angles of three consecutive rotations about the axes of the 3D coordinate system (Luhmann et al., 2006). In Figure 2.3, let *A* be a

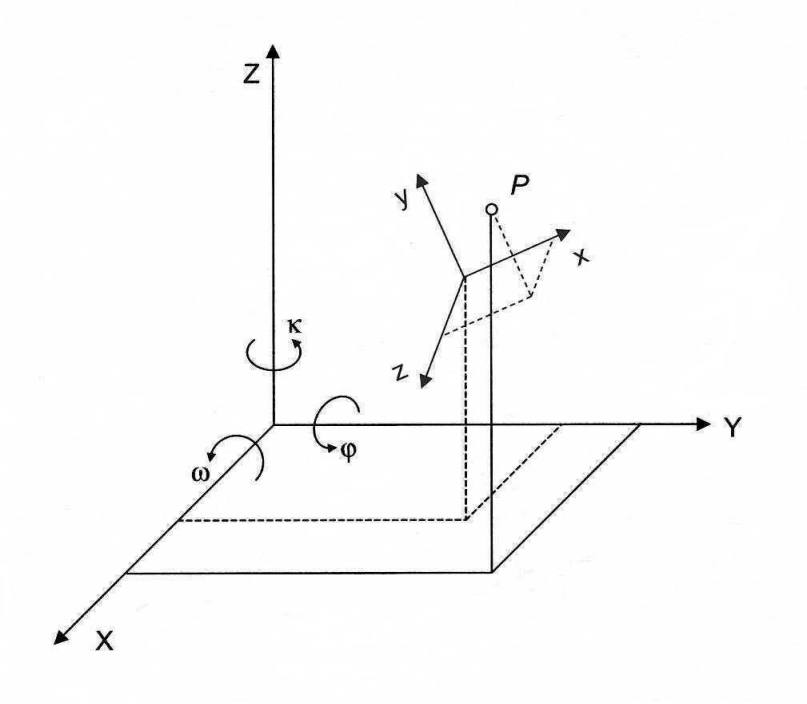

Figure 2.2: Parameters of a 3D Helmert Transformation (form Luhmann et al., 2006).

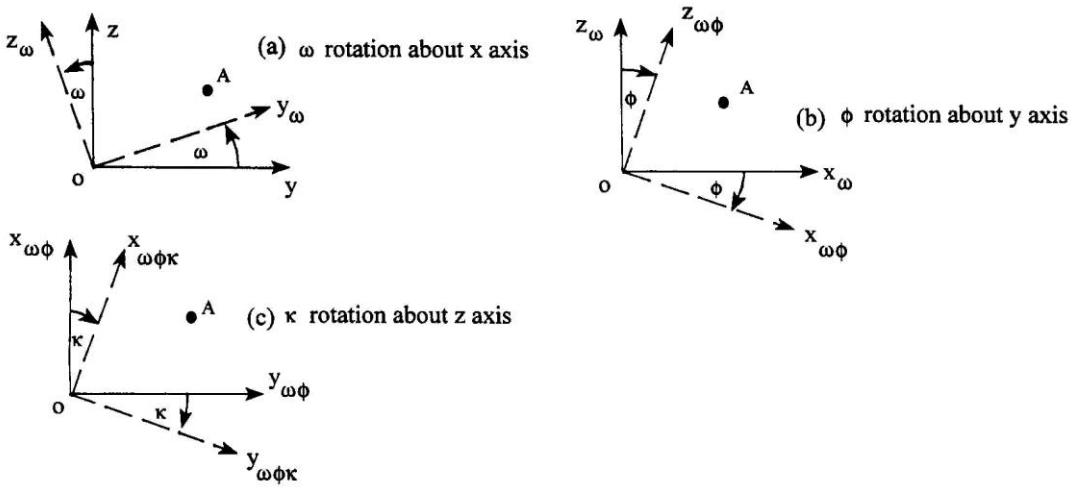

Figure 2.3: Consecutive rotations in 3D space (from Cooper and Robson, 2001).

point with its 3D position in the source coordinate system represented by $\mathbf{x} = [x\ y\ z]^{\mathrm{T}}$ and its position in the target coordinate system represented by $\mathbf{X} = [X\ Y\ Z]^{\mathrm{T}}$. The three consecutive rotations that lead from the source system to the target system are shown in Figure 2.3. Viewed from the positive rotation axis towards the origin of the coordinate system, a positive rotation (positive rotation angle) rotates the axes in a counter clockwise direction (Luhmann et al., 2006).

The first rotation is about the *x*-axis by the angle ω. As a result the $(x_\omega\ y_\omega\ z_\omega)$ coordinates of *A* are derived as follows:

$$\begin{aligned} x_\omega &= x \\ y_\omega &= y\cos\omega - z\sin\omega \\ z_\omega &= y\sin\omega + z\cos\omega \end{aligned} \tag{2.1}$$

or in matrix form

$$\mathbf{x}_\omega = \mathbf{R}_\omega \mathbf{x} = \begin{bmatrix} x_\omega \\ y_\omega \\ z_\omega \end{bmatrix} = \begin{bmatrix} 1 & 0 & 0 \\ 0 & \cos\omega & -\sin\omega \\ 0 & \sin\omega & \cos\omega \end{bmatrix} \begin{bmatrix} x \\ y \\ z \end{bmatrix} \tag{2.2}$$

Subsequently the second rotation is counter clockwise about the y_ω-axis by the angle φ. The $(x_{\omega\varphi}\ y_{\omega\varphi}\ z_{\omega\varphi})$ coordinates of *A* are calculated by

$$\begin{aligned} x_{\omega\varphi} &= x_\omega\cos\varphi + z_\omega\sin\varphi \\ y_{\omega\varphi} &= y_\omega \\ z_{\omega\varphi} &= -x_\omega\sin\varphi + z_\omega\cos\varphi \end{aligned} \tag{2.3}$$

or in matrix form

$$\mathbf{x}_{\omega\varphi} = \mathbf{R}_\varphi \mathbf{x}_\omega = \begin{bmatrix} x_{\omega\varphi} \\ y_{\omega\varphi} \\ z_{\omega\varphi} \end{bmatrix} = \begin{bmatrix} \cos\varphi & 0 & \sin\varphi \\ 0 & 1 & 0 \\ -\sin\varphi & 0 & \cos\varphi \end{bmatrix} \begin{bmatrix} x_\omega \\ y_\omega \\ z_\omega \end{bmatrix} \tag{2.4}$$

After the third rotation about the $z_{\omega\varphi}$-axis by the angle κ, the $(x_{\omega\varphi\kappa}\ y_{\omega\varphi\kappa}\ z_{\omega\varphi\kappa})$ coordinates of *A* are calculated by

$$\begin{aligned} x_{\omega\varphi\kappa} &= x_{\omega\varphi}\cos\kappa - y_{\omega\varphi}\sin\kappa \\ y_{\omega\varphi\kappa} &= x_{\omega\varphi}\sin\kappa + y_{\omega\varphi}\cos\kappa \\ z_{\omega\varphi\kappa} &= z_{\omega\kappa} \end{aligned} \tag{2.5}$$

or in matrix form

$$\mathbf{x}_{\omega\varphi\kappa} = \mathbf{R}_{\kappa}\mathbf{x}_{\omega\varphi} = \begin{bmatrix} x_{\omega\varphi\kappa} \\ y_{\omega\varphi\kappa} \\ z_{\omega\varphi\kappa} \end{bmatrix} = \begin{bmatrix} \cos\kappa & -\sin\kappa & 0 \\ \sin\kappa & \cos\kappa & 0 \\ 0 & 0 & 1 \end{bmatrix} \begin{bmatrix} x_{\omega\varphi} \\ y_{\omega\varphi} \\ z_{\omega\varphi} \end{bmatrix} \tag{2.6}$$

By combining the three rotations above, the whole rotation can be described by

$$\mathbf{X} = \mathbf{R}_{\kappa\varphi\omega}\mathbf{x} \tag{2.7}$$

where

$$\mathbf{R}_{\kappa\varphi\omega} = \mathbf{R}_{\kappa}\mathbf{R}_{\varphi}\mathbf{R}_{\omega} \tag{2.8}$$

and

$$\mathbf{X} = \mathbf{x}_{\boldsymbol{\omega\varphi\kappa}} \tag{2.9}$$

which leads to the full rotation matrix

$$\mathbf{R}_{\kappa\varphi\omega} = \begin{bmatrix} \cos\varphi\cos\kappa & \sin\omega\sin\varphi\cos\kappa + \cos\omega\sin\kappa & -\cos\omega\sin\varphi\cos\kappa + \sin\omega\sin\kappa \\ -\cos\varphi\sin\kappa & -\sin\omega\sin\varphi\sin\kappa + \cos\omega\cos\kappa & \cos\omega\sin\varphi\sin\kappa + \sin\omega\cos\kappa \\ \sin\varphi & -\sin\omega\cos\varphi & \cos\omega\cos\varphi \end{bmatrix} \tag{2.10}$$

Introducing the shift parameters $\mathbf{X}_0 = [X_0 \;\; Y_0 \;\; Z_0]^{\mathrm{T}}$ and the scale parameter λ the coordinate transformation can be defined as follows:

$$\mathbf{X} = \lambda\mathbf{R}_{\kappa\varphi\omega}\mathbf{x} + \mathbf{X}_0 \tag{2.11}$$

or in matrix form

$$\begin{bmatrix} X \\ Y \\ Z \end{bmatrix} = \lambda \begin{bmatrix} a_{11} & a_{12} & a_{13} \\ a_{21} & a_{22} & a_{23} \\ a_{31} & a_{32} & a_{33} \end{bmatrix} \begin{bmatrix} x \\ y \\ z \end{bmatrix} + \begin{bmatrix} X_0 \\ Y_0 \\ Z_0 \end{bmatrix} \tag{2.12}$$

The rotation matrix is an orthogonal matrix, therefore

$$\mathbf{R}_{\kappa\varphi\omega}{}^{-1} = \mathbf{R}_{\kappa\varphi\omega}{}^{\mathrm{T}} \tag{2.13}$$

For rotating backwards from the target system to the source system, the inverse (or transposed) rotation matrix is used:

$$\mathbf{x} = \frac{1}{\lambda}\mathbf{R}_{\kappa\varphi\omega}{}^{-1}\mathbf{X} - \mathbf{X}_0 \tag{2.14}$$

Spatial rotation can also be expressed by the direction cosines of the angles between the source and the target coordinate system. Therefore, the rotation matrix can also be regarded as a direction cosine matrix:

$$\mathbf{R} = \begin{bmatrix} cos(Xx) & cos(Yx) & cos(Zx) \\ cos(Xy) & cos(Yy) & cos(Zy) \\ cos(Xy) & cos(Yz) & cos(Zz) \end{bmatrix} = [\mathbf{i}\ \ \mathbf{j}\ \ \mathbf{k}] \tag{2.15}$$

where **i**, **j**, **k** are the unit vectors in the direction of the coordinate axes in the target system (Luhmann et al., 2006). A graphic representation of direction cosines can be seen in Figure 2.4.

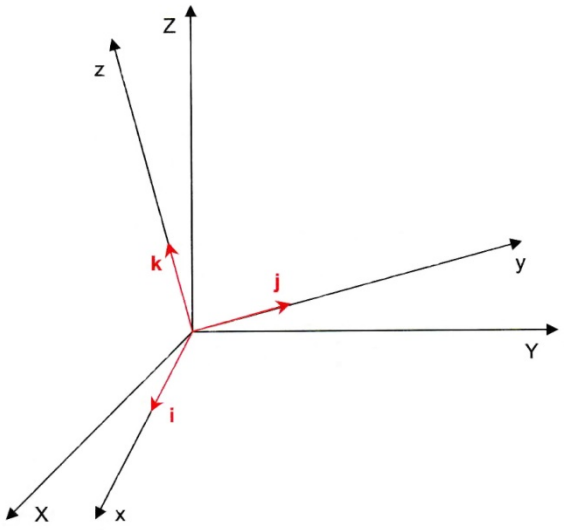

Figure 2.4: Description of a target coordinate system as direction cosines of a source system (from Luhmann et al., 2006).

2.3.2.2 Collinearity equations

In photogrammetry two different coordinate systems are used. One is the image coordinate system, which is used to represent a point in image space. The other one is the object coordinate system, which is used to represent a point in object space. The image coordinate system is a two-dimensional coordinate system that is defined by fiducial marks in analogue photogrammetry or by the array of sensor elements in digital photogrammetry, respectively (Figure 2.5) (Luhmann et al., 2006).

The camera coordinate system is equivalent to the image coordinate system extended by a *z*-axis that is normal to the image plane and passes through the perspective centre *O* (Figure 2.6). This axis is also called the perspective axis and the point where it intersects the image plane is the principal point *P*. The distance between principal point and perspective centre is called principal distance *c* or focal length *f*. The origin of the camera coordinate system is at the perspective centre *O*. The object coordinate system can be any 3D Cartesian coordinate system, typically defined by reference points on the object (Cooper and Robson, 2001; Luhmann et al., 2006).

Image coordinates are related to the object space using central perspective projection (Figure 2.6). Any object point *A* lies on a straight or collinear line, which coincides with its corresponding image point a' and the perspective centre *O*. The projection of an image point into the equivalent object point can be described by the 3D Helmert Transformation (Luhmann et al., 2006).

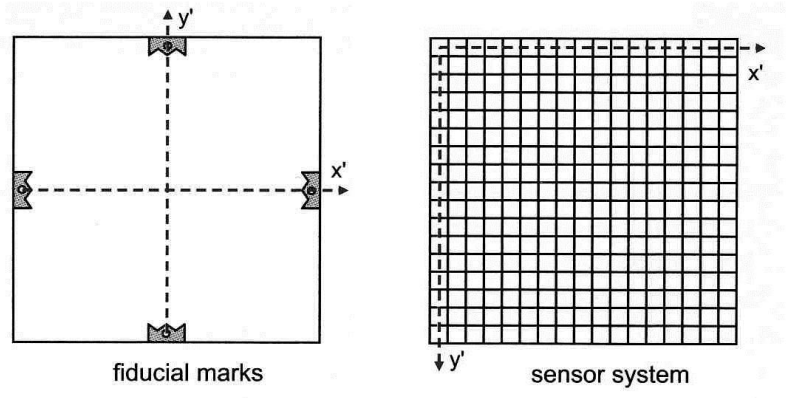

Figure 2.5: Image coordinate systems in analogue (left) and digital (right) photogrammetry (from Luhmann et al., 2006).

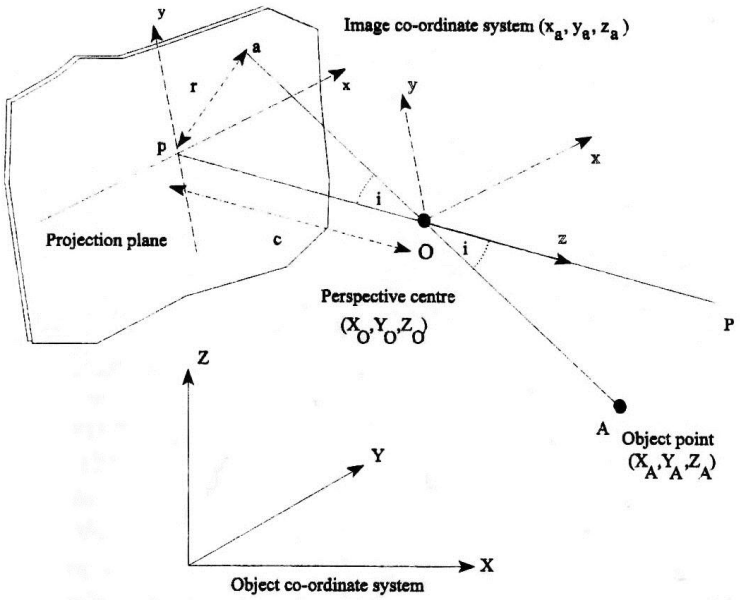

Figure 2.6: Camera coordinate system and central perspective projection (from Cooper and Robson, 2001).

The image coordinates x' and y' can be derived from the object coordinates by inverting the Helmert Transformation (Equation 2.11), substituting the coordinates of the source system $\mathbf{x}$ with image coordinates and principal distance c in $\mathbf{x}' = [x' \;\; y' \;\; c]^{\mathrm{T}}$, and introducing principal point $P = [x'_0 \;\; y'_0]$ and corrections for image distortion $\boldsymbol{\Delta\mathbf{x}'}$ (Equations 2.16 and 2.17).

$$\mathbf{x}' - \mathbf{x}'_0 - \boldsymbol{\Delta}\mathbf{x}' = \frac{1}{\lambda}\mathbf{R}_{\kappa\varphi\omega}{}^{-1}(\mathbf{X} - \mathbf{X}_0) \tag{2.16}$$

$$\begin{bmatrix} x' - x'_0 - \Delta x' \\ y' - y'_0 - \Delta y' \\ c \end{bmatrix} = \frac{1}{\lambda}\begin{bmatrix} a_{11} & a_{12} & a_{13} \\ a_{21} & a_{22} & a_{23} \\ a_{31} & a_{32} & a_{33} \end{bmatrix}\begin{bmatrix} X - X_0 \\ Y - Y_0 \\ Z - Z_0 \end{bmatrix} \tag{2.17}$$

The scale factor λ is unknown and varies for each point. It can be removed by dividing each of the first two lines of Equation 2.17 ($x' - x'_0 - \Delta x'$ and $y' - y'_0 - \Delta y'$, respectively) by the third line (c). This leads to development of the collinearity equations, which are the basis for calculating the photo coordinates of an object point (Equation 2.18).

$$x' = x'_0 + c\frac{a_{11}(X - X_0) + a_{21}(Y - Y_0) + a_{31}(Z - Z_0)}{a_{13}(X - X_0) + a_{23}(Y - Y_0) + a_{33}(Z - Z_0)} + \Delta x'$$
$$y' = y'_0 + c\frac{a_{12}(X - X_0) + a_{22}(Y - Y_0) + a_{32}(Z - Z_0)}{a_{13}(X - X_0) + a_{23}(Y - Y_0) + a_{33}(Z - Z_0)} + \Delta y' \quad (2.18)$$

where x'_0, y'_0, c, $\Delta x'$, $\Delta y'$ are the interior orientation parameters and X_0, Y_0, Z_0, ω, φ, κ are the exterior orientation parameters. The collinearity equations are the basis for bundle adjustment, where the exterior orientation of an unlimited number of images can be determined (Luhmann et al., 2006).

2.3.3 Exterior orientation determination

The exterior orientation consists of six parameters describing the position (X_0, Y_0, Z_0) and orientation (ω, φ, κ) of a camera coordinate system in the object coordinate system. The parameters of the exterior orientation, together with the parameters of the interior orientation establish the relationship between image coordinates and the corresponding object points (Luhmann et al., 2006). There is both an indirect and a direct method to determine exterior orientation parameters.

For the indirect method, points with known object coordinates (control points) have to be visible in images in order to derive their image coordinates. The measured image coordinates and possibly known interior orientation parameters derived during camera calibration (Section 2.4.3) are inserted in the collinearity equations, which are then solved for the six unknowns of the exterior orientation. The minimum number of the required control points depends on the number of images to be oriented and whether the interior orientation is known (Luhmann et al., 2006).

In a bundle adjustment an unlimited number of images can be oriented concurrently using a relatively low number of control points. It utilises the method of "least-squares", which implements the collinearity equations and minimises residuals of the observations (Cooper and Robson, 2001). One advantage of this method is that it can be applied using almost arbitrary image configurations, which is the general case in close-range applications. Using multiple, and arbitrary, image configurations reduces the number and size of occluded areas. It also facilitates full recording of large objects, without diminishing accuracy and data resolution, by only taking small scale

photographs. Multiple images also provide redundant observations, which increase precision and reliability and, if a stronger intersection geometry of bundles of rays is achieved, accuracy can be increased (Luhmann et al., 2006; Fryer et al., 2007).
Exterior orientation can also be estimated and incorporated directly by the utilisation of an integrated Global Navigation Satellite System (GNSS) and Inertial Navigation System (INS) system. The GNSS provides the three-dimensional position and the INS is primarily used to determine the orientation (further described in section 2.7). This method is mainly applied for airborne systems (Mikhail et a., 2001; Cramer and Stallmann, 2002; Heipke et al., 2002) but also in terrestrial mobile mapping applications (Manzoni et al., 2005; Niu et al., 2006; Guarnieri et al., 2008).

2.4 Close-range photogrammetry

2.4.1 Definition and differences to aerial photogrammetry

There is no generally accepted definition for close-range photogrammetry. According to Karara (1979) and Luhmann et al. (2006) close-range photogrammetry encompasses all photogrammetric work where the object to camera distance is no longer than 300 m. Cooper and Robson (2001) define close-range photogrammetry as a photogrammetric technique where the size of the object to be measured does not exceed 100 m and the camera is positioned close to the object. Most developments in photogrammetry have focussed on aerial applications (Albertz and Wiedemann, 1996) and mapping, but the basic principles also apply to close-range configurations (Mikhail et al., 2001; Luhmann et al., 2006). However, there are some factors that complicate the transfer of findings from aerial to close-range photogrammetry (Albertz and Wiedemann, 1996). In close-range photogrammetry the optical axis of the camera usually is not vertical but either horizontal or oblique. Furthermore, photographs are acquired from arbitrary locations with convergent orientation, which leads to more complex image configurations. Lens focus settings vary due to small and varying camera-to-object distances, causing variable principal distances. If fixed, images cannot always be in focus, unless the “depth of field” is considered and adjusted using an appropriate aperture and exposure settings. Further complications

that are more likely to occur in close-range photogrammetry are occlusions and differences in illumination (Albertz and Wiedemann, 1996; Mikhail et al., 2001; Luhmann et al., 2006).

2.4.2 Use of consumer-grade digital cameras

Consumer-grade cameras are not specifically designed for photogrammetric use and are therefore categorised as non-metric cameras. Non-metric cameras do not provide any additional aids for defining the interior orientation, while metric cameras are produced to meet high specifications for interior orientation stability (Luhmann et al., 2006). In the 1970s non-metric cameras were already considered to have photogrammetric potential and were increasingly used in photogrammetry (Karara, 1979). Schwidefsky (1970) proposed that close-range photogrammetry must be independent of the availability of metric cameras in order to extend its utilisation.

Low-cost, high resolution digital sensors are now available, boosted by the increased demand for digital cameras from the consumer market (Luhmann et al., 2006). Consumer-grade cameras, as part of a low-cost photogrammetric system, can enhance the attractiveness of photogrammetry for many applications, ranging from architectural documentation to recording of geological features (Mikhail et al., 2001; Ordóñez et al., 2008). Recent research aims to enable non-specialists to use photogrammetric methods in their respective field of work (Chandler and Fryer, 2005; Boochs et al., 2007; Bryan and Chandler, 2008; Ordóñez et al., 2008).

Even if consumer-grade cameras cannot obtain the accuracy level of metric cameras (Mikhail et al., 2001), recent publications (Chandler and Fryer, 2005; Luhmann et al., 2006; Boochs et al., 2007; Bryan and Chandler, 2008; Ordóñez et al., 2008) suggest that accuracy requirements can be met for many applications, while reducing cost and enhancing ease of use.

In recent years several cameras with integrated GPS receivers and sometimes even compass and tilt sensors have appeared on the market. These features can be considered as an extension of the photogrammetric usability (Gruen and Akca, 2008). The G700SE digital camera of Ricoh has a GPS positioning accuracy of 5 to 10 m and a built-in digital compass for direction recording. This camera has functionality to online export image and position data to online mapping platforms, such as Google

Maps and Google Earth (KOREC, n.d.; Ricoh, 2010). Other examples of consumer-grade cameras with integrated GPS functionality are the EX-H20G from Casio, which also has motion sensors for indoor positioning (Casio America, 2010), and the Leica V-LUX 20 camera (Leica Camera, n.d.).

A recent development is the integration of digital cameras in mobile phones. Mobile phone cameras with 10 megapixel (MP) resolution are available, due to the fast development in mobile phone technology. This and their inexpensiveness and ease-of-use indicate potential for spatial measurement. Mobile phones with integrated GPS receiver and motion sensors are also available, increasing their applicability even more (Gruen and Akca, 2008; Chikatsu and Takahashi, 2009). Comparative performance tests (Akca and Gruen, 2009; Chikatsu and Takahashi, 2009) indicated that with accurate calibration, mobile phone cameras can be used in photogrammetry similar to consumer-grade cameras.

2.4.3 Calibration of consumer-grade cameras

The purpose of camera calibration is to define the interior orientation parameters of a camera, which are crucial for accurate photogrammetric measurement (Bosch et al., 2005; Chandler et al., 2005; Wackrow et al., 2007). The interior orientation parameters are the principal point offsets x'_0 and y'_0, the principal distance c, and corrections for image distortions $\Delta x'$ and $\Delta y'$ (Luhmann et al., 2006).

There are different methods available to calibrate a camera. "Laboratory calibration" normally is a method for metric cameras and is rarely used in close-range photogrammetry where cheaper and easier to apply methods prevail (Luhmann et al., 2006).

"Test field calibration" utilises a field with coordinated targets. Images of this test field are taken from several positions and with different orientations. The object and photo coordinates of the targets are used to derive the interior orientation parameters in a bundle adjustment (Luhmann et al., 2006).

"On-the-job calibration" is a combination of test field calibration and actual object measurement. A portable test field is placed close to the object requiring measurement and is photographed together with the object (Luhmann et al., 2006).

"Self-calibration" can be regarded as an extension to test field calibration where the object to be measured replaces the test field. The images acquired for object measurement are simultaneously used for calibration (Luhmann et al., 2006).

The interior orientation of consumer-grade cameras can be subject to variations, although they can be calibrated in order to derive accurate measurements of an object. Recent research concerning the stability of these cameras (Bosch et al., 2005; Wackrow et al., 2007) revealed sufficient stability for many applications of medium accuracy for a period of at least one year.

An important issue when calibrating consumer-grade cameras is lens distortion, which has a significant influence on the accuracy of image measurements and should be modelled appropriately (Chandler et al., 2005). Wackrow and Chandler (2008) state that the measurement accuracy is decreased significantly by the presence of small residual errors in the lens model. These are discernible in photogrammetrically derived DEMs as systematic error surfaces or "domes" when measuring planar surfaces. This effect can be compensated by using slightly convergent imagery (Wackrow and Chandler, 2008; Wackrow and Chandler, 2011).

2.5 Orientation sensors

2.5.1 Measuring principles

2.5.1.1 Magnetometers

Magnetometers are sensors that measure magnetic fields and are used in a wide range of applications. In Lenz and Edelstein (2006) an account of the numerous and diverse measurement principles and applications can be found. Magnetometers can be distinguished by those measuring the total strength of a magnetic field and those measuring the strength only in a particular direction, which is a vector component of the field. Using three orthogonal vector magnetometers, the total strength of a magnetic field can be derived.

Magnetometers can be further distinguished according to their field of application. For this research project only the magnetic compass approach is relevant. Here the

magnetic field of the Earth is measured to derive the orientation of the sensor with respect to that field. The magnetic field is not horizontal (Kemp et al., 1998) and in order to obtain horizontal heading information the measurement has to be projected onto a horizontal plane.

Magnetometer readings are susceptible to local anomalies or distortions in the magnetic field of the Earth, which can be caused by any object with a magnetic signature. It is possible to determine corrections for these anomalies by comparing compass measurements with truth data. The corrections are valid provided the magnetic field in the area where the compass is located does not change (Lenz and Edelstein, 2006).

2.5.1.2 Accelerometers

Accelerometers belong to the group of inertial sensors, because they measure a linear shift in momentum (Corke et al., 2007). There is no unique design for accelerometers, but they are based on Newton's second law, $F = m * a$, where the force F on an object can be derived by multiplying the mass m of the object by acceleration a (Grewal et al., 2001). Therefore, an accelerometer often consists of a proof mass connected to a spring or cantilever beam that allows movement only in one direction (Grewal et al., 2001; Corke et al., 2007).

Momentum change is not the only force measured by accelerometers; measured values include acceleration due to gravity as well as movement (Corke et al., 2007). If the acceleration due to movement is very small the gravity component is measured only, which allows the vertical inclination of the sensor to be derived (Kemp et al., 1998; Speller and Yu, 2004).

A single accelerometer measures only one vector component, defined by the axis along which the proof mass can move. Multi-axis sensors are necessary for measuring more than one component (Grewal et al., 2001).

2.5.1.3 Gyroscopes

Gyroscopes also belong to the group of inertial sensors, but unlike accelerometers they measure angular motion (Corke et al., 2007). They are available in many designs for a variety of applications, mainly steering and stabilising. Two types of gyroscopes

can be distinguished: rate gyroscopes for measuring angular rates and displacement gyroscopes for measuring rotation angles (Grewal et al., 2001).

A gyroscope is basically a wheel spinning around an axis. A rotating body tends to retain its orientation due to inertia. If it is built in a gimballed system, the gyroscope is separated from angular movements of the body and stays in its orientation. The rotation angle of the body can then be derived from the angular displacement of the new orientation from the initial orientation (Grewal et al., 2001). In a "strap-down" system, the gyroscope is forced to move in the same way as the body. If the body rotates, the resisting torque of the gyroscope indicates the angular rate (Corke et al., 2007).

There are gyroscopes that are not based on a spinning wheel but a vibrating structure. Rotating the structure induces a Coriolis force, which can be used to derive the angular rate (Grewal et al., 2001; Corke et al., 2007).

2.5.2 Micro-Electro-Mechanical System (MEMS)

In order to find and develop new fields of application for sensors, researchers seek low-cost and small-size solutions. Niu et al. (2006) describe that Mobile Mapping Systems (MMS) that employ high-grade IMUs are too restricted in their utilisation, due to their large size and high cost. Popovic et al. (1996) state that the commercial viability of magnetometers does not exclusively depend on performance, but also on the potential to incorporate them in small-size devices.

MEMS technology has enabled the development of low-cost sensors that have a size in millimetre range, weigh a few milligrams, and consume little power (Niu et al., 2006). Orientation sensors based on MEMS are applied in a range of different fields. Kemp et al. (1998) and Luinge and Veltink (2004) used small-size accelerometers to measure body movement. Corke et al. (2007) showed how MEMS gyroscopes and accelerometer measurements can be fused with visual navigation in robotics. The capabilities of low-cost navigation sensors in mobile mapping applications were tested by Niu et al. (2006) and Guarnieri et al. (2008).

Niu et al. (2006) consider MEMS inertial sensors less accurate compared to the equivalent high-end sensors, due to their high noise level and bias instability. In their research, the performance of an IMU based on MEMS was assessed using data from a

high-end IMU as reference. Utilising different data processing methods they achieved an attitude Root Mean Square Error (RMSE) ranging from 0.35º to 1.5º.

Another test of the performance of orientation sensors was conducted by Brodie et al. (2008). Five identical IMUs containing accelerometers, magnetometers and gyroscopes were tested, using as reference a gauging rig, where the exact orientation could be determined. The maximum error derived in this test was 5.2° while the sensor specifications stated 1°. The mean RMSE of the component angles were 2.2° for roll, 2.2° for pitch, and 5.2° for yaw. The accuracy was improved to error values of less than 1°, after the sensors were re-initialised using a new method for estimating corrections for measurements from the IMU components.

An indication of nominal MEMS orientation sensor performance is given in product specifications of commercially available sensors. For example, the TCM5 orientation sensor of PNI used in this research project consists of a tri-axis accelerometer and a tri-axis magnetometer and measures orientation in three directions. It is supposed to deliver tilt-depending heading accuracy of 0.3° – 0.5°, pitch accuracy of 0.2° and roll accuracy between 0.2° to 1.0°, depending on the pitch angle (PNI, 2009). In 2009 the cost for this sensor was approximately £ 1,600. Xsens offers a comparable system with static roll and pitch accuracy of 0.5° and heading accuracy of 1.0°. This sensor has also a Global Positioning System (GPS) receiver integrated with position accuracy of 2.5 m (Xsens Technologies, 2009).

2.5.3 Sensor initialisation and offset calibration

The orientation of a system component, for example a digital camera, can be determined using an orientation sensor. To derive the orientation of the system component, two steps are usually necessary. First, the orientation sensor has to be initialised to yield accurate readings relative to the earth system. Initialisation comprises the gauging and correction of bias in the orientation sensor element measurements. The second step is to calibrate the rotational offsets between the orientation sensor and the system component.

In Vandeportaele et al. (2006), a system consisting of a camera and an orientation sensor was initialised. First the sensor components, accelerometers and magnetometers, were initialised separately followed by determining the local vertical

component of the magnetic field of the Earth. Several images of a calibration field were captured and the orientation of the camera for each image was determined. The rotational offset between the camera and the sensor was derived by comparing those values and the reading of the orientation sensor.

Alves et al. (2003) initialised an IMU to be used with a camera. The IMU was attached to a pendulum, which allowed true values of orientation and acceleration to be determined for the moving sensor. The rotational offset between camera and IMU was determined by measuring the vertical direction of camera and IMU. This was achieved by defining the vanishing point of vertical lines in images acquired with the camera and sensing gravity, respectively. The same approach was used in Lobo and Dias (2007), where it was extended by a method to determine the translation between camera and IMU, because the translation could influence the overall accuracy.

Kelly and Sukhatme (2008) restricted their research to offset calibration. The rotation and translation between a camera and an IMU was determined simultaneously using an "Unscented Kalman" filter. The only additional equipment needed for this method is a camera calibration field. The authors claim the method to be suitable for re-calibrating the system if necessary.

2.6 Positioning sensors

2.6.1 Global Navigation Satellite System (GNSS)

GNSS can be used to determine 3D position anywhere on the Earth. They rely on a network of satellites orbiting the Earth and sending electro-magnetic signals to the ground. Currently there are four systems, which are all based on similar principles: GPS, GLONASS, Galileo, and Compass (El-Rabbany, 2006; Chiang et al., 2010). At present Galileo is not fully operational and Compass is being extended from a regional system restricted to China and neighbouring countries to a global system that is expected to be operational by 2013 (Chiang et al., 2010). GPS and GLONASS can be used for positioning and modern receivers make use of signals of both systems to increase performance. GPS is the GNSS that is relevant to this literature review, because this system was used in this particular research project. GPS is operated by

the American Department of Defense and consists of three segments: space segment, earth-based control segment, and user segment. The space segment encompasses a network of a nominal 24 satellites. Their operability is monitored and ensured by the control segment. The user segment consists of everyone who utilises GPS (El-Rabbany, 2006).

The signal permanently sent by the satellite consists of at least two codes on two carrier waves (L1 and L2) and a message containing the current position of the satellite. Only the Standard Position System (SPS) code is available to all users. The structure of the SPS code is unique to each satellite and is repeated regularly (El-Rabbany, 2006). GPS receivers replicate the SPS code for each satellite at theoretically the same time as the satellite produces the code. The satellite signal arrives at the receiver with a time shift and, therefore, the satellite code does not match the receiver code at the time of arrival. The magnitude of the time shift is determined by time shifting the receiver code until it correlates with the satellite code (Van Sickle, 2008). The time shift indicates the time the signal takes to travel from the satellite to the receiver and is used to calculate the distance or 'range' between satellite and receiver. Having at least distances to three satellites at the same time allows a trilateration technique to be used to determine the position of the receiver (Figure 2.7) (El-Rabbany, 2006). However, a fraction of the time shift is due to offsets between satellite and receiver clocks (Van Sickle, 2008). Synchronisation of satellite and receiver clocks to the precision necessary requires very accurate and hence expensive clocks. It is far cheaper to integrate unsynchronised clocks in receivers and

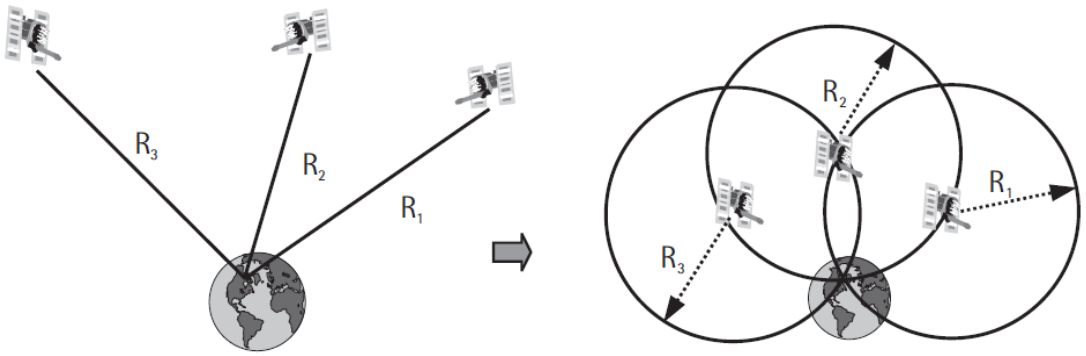

Figure 2.7: Basic principle of GPS positioning (from El-Rabbany, 2006).

include the time offset between the two clocks as an additional unknown. As a result, at least one more satellite is needed for position determination. This "code" based method for positioning can yield planimetric coordinates with a maximum error of 10 m and height coordinates with an error up to 19 m and meets most accuracy requirements necessary for navigation (El-Rabbany, 2006).

2.6.2 Differential Global Positioning System (DGPS)

The accuracy of GPS positioning is degraded by different factors: inaccurate position of the satellite, satellite clock error, and errors in signal propagation caused by the signal passing through the atmosphere (El-Rabbany, 2006). These factors affect the accuracy of the "code" based method but can be reduced by using DGPS. The accuracy achievable with DGPS is normally in the range of a few metres and suitable for some mapping applications. A second receiver is positioned as a base or reference station at a point with known coordinates. In that way, a series of GPS derived positions can be compared to the accepted position and correction values are calculated as a function of time. These are used to correct the computed position of the first receiver (rover) in real-time or by using a post-processing method. In this technique it is assumed that both base station and rover experience the same positional errors. In order to achieve this they have to be located close to each other so that they observe the same satellites. A general principle is that the achievable accuracy increases with decreasing distance between base station and rover (Grewal et al., 2001; El-Rabbany, 2006).

DGPS can be categorised in local-area and wide-area DGPS. In the local-area category the rover is very close to the base station, often in line of sight, and it is assumed that the corrections due to atmospheric interference are the same for both receivers. In the wide-area category corrections are determined by a geographically wide spread network of permanent reference stations. Local-area DGPS achieves a higher accuracy, because the wide-area approach cannot completely correct for errors in the signal propagation due to the usually long distance between rover and base station (Grewal et al., 2001). This problem can be reduced by using a dual-frequency receiver. This type of receiver compares both carrier waves sent by the satellite. These are affected differently by the atmosphere and appropriate correction values can be

derived (El-Rabbany, 2006). Another solution to this problem is the utilisation of "virtual reference stations". A virtual reference station is a base station that is fictitiously located close to the rover position. Its observations are interpolated from surrounding stations of a wide-area network (Wanninger, 1999). The GNSS equipment manufacturer Trimble currently provides a service that creates virtual reference stations in real-time (Trimble Navigation, 2010). However, this service is not free of charge.

A further accuracy improvement important for survey-grade DGPS is possible when measuring the number of full carrier wave cycles and the fraction of cycles at the sending and the receiving end. This "phase comparison" method gives a more precise estimate of the distance between satellite and receiver and hence a higher accuracy in positioning (El-Rabbany, 2006). However, the carrier consists of identical sinusoidal waves and the number of full carrier wave cycles between receiver and the satellite is not immediately known. The unknown number of full cycles N is often referred to as the initial cycle ambiguity. From the time the receiver is switched on, it can count full cycles that it has received and measure fraction of cycles, but the initial cycle ambiguity need to be resolved in order to achieve high accuracy positioning (El-Rabbany, 2006). This is normally achieved using double-differencing. In double-differencing two GPS receivers (base station and rover) observe the same pair of satellites at the same time. The observations made in double differencing are: differences in carrier phase measurements between two satellites observed by the same receiver (Figure 2.8a) and differences in carrier phase measurement between two receivers observing the same satellite (Figure 2.8b). The initial cycle ambiguity can be resolved by combining double-differencing observations during two consecutive points in time (epochs) and determining the differences between the observations (Figure 2.9). This is also known as "triple differencing" (Van Sickle, 2008). The initial cycle ambiguity is valid as long as the receiver can maintain "lock" with the satellite signal. When the receiver loses the satellite signal, a discontinuity of the carrier phase measurement (cycle slip) occurs and the initial cycle ambiguity has to be re-calculated in order to maintain high accuracy measurements (El-Rabbany, 2006, Van Sickle, 2008). With carrier phase measurements accuracies to the centimetre level can be achieved, when the rover only stays a short time on a spot to be measured (rapid static mode). In a static mode, where both receivers are fixed at a location from

20 minutes up to several hours, accuracies at a range of 5 to 10 mm can be obtained (El-Rabbany, 2006).

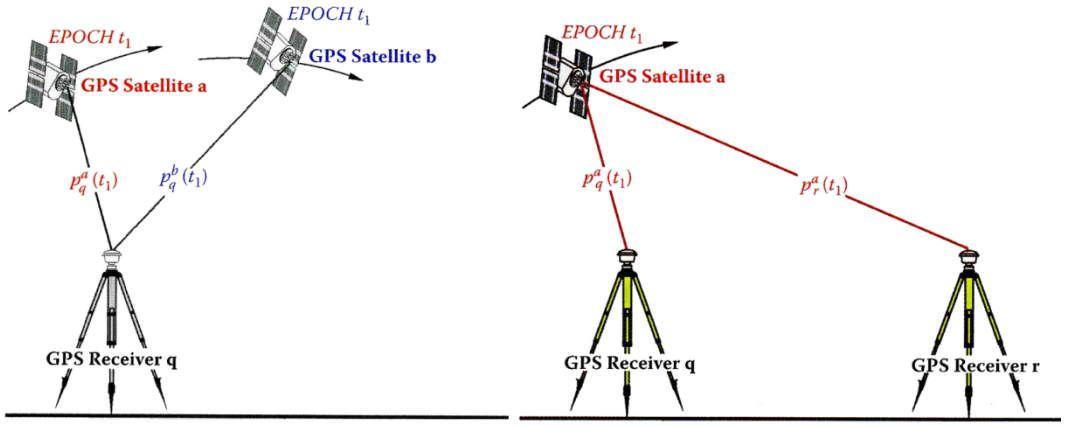

Figure 2.8: Observations made in double differencing (from Van Sickle, 2008).

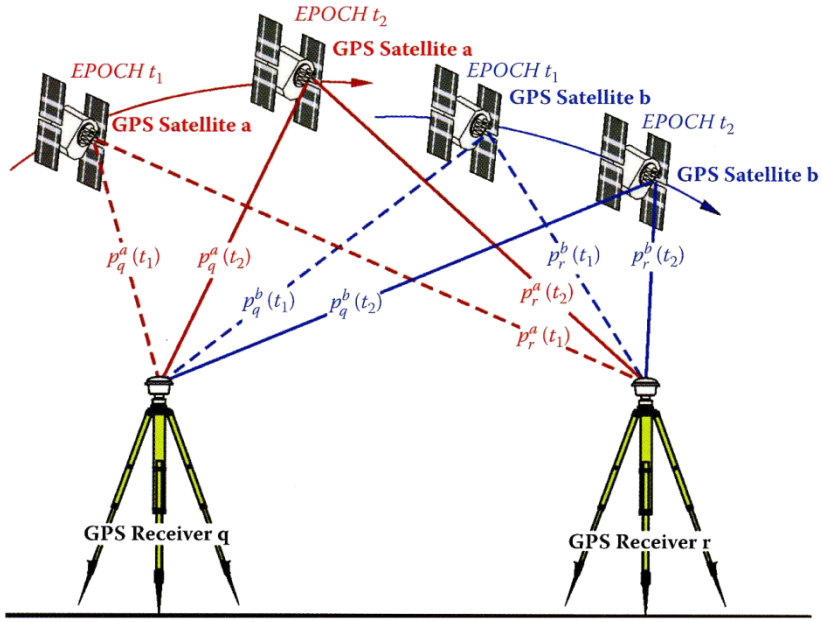

Figure 2.9: Double differencing over two epochs or triple differencing (from Van Sickle, 2008).

2.6.3 Multipath

The previous section explained how some error sources that affect GPS positioning accuracy can be attenuated by using DGPS. However, DGPS cannot reduce the effect of multipath. Multipath error is caused by the satellite signal arriving at the antenna from different paths and not only from the direct line of sight between antenna and satellite. Satellite signals that do not arrive from the direct line of sight have been reflected from objects surrounding the DGPS antenna, in particular the ground (Figure 2.10). The travelling time for reflected signals is longer than for the direct signal, but they cannot easily be distinguished from each other. As a consequence the reflected signals distort the direct signals when they arrive at the antenna, resulting in a ranging-error (Grewal et al., 2001; El-Rabbany, 2006). Multipath affects both code and carrier phase measurements and according to El-Rabbany (2006) multipath can cause errors in code measurements of tens of meters. In carrier phase measurements the maximum multipath error is a quarter of a cycle. For the L1 carrier wave this would be a magnitude of 4.8 cm. Multipath is widely recognised as a very significant error source in satellite-based positioning (Braasch, 1996; Grewal et al., 2001; El-Rabbany, 2006). It is highly localised and can therefore not be reduced using DGPS. Several hard- and software based methods exist that aim to attenuate the effect of multipath (Braasch, 1996; Grewal et al., 2001; El-Rabbany, 2006; Van Sickle, 2008).

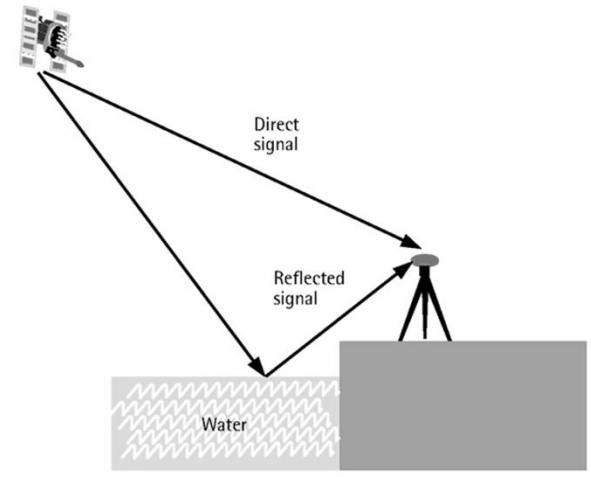

Figure 2.10: Multipath effect (from El-Rabbany, 2006).

The hardware approaches are generally concerned with antenna design. Metal groundplanes at the bottom of the antenna are used to reduce multipath from the ground. However, when multipath arrives at the edge of the groundplane, it still affects the measurements. Choke ring antennas contain concentric circular troughs that reduce this effect (Van Sickle, 2008). The software approaches are implemented in the receiver and use distinguishing factors between direct and reflected signals for enhancing the distorted signal within the receiver (Grewal et al., 2001; Van Sickle, 2008). These factors include the comparatively lower strength and higher diffusion of the reflected signal and a change in signal polarisation (Van Sickle, 2008).

2.6.4 Low-cost systems

The low-cost segment of the GPS market utilises the "code" based approach and offers handheld devices with a nominal accuracy of 1 to 10 m (Schwieger and Gläser, 2005). However, El-Rabbany (2006) states the achievable accuracy of the "code" based approach with 10 m in plan and 19 m in height. Wing et al. (2005) tested some of these receivers under varying conditions from "open sky" to "under canopy". Results described average errors ranging from 0.8 m up to 26 m with most errors smaller than 10 m.

Schwieger and Gläser (2005) developed a method to improve the accuracy of low-cost GPS receivers so that they can be used in geodetic surveys. The method is restricted to static baseline surveys and utilises two receivers, which can track carrier phase data. These receivers do not use the carrier phase data for "phase comparison" but for smoothing the signal. The raw code and carrier phase data were extracted and post-processed using software developed for utilising all data collected by the two low-cost receivers. Therefore, the full code and carrier phase information could be used for positioning. The method achieved a maximum deviation from the true values of 8 cm after a 30 minute observation period.

In October 2010 GENEQ announced their new small-size GPS receiver SXBlue III (Lauture, J.-Y., 2010). According to the specifications (GENEQ, 2010a) the SXBlue III is a dual frequency receiver that utilises DGPS and carrier phase measurements to provide centimetre accuracy in positioning. This receiver with a price of £ 3,150 (not including VAT) (Stevens, 2010) is more expensive than low-cost systems (available

from approximately £ 90 to £ 500 in 2012) (Garmin, 2012). However, it is significantly more cost effective when compared with survey-grade receivers, and the manufacturer believes that this will set a new standard for pricing of high accuracy GPS receivers (GENEQ, 2010a).

2.7 GPS/INS

The benefit of integrating GPS and INS, rather than using them standalone, is that they are complementary to each other, which allows more reliable positioning (Cramer and Stallmann, 2002). The integration of GPS and INS was initially carried out for direct georeferencing of airborne laser scanner data. GPS/INS systems were later also used in aerial photogrammetry, either for direct exterior orientation determination or integrated in a bundle adjustment.

The INS consists of an IMU containing accelerometers and gyroscopes and software for data processing (Heipke et al., 2002). It measures angular and linear movement and can be used for navigation on its own, but due to accumulating errors of the sensors, position data are only reliable for short time periods. An integrated GPS can solve this problem by providing low frequency reference positions to the INS but over longer periods. In return the INS provides high frequency navigation information, valuable if the GPS temporarily loses satellite signal or the number of available satellites falls below the required four (Cramer and Stallmann, 2002). Integrating GPS and INS data is usually performed using a Kalman filter, which requires the physical offset between the GPS and INS sensors to be considered (Mirzaei and Roumeliotis, 2008). Furthermore, accurate direct georeferencing is only possible if the offsets between GPS/INS and camera can be accounted for and the time is correctly aligned (Cramer and Stallmann, 2002). These offsets can be derived in a calibration procedure that compares exterior orientation parameters derived indirectly based on control points with the results from the GPS/INS measurement (Forlani and Pinto, 2002; Niu et al., 2006).

GPS/INS is particularly suited for dynamic applications or in areas where the GPS signal is lost easily and therefore sufficient for mapping projects (El-Rabbany, 2006). There are also examples of terrestrial applications for GPS/INS, mainly for mobile

mapping from a van: Reulke et al. (2004) and Manzoni et al. (2005) utilise high-end and expensive INS, while Niu et al. (2006) and Guarnieri et al. (2008) integrate GPS with low-cost INS based on MEMS technology.

2.8 Low-cost recording system approaches

The availability of consumer-grade cameras and low-cost devices for orientation determination facilitated the development of easy-to-use and low-cost methods and systems for image-based recording. In Bosch et al. (2005) cost reduction in cultural heritage recording is sought by utilising consumer-grade digital cameras. Although this achieves some savings, exterior orientation estimation relies on reference points and a surveyor and professional equipment is necessary. Boochs et al. (2007) enhanced the usability of photogrammetry for non-experts by providing a device for easy stereo image acquisition with consumer-grade cameras. In their method, control is provided by coordinated reference points, but measured object distances can also be used, when the restriction to scaled measurements is acceptable. Ordóñez et al. (2008) avoid additional costs for surveying reference points by measuring the camera-object distance. The authors mount a camera and a handheld laser distance meter on a rigid support device. Having information about the camera-object distance enabled scaled measurements in the images. An alternative way to provide scale reference can be found in Bryan and Chandler (2008). They developed and tested a technique for rock-art recording by non-specialists. To keep it simple, scale bars are used to provide scale in the object space. Non-specialist volunteers were successfully trained in applying this technique, which resulted in a further reduction in recording cost. Scale bars for reference are also used in Chandler and Fryer (2005). They state that scale bars are sufficient for simple sites but recording in a 3D national reference system is preferable and can be achieved by surveying control points. A known distance can only provide a scale constraint, but provides no orientation and position information of the object.

There are some examples where the exterior orientation of a camera was determined directly, similar to integrated GPS/INS for airborne sensors. In these examples small-size, low-cost orientation sensors substituted expensive INS devices.

Fiani and Pistillo (2004) developed a portable system for recording sea cliffs where images were taken from a motorboat. It consists of a dual-frequency GPS receiver, digital compass, and a digital consumer-grade camera. The compass includes inclinometers and is capable of measuring three-dimensional orientation with a nominal accuracy of 0.5° for heading and 0.15° to 2.0° for both pitch and roll. All components are fixed on an aluminium bar and the offsets in the whole system are calibrated at millimetre accuracy. The system was first tested on a building where surveyed reference points are used to derive exterior orientation in a conventional way. The authors report significant differences when conventionally derived exterior orientation parameters were compared to values directly provided by GPS and compass. They suggest that the result could be improved by enhancing the calibration procedure and including geometrical constraints.

Coppa et al. (2007) built a pedestrian MMS using the same compass used in the recording system described previously, an equivalent GPS receiver, and digital camera. The offsets of the system components were calibrated using a calibration field established on the outside wall of a building. When testing the system an absolute path displacement of 60 to 150 cm was achieved. Relative distance measurements yield differences between 20 and 40 cm. These high differences are attributed to poor image geometry, poor image point measurement, poor lighting conditions, poor performance of GPS in built-up areas, and deviations in the compass reading due to possible magnetic distortions.

Niu et al. (2006) used a MEMS-based GPS/INS navigation system mounted on a van for mobile mapping. The authors conducted tests on two different sites and achieved a 3D RMSE of 10.5 cm and 42.6 cm, respectively, using a high-end GPS/INS system to provide reference data.

2.9 Low-cost online geographic data visualisation and sharing

In recent years advances in technology, especially computer graphics, and the availability of broadband internet have enabled the development of tools that provide

opportunity to visualise, share, and create geographic data on the internet (Goodchild, 2007a; Craglia et al., 2008; Elvidge and Tuttle, 2008). A number of free platforms provide tools to anyone who has internet access. Well known examples are virtual globes such as Google Earth, NASA World Wind, and ESRI ArcGIS Explorer as well as the online digital maps OpenStreetMap and Wikimapia (Goodchild, 2007a; Elvidge and Tuttle, 2008; Muggah and Mioc, 2010). Generally, these platforms enable users to superimpose their own geographic data on the underlying basic geographic data, such as digital maps and satellite imagery (Blower et al., 2007; Goodchild, 2007a; Stensgaard et al., 2009). In this context geographic data is generally defined as data that can be georeferenced in some way (Bell et al., 2007).

2.9.1 Benefits and risks

The success of platforms that allow users to create and disseminate geographic data online, is often credited to their ease-of-use, the straightforward approach of adding data, and the fact that use usually is free and theoretically accessible by everyone (Butler, 2006; Blower et al., 2007; Craglia et al., 2008). These platforms are designed to be used by lay-people and no specific technical knowledge is necessary to contribute data to them (Bell et al., 2007; Blower et al., 2007; Goodchild, 2007a). This has also increased the interest of the scientific community in using such platforms. Scientist are able to visualise and share their data and research results with colleagues worldwide, without any additional technical support or cost (Butler, 2006; Blower et al., 2007; Chen et al., 2009; Stensgaard et al., 2009). Another benefit of using such platforms is that they often facilitate the combined visualisation of data from different sources (Bell et al., 2007; Blower et al., 2007; Stensgaard et al., 2009). Furthermore, these platforms offer means to communicate research results to a wide audience of non-scientists, such as people in the government and the general public (Blower et al., 2007; Elvidge and Tuttle, 2008; Sheppard and Cizek, 2009; Stensgaard et al., 2009). The acceptance of this technology by scientist is indicated by the increased number of publications where the use of virtual globes and digital maps in a scientific context is discussed (Elvidge and Tuttle, 2008; Sheppard and Cizek, 2009; Stensgaard et al., 2009). The fields in which online data visualisation platforms have been utilised in scientific research ranges from health science and disease control (Stensgaard et al.,

2009) to real-time monitoring and mapping (Eugster and Nebiker, 2008). In Chen et al. (2009) general solutions for visualising results of earth science data analysis in Google Earth are discussed. Muggah and Mioc (2010) investigated the usability of Google Maps for visualising bathymetric data, aiming to enhance data viewing by users. Further examples can be found in Blower et al. (2007) and Boschetti et al. (2008).

Besides these benefits, there are also risks in using open access online platforms for visualising and sharing geographic data. One issue is the uncertainty about the validity and reliability of data provided by others. Even data that was produced by scientists and experts can contain unintended errors (Sheppard and Cizek, 2009). Goodchild (2007a) reports on errors in the georeferencing of Google Earth imagery in Santa Barbara, California. It is also reported that subsequently, Google has reduced these errors significantly, but all data derived or georeferenced using this imagery during that time would have inherited the original error. Data errors are not only a risk for data users but also for the data provider. Sheppard and Cizek (2009) note that errors occurring on publicly accessible visualisation platforms can damage the reputation of the data provider. Another common problem is the lack of information about data quality that prevents users from being able to judge the usability of the data for their purposes (Sheppard and Cizek, 2009). Eugster and Nebiker (2008) stated that the earth model underlying virtual globes is often not known. Therefore, the authors created their own virtual globe to be able to accurately integrate their geographic research data. These online platforms use altruistic principles for data sharing, which introduces a further risk. Everyone may add and create data, which allows the intentional introduction of errors to achieve personal or political goals (Goodchild, 2007a; Sheppard and Cizek, 2009). Several authors (Goodchild, 2007b; Craglia et al., 2008; Sheppard and Cizek, 2009) note that there is a need for mechanisms and standards that ensure data validity and reliability, which is crucial for building a higher level of trust in the data on online geographic data visualisation platforms.

2.9.2 Virtual globes

Virtual globes are probably the most popular online geographic data visualisation platforms. According to the definitions that can be found in the literature (Bell et al.,

2007; Blower et al., 2007; Boschetti et al., 2008; Craglia et al., 2008; Elvidge and Tuttle, 2008; Chen et al., 2009; Stensgaard et al., 2009) a virtual globe is a software application that displays a 3D representation of the real world. The display is usually based on satellite and airborne imagery as well as map data, on which additional information can be superimposed. Users can freely move around by panning and zooming. Virtual globes are also considered to be an easy-to-use, lightweight form of Geographic Information Systems (GIS) with basic analysis functionalities (Blower et al., 2007; Stensgaard et al., 2009). These provide the possibility to organise data geographically and are often used as browsers for geographic information (Bell et al., 2007; Cragila et al., 2008; Stensgaard et al., 2009).

Blower et al. (2007) report at least 30 virtual globes existed in 2007. Simultaneous display of multiple data sets and use of simple file formats are common features of all virtual globes, but other capabilities vary (Blower et al., 2007). Three examples of virtual globes are presented in the subsequent sections.

2.9.2.1 Google Earth

Google Earth was released in 2005 after Google had bought the "Earth Viewer" of Keyhole in 2004 (Cragila et al., 2008). It is the leader in the virtual globe market (Schöning et al., 2008; Stensgaard et al., 2009) and according to Schöning et al. (2008) was downloaded over 100 million times within the first 15 months of its release. Google Earth is closed source software that runs on different computer platforms and is focused on use by the general public (Blower et al., 2007; Schöning et al., 2008, Stensgaard et al., 2009). Beside the basic free version, two commercial versions are available, exhibiting enhanced capabilities: Google Earth Pro and Google Earth Enterprise (Google, 2011a). Through Google Earth, the user gains access to commercial satellite and airborne imagery (Beck, 2006; World Wind Central, 2010a).

All geographic data visualising and organising tasks in Google Earth are accomplished utilising Keyhole Markup Language (KML) (Chen et al., 2009). KML is a language for storing and distributing geographic data for visualisation in virtual globes that is based on Extensible Markup Language (XML) (Open Geospatial Consortium, 2008). Since 2008, KML is an international standard that is maintained by the Open Geospatial Consortium (OGC) (Google Inc., 2010). KML features that are implemented by Google Earth include near real-time visualisation

("NetworkLink"), display of photographs with specified viewing parameters ("PhotoOverlay"), and creation of KML archive file (KMZ). KMZ files contain the KML code file together with supporting data files, such as images, and appear to the user as one single file (Blower et al., 2007; Google, 2011b).

2.9.2.2 World Wind

World Wind was released in 2004 (Bell et al., 2007; World Wind Central, 2010b) and is the second biggest virtual globe (Schöning et al., 2008). According to Bell et al. (2007) it had been downloaded over 10 million times by 2007 with users requesting an average of 6.5 million images daily. The focus of World Wind is on scientific applications and it is possible to customise it for specialised groups or integrate it into other applications (Butler, 2006; Bell et al., 2007; Blower et al., 2007; Schöning et al., 2008). World Wind is open source software and computer operating system independent (Bell et al., 2007; Blower et al., 2007; Boschetti et al., 2008). It was developed by the National Aeronautics and Space Administration (NASA) and partners, but being open source software, many features are contributed by members of the open source community (Bell et al., 2007). Beside imagery and elevation data collected by NASA, users have also access to other image data sources in the public domain (Bell et al., 2007). The data provided with World Wind is not restricted to the Earth, but also comprises imagery and elevation models for Moon, Mars, Venus, and Jupiter as well as imagery of stars and galaxies (Bell et al., 2007; World Wind Central, 2010b). Web Mapping Service (WMS), a widely accepted standard maintained by OGC, is supported by World Wind as data input protocol (Bell et al., 2007). Basic support for KML, which is being continuously extended, is also available (Blower et al., 2007; World Wind Central, 2010a).

2.9.2.3 ArcGIS Explorer

ArcGIS Explorer was released by ESRI, the market leader in GIS, as a client for ArcGIS Server, but it can also be used as a standalone program (Blower et al., 2007; Schöning et al., 2008). The software is computer operating system dependent and runs on Windows systems only (Blower et al., 2007). Different to Google Earth or World Wind, ArcGIS Explorer can perform basic spatial analysis and supports a range of

different files and services for data input such as WMS, KML, shapefiles, and geodatabases (Butler, 2006; Blower et al., 2007; Schöning et al., 2008; ESRI, 2009)

2.9.3 Other online platforms

Besides virtual globes there are other online platforms that can be used for displaying basic geographic data. Some of these platforms are highlighted in this section.

One well known platform is Google Maps. It can be considered as the web-based equivalent to Google Earth, but is not a virtual globe, because it is restricted to a 2D view (Stensgaard et al., 2009). One benefit of Google Maps is that it is completely web-based and it is not necessary to install any additional software (Stensgaard et al., 2009). Furthermore, Google provides free code and references to embed Google base maps in other websites and superimpose the maps with geographic data (Muggah and Mioc, 2010). Similar services are provided by Yahoo! Maps. Users can embed maps in their own website and superimpose their own or third party geographic data (Yahoo!, 2011).

Another online platform is Wikimapia. It is basically an editable and interactive online map that aims to provide a free, complete, and multilingual map of the world (Wikimapia, 2010). Everyone with access to internet can select a location on the Earth and provide text and image data for this location. The location itself is defined by geodetic coordinates and the accuracy and significance of the entry is checked by volunteer reviewers (Goodchild, 2007a).

Geographic data can also be displayed on online platforms that are not focussed on providing maps. On Flickr, users can upload images that are georeferenced by geodetic coordinates (Goodchild, 2007a). A basic map is provided where images can be searched based on location and keywords (Flickr, 2011).

Microsoft Photosynth enables users to create panoramic views or image models from their own photo collections using image matching techniques (Microsoft, n.d. a). Image models consist of images capturing the same scene or object from differing vantage points. Users can navigate through the model by changing their vantage point. The panoramas and image models can be shared on the Photosynth website but can also be published on Microsoft Bing Maps (Microsoft, n.d. b). This allows searching and viewing the images in connection with their geographic location.

2.10 Summary

This literature review demonstrated that cultural heritage has an important role in society. One important benefit of preserving heritage is provision of a detailed and accurate spatial record of heritage objects that can either be used for planning in conservation projects or archived to secure them for the future. There are a number of methods for heritage recording, but close-range photogrammetry has proven to have clear advantages over other methods. It can be comparably cheap when consumer-grade cameras are utilised, because the recording equipment cost is reduced. Although these cameras are not specifically designed for utilisation for photogrammetric measurement, sufficient accuracy can be achieved when they are calibrated. Furthermore, very detailed geometric and textural data can be recorded in a short period of time. One significant drawback is that there is still the need to provide surveyed control points in order to record features in a 3D national reference frame. Using a survey staff or camera-to-object distance measurements instead of control points enables only scaled but not georeferenced measurements. One solution could be the direct determination of exterior orientation using a method similar to the integrated GPS/INS for airborne sensors. The expensive and bulky components of the GPS/INS can partly be substituted by low-cost and small-size sensors based on MEMS technology. There are a range of orientation sensors available, which may provide a suitable level of accuracy, whereas low-cost GPS receivers cannot currently provide the required positional accuracy. This explains why in approaches to implement such systems for direct exterior orientation determination, survey-grade GPS has been utilised instead of low-cost receivers. However, the recent announcement of a small-size GPS receiver (SXBlue III) that can provide centimetre positioning accuracy at lower cost than conventional survey-grade GPS receivers indicates that high accuracy in the low-cost segment might be available in the future. A basic combination of low-cost orientation and position sensors has revealed some difficulties, but further research is justified, particularly if multiple image configurations are considered.

The literature also demonstrated that there is an increased interest in making cultural heritage data widely accessible to experts and the general public in order to increase

research efficiency and learning. As heritage data usually has a geographic component, online geographic visualisation platforms, such as virtual globes, can be utilised to make heritage data accessible. The advantage of these platforms is that they are easy and free to use and theoretically accessible worldwide.

3 Methodology

This chapter describes resources and methods used to achieve the aim and objectives of this research (Section 1.1). Soft- and hardware utilised during recording system development and testing are described, followed by an explanation of algorithms and workflows developed for data processing and utilisation. Difficulties that occurred in the course of this research are discussed and solutions to these difficulties presented.

3.1 Bundle adjustment software

Bundle adjustment is a key method for data processing and analysis in this research project. It is used for camera calibration (Section 3.3.1.1), truth data creation for offset calibration (Section 3.5.1), and accuracy assessment (Section 3.6.3). In this research, two computer programs capable of performing bundle adjustment were utilised: Leica Photogrammetric Suite (LPS 9.3) (Section 3.1.1) and General Adjustment Program (GAP) (Section 3.1.2). Their differing characteristics complemented each other, allowing optimisation of data processing and analysis.

3.1.1 Leica Photogrammetric Suite (LPS) PRO 9.3

ERDAS IMAGINE LPS PRO 9.3 is a commercial software package for digital photogrammetry and remote sensing. Among other things, it facilitates manual target point measurement, automatic tie point generation, and a bundle adjustment algorithm for processing image data acquired by a variety of cameras (ERDAS, 2008). In this

research, LPS was utilised for image point measurement, because it offers an easy-to-use graphical point measuring tool. These measured points can be classified as one of three types. When corresponding object space coordinates are available, the image points can be defined as either control or check points. The image and object coordinates of control points are utilised in bundle adjustment calculations. In LPS, it is possible to assign individual precision values to each single point, in order to constrain them in the bundle adjustment. Check point coordinates are not used for image restitution, but can provide an independent measure of accuracy. Tie points are the third type of point that can be used in a bundle adjustment in LPS. They provide image coordinate without corresponding known object space coordinates. Tie points increase the number of measured values (image coordinates) in bundle adjustment calculations, thus increasing the precision of the result. They can be either measured manually or automatically using the tie point generation tool (Section 3.3.1.1). When tie points are measured automatically, outliers that degrade the precision can occur. These outliers need to be identified and removed after tie point generation.

When interior orientation parameters and lens model of a camera are available, they can be incorporated into an LPS project either manually or automatically using an LPS camera calibration file. For digital cameras the sensor pixel size in micrometre has to be added manually. When interior orientation parameters and lens model are not known, LPS facilitates camera self-calibration during bundle adjustment. Wackrow (2008) notes that camera self-calibration in a previous version of LPS (Version 8.3) was not sufficiently flexible to be used for calibrating consumer-grade cameras. It was unknown whether flexibility has improved in the version used in this project (LPS 9.3). Therefore, it was decided to use LPS during camera calibration only for image point measurements, tie point generation, and providing initial values for camera self-calibration in GAP (Section 3.1.2).

LPS allows saving detailed bundle adjustment results in text format to a report. This report contains input image coordinates, exterior and interior orientation parameters, residuals of control point coordinates, adjusted control point coordinates, and image coordinate residuals of control and tie points.

3.1.2 General Adjustment Program (GAP)

The general adjustment program (GAP) was developed by Clark (Chandler and Clark, 1992). It is a least-squares estimation program that can be used for simultaneous network adjustment in survey or photogrammetry-related projects (Engineering Surveying Research Centre, 1994). GAP runs from a console window and has no graphical image point measurement tool, different to LPS. Image coordinates have to be provided by other sources. In this research, image coordinates were measured in LPS. In order to use these measurements in GAP, an initial bundle adjustment was performed in LPS and the results saved in an LPS report. These results included exterior and interior orientation parameters as well as image and object point coordinates. This information was used as input data for GAP. Figure 3.1 depicts a schematic representation of the required input files for GAP and the resulting output files. The file containing the "interior orientation" also includes estimated parameters for radial and tangential lens distortion. All parameters can be selectively set to fix, unknown, or constrained by a known standard deviation, enabling camera self-calibration during bundle adjustment. The flexibility of GAP in interior orientation parameter selection is an advantage for consumer-grade camera calibration (Wackrow, 2008). GAP has been successfully used in this area (Chandler et al., 2005;

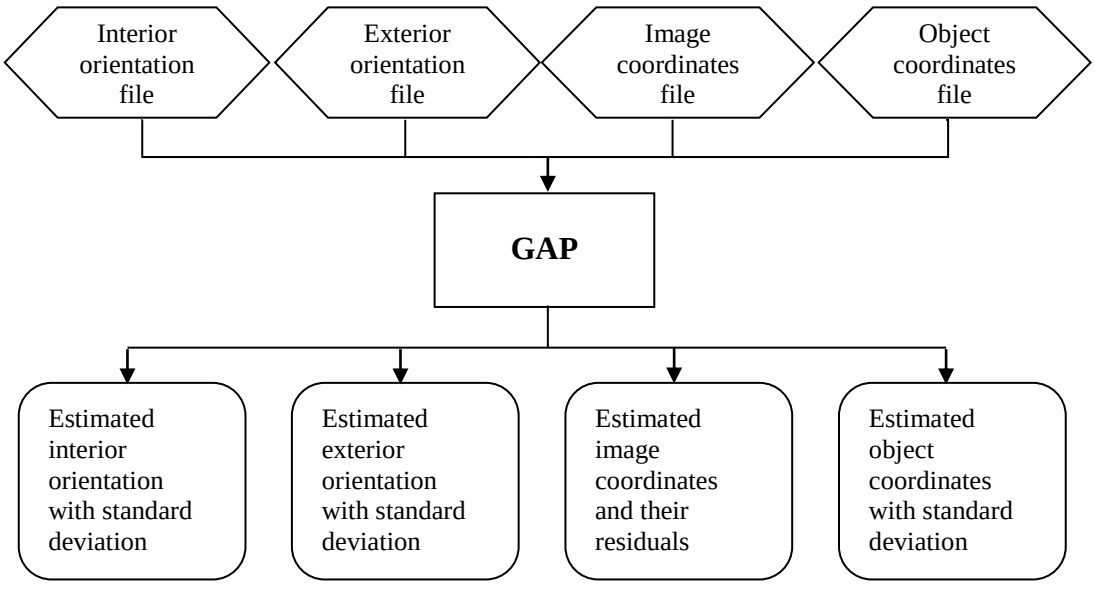

Figure 3.1: Schematic representation of GAP input and output files.

Wackrow, 2008) and it was decided to also use this software for camera calibration in this research project (Section 3.3.1.1).

All parameters and coordinates contained in the GAP input files are selective in the same way as the interior orientation parameters (fix, unknown, or constrained by known standard deviation). This enables constraining the parameters of each image in the GAP exterior orientation input file individually. The object coordinate input file contains object coordinates of target points. Points that are fixed or constrained by a known standard deviation serve as control points. The coordinates of the unknown points will be re-estimated during bundle adjustment. Therefore, these points can be used as check points or just serve as tie points. The possibility to individually constrain parameters provides high flexibility in data processing. Furthermore, the GAP input and output files are in an American Standard Code for Information Interchange (ASCII) text file format, which facilitates easy access and quick changes to the file content. This demonstrates the high flexibility and easy access to data provided in GAP and it was decided to use this program during recording system accuracy assessment (Section 3.6.3).

The calculations in GAP are based on the "least-squares" method and can also be used for simultaneously adjusting data from topographic surveys, either with or without photo observations (Section 3.2.1). In the latter case GAP requires an object coordinates input file, containing initial coordinates of the surveyed points, and a survey observation input file. The GAP adjustment results in one file with estimated coordinates of survey points and one with residuals of survey observations.

3.2 Test sites

3.2.1 Test field

For developing and initially testing the recording system, as well as for camera calibration, easily accessible test sites were required. The first test site was established in February 2009 on an outside wall of the Civil Engineering laboratory at Loughborough University (Figure 3.2) and will be referred to as "test field". The wall

Figure 3.2: Test field at Loughborough University campus.

was chosen for its ease of access and the open space in front of the wall, from where data (imagery, orientations, and positions) could be collected. The test field was considered representative for heritage object types that are vertically structured and have a comparatively large footprint. 43 surveying targets were attached to the test field to mark the location of coordinated points. The flatness of the test field was considered a disadvantage, as all coordinated points would be located in the same plane. Therefore, some of the targets were also attached to objects protruding from the wall (for example lamps and ventilation boxes) in order to achieve a greater variation in depth. It was decided to use silicone sealant for attaching the targets, as this enabled a firm attachment while detaching without leaving residue on the wall was still possible. The targets were arranged in 5 rows of 8 to 9 targets with an approximate separation of 1.5 m. This resulted in a test field with dimensions of approximately 11 m by 6 m. Two survey stations were established adjacent to the test field using Leica System 500 DGPS (Figure 3.3). Each survey station was occupied by the DGPS receiver for 30 minutes and GPS data was sampled every 2 seconds. The DGPS base station was located on a coordinated point on Loughborough University campus, which had previously been linked to an Ordnance Survey passive point known as "Charnwood" (Ordnance Survey, 2011a). The DGPS measurements were post-processed in Leica SKI-Pro software. The resulting Cartesian coordinates of the survey stations were transformed into Ordnance Survey Great Britain 1936 (OSGB36)

Figure 3.3: Survey stations adjacent to test field.

grid coordinates using the Grid InQuest coordinate transformation software provided by Ordnance Survey (2011b). OSGB36 coordinates of the targets were derived using a Leica TCR405 Total Station and observations (vertical and horizontal angles and distances to each target point) acquired from both survey stations. Mean sea level and grid scale factor corrections were applied to the horizontal distances to each target. From the measured angles, the corrected distances, assumed measurement precisions, and the survey station coordinates, the best estimates for the coordinates of the target points were derived in a least squares adjustment using GAP. The standard deviation extracted from the estimated coordinates of the survey points output file indicates the local precision of these coordinates (2 mm in plan and 1 mm in height).

This test field was used for camera calibration (Section 3.3.1.1) and for recording system tests (Section 3.6).

3.2.2 Test object

The test field presented in the previous section is representative for vertical structures with a large footprint. However, it was considered not representative for the type of

heritage object found at the location of the first case study. The first case study was conducted at St. Catherine's Oratory on the Isle of Wight, UK (Section 5.1). The heritage object at this location is a vertical structure with a small diameter on the ground and is accessible from all sides. In order to validate the operability of the recording system and the data collection workflow prior to application in the field, conditions at the case study site were simulated in a preparatory test. For this purpose a second test site was established in May 2010. A metal piece of art (Figure 3.4) located at Loughborough University campus was considered similar to St. Catherine's Oratory and was chosen as test site. This test site will be referred to as "test object".

The lower part could be reached without auxiliary means (approximately up to 2 m) and so 9 survey targets were attached to the test object using silicone sealant. For the upper part, natural points defined by distinctive features, such as corners and intersections, were selected. In total 9 targeted and 8 natural points were established on the southern side of the test object. Compared to the test field, the points could be distributed with a greater variation in depth. Two survey stations were established on the southern side of the test object (Figure 3.5) using DGPS, with the base station

Figure 3.4: Test object at Loughborough University campus.

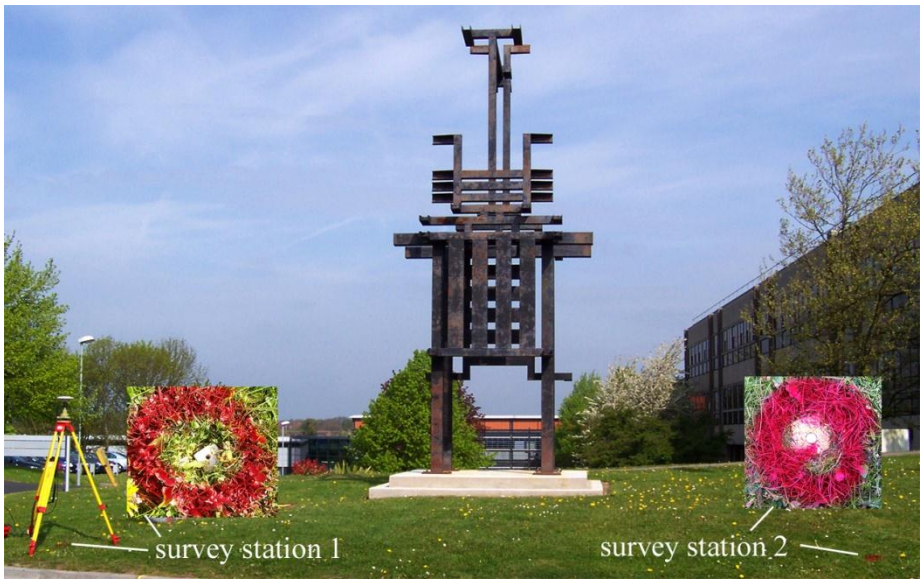

Figure 3.5: Test object survey stations 1 and 2.

located at a previously coordinated point on Loughborough University campus. Each survey station was occupied by a DGPS receiver for 30 minutes with a data collection rate of 2 seconds. The DGPS data was post-processed in Leica SKI-Pro and the resulting Cartesian coordinates transformed to OSGB36 coordinates using Grid InQuest. The coordinates of the targeted and natural points were determined using a Leica TCR405 Total Station and observations acquired from one survey station only. This was considered sufficient, because the test object was used in the preliminary test for the case study only and was not used for camera calibration. Mean sea level and grid scale factor corrections were applied to the horizontal distances and the OSGB36 coordinates of each point determined. The precision of the target point coordinates was assumed to be similar to that achieved for the "test field" (Section 3.2.1). The precision of the natural point coordinates was estimated using LPS bundle adjustments. Based on the results it was decided to assume a precision of 5 mm.

3.3 Recording system

The recording system developed during this research project (Figure 3.6) comprises a consumer-grade digital camera for image acquisition, a 3D orientation sensor for

Figure 3.6: Components of recording system.

orientation determination, a differential GPS (DGPS) receiver for positioning, and a laptop for data recording. The system also facilitates positioning using a Total Station as an alternative to DGPS.

3.3.1 Components

3.3.1.1 Consumer-grade digital camera

The camera used for image acquisition is a Nikon D80 consumer-grade, digital camera. An overview of the characteristics of the Nikon D80 camera is provided in Table 3.1. A Nikkor autofocus 1:2.8D lens with a fixed focal length of 24 mm was attached. Imagery captured was stored in the Joint Photographic Experts Group (JPEG) image file format using the "high quality" setting. Information concerning each image, such as date and time of file creation, was automatically stored in the Exchangeable Image File Format (Exif) header of the JPEG image file.

The interior orientation of the camera and the lens distortion was estimated in a camera calibration process. In order to maintain stability, the focus setting was fixed to infinity by wrapping electrical tape around the lens and the auto focus feature was

Table 3.1: Characteristics of Nikon D80.

Feature	*Nikon D80*
Camera type	Single lens reflex (SLR)
Image size (pixel)	3872 x 2592
Effective pixels	10.2 million
Sensor size (mm)	23.6 x 15.8
Pixel dimension (μm)	6.095 x 6.095
Auto focus	Yes
Manual focus	Yes
Camera dimension (mm)	132 x 103 x 77
Weight (g)	668
Cost in 2006 (£)	900

switched off. In March 2009, 13 images of the test field were taken from different positions at an approximate camera-to-object distance of 7 m. Of these images, 3 were acquired with a 90° rotation, in order to more accurately derive principal point offsets. In LPS image coordinates of the target points were measured manually and tie points were generated automatically. The sensor pixel size of the camera was obtained from an online source (Askey, 2006). An initial LPS bundle adjustment was conducted in order to provide data for camera self-calibration in a GAP bundle adjustment. The adjusted interior orientation and lens distortion parameters resulting from the GAP bundle adjustment were tested for their significance by comparing them to their standard deviation. When the standard deviation was smaller than its corresponding parameter, the parameter was considered significant for camera calibration. Insignificant parameters were excluded from the calibration process and the remaining parameters re-estimated in another bundle adjustment. This resulted in estimates for focal length, principal point offset, and two radial lens distortion parameters. In order to have the parameters available for further use, they were re-imported into LPS and saved to an LPS camera file. Focal length and principal point offset could be manually copied into LPS. The radial lens distortion could only be imported into LPS by first

calculating distortions for a range of radial distances in a Microsoft Excel spread sheet, which were then copied into LPS.

3.3.1.2 Orientation sensor

The orientation sensor used in this research project is the TCM5 (Figure 3.7) manufactured by PNI and costing £ 1,600 in 2009. The TCM5 is an MEMS-based 3D orientation sensor, utilising a 3-axis magnetometer and a 3-axis accelerometer that measures heading (*h*), pitch (*p*), and roll (*r*). The accuracy specified by the manufacturer is 0.3° to 0.5° for heading, 0.2° for pitch, and 0.2° to 1.0° for roll, depending on the pitch angle (Table 3.2) (PNI, 2009).

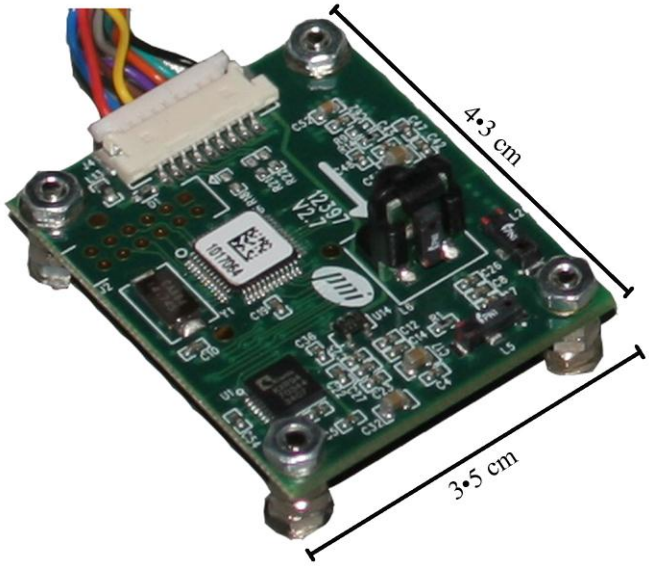

Figure 3.7: TCM5 3D orientation sensor.

Table 3.2: Accuracy of TCM5 measurements specified in PNI (2009).

Angle	*Condition*	*Root Mean Square (°)*
Heading	Tilt < 70°	0.3
	Tilt > 70°	0.5
Pitch	-	0.2
Roll	Pitch < 65°	0.2
	Pitch < 80°	0.5
	Pitch < 86°	1.0

The orientation sensor uses the magnetic field of the Earth to determine heading. Components built in the recording system or objects close to the recording system can distort this field locally and cause erroneous heading measurements. To achieve measurements with the specified accuracy it is necessary to identify these distortions during an initialisation process. In this process, the recording system is sequentially rotated and tilted in different orientations while the orientation sensor measures the magnetic field. An algorithm built into the orientation sensor software uses these measurements to estimate the distortions and to adjust subsequent measurements accordingly. Only distortions that are consistent with respect to the orientation sensor can be compensated. When an object causing distortions in the local magnetic field and the orientation sensor are moved with respect to each other, heading measurements can no longer be correctly adjusted (PNI, 2009).

The settings of the orientation sensor allow heading to be measured either with respect to the magnetic North Pole ("magnetic north") or to the geographic North Pole ("true north"). In the latter case a magnetic declination value has to be supplied.

For protection, the orientation sensor was housed in a 10 by 10 by 6 cm dust and waterproof plastic box. A cable for data transmission and power supply connects this box to an identical box that houses 3 alkaline 1.5 Volt batteries as power supply and that can be connected to the laptop (Section 3.3.1.3) via conventional RS232 cable and an RS232-to-USB converter.

3.3.1.3 Laptop

The orientation sensor was operated using software provided by PNI (TCMStudio35), running on an off-the-shelf laptop (Toshiba Satellite Pro). The orientation sensor has no internal measurement storage capability and the laptop was also used to store the orientation sensor measurements. The TCMStudio35 software records time coded measurements transmitted from the orientation sensor and information regarding the operation of the sensor. These records can be saved in text format to a data log file and a system log file, respectively. The data log file consists of a time coded list of continuous orientation measurements. The orientation sensor software achieves time coding by assigning the "tick" count at the time of measurement to each set of orientation measurements (heading, pitch, and roll measurement at one point in time). A "tick" is the measurement unit the orientation sensor uses for time reference. The

length of a "tick" is equivalent to 1/60 second (PNI, 2009). In the system log file key information about orientation sensor operation is stored, including the laptop system date and time of data logging start and stop. This information was used to assign date and time to the "tick" counts in the data log file.

To be able to later retrieve orientation measurements corresponding to each image from the data log file, the internal clock of the camera clock has to be synchronised with the laptop clock, ideally before data collection. This was achieved using synchronisation functionality of Nikon PictureProject software, provided with the Nikon D80 camera.

3.3.1.4 Differential GPS

When the recording system was assembled in January 2010, no low-cost, small-size DGPS receivers were available on the market to provide centimetre accuracy required in this project. Therefore, it was decided to use a survey-grade Leica System 500 dual-frequency DGPS receiver, capable of carrier phase measurements and enabling positioning with centimetre accuracy. Although this is certainly not a low-cost component (approximately £ 8,000 in 2006), it facilitates the testing of the principles of direct exterior orientation determination for close-range photogrammetry. These principles will also be applicable when small-size, low-cost GPS receivers for high accuracy positioning emerge on the market. The potential for this kind of GPS receivers was subsequently demonstrated by the announcement of the SXBlue III (GENEQ, 2010a), costing £ 3,150 in 2010 (Stevens, 2010).

3.3.1.5 Total Station

Positioning of the recording system using a Total Station is possible, when the DGPS antenna is replaced by a prism. This option facilitates the utilisation of the recording system when GPS is not available, for example inside buildings or under the canopy in forested areas. However, Total Stations are high-end devices and non-experts might find it difficult to use them (Bryan and Chandler, 2008) and so positioning in this research project was focused on utilising GPS, which perhaps is easier to operate for non-specialists (Section 6.3.2). In order to demonstrate the usability of Total Station for recording system positioning, one test was conducted using a Leica TCR405 Total Station (Section 3.6).

3.3.2 Assembled recording system

The recording system was assembled in January 2010. A rigid mounting frame (Figure 3.8) was designed to enable securing the camera, orientation sensor, and DGPS antenna or prism in a fixed position relative to each other. The fixtures of these components to the mounting frame were expected to prevent rotation or shift between components and their stability was considered crucial for stable offset calibration (Section 3.5). The DGPS receiver was connected to the DGPS antenna via coaxial cable and the laptop was connected to the orientation sensor via RS232 cable connected to a RS232-to-USB converter.

3.3.2.1 Mounting frame

The mounting frame was designed as a box with an open front and back side, one partition, and a spigot on top (Figure 3.8) and was purposely built by technicians working in the Wolfson School of Mechanical and Manufacturing Engineering. The main part of the frame was made from aluminium in order to provide sufficient

Figure 3.8: Recording system mounting frame with camera, orientation sensor, and DGPS antenna.

stability of the frame, whilst keeping weight low. In addition, aluminium is non-magnetic and was therefore considered to have no influence on the magnetometer readings of the orientation sensor. The spigot was incorporated into the mounting frame to facilitate attaching and detaching the DGPS antenna or prism without positional offset changes. It was made of steel, in order to increase its durability against the stresses of frequently re-attaching DGPS antenna or prism. The box housing the orientation sensor was attached to the partition of the mounting frame by 4 nuts and bolts located in the corners of the box. The camera was attached to the bottom of the mounting frame (Section 3.3.2.2). At the bottom is also a 1/4" British Standard Whitworth (BSW) socket that allows the mounting frame to be attached to a conventional camera tripod.

3.3.2.2 Camera fixture

In this research two different approaches to attach the camera to the mounting frame were used. Initially, the camera was fitted into a purposely build wooden enclosure (Figure 3.9). The wooden enclosure consisted of a rectangular bottom plate with two perpendicular plates on the small sides. The distance between the inner surfaces of the perpendicular plates was equivalent to the width of the camera. The camera was placed between the two perpendicular plates, which were designed to prevent the camera from rotating by restricting movement of its small sides. A 1/4" BSW bolt through a hole in the bottom plate into the tripod socket of the camera fixed the camera in position. For additional stability another plate that partly covered the back

a: front b: back

Figure 3.9: Initial approach of camera fixture: wooden enclosure.

of the camera (Figure 3.9b) was added to the enclosure. The enclosure could be slid into the lower part of the mounting frame and was fixed by a metal bar in the front and two conventional bolts and nuts in the back. For accessing the camera battery, memory card, and for synchronising the camera clock with the laptop clock, it was necessary to completely detach the camera from the mounting frame and the wooden enclosure.

Initial results of data analysis suggested that this approach of attaching the camera to the mounting frame was not sufficiently stable. It was therefore decided to use a more rigid approach for fixing the camera to the mounting frame (Figure 3.10). This required some modifications to the mounting frame (for example one additional hole and a frame extension), because it had been originally designed to best suit the initial approach to attach the camera. In the second approach the camera was fixed to the mounting frame at two points. The first fixing point is a 1/4" BSW bolt through an additional hole in the bottom plate of the mounting frame into the tripod socket of the camera. This fixed the position of the camera in the mounting frame. The modified fixture involved a modified hose clip tightly clamped around the lens and fixed to the mounting frame. The modification to the hose clip consisted of a conventional bolt through the hose clip that pointed downwards when the clip was clamped around the lens. This bolt fixed the hose clip to an extension of the mounting frame, consisting of three aluminium bars. Two bars were fixed horizontally to the mounting frame bottom plate on either side of the camera, protruding from the mounting frame by

Figure 3.10: Modified approach of camera fixture: hose clip.

approximately 20 mm. The hose clip was bolted onto the third bar, which was fixed across the protruding ends of the other bars. This fixed the lens in position and was expected to fully disable rotation of the whole camera.

In later tests it was revealed that the seeming instability of the initial camera fixture was caused mainly by an error in the transformation algorithm (Section 3.4), which was subsequently corrected. However, the modified camera fixture also enhanced the handling of the camera by making the memory card easily accessible and allowing camera and laptop clock synchronisation without detaching the camera from the mounting frame.

3.4 Transformation algorithm

In this project the TCM5 orientation sensor was used to determine three of the six exterior orientation parameters directly. The desired parameters for utilisation in photogrammetric software were the photogrammetric rotation angles omega (ω), phi (φ), and kappa (κ) used to describe a 3D rotation by three consecutive rotations (Section 2.3.2.1) about rotated axes. In contrast, the angles heading (h), pitch (p), and roll (r) actually measured by the orientation sensor, describe rotations about fixed axes. In the orientation sensor coordinate system h is the rotation angle about the z-axis and is always measured with respect to north. The angles p and r are the rotation angles about the non-rotated y-axis and the x-axis, respectively. Both are measured with respect to the local horizontal plane, which is defined by local gravity (PNI, 2009). The alignment of the orientation sensor axes in the recording system mounting frame with respect to the camera coordinate system is depicted in Figure 3.11. Due to this alignment, changes in h have a strong correlation with changes in the rotation angle value of φ in the camera coordinate system. Changes in p and r are strongly related to changes in ω and κ, respectively.

Despite these correlations between the rotation angles, the two different methods of describing these angles required algorithms transforming ω, φ, and κ to their equivalent h, p, and r values, and vice versa. Although an exhaustive literature research was conducted, no easily implementable algorithm could be found.

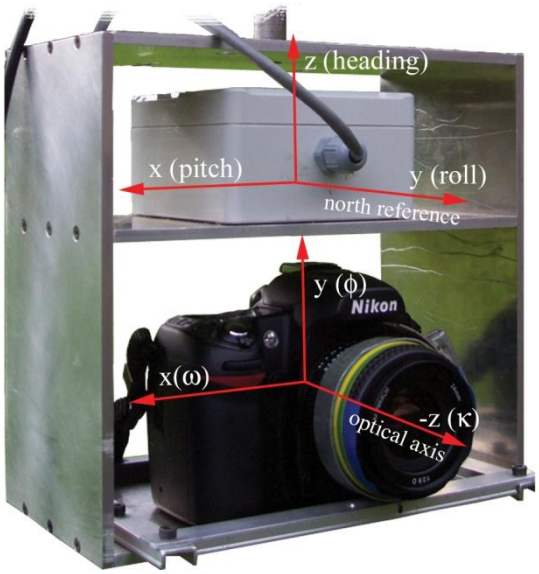

Figure 3.11: Approximate alignment of orientation sensor and camera coordinate system in the mounting frame.

Therefore, two angle transformation algorithms were developed in this research project. These are explained in detail in the subsequent sections. Both algorithms were developed in MatLab and applied during rotational offset calibration and direct exterior orientation determination (Section 3.5.2).

3.4.1 Omega, phi, kappa to heading, pitch, roll

A geometric approach was chosen to convert omega (ω_P), phi (φ_P), and kappa (κ_P) into their equivalent heading (h_P), pitch (p_P), and roll (r_P) values. The subscript "$_P$" denotes values that were derived photogrammetrically in a bundle adjustment. In this approach the inverse of a rotation matrix $\mathbf{R}_{\kappa\varphi\omega}$ derived from ω_P, φ_P, and κ_P (Section 2.3.2.1) was used to rotate two vectors representing the non-rotated positive and negative camera axis, $\mathbf{a1} = [0\ \ 0\ \ 1]^T$ and $\mathbf{a2} = [0\ \ 0\ \ -1]^T$, and one vector, $\mathbf{a3} = [1\ \ 0\ \ 0]^T$, representing an axis perpendicular to the camera axis. This resulted in the rotated vectors

$$\mathbf{b1} = \begin{bmatrix} x1 \\ y1 \\ z1 \end{bmatrix} = \mathbf{R}_{\kappa\varphi\omega}{}^{-1}\mathbf{a1} \tag{3.1}$$

$$\mathbf{b2} = \begin{bmatrix} x2 \\ y2 \\ z2 \end{bmatrix} = \mathbf{R}_{\kappa\varphi\omega}{}^{-1}\mathbf{a2} \tag{3.2}$$

$$\mathbf{b3} = \begin{bmatrix} x3 \\ y3 \\ z3 \end{bmatrix} = \mathbf{R}_{\kappa\varphi\omega}{}^{-1}\mathbf{a3} \tag{3.3}$$

The vectors $\mathbf{b1}$ and $\mathbf{b2}$ represent the rotated positive and negative camera axis. From the horizontal components of $\mathbf{b1}$ and $\mathbf{b2}$, the angle h_P can be derived as follows:

$$h_P = \arctan2\left(\frac{x2 - x1}{y2 - y1}\right) \tag{3.4}$$

Note: arctan2 is the four-quadrant inverse tangent.
In cases where the value of h_P is negative, 360° were added to the result. This ensures comparability between measured and photogrammetrically derived heading, because the orientation sensor measures heading in the range of 0° to 360°. The angle p_P can be derived from the height difference of $\mathbf{b1}$ and $\mathbf{b2}$ and the combined length of both vectors projected in the 2D plane (Equation 3.5).

$$p_P = \arctan2\left(\frac{z2 - z1}{\sqrt{(x2 - x1)^2 + (y2 - y1)^2}}\right) \tag{3.5}$$

The vector $\mathbf{b3}$ represents the perpendicular to the rotated camera axis. The angle established by the z-value of $\mathbf{b3}$ and the length of $\mathbf{b3}$ projected in the 2D plane represents r_P (Equation 3.6).

$$r_P = \arctan2\left(\frac{0 - z3}{\sqrt{x3^2 + y3^2}}\right) \tag{3.6}$$

3.4.2 Heading, pitch, roll to omega, phi, kappa

To transform directly measured h_D, p_D, and r_D into their equivalent photogrammetric angles ω_D, φ_D, κ_D a method utilising direction cosines was devised. The subscript "$_D$" denotes values that were derived directly by orientation sensor measurements. In this

approach the direction cosines of the rotated orientation sensor coordinate axes *X*, *Y*, and Z (target system) relative to the non-rotated orientation sensor coordinate axes *x*, *y*, and *z* (source system) were derived.

The vector $\mathbf{j} = [\cos(Yx)\ \ \cos(Yy)\ \ \cos(Yz)]^{\mathrm{T}}$ is the direction cosine vector of the *Y*-axis in the rotated coordinate system. The rotation matrix $\mathbf{R}_p$ (Equation 3.7) describes a rotation about the non-rotated *x*-axis $\mathbf{x}_0 = [1\ \ 0\ \ 0]^{\mathrm{T}}$ by the angle p_D. To derive **j**, $\mathbf{R}_p$ is used to rotate the non-rotated *y*-axis $\mathbf{y}_0 = [0\ \ 1\ \ 0]^{\mathrm{T}}$ (Equation 3.8).

$$\mathbf{R}_p = \begin{bmatrix} 1 & 0 & 0 \\ 0 & \cos(p_D) & -\sin(p_D) \\ 0 & \sin(p_D) & \cos(p_D) \end{bmatrix} \tag{3.7}$$

$$\mathbf{y}_p = \mathbf{R}_p * \mathbf{y}_0 \tag{3.8}$$

The resulting vector $\mathbf{y}_p$ is subsequently rotated about the non-rotated *z*-axis $\mathbf{z}_0 = [0\ \ 0\ \ 1]^{\mathrm{T}}$ by the angle h_D (Equation 3.10) using the rotation matrix $\mathbf{R}_h$ (Equation 3.9). The result of this rotation is the direction cosine vector **j**.

$$\mathbf{R}_h = \begin{bmatrix} \cos(h_D) & -\sin(h_D) & 0 \\ \sin(h_D) & \cos(h_D) & 0 \\ 0 & 0 & 1 \end{bmatrix} \tag{3.9}$$

$$\mathbf{j} = \begin{bmatrix} \cos(Yx) \\ \cos(Yy) \\ \cos(Yz) \end{bmatrix} = \mathbf{R}_h * \mathbf{y}_p \tag{3.10}$$

The vector $\mathbf{i} = [\cos(Xx)\ \ \cos(Xy)\ \ \cos(Xz)]^{\mathrm{T}}$ contains the direction cosines of the *X*-axis in the rotated (target) coordinate system and must meet two conditions. The first condition is met when the angle between **i** and the $\mathbf{x}_0$-$\mathbf{y}_0$-plane equals r_D. This is achieved by using the rotation matrix $\mathbf{R}_r$ (Equation 3.11) to rotate $\mathbf{x}_0$ about $\mathbf{y}_0$ by the angle r_D (Equation 3.12).

$$\mathbf{R}_r = \begin{bmatrix} \cos(r_D) & 0 & \sin(r_D) \\ 0 & 1 & 0 \\ -\sin(r_D) & 0 & \cos(r_D) \end{bmatrix} \tag{3.11}$$

$$\mathbf{x}_r = \begin{bmatrix} x_{r1} \\ x_{r2} \\ x_{r3} \end{bmatrix} = \mathbf{R}_r * \mathbf{x}_0 \tag{3.12}$$

The second condition is met when **i** is perpendicular to **j**. To achieve this, the vector $\mathbf{x}_r$ is rotated about $\mathbf{z}_0$ by h_D and an additional angle *h2*. Figure 3.12 explains why *h2* is required in order to meet the second condition. For simplification it is assumed that h_D equals 0. In this case **i** is perpendicular to **j**, when **i** lies in a plane formed by the $\mathbf{x}_0$-axis and the vector $\mathbf{z}_p$. The vector $\mathbf{z}_p$ is derived by rotating $\mathbf{z}_0$ about $\mathbf{x}_0$ by the angle p_D. The angle *h2* rotates the vector $\mathbf{x}_r$ into the $\mathbf{x}_0$-$\mathbf{z}_p$ plane. The resulting direction cosine vector **i** maintains the angle r_D to the $\mathbf{x}_0$-$\mathbf{y}_0$ plane (first condition), because this is a rotation about $\mathbf{z}_0$. The calculation of *h2* is also valid for any value of h_D that does not equal 0, because both **i** and **j** will be rotated about $\mathbf{z}_0$ by the same magnitude, which maintains both conditions. The magnitude of *h2* depends on the angles r_D and p_D (Equation 3.13).

$$h2 = \arcsin\left(\frac{x_{r3}}{\tan(90 - p_D) * \cos(r_D)}\right)(-1) \tag{3.13}$$

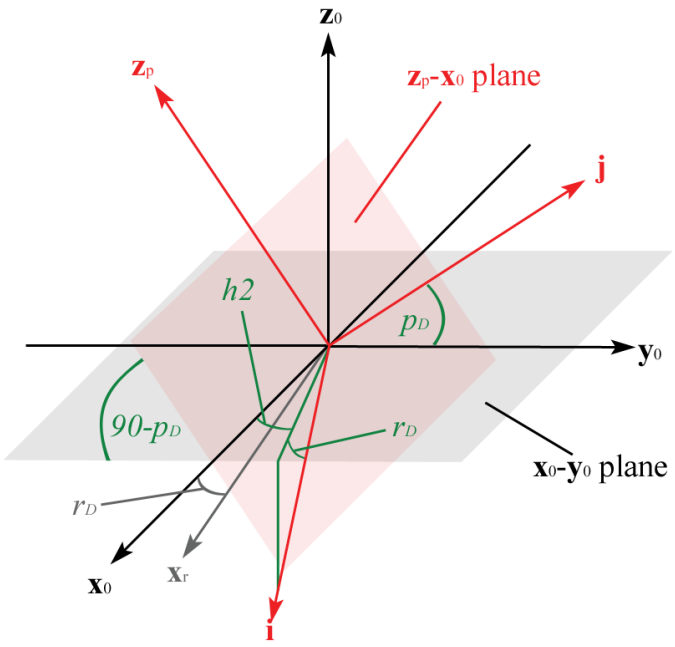

Figure 3.12: Graphical description of the derivation of *h2* (assumption $h_D = 0$).

Equation 3.13 can be solved under the condition $-1 \leq \frac{x_{r3}}{\tan(90-p_D)*\cos(r_D)} \geq 1$. This condition is met when $|p_D| + |r_D| \leq 90$, where $|p_D|$ and $|r_D|$ are the absolute values of angles p_D and r_D. This condition is met when extreme pitch and roll do not occur at the same time, which is considered to be the case in most practical recording situations.

The rotation matrix $\mathbf{R}_{h2}$ (3.14) combines the two rotation angles h_D and $h2$ and is used to derive **i** by rotating $\mathbf{x}_r$ about $\mathbf{z}_0$ (Equation 3.15).

$$\mathbf{R}_{h2} = \begin{bmatrix} \cos(h_D + h2) & -\sin(h_D + h2) & 0 \\ \sin(h_D + h2) & \cos(h_D + h2) & 0 \\ 0 & 0 & 1 \end{bmatrix} \tag{3.14}$$

$$\mathbf{i} = \begin{bmatrix} \cos(Xx) \\ \cos(Xy) \\ \cos(Xz) \end{bmatrix} = \mathbf{R}_{h2} * \mathbf{x}_r \tag{3.15}$$

The direction cosine vector representing the *z*-axis in the rotated coordinate system is $\mathbf{k} = [\cos(Zx)\ \cos(Zy)\ \cos(Zz)]^{\mathrm{T}}$. The axes of the orientation sensor coordinate system are perpendicular to each other. Therefore, **k** can be derived as the cross-product of the vectors **i** and **j** (Equation 3.16).

$$\mathbf{k} = \begin{bmatrix} \cos(Zx) \\ \cos(Zy) \\ \cos(Zz) \end{bmatrix} = \mathbf{i} \times \mathbf{j} \tag{3.16}$$

From the direction cosine vectors **i**, **j**, and **k** the rotation matrix $\mathbf{R}_D$, describing the rotation from the (*x y z*) source system to the (*X Y Z*) target system, is derived by

$$\mathbf{R}_D = [\mathbf{i}\ \mathbf{j}\ \mathbf{k}] \tag{3.17}$$

Figure 3.11 demonstrates that the camera is oriented in the close-range case of photogrammetry. The camera coordinate system is permanently rotated with respect to the normal case of photogrammetry where the optical axis is oriented along the vertical and points down. In order to extract rotation angles relating to the normal case of photogrammetry, this permanent rotational offset was included by multiplying the rotation matrix $\mathbf{R}_{CN}$ (Equation 3.18) with $\mathbf{R}_D$ (Equation 3.19).

$$\mathbf{R}_{CN} = \begin{bmatrix} 1 & 0 & 0 \\ 0 & 0 & -1 \\ 0 & 1 & 0 \end{bmatrix} \tag{3.18}$$

$$\mathbf{R}_N = \mathbf{R}_D * \mathbf{R}_{CN} = \begin{bmatrix} a_{11} & a_{12} & a_{13} \\ a_{21} & a_{22} & a_{23} \\ a_{31} & a_{32} & a_{33} \end{bmatrix} \tag{3.19}$$

From the rotation matrix $\mathbf{R}_N$ in Equation 3.19 the angles ω_D, φ_D, κ_D were derived as follows:

$$\omega_D = \arctan2\left(\frac{-a_{23}}{a_{33}}\right) \tag{3.20}$$

$$\varphi_D = \arcsin(a_{13}) \tag{3.21}$$

$$\kappa_D = \arctan2\left(\frac{-a_{12}}{a_{11}}\right) \tag{3.22}$$

3.5 Offset calibration

When assembling the recording system, rotational and positional offsets between the recording system components are introduced. Ideally these offsets are fixed. To be able to directly derive exterior orientation of the camera, the rotational offsets between camera and orientation sensor and the positional offsets between camera and DGPS antenna or prism have to be determined or calibrated. This was achieved by comparing the directly measured DGPS or Total Station coordinates (X_D, Y_D, Z_D) and orientation angles (h_D, p_D, r_D) with the true exterior orientation parameters (Section 3.5.1). This resulted in estimates of three rotational and three positional offset calibration values (Δh, Δp, Δr, Δx, Δy, Δz) and also provided indicators of the calibration precision. The calculations were conducted using a MatLab routine coded for this purpose (Appendix A).

3.5.1 Truth data

LPS Version 9.3 was utilised to derive the exterior orientation parameters (ω_P, φ_P, κ_P, X_P, Y_P, Z_P) of acquired images indirectly in a bundle adjustment. These parameters were considered to be the true exterior orientation. They were used to validate the exterior orientation parameters derived from the orientation sensor and DGPS or Total Station measurements.

In LPS the interior orientation and lens distortion of the camera was provided by the camera file resulting from the camera calibration process (Section 3.3.1.1). To reduce time spent on truth data generation, it was decided to use only 22 of the 43 available coordinated target points of the test field for image coordinate measurement. This number of points was considered sufficient, because it resulted in typically 10 to 20 control points measured in each image. In the case of the test that was conducted using the test object, all available artificial and natural control points were measured. In the bundle adjustment process the interior orientation of the camera was considered fixed for all images and the control points were constrained by standard deviations which were assumed equivalent to their accuracy (Section 3.2). The resulting exterior orientation parameters of each image were saved in a text file in the same sequence of image acquisition.

3.5.2 Rotational offset calibration

For estimating the rotational offsets, the photogrammetric exterior orientation angles of n camera stations i (ω_{Pi}, φ_{Pi}, κ_{Pi}) were transformed into their equivalent heading (h_{Pi}), pitch (p_{Pi}), and roll (r_{Pi}) using the algorithm described in Section 3.4.1. A camera station is defined as the position and orientation of the camera at the time of image acquisition.

The calibration values Δp and Δr were derived by calculating the arithmetic mean of the differences between the true (p_{Pi} and r_{Pi}) and the directly measured (p_{Di} and r_{Di}) pitch and roll angles (Equation 3.23 and Equation 3.24).

$$\Delta p = \frac{1}{n}\sum_{i=1}^{n}(p_{Pi} - p_{Di}) \tag{3.23}$$

$$\Delta r = \frac{1}{n}\sum_{i=1}^{n}(r_{Pi} - r_{Di}) \tag{3.24}$$

The heading offset calibration value was derived in a slightly different way. Instead of averaging all differences, Δh was calculated as the arithmetic mean of the differences $(h_{Pi} - h_{Di})$ for all i that represent the m camera stations at the location of orientation sensor initialisation. The camera tripod was not moved between these stations and only the mounting frame was tilted differently. This approach recognised that magnetometer readings become increasingly invalid when the recording system is moved away from the location of orientation sensor initialisation (Section 3.3.1.2). In order to avoid heading measurements with invalid magnetometer gauging being used for offset calibration, it was decided to limit the calculation of Δh to the m images obtained at the location of orientation sensor initialisation (Equation 3.25).

$$\Delta h = \frac{1}{m}\sum_{i=1}^{m}(h_{Pi} - h_{Di}) \tag{3.25}$$

Besides the calibration values Δh, Δp, and Δr, their respective standard deviations s_h, s_p, and s_r were also calculated (Equations 3.26 to 3.28).

$$s_h = \sqrt{\frac{1}{m}\sum_{i=1}^{m}(h_{Pi} - h_{Di} - \Delta h)^2} \tag{3.26}$$

$$s_p = \sqrt{\frac{1}{n}\sum_{i=1}^{n}(p_{Pi} - p_{Di} - \Delta p)^2} \tag{3.27}$$

$$s_r = \sqrt{\frac{1}{n}\sum_{i=1}^{n}(r_{Pi} - r_{Di} - \Delta r)^2} \tag{3.28}$$

The standard deviation indicates the precision of the calibration values. In the case of Δh the significance of the standard deviation s_h is reduced, due to the reduced number of measurements used to calculate Δh. At the location of orientation sensor initialisation, data was typically collected at 2 camera stations and used for calculating the heading offset calibration value Δh. This sample size was considered to be insufficient to yield representative standard deviations. Therefore, it was decided to additionally derive the span or range of heading offsets $s\Delta h$, which is the maximum difference between Δh and any value of $(h_{Pi} - h_{Di})$ (Equation 3.29).

$$s\Delta h = \max(|(h_{Pi} - h_{Di}) - \Delta h|) \tag{3.29}$$

This value indicates the suitability of Δh as an offset calibration value for heading measurements at camera stations that were not used to derive Δh.

Using the calibration values Δh, Δp, and Δr, orientation sensor measurements could be corrected for rotational offsets due to inexact alignment between the camera and the orientation sensor. The corrected orientation angles h_{Ci}, p_{Ci}, and r_{Ci} were obtained by adding the calibration values to their respective orientation sensor measurements (Equations 3.30 to 3.32).

$$h_{Ci} = h_{Di} + \Delta h \tag{3.30}$$

$$p_{Ci} = p_{Di} + \Delta p \tag{3.31}$$

$$r_{Ci} = r_{Di} + \Delta r \tag{3.32}$$

The final step of the rotational offset calibration process was to transform the corrected angles h_{Ci}, p_{Ci}, and r_{Ci} into photogrammetric angles ω_{Ci}, φ_{Ci}, and κ_{Ci} that can be used as exterior orientation parameters in a bundle adjustment. This was achieved by utilising the "heading, pitch, roll to omega, phi, kappa" transformation algorithm (Section 3.4.2). This algorithm was also applied to the standard deviations s_h, s_p, and

s_r in order to provide an indicator of precision corresponding to photogrammetric angles.

3.5.3 Positional offset calibration

To determine positional offset calibration values it has to be recognised that varying heading, pitch, and roll during data collection cause the absolute positional offsets between camera and DGPS antenna or prism to change. It is essential to derive an estimate for three fixed components relative to the camera using all *n* camera stations. This was achieved by rotating the absolute positional offsets into the non-rotated camera coordinate system (normal case of photogrammetry). In a non-rotated system the relative positional offsets are theoretically of equal magnitude for all sensor orientations. The absolute positional offsets $\mathbf{d}_{ai}$ were calculated by subtracting the directly measured DGPS or Total Station positions (X_{Di}, Y_{Di}, Z_{Di}) from the photogrammetrically derived positions (X_{Pi}, Y_{Pi}, Z_{Pi}) (Equation 3.33).

$$\mathbf{d}_{ai} = \begin{bmatrix} (X_{Pi} - X_{Di}) \\ (Y_{Pi} - Y_{Di}) \\ (Z_{Pi} - Z_{Di}) \end{bmatrix} \tag{3.33}$$

Using the photogrammetrically derived angles ω_{Pi}, φ_{Pi}, and κ_{Pi} in the rotation matrix in Equation 2.10, the rotation matrix $\mathbf{R}_{Pi}$ was derived for each camera station *i*. This matrix was used to rotate absolute positional offsets $\mathbf{d}_{ai}$ into the non-rotated camera coordinate system, resulting in relative positional offsets $\mathbf{d}_{ri} = [X_{ri}\ Y_{ri}\ Z_{ri}]^T$ (Equation 3.34).

$$\mathbf{d}_{ri} = \mathbf{R}_{Pi} * \mathbf{d}_{ai} \tag{3.34}$$

A simplified illustration of absolute and relative positional offsets is depicted in Figure 3.13.

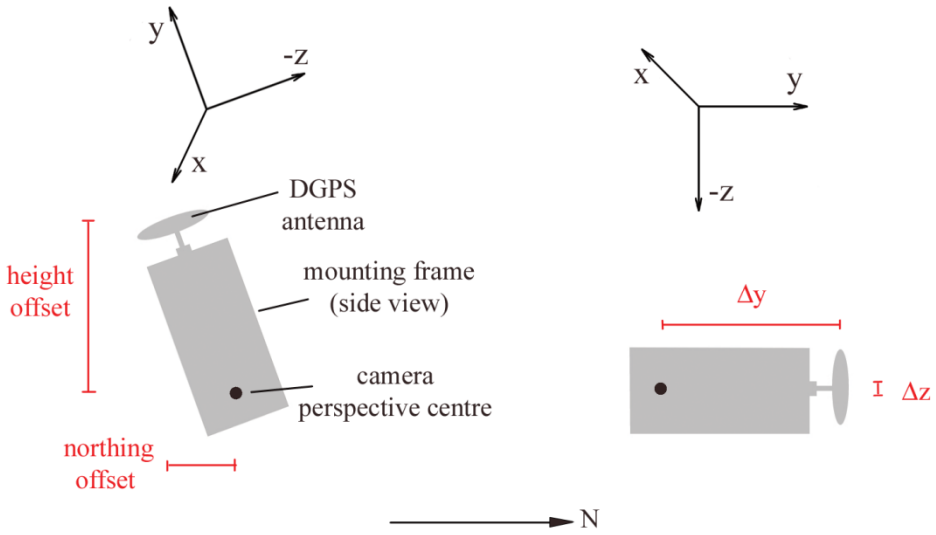

a: rotated camera coordinate system

b: non-rotated camera coordinate system (normal case)

Figure 3.13: Positional offsets in the rotated camera coordinate system and in the non-rotated camera coordinate system.

From the relative positional offsets the relative calibration values Δx, Δy, and Δz were derived by calculating the arithmetic means of X_{ri}, Y_{ri}, and Z_{ri}, respectively (Equations 3.35 to 3.37).

$$\Delta x = \frac{1}{n}\sum_{i=1}^{n} X_{ri} \tag{3.35}$$

$$\Delta y = \frac{1}{n}\sum_{i=1}^{n} Y_{ri} \tag{3.36}$$

$$\Delta z = \frac{1}{n}\sum_{i=1}^{n} Z_{ri} \tag{3.37}$$

The standard deviations s_x, s_y, and s_z were also calculated (Equations 3.38 to 3.40). These indicate the precision of their corresponding positional offset calibration value.

$$s_x = \sqrt{\frac{1}{n}\sum_{i=1}^{n}(X_{ri} - \Delta x)^2} \tag{3.38}$$

$$s_y = \sqrt{\frac{1}{n}\sum_{i=1}^{n}(Y_{ri} - \Delta y)^2} \tag{3.39}$$

$$s_z = \sqrt{\frac{1}{n}\sum_{i=1}^{n}(Z_{ri} - \Delta z)^2} \tag{3.40}$$

To correct direct position measurements (DGPS or Total Station) for positional offsets, absolute calibration values $\mathbf{c}_{ai} = [\Delta x_{ai}\ \ \Delta y_{ai}\ \ \Delta z_{ai}]^T$ for each camera station i were derived by rotating the vector of relative calibration values $\mathbf{c}_0 = [\Delta x\ \ \Delta y\ \ \Delta z]^T$ into the rotated camera coordinate systems of each camera station *i*. This was achieved by inserting the orientation sensor angles corrected for rotational offsets and transformed into photogrammetric angles ω_{Ci}, φ_{Ci}, and κ_{Ci} (Section 3.5.2) into the rotation matrix in Equation 2.10. This resulted in a rotation matrix $\mathbf{R}_{Ci}$ for each camera station *i*. Applying the inverse of $\mathbf{R}_{Ci}$ to $\mathbf{c}_0$ results in a vector of absolute calibration values $\mathbf{c}_{ai}$ (Equation 3.41).

$$\mathbf{c}_{ai} = \mathbf{R}_{Ci}{}^{-1} * \mathbf{c}_0 \tag{3.41}$$

The corrected DGPS or Total Station positions (X_{Ci}, Y_{Ci}, Z_{Ci}) are then calculated by adding Δx_{ai}, Δy_{ai}, and Δz_{ai} to their corresponding direct position measurements X_D, Y_D, and Z_D (Equations 3.42 to 3.44).

$$X_{Ci} = X_{Di} + \Delta x_{ai} \tag{3.42}$$

$$Y_{Ci} = Y_{Di} + \Delta y_{ai} \tag{3.43}$$

$$Z_{Ci} = Z_{Di} + \Delta z_{ai} \tag{3.44}$$

These corrected values can be used to provide initial exterior orientation parameters in a bundle adjustment. The relative standard deviations were not transformed into absolute values. However, when these values are used in calculations together with absolute values, the orientation of the mounting frame during data collection has to be considered. Figure 3.13 demonstrates that when the mounting frame is oriented approximately vertical during data collection, the absolute height offset (Z_{Pi} - Z_{Di}) derived in the rotated camera system is the main contributor to the Y_{0i} offset in the non-rotated camera system. Therefore, in the case depicted in Figure 3.13, s_y essentially corresponds to absolute height offsets and s_z to absolute planimetric offsets.

3.6 Initial recording system tests

The recording system was initially tested at the two test sites at Loughborough University (Section 3.2). The aim of testing was to assess achievable accuracy as well as calibration stability and precision. From January 2010 to February 2011, 9 tests (Test1 to Test9) were conducted, resulting in 9 data sets. A data set comprises of images of the test site, continuous heading, pitch, and roll measurements of the orientation sensor, and position data for each image derived by either DGPS or Total Station. The tests varied in the camera fixture, the method used for positioning (DGPS or Total Station), the test site, and whether the camera was detached from the mounting frame between tests. Table 3.3 provides an overview of the characteristics of each recording system test conducted at the two test sites at Loughborough University. During the first three tests the camera was attached to the mounting frame using the wooden enclosure described in Section 3.3.2.2. Therefore, the camera was completely detached from the mounting frame after each test, in order to be able to extract image data. From Test4 the modified camera fixture (Section 3.3.2.2) was used. In Test4 a prism was attached to the mounting frame instead of the DGPS antenna to test the usability of Total Station for positioning the recording system. Test5 was conducted as preparation test for the first case study (Section 5.1) at the test object. After Test4 and Test5 the camera was also detached. By comparing calibration

Table 3.3: Overview of initial tests conducted at Loughborough University campus.

TestID	*Date*	*Number images*	*Positioning*	*Test site*	*Camera fixture*	*Camera detached between tests*
Test1	18-01-2010	9	DGPS	test field	wooden	yes (18 mm lens)
Test2	19-02-2010	9	DGPS	test field	wooden	yes
Test3	04-03-2010	12	DGPS	test field	wooden	yes
Test4	22-04-2010	18	Total Station	test field	hose clip	yes
Test5	06-05-2010	11	DGPS	test object	hose clip	yes
Test6	20-09-2010	34	DGPS	test field	hose clip	no
Test7	22-09-2010	27	DGPS	test field	hose clip	no
Test8	29-09-2010	18	DGPS	test field	hose clip	no
Test9	24-02-2011	20	DGPS	test field	hose clip	no

results of these two tests, it was realised that the camera cannot be re-attached to the mounting frame without rotational offset changes. Therefore, it was decided not to detach the camera after Test6 and for the remaining subsequent tests.

Another variation between the initial tests occurred for Test1. Data was accidentally collected using a camera different to the originally calibrated Nikon D80 with 24 mm lens (Section 3.3.1.1). This camera was also a Nikon D80 but with an 18-70 mm zoom lens fixed to 18 mm using electrical tape. This camera was calibrated after data collection and the camera calibration parameters were used for photogrammetric data processing in Test1. This ensured usability of the data collected in Test1 and comparability to the other initial recording system tests.

3.6.1 Data collection

The procedures adopted during data collection were the same for all initial recording system tests. Prior to data collection, the internal clock of the camera was synchronised with the laptop clock and the orientation sensor was initialised at the location of the first camera station. Imagery, orientation and position data were collected at a varying number of camera stations adjacent to the test site. The camera stations at the test field (Section 3.2.1) were arranged with camera-to-object distances varying from approximately 7 m to 10 m. Figure 3.14 provides a typical representation of the camera station arrangement using camera stations of Test8.

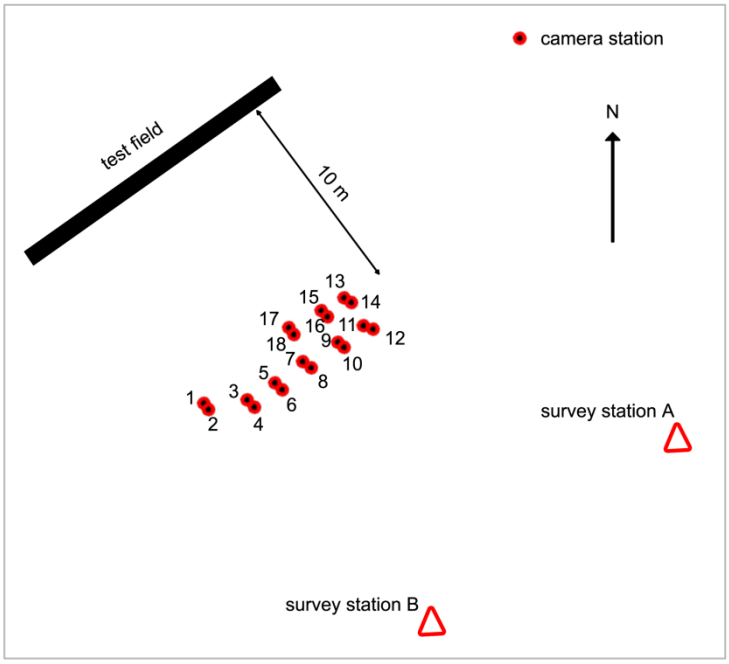

Figure 3.14: Approximate arrangement of camera stations (1-18) in Test8.

Imagery was collected in landscape format. At the given camera-to-object distance, targets representing the lower part of the test field were captured throughout the image format. To capture the upper targets at these distances, the mounting frame was tilted upwards, resulting in an increased range of measured pitch values. Some camera stations are in close proximity to each other (Figure 3.14), because images capturing the lower and the upper part of the test field were usually taken from a tripod at the same location. The test field is approximately planar and so the range of heading values measured would inevitably be comparatively limited. To be able to test the recording system with a greater range of heading values that would be likely to occur in heritage recording projects, some images were deliberately acquired with a slightly oblique view in relation to the test field.

The “modern art” test object (Section 3.2.2) is a vertical structure with a small diameter on the ground and is accessible from all sites. Therefore, camera stations in Test5 were arranged in an arc around the southern side of the test object (Figure 3.15), where control points were visible. This enabled data collection with a greater variation in heading values compared to data collection at the planar test field. The approximate average camera-to-object distance was 5 m to 6 m. It was necessary to acquire three

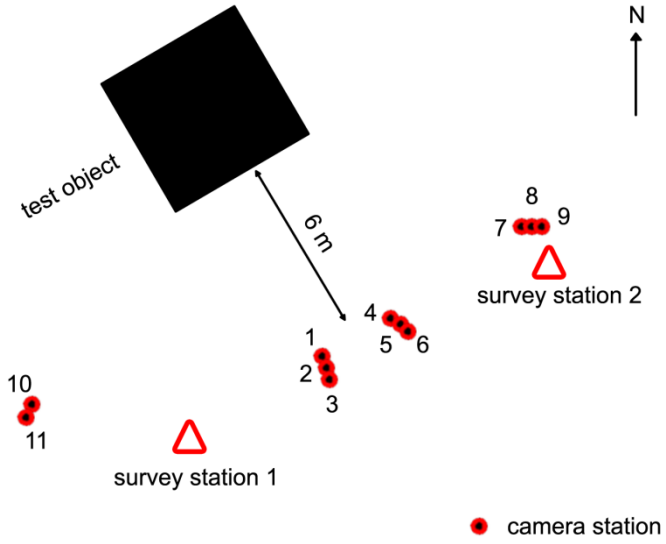

Figure 3.15: Approximate arrangement of camera station in Test6.

images from the same location with varying pitch of the mounting frame to capture the entire height of the test object at this distance. This resulted in a higher range of pitch values compared to data sets collected at the test field.

During data collection the orientation sensor continuously recorded heading, pitch, and roll with an interval of 0.5 seconds, while images and discrete DGPS or Total Station positions were acquired for every camera station. During tests where DGPS was used for positioning, a DGPS base station was set up at one of the survey stations adjacent to the test site. At the first camera stations GPS data was acquired for 10 minutes at a sampling rate of 2 seconds without moving the recording system. This enabled carrier-phase measurement by providing sufficient data for resolving the initial cycle ambiguity of the GPS signal (Section 2.6.2). For each subsequent camera station it was sufficient to acquire GPS data for 1 minute only, as long as the receiver could maintain "lock" with the satellite signal. In Test4 a Total Station and a prism were positioned at the two survey stations adjacent to the test field, in order to determine the position of the prism attached to the mounting frame.

3.6.2 Data processing

As preparation for data analysis the data of each data set was further processed. The DGPS positions were post-processed using Leica SKI Pro software, utilising GPS data

captured by both the rover and the DGPS base station. The resulting Cartesian coordinates were transformed into OSGB36 coordinates using the Grid InQuest transformation software provided by Ordnance Survey. The Total Station positions were calculated in a spread sheet using Total Station observations and survey station coordinates, utilising mean sea level and grid scale factor corrections.

Furthermore, time information stored in the Exif-header of the JPEG image files was used to extract corresponding heading, pitch, and roll measurements from the continuous record of orientation sensor data. The image acquisition time was manually extracted from the Exif header of each image and saved to a text file. Software for extracting data from the orientation sensor data log file (ExtractOrientationData) had been coded in the programming language "C sharp" (C#). This software program utilises information stored in the time text file, the data log, and the system log of the orientation sensor to extract heading, pitch, and roll at the time of image acquisition.

For this research project it was decided to set the orientation sensor to measure heading with respect to magnetic north. This prevented incorrect heading measurement due to erroneous magnetic declination value input. In order to achieve heading with respect to the north direction defined by OSGB36 coordinates ("grid north"), the measured heading was corrected by adding values for magnetic declination and grid convergence. The magnetic declination is the angular difference between magnetic north and true north and is location and time dependent. The American National Oceanic and Atmospheric Administration (NOAA) National Geophysical Data Center provides an online magnetic declination estimation tool (NOAA, 2011), which was utilised to obtain the actual magnetic declination for each date and location of data collection. Grid convergence is the angular difference between true north and grid north. The grid convergence angle is location dependent. A Microsoft Excel spread sheet provided on the Ordnance Survey website (Ordnance Survey, 2007) facilitated the determination of the grid convergence angle for each location of data collection. In subsequent calculations heading always referred to grid north heading.

The last step in data preparation was creation and application of offset calibration values (Section 3.5). From each test data set, rotational and positional offset calibration values and their standard deviations were derived. For applying calibration

values to measurements, two groups of data sets were distinguished. The first group comprises data sets where the camera was detached from the mounting frame between the tests (Test1-Test5). Therefore, the calibration values derived from each test data set of this group were considered not suitable to correct orientation and position measurements of any other test data set. As a result, measured orientation and position of each test in the first group were corrected using calibration values that were derived from data of the same test. Assuming that the best suitable calibration values are derived from data of the same test, the results of accuracy assessment (Section 3.6.3) in Test1 to Test6 indicate the theoretically highest accuracy achievable.

The second group comprises Test6 to Test9. The camera was not detached from the mounting frame between these tests. Therefore, calibration values derived from each of these test data sets were considered suitable to correct orientation and position measurements of other data sets in the second group. Calibration values derived from data of each test in the second group were applied to measurements of the other tests in this group. Additionally, orientation and position measurements of tests in the second group were also corrected for rotational and positional offsets using calibration values derived from the same data set. This enabled comparison between accuracy achieved using best suitable offset calibration values and accuracy achieved using independently derived offset calibration values. As a result, four sets of corrected measurements were obtained for each test in the second group.

3.6.3 Accuracy assessment

The corrected orientation and position measurements of both recording system test groups were used to provide initial exterior orientation parameters (ω, φ, κ, X_0, Y_0, Z_0) in a GAP bundle adjustment. The input files for each GAP bundle adjustment were derived from an LPS bundle adjustment report (Section 3.1.2) created using the imagery of the corresponding test data set. Prior to conducting the GAP bundle adjustment, the parameters in the "extracted exterior orientation parameters" input file (Figure 3.1) were substituted by the direct orientation and position measurements corrected for rotational and positional offsets. Except for φ, these parameters were constrained by the standard deviations of their corresponding offset calibration values. During data collection the mounting frame was oriented approximately vertical and,

therefore, s_z was used as corresponding standard deviation for the parameter Y_0 (northing) and s_y for the parameter Z_0 (height) (Section 3.5.3). The parameter φ is strongly related to the measured heading value (Figure 3.11). The heading calibration value Δh was derived solely from data of camera stations at the location of orientation sensor initialisation. The calibration value Δh was considered not ideal for correcting heading measurements at other camera stations, because of potential erroneous heading measurements due to local magnetic field distortions. Therefore φ is constrained by two different values, depending on the location where the corresponding heading data was collected. For camera stations at the location of orientation sensor initialisation, it was assumed that the measured heading is not subjected to inaccuracies due to local magnetic field distortions. Therefore, the heading accuracy of the orientation sensor specifications (Table 3.2) was used as a stochastical constraint. For all other camera stations, the range of heading offsets $s\Delta h$ was used. In that way, camera stations where the direct heading measurement is less reliable would provide a reduced effect in the bundle adjustment process.

In the GAP bundle adjustment, no control points were used, so relying on the exterior orientation parameters derived from the orientation sensor and DGPS or Total Station only. The coordinated points of the test sites could then be used as check points, with their OSGB36 coordinates estimated in the bundle adjustment. These estimated coordinates were compared to the known coordinates of the points. This allowed the calculation of the RMSE for easting, northing, and height, critically allowing absolute accuracy to be determined. Relative accuracy was assessed also. Easting, northing, and height distances between all possible pairs of coordinated points were calculated from the check point coordinates estimated in the bundle adjustment. These distances were compared to corresponding distances calculated from the original check point coordinates. The RMSE of the distance differences provides a measure of the one-dimensional (1D) relative accuracy and the 2D and 3D relative accuracy was derived also. 2D relative accuracy was calculated analogous to 1D relative accuracy, but using planar or horizontal distances calculated from easting and northing coordinates. 3D or slope distances between all possible pairs of check points were used to derive the 3D relative accuracy.

3.7 Enhancing usage and accessibility of cultural heritage data

One objective of this research project (Section 1.1) is to demonstrate the usability of simple and low-cost methods for enhancing usage and accessibility of photogrammetric cultural heritage data. Usage of photogrammetric data can be improved by storing exterior orientation parameters in the same file as their corresponding image. This reduces the number of files that have to be handled in a project, which eases exchanging data between researchers or other stakeholders. Furthermore, ambiguities in attributing exterior orientation parameters to their corresponding image can be avoided, because correct attribution would always be defined. This is a significant advantage in recording projects where cultural heritage objects are recorded for safekeeping over comparably long periods of time and information about attributing exterior orientation to images might get mislaid.

In this research project, a method to store exterior orientation parameters and image in one file was investigated (Section 3.7.1). This method also enhanced data accessibility by providing opportunity for visualisation on the internet (Section 3.7.2). The practicability of this method was demonstrated using photogrammetric data collected at the Roughting Linn case study site (Section 5.2).

3.7.1 Combined storage of exterior orientation and imagery

It was decided to exclusively use standardised approaches for storing exterior orientation parameters and image data in one file, in order to guarantee usability of data. The first approach that was considered for this purpose was storing data in the Exif-header of the JPEG image file. Exif is a standard for storing image data and image metadata in one file. It is maintained by Camera & Imaging Product Association and Japan Electronics and Information Technology Industries Association (JEITA) (Camera & Imaging Product Association, 2010). The version at the time of

writing is Exif 2.3 and facilitates storage of 3D position and heading, indicating the potential of Exif for storing exterior orientation information. However, the storage of 3D orientation is currently not supported and it was decided not to use this approach in this research project. An alternative approach involved the "KML format". The current KML specification (Open Geospatial Consortium, 2008) allows adding 3D position and 3D orientation information to a KML file and this information can be linked to the corresponding image file. Both, the KML file and the image, can be stored together in a KML archive file (KMZ file), which appears to the user as one single file (Blower et al., 2007). A software routine was programmed in C# that creates one single KMZ file for each image. In order to comply with the KML standard, the directly determined exterior orientation parameters were converted to suitable KML input parameters previous to KMZ generation. The KML standard requires horizontal position being provided in geodetic coordinates of the World Geodetic System 1984 (WGS 84) and height position being provided relative to the Earth Gravitational Model 1996 (EGM 96) geoid. The horizontal position in OSGB36 coordinates was transformed to geodetic coordinates of WGS 84 (longitude, latitude) in decimal degrees using the online coordinate transformation software provided by Synthetics Technical Consulting (Synthetics Technical Consulting, 2011). The height relative to the EGM 96 geoid was derived by first converting the height coordinate in the OSGB36 system into height above the Geodetic Reference System 1980 (GRS 80) ellipsoid using Grid InQuest transformation software provided by Ordnance Survey. In a second step the height difference between the EGM 96 geoid and the GRS 80 ellipsoid at the given location was derived from the National Geospatial-Intelligence Agency (NGA) online EGM 96 geoid calculator (National Geospatial-Intelligence Agency, n.d.). This value was applied to the height output of the Grid InQuest transformation (height above GRS 80 ellipsoid), resulting in height relative to the EGM 96 geoid, suitable for usage within the KML standard. The rotation angles were transformed also. In the KML standard, rotation is defined by three sequential rotations about the axes of the camera coordinate system. However, orientation angles in KML describe rotation using a rotation sequence different to the sequence used with photogrammetric angles (ω, φ, κ). The rotation sequence for KML angles is: first angle about the camera z-axis, second angle about the rotated x-axis, and third angle about the rotated z-axis. The directly determined photogrammetric angles were

converted to angles suitable for KML using MatLab. A built-in MatLab function known as "dcm2angle" allows extracting rotation angles from a rotation matrix depending on a certain rotation sequence. A rotation matrix was created by inserting the directly determined photogrammetric orientation angles (ω, φ, κ) into Equation 2.10. This matrix was used as input in the "dcm2angle" function of MatLab and the rotation sequence "ZXZ" was specified. The unit of the three output angles is radians. Therefore, they were converted into decimal degrees prior to utilisation in KML. In its default setting the heading angle output of "dcm2angle" is in the range of -180° to 180° with positive rotations in counter-clockwise direction. The heading range for KML is specified as 0° to 360° and rotating in clockwise direction. In order to obtain heading suitable for KML in a final step positive heading outputs were subtracted from 360 and negative outputs were multiplied by -1.

3.7.2 Visualisation in Google Earth

The KMZ approach for storing exterior orientation information and images in one file was also chosen because the KMZ file can be used directly for visualisation in Google Earth. The current version of the KML standard (Open Geospatial Consortium, 2008) implements a feature ("PhotoOverlay") that enables displaying images in their orientation and position at the time of image acquisition. Figure 3.16 provides an example of "PhotoOverlay" displayed in Google Earth. It depicts an oblique aerial image of a landslide close to Charmouth in Dorset, UK, which is superimposed on the Google Earth background data in its orientation and position during exposure.

The main elements of "PhotoOverlay" are position and orientation of an image, the image to be displayed, and additional viewing parameters that define the field of view and the distance from camera position to image. The combination of position, orientation, and image in a KMZ file was described in Section 3.7.1. Therefore, the software routine that created the KMZ file was modified to also include the additional viewing parameters in the KML part of the KMZ file. The field of view can be compared to the lens opening of a camera (Open Geospatial Consortium, 2008) and, therefore, was calculated using the focal length of the camera (f) and the camera image sensor size. In KML the field of view is defined by four angles: right field of

Figure 3.16: Photo overlay of an oblique aerial image in Google Earth.

view (*rightFoV*), left field of view (*leftFoV*), top field of view (*topFoV*), and bottom field of view (*bottomFoV*). The angles *rightFoV* and *leftFoV* define the horizontal lens opening angle of the camera. They are equal in their absolute magnitude and only differ in their algebraic sign (Equations 3.45 and 3.46).

$$rightFoV = \arctan\left(\frac{hz}{2 * f}\right) \tag{3.45}$$

$$leftFoV = -\arctan\left(\frac{hz}{2 * f}\right) \tag{3.46}$$

Note: hz is the length of the camera image sensor in horizontal direction.

The angles *topFoV* and *bottomFoV* define the vertical lens opening angle. They are also equal in their absolute magnitude and only differ in their algebraic sign (Equations 3.47 and 3.48).

$$topFoV = \arctan\left(\frac{vt}{2 * f}\right) \tag{3.47}$$

$$bottomFoV = -\arctan\left(\frac{vt}{2 * f}\right) \tag{3.48}$$

Note: vt is the length of the camera image sensor in vertical direction.

The focal length *f* was also used to define the distance from camera to image in the KML file. The position, orientation, and viewing parameters can be used by Google Earth to display the corresponding image in a representation of its position and orientation at the time of exposure.

In order to demonstrate the usability of Google Earth for visualisation of cultural heritage data, KMZ files of 8 images and their corresponding exterior orientation parameters collected during the case study at Roughting Linn rock-art site (Section 5.2) were created. These KMZ files also included viewing parameters required for "PhotoOverlay" and were used to visualise rock-art images in Google Earth.

This approach was considered a low-cost and easy-to-use way to enhance cultural heritage data accessibility and usage, because no special knowledge in visualisation is needed and Google Earth is available without charge.

3.8 Summary

In this chapter hardware, software and methods used to achieve the aims and objectives of this research project (Section 1.1) were explained. It started with an introduction of the two bundle adjustment software programs, LPS and GAP, used in this research. The advantages and disadvantages of both programs and their application in this research project were explained.

Secondly, the test sites that had been established at Loughborough University were described. The process of establishing the test sites as well as their characteristics were explained in detail.

This was followed by a detailed description of the recording system and its components: camera, orientation sensor, DGPS receiver and antenna (or Total Station and prism), and laptop. The fixture of camera, orientation sensor, and DGPS antenna (or prism) to the recording system mounting frame was discussed. It was stated that the stability of the component fixture to the mounting frame is crucial for stable offset calibration, an issue discussed further in Section 6.1.1.

It was recognised that the orientation sensor uses a method to describe rotation angles different to the method used in photogrammetry. The algorithms devised to transform

photogrammetric angles to equivalent orientation sensor angles, and vice versa, have been described in detail.

Subsequently the offset calibration process was explained. The influence of local magnetic field distortions on heading measurements was identified as an important issue regarding the stability and accuracy of the heading offset calibration value. The calculation of the heading calibration value and its stochastic constraint was adjusted in order to reduce the effect of the local magnetic field distortion.

Furthermore initial recording system tests were described. This involved the description of variations between the tests as well as data collection and processing. An account of the data analysis process, including accuracy values derived in order to assess the recording system performance, was also given. The test results are presented in Chapter 4 and are discussed fully in Chapter 6.

This chapter concludes with a description of approaches to enhance usage and accessibility of photogrammetric cultural heritage data. Storing exterior orientation data and imagery in one file was considered important to enhance data usage and longevity. This was achieved by utilising the capabilities of KML for storing exterior orientation and the corresponding image in a single KMZ file. Using KMZ files also enhanced accessibility by enabling data visualisation in Google Earth. The case study conducted at Roughting Linn rock-art site utilised this KMZ based approach and is presented in Section 5.2.4.

4 Results

In this chapter results of nine initial recording system tests at Loughborough University (Section 3.6) are presented. First, the precision and stability of offset calibration values are investigated, which demonstrates whether the two camera fixture approaches achieve significantly different calibration precisions. These tests also investigate whether stable offset calibration can be achieved using either of the camera fixture approaches.

The second part of this chapter is focussed on the absolute and relative accuracy that was achieved in object space. Absolute and relative accuracy was assessed for test data sets collected using the original camera fixture and test data sets collected using the modified camera fixture. For a subset of test data sets, absolute and relative accuracy achievable using calibration values derived independently from different test data sets is investigated.

This chapter concludes with a brief summary.

4.1 Offset calibration results

Precise and stable calibration of the rotational offsets between camera and orientation sensor and the positional offsets between camera and DGPS antenna or prism is crucial for direct determination of exterior orientation parameters. Offset calibration values are applied to directly determined orientation and position measurements, in order to derive the exterior orientation of the camera. Calibration precision and stability have an influence on the quality of the exterior orientation parameters and

therefore also on the overall achievable recording system accuracy. In this section the offset calibration precision achieved in each test and the offset calibration stability over time are presented.

4.1.1 Calibration precision

The standard deviation of the calibration value calculated during offset calibration (Section 3.5) is an indicator of the precision and reliability of the calibration. For evaluating the precision, the expected accuracy of orientation sensor (Table 3.2) and DGPS or Total Station (Section 4.1.1.2), respectively, was used as reference. Values that exceed the expected accuracy indicate offset changes between the recording system components during data collection that are not caused by the expected measurement errors of the orientation and position measurement devices. Acceptable offset calibration precision is indicated by standard deviations that meet the expected accuracy of the corresponding measurement device, because this suggests expected measurement errors being the only reason for offset changes during data collection.

4.1.1.1 Precision of rotational offsets

For evaluating the precision of the rotational offsets, the accuracy values in the TCM5 orientation sensor specifications (Table 3.2) were used as reference. The standard deviations of the heading, pitch, and roll calibration values derived from the test data sets collected at Loughborough University test sites are listed in Table 4.1. The first column identifies the test data set used to derive the calibration values and their standard deviation. The subsequent three columns display the standard deviations in the order: heading (s_h), pitch (s_p), and roll (s_r). Table 4.1 also includes the range of heading offset ($s\Delta h$) for each test, which is displayed in the last column. These values indicate the suitability of the heading offset calibration value to correct heading measurements from camera stations that are not at the location of orientation sensor initialisation (Section 3.5.2). They were included in the calibration precision assessment, because the representativeness of the heading offset calibration value and its standard deviation is reduced (Section 3.5.2). The range of heading offset also demonstrates the effect distortions in the local magnetic field can have on the heading

Table 4.1: Rotational offset standard deviations and range of heading offset.

Test ID	s_h (°)	s_p (°)	s_r (°)	$s\Delta h$ (°)
Test1	0.05	0.06	0.06	0.22
Test2	0.14	0.13	0.13	1.03
Test3	0.12	0.12	0.08	0.50
Test4	0.12	0.13	0.12	0.58
Test5	0.45	0.15	0.34	2.24
Test6	0.08	0.10	0.19	0.40
Test7	0.05	0.10	0.20	0.35
Test8	0.15	0.07	0.14	0.27
Test9	0.01	0.13	0.14	0.48

measurement of the orientation sensor. The values of Table 4.1 are visualised in Figure 4.1 (standard deviations) and Figure 4.2 (range of heading offset) to enhance comparison between the values.

Figure 4.1 demonstrates that the standard deviation of the pitch calibration value s_p does not exceed the orientation sensor pitch accuracy (0.2°) in any of the initial recording system tests. This indicates a high precision and reliability of the pitch calibration values. Precise and reliable roll calibration was also achieved in all initial recording system tests, except for Test5. In Test5 the standard deviation of the roll calibration value s_r exceeds the expected orientation sensor roll accuracy (0.2°) by

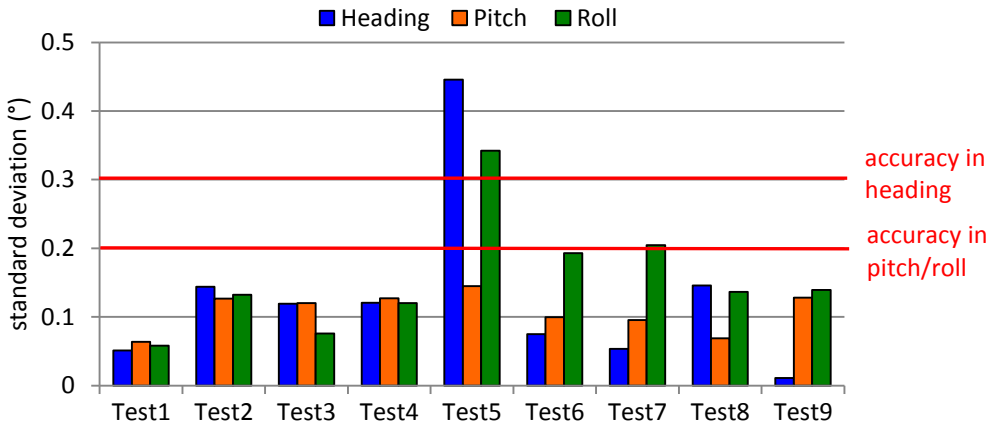

Figure 4.1: Rotational offset calibration precision.

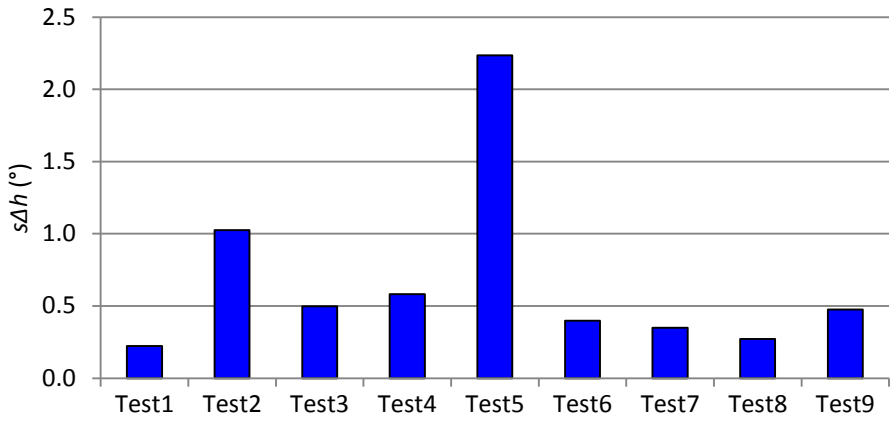

Figure 4.2: Range of heading offset (sΔh).

0.14°. This indicates a significant roll offset change that only occurs in Test5. The standard deviation of the heading calibration value s_h in Test5 is also significantly larger than the corresponding values of the other tests. It exceeds the expected heading accuracy (0.3°) by 0.15°. The significance of s_h is reduced due to the reduced number of measurements used to calculate the heading calibration value Δh (Section 3.5.2). However, the significant difference between s_h in Test5 and s_h in other tests indicates some difficulty in determining the heading offset at the camera stations used for heading calibration (Section 3.5.2) that only occurs in Test5. Another difference between Test5 and the other initial recording system tests is revealed by comparing the range of heading offset ($s\Delta h$) values with each other (Figure 4.2). In Test5 $s\Delta h$ is significantly larger than corresponding values in other tests and exceeds the second largest value (Test2) by 1.21°. This reveals significant changes in the heading offset when the recording system is moved away from the location of orientation sensor initialisation, suggesting a high influence of local magnetic distortion on the heading measurements in Test5.

Test5 was conducted at the test object (Section 3.2.2) while all other tests were conducted at the test field (Section 3.2.1). Therefore, the differences between Test5 and the other tests indicate test site specific influences on rotational offset calibration. The heading measurements appear to be particularly affected, which suggests erroneous orientation sensors magnetometer readings due to distortions in the local magnetic field. This will be further discussed in the "Discussion" chapter (Section 6.1.2).

If the results from Test5 are excluded, the standard deviations of all tests meet the expected accuracy of the orientation sensor (Figure 4.1). This indicates that rotational offset calibration values derived in tests utilising the original camera fixture approach (Test1 to Test3) achieve a similar precision as values derived in tests utilising the modified camera fixture (Test4 to Test9). Nevertheless, the modified camera fixture is considered the better approach for attaching the camera to the mounting frame. It enables access to the image data without detaching the camera from the mounting frame, which was later revealed to be essential for stable offset calibration (Section 4.1.2.1).

4.1.1.2 Precision of positional offsets

The precision of positional offset calibration values was evaluated using the expected accuracy of the positioning device utilised during the test. For DGPS the expected accuracy is 10 mm in plan and 30 mm in height (Konecny, 2003) and for the Leica TCR405 Total Station, which was used for positioning in Test4, the expected accuracy is 3 mm in plan and height (Leica Geosystems, 2006). Table 4.2 lists the standard deviations of the positional offset calibration values. The first column identifies the test data set used to derive the calibration values and their standard deviation. The subsequent three columns display the standard deviations calculated for the x- (s_x), y- (s_y), and z-direction (s_z) of the camera coordinate system. A graphical representation of the values of Table 4.2 can be found in Figure 4.3.

Except for Test5, the largest standard deviation in each test is achieved for the y-offset (s_y). During data collection for Test1 to Test9 the recording system mounting frame was oriented approximately vertical (Section 3.5.3 and Section 3.6.3). However, positional offset calibration values and their standard deviations were derived after absolute positional offsets were rotated in the non-rotated camera coordinate system (Section 3.5.3), in which the mounting frame is oriented horizontally (Figure 3.13). Therefore, the calibration value standard deviation s_y, derived in the non-rotated camera coordinate system, essentially corresponds to absolute height values measured in the rotated camera coordinate system. Therefore s_y is evaluated using the expected DGPS or Total Station height accuracy. For the same reason the standard deviation s_z essentially corresponds to absolute easting and northing measured in the

Table 4.2: Positional offset standard deviations.

Test ID	s_x *(mm)*	s_y *(mm)*	s_z *(mm)*
Test1	11	21	7
Test2	27	72	15
Test3	13	16	13
Test4	6	6	6
Test5	8	9	9
Test6	14	26	17
Test7	11	15	15
Test8	7	20	13
Test9	7	20	7

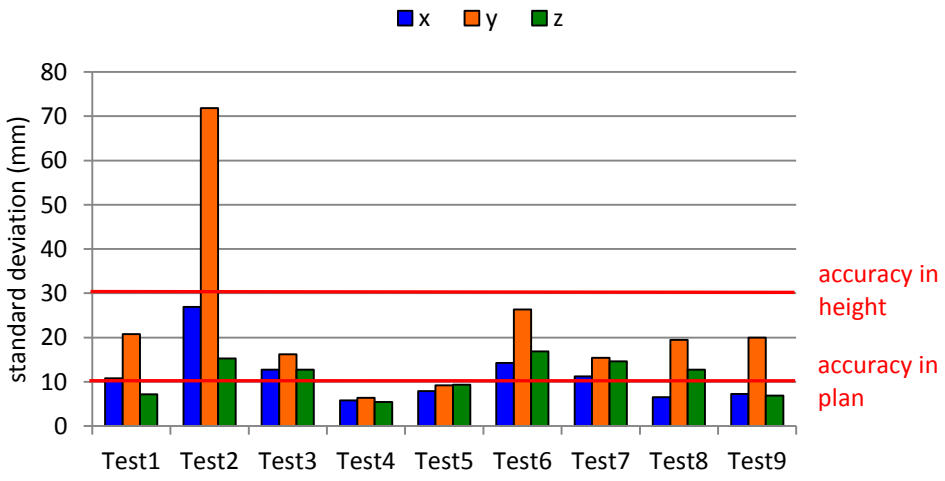

Figure 4.3: Positional offset calibration precision.

rotated camera coordinate system and is evaluated using the expected planimetric DGPS accuracy. Test2 is the only test where s_y does not meet the expected DGPS height accuracy, exceeding it by 42 mm. In the same test s_x and s_z exceed the expected planimetric DGPS accuracy by 17 mm and 5 mm, respectively. This indicates significant positional offset changes during data collection in Test2, which result in a low precision and reliability of the positional offset calibration values derived from this test data set. Less significant offset changes are indicated in Test1, 3, 6, 7, and 8 where the standard deviations of Δx and Δz exceed the planimetric DGPS accuracy by up to 7 mm. The smallest standard deviations were achieved in Test4 where Total

Station was used for positioning. However, the values exceed the expected Total Station positioning accuracy (3 mm) by up to 3 mm.

Based on these results the positional offset calibration is considered to be of lower precision than the rotational offset calibration. The significantly high standard deviations in Test2 can be explained by two gross errors in the camera station positions that were caused by a weak satellite constellation during data collection. Possible reasons for the standard deviations in the other test data sets exceeding the expected positioning accuracy include decrease in DGPS positioning accuracy due to tilt of the mounting frame and will be discussed in Section 6.1.3.

With the exception of Test2, positional offset calibration values were derived to similar precision in tests utilising the original camera fixture and in tests utilising the modified camera fixture. This indicates that both camera fixture approaches derived positional offset calibration values of similar precision.

4.1.2 Calibration stability

Calibration stability indicates the usability of calibration values derived from one test data set to correct orientation and position measurements of other test data sets. One objective in this research is to achieve offset calibration that is sufficiently stable or consistent to allow calibrating rotational and positional offsets prior to data collection (Section 1.1). The availability of consistent offset calibration is crucial for realising a practicable recording system, because it would enable recording without the need for coordinated points on site. The calibration is considered consistent when changes in the offset calibration value do not exceed the expected accuracy of orientation sensor and DGPS, respectively.

4.1.2.1 Stability of rotational offset calibration

The stability of rotational offset calibration indicates the suitability of rotational calibration values derived from one data set for correcting orientation measurements of other data sets. The rotational offset calibration values derived from Test1 to Test9 are listed in Table 4.3 with the first column identifying the test data set used to derive the calibration values and the subsequent columns displaying calibration values for heading (Δh), pitch (Δp), and roll (Δr).

When assessing the calibration value changes between the tests, it has to be considered that Test1 to Test3 were conducted using a camera fixture different to the one used in Test4 to Test9 (Table 3.3). Calibration stability between tests can only be assessed when the component fixture to the mounting frame was not changed. Figure 4.4 provides a graphical representation of the rotational offset calibration values grouped into tests utilising the initial camera fixture ("wooden enclosure") and tests utilising the modified camera fixture ("hose clip"). These two groups of tests were assessed separately.

Table 4.3: Rotational offset calibration values.

Test ID	*Δh (°)*	*Δp (°)*	*Δr (°)*
Test1	-6.09	-0.67	0.71
Test2	-9.33	-0.46	0.81
Test3	-6.13	-0.36	0.89
Test4	-5.75	1.32	-1.09
Test5	-3.32	1.89	0.20
Test6	-5.11	1.48	0.08
Test7	-5.45	1.37	0.10
Test8	-5.78	1.32	0.06
Test9	-5.63	1.26	0.04

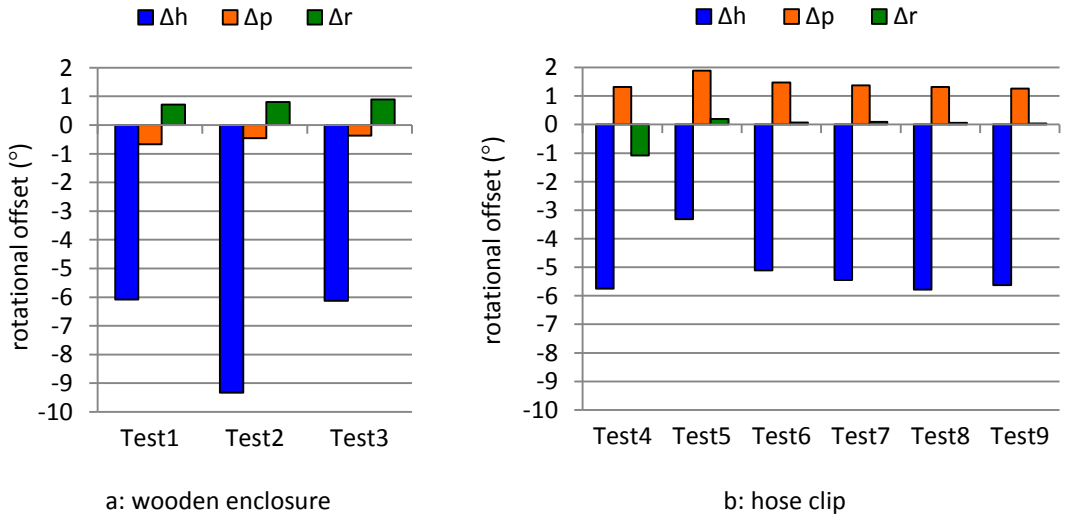

Figure 4.4: Rotational offset calibration values.

Figure 4.4a depicts rotational offset calibration values derived from test data sets where the initial camera fixture approach was used. As explained in Section 3.3.2.2, this camera fixture required the camera to be detached from the mounting frame after data collection in order to access the imagery stored on the camera memory card. As expected, Test1 to Test3 vary most in their heading calibration value, which changed from -6.09° in Test1 to -9.33° in Test2. The magnitude of the change (3.24°) exceeds the orientation sensor heading accuracy by 2.94°. The heading calibration value change from Test2 to Test3 is of similar magnitude (3.20°). Less significant offset changes occur for the pitch calibration value. The magnitude of change between Test1 and Test3 is 0.31° and exceeds the orientation sensor pitch accuracy (0.2°). This demonstrates that with the initial camera fixture approach the heading and pitch offset calibration is not sufficiently stable to allow offset calibration prior to data collection. The roll offset calibration values between Test1 and Test3 change by a magnitude smaller than the expected roll accuracy (0.2°) and is considered consistent. These results indicate that re-attaching the camera to the mounting frame using the original camera fixture approach introduces offset changes in heading and pitch but maintains the roll offset, which is expected.

Figure 4.4b depicts rotational offset calibration values derived in tests utilising the modified camera fixture (Test4 to Test9). The largest calibration value changes occur from Test4 to Test5. The heading calibration value changes from -5.75° in Test4 to -3.32° in Test5. The magnitude (2.43°) exceeds the orientation sensor heading accuracy by more than 2°. Between Test4 and Test5 the pitch and roll calibration values also change significantly. The change for pitch is 0.57° and for roll is 1.29°, which are both larger than the orientation sensor accuracy (0.2°). The second largest changes occur from Test5 to Test6 with a change of 1.79° in heading, 0.41° in pitch, and 0.12° in roll. Except for roll, these changes also exceed the expected orientation sensor accuracy. The camera was detached from the mounting frame between these three tests (Test4 to Test6). Therefore, these results indicate that the modified camera fixture also does not allow re-attaching the camera without requiring re-calibration of the rotational offsets. This is probably also the reason Test4 is the only test where the roll offset calibration value is negative. Handling the modified camera fixture after data collection of Test4 could have slightly bent the hose clip or the aluminium bars (Section 3.3.2.2). This will be further discussed in Section 6.1.1.

From Test6 to Test9 the camera remained attached to the mounting frame (Section 3.6). Compared to the calibration value changes occurring between Test4 to Test6, the magnitude of changes between Test6 to Test9 is radically reduced. The heading calibration value changes from Test6 to Test8 by 0.67°. This is the largest calibration value change occurring between the four tests that were conducted without detaching the camera from the mounting frame (Test6 to Test9). The magnitude of the change does still exceed the orientation sensor heading accuracy (0.3°) and indicates inconsistent heading offset calibration. However, the magnitude of heading calibration value change is smaller than the changes occurring from Test4 to Test6. The largest change for pitch (0.22°) occurs from Test6 to Test9. This value only exceeds the orientation sensor pitch accuracy by 0.02°. Furthermore, this change occurred over an entire 6 month period, when the camera was not detached from the mounting frame. This indicates a slight instability of the pitch calibration over a 6 month period. The roll calibration is the most stable with the highest difference being 0.06°, which is smaller than the orientation sensor roll accuracy (0.2°). These results demonstrate that the rotational offset calibration stability can be improved, when the camera remains attached to the mounting frame. Despite the instability of the heading offset calibration, the rotational offset calibration values derived during the period when the camera remained attached to the mounting frame were used to provide independently derived calibration values for accuracy assessment in Section 4.2.1.2 and Section 4.2.2.2.

4.1.2.2 Stability of positional offset calibration

The stability of positional offset calibration indicates the suitability of positional calibration values derived from one data set for correcting position measurements of other data sets. The positional offset calibration values derived in Test4 cannot be compared to calibration values derived in any other test, because this test was conducted using a Total Station for positioning. Therefore, Test4 is not part of the positional offset calibration stability assessment. In Table 4.4 the first column identifies the test data set used to derive the calibration values with corresponding Δx, Δy, and Δz displayed in the three subsequent columns. Calibration value changes that do not exceed the expected DGPS accuracy indicate stable positional offset

Table 4.4: Positional offset calibration values (not including Test4).

TestID	Δx *(mm)*	Δy *(mm)*	Δz *(mm)*
Test1	-72	-201	111
Test2	2	-264	-85
Test3	-7	-241	-100
Test5	-19	-233	-102
Test6	-19	-248	-134
Test7	-27	-219	-130
Test8	-8	-221	-131
Test9	-20	-217	-127

calibration. The offset calibration value Δy essentially corresponds to height measured by DGPS, and the offset calibration value Δz essentially corresponds to planimetric DGPS positions, equivalent to Section 4.1.1.2. Therefore, offset calibration value changes in Δy were evaluated using the expected DGPS accuracy in height (30 mm) as reference. Offset calibration value changes in Δz and Δx were evaluated using the expected DGPS accuracy in plan (10 mm) as reference.

The stability of positional offset calibration can only be assessed when the same camera fixture was used during data collection, similar to the assessment of the rotational offset calibration stability (Section 4.1.2.1). Figure 4.5 depicts the values of Table 4.4 separately for tests conducted using the original camera fixture (Figure 4.5a) and tests conducted using the modified camera fixture (Figure 4.5b). Figure 4.5 demonstrates that the changes between positional offset calibration values are more significant for Test1 to Test3 (Figure 4.5a) than for Test5 to Test9 (Figure 4.5b). The largest changes occurred from Test1 to Test2. The calibration value Δx changes by 75 mm, Δy by 62 mm, and Δz by 196 mm. These changes significantly exceed the expected DGPS positioning accuracy and are too large to be a result of changes in physical offsets between camera and DGPS antenna. An explanation for these changes could be errors in DGPS positioning in Test1, probably due to multipath effects and unfavourable satellite constellation. The changes from Test2 to Test3 are less significant and meet the expected DGPS accuracy for Δx (9 mm) and Δy (23 mm). For Δz (15 mm) the changes exceed the expected planimetric DGPS accuracy. In Test1 to

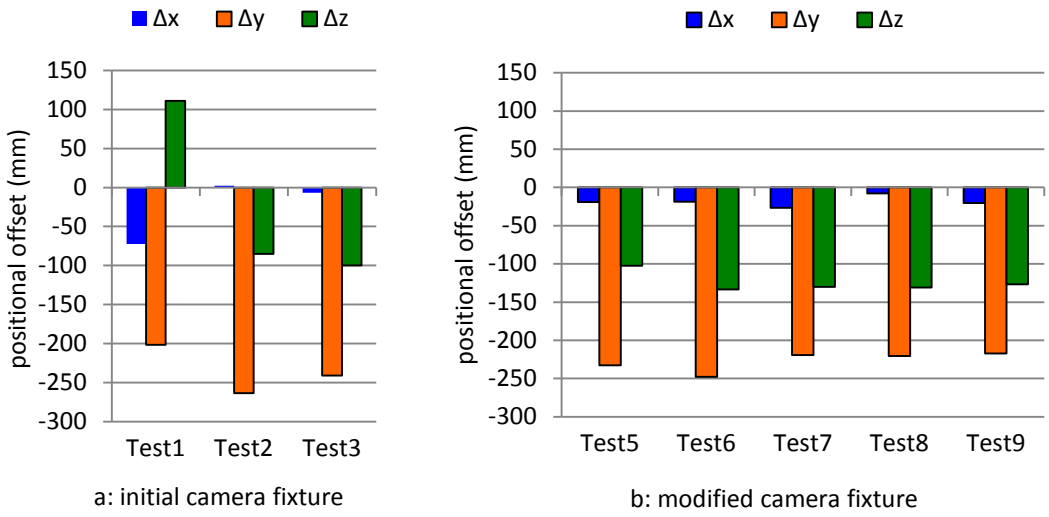

Figure 4.5: Positional offset calibration values (not including Test4).

Test3 the initial camera fixture was used. The camera was detached from the mounting frame after data collection of each test in order to access imagery stored on the memory card. Therefore, the positional offset changes between the tests are possibly introduced by re-attaching the camera. This demonstrates that stable positional offset calibration cannot be achieved using the initial camera fixture.

Figure 4.5b depicts positional calibration values derived in tests utilising the modified camera fixture approach (Test5 to Test9). The change of the z-offset calibration value (Δz) from -102 mm in Test5 to -134 mm in Test6 is the largest calibration value change between these tests. The magnitude of the change (31 mm) exceeds the expected planimetric DGPS accuracy. These calibration value changes indicate that the modified camera fixture is not capable of providing consistent positional offset calibration, when the camera is detached between the collection of differing data sets. The second largest change occurs from Δy in Test6 (-248 mm) to Δy in Test9 (-217 mm). The magnitude of the change (31 mm) only slightly exceeds the expected height accuracy of DGPS. Furthermore, this change occurred over the entire 6 month period when the camera was not detached from the mounting frame. This indicates either a slight instability of the y-offset calibration over a 6 month period or some other cause, which is further discussed in Section 6.1. The only other significant positional offset calibration value changes occur in relation to Test8. The x-offset calibration value (Δx) derived in Test8 deviates from corresponding calibration values

of Test5 to Test9 by magnitudes ranging from 11 mm to 19 mm, which exceed the expected DGPS accuracy in plan. A reason for this could be a decrease in DGPS positioning accuracy due to antenna tilt up to 32° (Section 6.1.3). The results presented in this section demonstrate that when the camera is permanently attached to the mounting frame, the positional offset calibration stability can be improved. Apart from the exception of Δx in Test8, the positional offset calibration achieved in Test6 to Test9 can be considered sufficiently stable to provide independently derived positional offset calibration values for accuracy assessment in Section 4.2.1.2 and Section 4.2.2.2.

4.2 Accuracy in object space

4.2.1 Absolute accuracy

Absolute accuracy quantifies the capability of the recording system to provide data for measurements that are accurate in relation to a national coordinate reference system. It is indicated by the RMSE of the differences between object coordinates of check points estimated in a GAP bundle adjustment using directly derived exterior orientation parameters and their true coordinates (Section 3.6.3). For Test5, all 17 coordinated points of the test object were used as check points while for all other tests every other point of the 43 coordinated test field points were used. Direct exterior orientation parameters were derived by applying calibration values to orientation and position measurements. Due to the results of the calibration stability investigation in Section 4.1.2, the achievable accuracy was assessed differently for Test1 to Test5 and for Test6 to Test9. The offset calibration achieved in Test1 to Test5 was not considered sufficiently stable to provide suitable independent calibration values for offset correction in other data sets. As a result, exterior orientation parameters for Test1 to Test5 were achieved by using offset calibration values derived from the same test data set as the direct orientation and position measurements. Exterior orientation parameters for Test6 to Test9 were derived from all possible combinations between calibration values and direct orientation and position measurements derived from Test6 to Test9 (Section 3.6.2).

4.2.1.1 Absolute accuracy achieved in Test1 to Test5

At the time absolute accuracy assessment for Test1 to Test5 was conducted, it was assumed that the best suited calibration values to correct orientation and position measurements of a data set are derived from the same data set (Section 3.6.2). The results in this section were considered to indicate the theoretically highest absolute accuracy achievable. During absolute accuracy assessment for Test6 to Test9 (Section 4.2.1.2) it was realised that calibration values derived from the same data set as the direct measurements do not always result in the highest accuracy achievable. Furthermore, there is a danger of circularity in the argument, when offset calibration values are used to correct the same measurements from where they originated. However, the results in this section are still considered to indicate the level of absolute accuracy achievable.

Table 4.5 lists the RMSE for easting, northing, and height differences between estimated and original check point coordinates achieved for Test1 to Test5. The first column identifies the test data set where calibration values and orientation and position measurements originated. The three subsequent columns display the RMSE achieved for easting, northing, and height in each test. To facilitate comparison, the RMSE of the check point coordinates is graphically represented in Figure 4.6. This figure also displays error margins for each RMSE value, indicating a 95 % confidence interval. The error margins are indicated by the vertical lines originating from the top of each bar. The resulting interval contains 95 % of all calculated check point coordinate differences and is a measure for the reliability of the calculated RMSE.

Table 4.5: Absolute accuracy (RMSE) achieved in Test1 to Test5.

Test ID	*RMSE (mm)*		
	Easting	*Northing*	*Height*
Test1	27	30	15
Test2	15	16	5
Test3	30	43	12
Test4	13	35	10
Test5	4	3	7

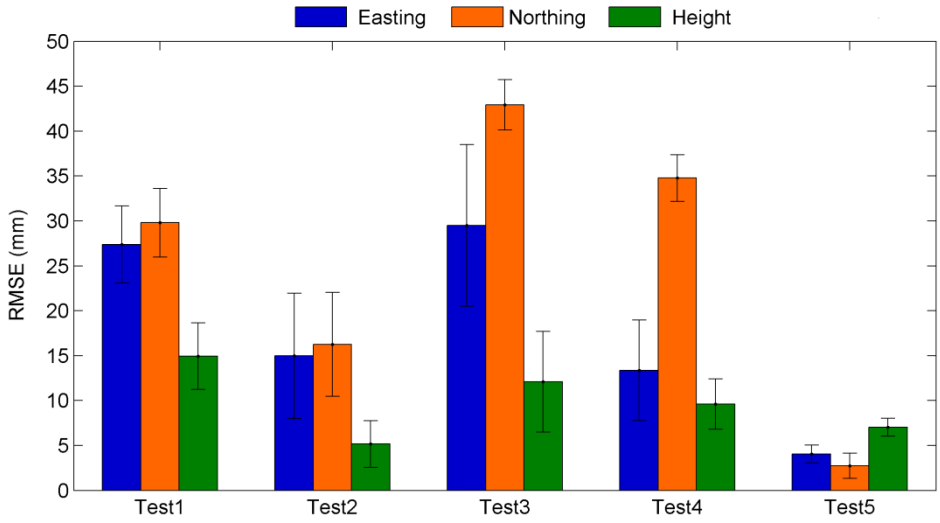

Figure 4.6: Absolute accuracy (RMSE) achieved in Test1 to Test5.

Table 4.5 and Figure 4.6 demonstrate that the recording system achieves at worst an absolute accuracy of 43 mm using the original camera fixture (Test1 to Test3) and of 35 mm using the modified camera fixture (Test4 and Test5). The error margins for the RMSE vary between 1 mm in Test5 and 9 mm in Test3 (Table 4.5). The larger margins indicate that estimated check point coordinates deviate from their true coordinates in different directions or by differing magnitudes, influencing the reliability of the RMSE.

The largest RMSE (43 mm) is achieved for northing in Test3. The smallest RMSE is achieved in Test5 with values for easting, northing, and height not exceeding 7 mm. It is striking that Test2 and Test5 achieve the two smallest RMSE (smaller than 17 mm), because in these tests some calibration value standard deviations are significantly larger than the expected orientation and positioning accuracy (Figure 4.1 and Figure 4.3). A large standard deviation indicates that the calibration value is not well suited to correct measurements at each camera station. This results in erroneous initial exterior orientation parameters at some camera stations. Test2 and Test5 suggest that these errors can be compensated during the bundle adjustment where the sum of squares of residuals are minimised, which is further discussed in Section 6.2.1.1.

Figure 4.6 also reveals inconsistency of the absolute accuracy levels achieved in each test. The achieved absolute accuracy varies between 3 mm (northing in Test5) and 43 mm (northing in Test3). A possible explanation for this could be the slightly

different image configurations used. The number of images used for accuracy assessment in each test differed slightly. Furthermore, the orientations and positions of the images slightly vary between differing test data sets. Both factors can influence the results of the bundle adjustment and could cause differences between the accuracy achieved in each test and the reliability of the accuracy value (RMSE). This could also explain why the second largest RMSE (35 mm for northing) is achieved in Test4, where Total Station was used for positioning. Positioning with Total Station is considered to be more accurate than positioning with DGPS. The higher positioning accuracy was expected to be reflected in the absolute recording system accuracy achieved in this test. The influence of image configuration on the achievable accuracy will be further discussed in Section 6.2.1.1.

4.2.1.2 Absolute accuracy achieved in Test6 to Test9

Despite some changes between offset calibration values derived from data sets of Test6 to Test9, the calibration was considered sufficiently stable to be applied to measured orientation and position parameters of any of these four tests (Test6 to Test9). The absolute accuracy achievable was assessed for all possible combinations of calibration values and direct orientation and position measurements. This also includes combinations of calibration values and orientation and position measurements originating from the same test data set. This allows the absolute accuracy achievable with independently derived calibration values to be assessed as well as comparison to the absolute accuracy achievable with theoretically best suited calibration values.

Table 4.6 contains RMSE for easting, northing, and height achieved for different combinations of calibration values and direct orientation and position measurements. The first column indicates the test data set from where the orientation and position measurements originated. This is followed by a column identifying the test data set from where the calibration values were derived. The remaining columns contain the RMSE for easting, northing, and height differences between estimated and original check point coordinates.

A graphical representation of the RMSE in Table 4.6 is provided in Figure 4.7. The upper labelling of the horizontal axis identifies the test data set from where the

Table 4.6: Absolute accuracy achieved in Test6 to Test9.

Measured parameters	*Calibration values*	*RMSE (mm)*		
		Easting	*Northing*	*Height*
Test6	Test6	13	16	3
	Test7	11	6	17
	Test8	15	13	13
	Test9	8	9	9
Test7	Test6	11	19	16
	Test7	4	6	2
	Test8	21	15	5
	Test9	7	16	8
Test8	Test6	40	31	9
	Test7	5	5	5
	Test8	10	12	3
	Test9	22	10	11
Test9	Test6	34	24	8
	Test7	9	10	10
	Test8	11	12	6
	Test9	10	10	5

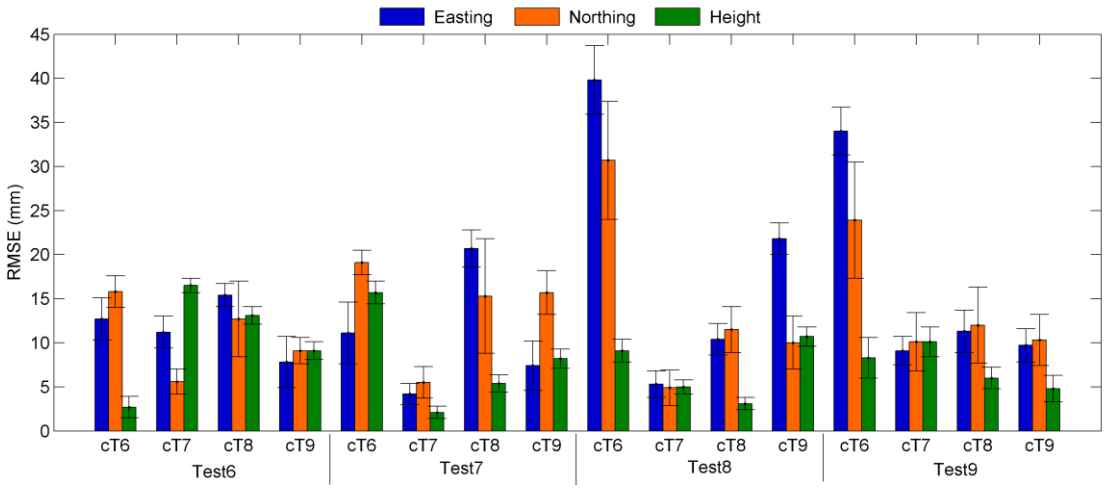

Figure 4.7: Absolute accuracy (RMSE) achieved in Test6 to Test9.

calibration values were derived. For display reasons the abbreviation “cTX” is used to denote a data set from where calibration values were derived, with “X” being a variable for the test number (6 – 9). The lower labelling identifies the test data set from where the orientation and position measurements originated.

The results displayed in Table 4.6 and Figure 4.7 demonstrate that the recording system can provide data with an absolute positional accuracy of at worst 40 mm in object space, when calibration values are derived independently of the data set to which they are applied. The RMSE for Test6 to Test9 were also calculated with a higher reliability than in Tests 1 to 5: the error margins vary only between 1 mm and 7 mm, with most margins smaller 3 mm. This suggests that estimated check point coordinates in these tests deviate from the true coordinates in the same direction and by a similar magnitude.

The largest RMSE (40 mm) was achieved when calibration values of Test6 were used to correct the measurements in Test8. The second largest RMSE (34 mm) was achieved when the same calibration values are used to correct measurements in Test9. However, most combinations achieve RMSE smaller than 20 mm. In fact, in 7 of the 16 different combinations the achieved RMSE is even smaller than 15 mm. The optimum result with the smallest RMSE is achieved when the calibration values derived from Test7 are applied to the measurements in Test8. The RMSE achieved with this combination is 5 mm in easting, northing, and height. These varied results demonstrate a significant inconsistency in the achievable absolute accuracy. It was already mentioned in Section 4.2.1.1 that this can possibly be explained by variations in the image configuration. However, variations of achievable absolute accuracy also occur when the image configuration remains unchanged. For example, all combinations where orientation and position measurements originated from Test8 were processed using identical images. Despite that, the absolute accuracy achieved varies between 5 mm when calibration values derived in Test7 were used and 40 mm when calibration values derived in Test6 were used. This indicates that the differences in calibration values can result in high variations in achieved accuracy. This issue will be further discussed in Section 6.2.1.

Furthermore, Figure 4.7 demonstrates that Test7 is the only data set where calibration values and orientation and position measurements derived from the same test data set achieved the highest absolute accuracy for this test data set. In all other cases the

highest absolute accuracy is achieved using independently derived calibration values. This indicates that using calibration values derived from the same data set as the orientation and position measurements does not generally result in the highest achievable accuracy. Therefore, the best suited calibration values for correcting direct measurements might not always be derived from the same data set. These findings suggest that the bundle adjustment minimises residuals differently for differing combinations of calibration values and direct measurements. This could have also caused the inconsistency of absolute accuracy in Test1 to Test5 (Section 4.2.1.1) and will be further discussed in Section 6.2.1.

4.2.2 Relative accuracy

The relative or inner accuracy quantifies the capability of the recording system to provide data for measurements that are accurate in relation to each other. This was assessed by comparing distances between check point coordinates estimated in a bundle adjustment with equivalent distances derived from true coordinates (Section 3.6.3). For Test5, all 17 coordinated points of the test object were used as check points while for all other tests every other point of the 43 coordinated test field points were used. Relative accuracy was assessed relating to 1D (easting, northing, and height), 2D, and 3D distances. 2D relative accuracy is the planar measurement accuracy achievable by the recording system. It combines relative easting and northing distance into a horizontal distance. 3D relative accuracy is the measurement accuracy in three dimensions combining relative easting, northing, and height distance into a slope distance. The RMSE of the distance differences indicates the relative accuracy. Relative accuracy results are presented for Test1 to Test5 and Test6 to Test9 separately, similar to Section 4.2.1.

4.2.2.1 Relative accuracy achieved in Test1 to Test5

In Section 4.2.1.2 it was revealed that calibration values and direct measurements originating from the same data set do not always result in the best absolute accuracy achievable. However, it was decided to assess the relative accuracy in Test1 to Test5 corresponding to the absolute accuracy assessment for these tests (Section 4.2.1.1).

Even when the results do not represent the best achievable relative accuracy, they provide an indicator for the level of relative accuracy achievable.

Relative accuracy values (RMSE) for easting, northing, height, horizontal and slope distances achieved for Test1 to Test5 are contained in Table 4.7. The first column of Table 4.7 identifies the test data set from where calibration values and orientation and position measurements originated. In the subsequent columns easting, northing, height, horizontal, and slope relative accuracy are displayed. RMSE for 1D distances in Table 4.7 are graphically displayed in Figure 4.8, horizontal and slope distances are displayed in Figure 4.9.

Table 4.7: Relative accuracy achieved in Test1 to Test5.

Test ID	*RMSE (mm)*				
	Easting	*Northing*	*Height*	*Horizontal*	*Slope*
Test1	19	16	18	21	26
Test2	20	17	7	8	10
Test3	26	8	16	23	28
Test4	19	9	9	18	20
Test5	3	4	3	3	3

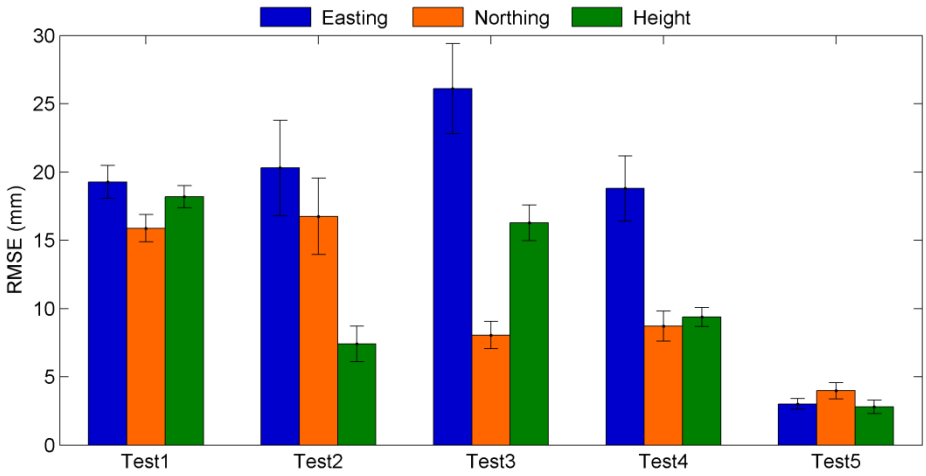

Figure 4.8: 1D relative accuracy achieved in Test1 to Test5.

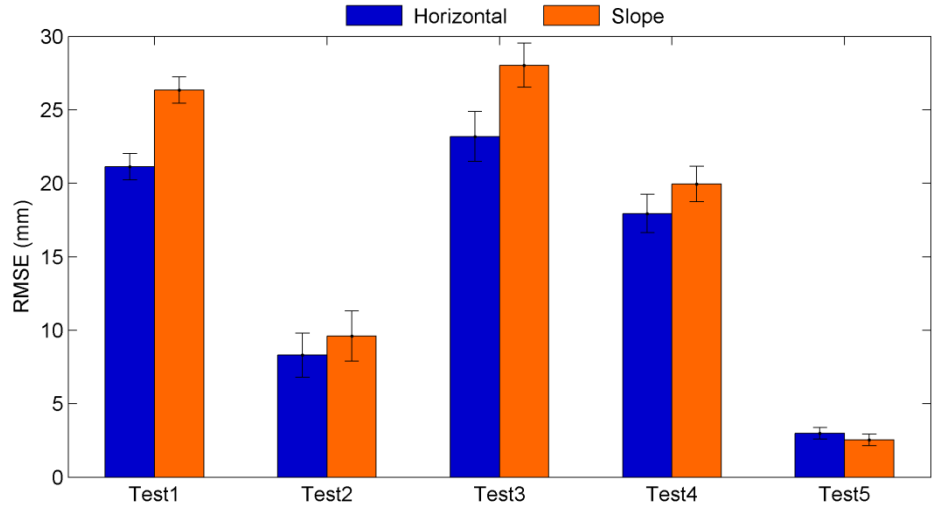

Figure 4.9: 2D and 3D relative accuracy achieved in Test1 to Test5.

Except for Test5, the largest RMSE in all tests is achieved for easting, with values ranging from 19 mm (Test4) to 26 mm (Test3). The values for northing and height are smaller than 19 mm, with some values smaller than 10 mm. The results achieved in Test5 are significantly improved compared to results achieved in the other tests, with a RMSE for easting of 3 mm, for northing of 4 mm, and for height of 3 mm. These results demonstrate that the relative accuracy achieved for Test1 to Test5 is generally improved in comparison to the corresponding absolute accuracy (Section 4.2.1.1). The error margins for relative accuracy are also smaller (1 mm to 4 mm), indicating that relative accuracy can be determined with higher reliability. However, the results in Table 4.7 also reveal inconsistency of relative accuracy achievable in differing test data sets. The inconsistency could be caused by varying image configurations between the tests, similar to the absolute accuracy assessment for these tests. Furthermore, the absolute accuracy depicted in Figure 4.6 and the relative accuracy depicted in Figure 4.8 present a similar pattern of accuracy value distribution with the smallest RMSE achieved in Test5 and the largest RMSE achieved in Test3. Therefore, it is very likely that the reason for the inconsistency in the achievable absolute accuracy is the same for the inconsistency in the relative accuracy. These findings will be further discussed in Section 6.2.

Figure 4.9 provides a graphical representation of the 2D (horizontal) and 3D (slope) RMSE achieved in Test1 to Test5 with corresponding values listed in Table 4.7. The largest RMSE was achieved in Test3 with 23 mm in 2D and 28 mm in 3D, similar to

the results for 1D relative accuracy (Figure 4.8). The smallest RMSE for both 2D and 3D is achieved in Test5 with 3 mm for 2D and 3 mm for 3D. This range of achieved RMSE again reflects the inconsistency of relative accuracy demonstrated in Figure 4.8.

Comparing 2D and 3D relative accuracy in Figure 4.9 with each other reveals that 3D relative accuracy RMSE are larger than 2D accuracy RMSE, except for Test5. This was expected, because the 3D accuracy computation includes height distance, which adds an additional error component. However, Test5 indicates that even when an additional error component is included the achieved accuracy is not always decreased compared to the accuracy achieved without the additional error component. This becomes clear also when 2D and 3D relative accuracy is compared to the corresponding 1D relative accuracy. 2D and 3D relative accuracy RMSE are derived from the combined easting, northing, and height distances and were expected to be larger than their corresponding 1D RMSE. Comparing the values in Table 4.7 it is evident that this expectation was not met in all tests. In Test2 the 2D and 3D values (8 mm and 10 mm) are significantly smaller than the corresponding easting and northing values (20 mm and 17 mm). Also in Test5, 2D and 3D relative accuracy values (3 mm) are smaller than or equal to corresponding easting and northing values (3 mm and 4 mm). This indicates that estimated coordinates of check points are rotated with respect to the national reference system (OSGB36). A reason for this rotation could be insufficiently accurate rotational offset calibration between orientation sensor and camera of the recording system. Further discussion will be provided in Section 6.2.2.

4.2.2.2 Relative accuracy achieved in Test6 to Test9

For Test6 to Test9 the achievable relative accuracy was investigated for different combinations of calibration values and direct orientation and position measurements. Table 4.8 lists the RMSE for achieved relative accuracy in Test6 to Test9. The first column identifies the test from where the orientation and position measurements originated and the second column identifies the test that was used to derive the calibration values. The following columns contain the RMSE for easting, northing, height, horizontal, and slope distances.

Table 4.8: Relative accuracy achieved in Test6 to Test9.

Measured parameters	*Calibration values*	*RMSE (mm)*				
		Easting	*Northing*	*Height*	*Horizontal*	*Slope*
Test6	Test6	8	6	4	4	4
	Test7	6	5	4	7	7
	Test8	5	15	5	7	8
	Test9	10	6	5	7	8
Test7	Test6	12	6	6	10	10
	Test7	4	6	3	3	3
	Test8	7	22	6	10	10
	Test9	10	9	6	11	12
Test8	Test6	13	23	6	5	6
	Test7	5	7	4	3	3
	Test8	6	10	3	3	3
	Test9	6	11	5	8	7
Test9	Test6	9	23	8	8	9
	Test7	5	11	6	6	7
	Test8	8	15	4	6	5
	Test9	7	9	5	6	7

A graphical representation of the 1D relative accuracy values can be found in Figure 4.10. The upper labelling of the horizontal axis identifies the test data set used to derive the calibration values and the lower labelling identifies the test data set from where orientation and position measurements originated. Figure 4.10 reveals that in most cases the smallest RMSE of any one combination is achieved for height and the largest RMSE is achieved for northing. This indicates that height measurements can be better defined in relation to each other than planar measurements.

As expected, the relative accuracy achieved in Test6 to Test9 is notably improved when compared to the corresponding absolute accuracy achieved in these tests. The largest RMSE achieved for 1D distances is 23 mm in northing for Test8 using calibration values derived in Test6. The 15 mm accuracy level is also exceeded by northing in Test9 using calibration values derived in Test6 (23 mm) and in Test7 using

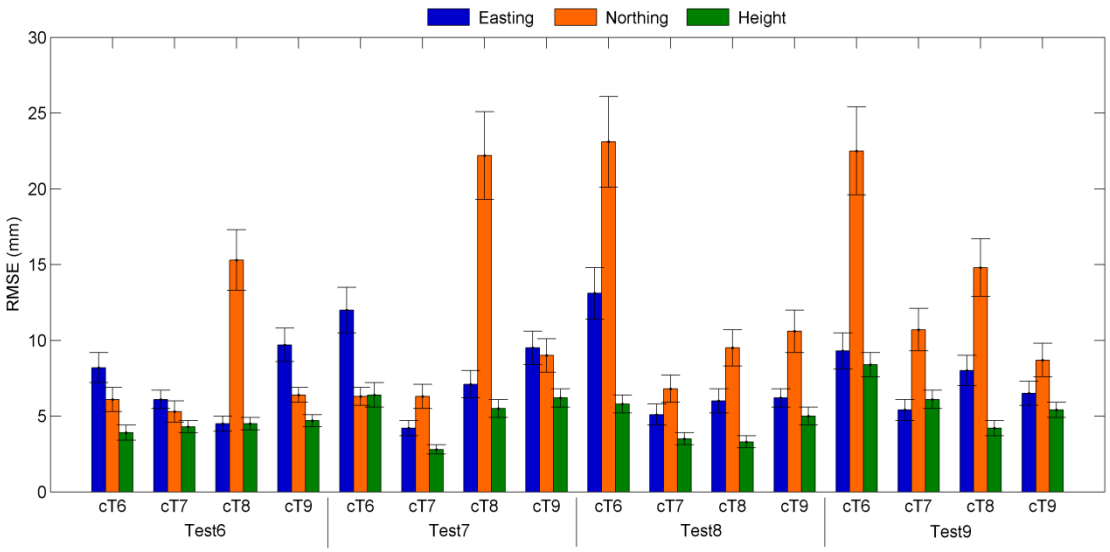

Figure 4.10: 1D relative accuracy achieved in Test6 to Test9.

calibration values derived in Test8 (22 mm). Most of the other values do not exceed 10 mm. The optimum accuracy is achieved in Test6 when calibration values derived in Test7 were used. For this combination the RMSE ranges from 4 mm for height to 6 mm for easting. Using calibration values derived from the same test data set as the direct orientation and position measurements does not always result in the smallest RMSE achieved for this test data set, similar to the absolute accuracy results presented in Section 4.2.1.2. Only in Test7 and in Test9 the smallest RMSE is achieved using calibration values and orientation and position measurements derived from the same test data set. These results again demonstrate inconsistency of the achievable relative accuracy. This inconsistency also occurs within one data set and cannot be only caused by differences in image configuration. Therefore, the inconsistency in achievable relative accuracy could also indicate that the bundle adjustment minimises residuals differently for the differing combinations of calibration values and direct measurements (Section 4.2.1.2). Furthermore, the relative accuracy results displayed in Figure 4.10 show a similar pattern of accuracy value distribution as the corresponding absolute accuracy results in Figure 4.7 (Section 4.2.1.2). The two largest RMSE in absolute and relative accuracy assessment were achieved in Test8 and Test9 when calibration values of Test6 were used. The accuracies achieved in Test7 and in Test8 using calibration values of Test7 are between the three smallest RMSE achieved for absolute and relative accuracy. This indicates correlation between

absolute accuracy achievable using one combination of calibration values and direct measurements, and relative accuracy achievable using the same combination. Therefore, the inconsistency in both, absolute and relative accuracy, probably have the same source. The reasons for the inconsistency in achievable relative accuracy will be discussed in Section 6.2.2.

Figure 4.11 displays horizontal and slope relative accuracy corresponding to the values in Table 4.8. The upper labelling of the horizontal axis identifies the origin of the calibration values used and the lower labelling identifies the origin of orientation and position measurements.

Figure 4.11 demonstrates that the recording system can achieve 2D and 3D relative accuracy of 12 mm when independently derived calibration values are used. The largest RMSE of 2D relative accuracy (11 mm) was achieved in Test7 using calibration values of Test9. The largest RMSE of 3D relative accuracy (12 mm) was also achieved in Test7 using calibration values derived from Test9. All other combinations achieve RMSE smaller than 10 mm, with most values being even smaller than 8 mm. The 3D relative accuracy achieved is in some cases higher than the 2D relative accuracy, similar to the relative accuracy results in Test1 to Test5. As already noted in Section 4.2.2.1, this indicates that the accuracy of a combination of relative distances is not always degraded compared to the accuracy of the single relative distances. Furthermore, in many cases 2D and 3D relative accuracy is

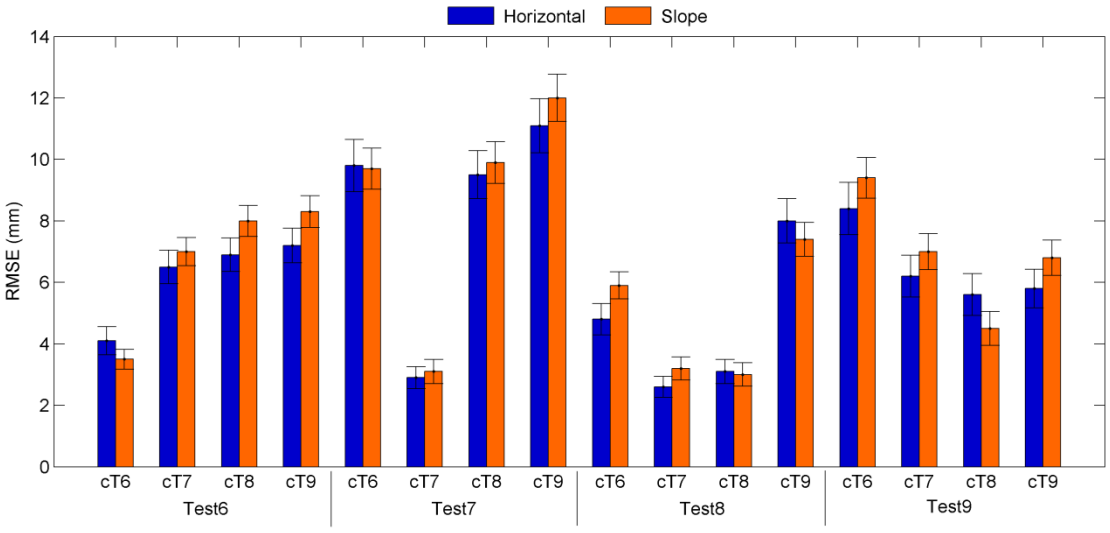

Figure 4.11: 2D and 3D relative accuracy achieved in Test6 to Test9.

significantly higher than the corresponding 1D accuracies. For example, in Test8 using calibration values of Test6, 2D and 3D relative accuracy values (5 mm and 6 mm, respectively) are less than a third of the achieved relative northing accuracy (23 mm) and less than half of the achieved easting accuracy (13 mm) (Table 4.8). This is further emphasised when the largest RMSE achieved for 1D relative accuracy and for 2D as well as 3D relative accuracy are compared. While the three largest RMSE for 1D relative accuracy are 23 mm and 22 mm, the three largest values for 2D and 3D relative accuracy are 12 mm, 11 mm, and 10 mm. As already stated in Section 4.2.2.1, the RMSE indicating 2D and 3D relative accuracy would be expected to be larger than the corresponding RMSE for 1D accuracy. Therefore, the relative accuracy results of Test6 to Test9 also suggest a small rotation of the check point coordinates with respect to the national reference system (OSGB36), due to possibly not sufficiently accurate rotational offsets. This will be further discussed in Section 6.2.2.

4.3 Summary

This chapter presented the calibration and accuracy assessment results of the initial recording system tests described in Section 3.6. It was demonstrated that similar levels of calibration value precision can be achieved with the original and the modified camera fixture. The precision of rotational offset calibration values was generally higher than the precision of the positional offset calibration values, which indicated slight positional offset changes during data collection. Further, it was revealed that stable offset calibration is only achievable when the camera remains attached to the mounting frame. However, even in this case, significant changes in the heading and the x-offset calibration values were identified.

The accuracy assessment demonstrated that the recording system can achieve an absolute accuracy of 40 mm, when independently derived calibration values are used for offset correction. The achieved relative accuracy was higher than the absolute accuracy, with 25 mm for 1D relative accuracy and 12 mm for 2D and 3D relative accuracy. The lower 2D and 3D relative accuracy indicates a small rotation of estimated check point coordinates with respect to the national reference system (OSGB36).

For absolute and relative accuracy, a significant inconsistency of achieved RMSE was noticed. Varying image configurations, calibration value changes, and the bundle adjustment minimising residuals differently for differing combinations between calibration values and direct measurements, were identified as possible sources of this inconsistency. The results and findings presented in this chapter will be further discussed in Chapter 6.

5 Cultural heritage case studies

Results presented in Chapter 4 demonstrated the potential of the recording system for image-based recording. However, these results were not obtained in a real cultural heritage recording environment. To verify the applicability of the recording system for image-based cultural heritage recording, two case studies were carried out at heritage sites located in the United Kingdom.

The first case study was conducted at St. Catherine's Oratory on the Isle of Wight. The exposed location of the site on top of a hill provided ideal conditions for utilisation of DGPS for positioning. Furthermore, the vertical structure of the case study object allowed testing the recording system for its applicability when the mounting frame is oriented approximately vertical or is slightly pitched during data collection. This is similar to the mounting frame orientation during data collection for the initial recording system tests (Section 3.6). The shape and size of the object also allowed circulating around the object during data capture. This provided an opportunity to test the recording system for a comparatively high range of measured headings. In this case study, the achievable accuracy was assessed for differing camera-to-object distances. Furthermore, the effect of the availability of a single control point on the achievable absolute and relative accuracy was investigated. The characteristics of this heritage site, data collection and findings of the case study are presented in Section 5.1.

The second case study was conducted at Roughting Linn rock-art site in Northumberland. The object that was recorded during this case study is a slightly sloping rock-outcrop with Neolithic "petroglyphs" (rock engravings). This allowed testing the recording system performance under conditions different to the initial

recording system tests (Section 3.6) and the St. Catherine's Oratory case study. A major difference was the larger pitch of the mounting frame during data collection. Data collected at Roughting Linn was also used to investigate the practicability of Google Earth to enhance access to digital cultural heritage data. Furthermore, the capability of KML to store imagery and corresponding exterior orientation parameters in a single file was developed and tested. The performance of the recording system in the Roughting Linn case study and the results of using Google Earth and KML for data visualisation and storage are presented in Section 5.2. This chapter concludes in a short summary.

5.1 St. Catherine's Oratory

St. Catherine's Oratory is located in the south of the Isle of Wight, close to the coast and on one of the highest parts of the island (English Heritage, n.d.). The monument consists of a tower and the remains of a chapel dating back to the fourteenth century, with possible repairs and rebuilding carried out in later periods (Currie, 2001; Roberts, 2004). Today, St. Catherine's Oratory is legally protected as a "Scheduled Monument" and is owned and managed by the National Trust (Roberts, 2004). In the case study, only the tower of St. Catherine's Oratory (Figure 5.1) was used for data collection. The tower of St. Catherine's Oratory is approximately 11 m high and an octagonal "Greensand" stone structure (Roberts, 2004). Including the four buttresses on the outside, the tower has a diameter on ground of approximately 4.5 m. This small ground footprint enables accessibility from all sides.

5.1.1 Data collection at St. Catherine's Oratory

Data collection at St. Catherine's Oratory was carried out from 1st to 2nd June 2010. This date is within the time period between data collection of Test5 and Test6 (Section 3.6). On the first day of the case study two survey stations, denoted SCOA and SCOB, were established adjacent to the eastern side of the tower in a static DGPS survey. Each station was occupied by the DGPS receiver for 30 minutes and GPS data

Figure 5.1:Tower of St. Catherine's Oratory on the Isle of Wight, UK.

was sampled in 2 second intervals. No coordinated point suitable for setting up a DGPS base station for this survey was available at the case study site. As a result, an active Ordnance Survey GPS Network station was used as reference. This station, which is known as "SANO", is located on the Isle of Wight within a distance of 9 km from St. Catherine's Oratory (Ordnance Survey, 2011c). At this distance the reference station "SANO" and the rover stations (SCOA and SCOB, respectively) were considered to observe the same satellites and experience similar errors due to atmospheric interference (Section 2.6.2). The DGPS measurements at SCOA and SCOB were post-processed in Leica SKI-Pro software using reference data derived from "SANO". The resulting Cartesian coordinates were converted into OSGB36 coordinates using the Grid InQuest software provided by Ordnance Survey (2011b). From SCOA and SCOB 22 points established on the eastern facade of the tower were coordinated using a Leica TCR405 Total Station. 12 of these points were marked using survey targets attached to the lower part of the tower (Figure 5.2a) that could be

reached without auxiliary means (approximately up to 2 m), analogous to the test object at Loughborough University (Section 3.2.2). Silicone sealant was used to enable a firm attachment, whilst detaching without leaving residue on the façade was still possible. For the upper part (approximately 2 m to 11 m), 10 natural points defined by distinctive features, such as corners and intersections of Greensand blocks, were selected (Figure 5.2b). From Total Station observations and survey stations coordinates, OSGB36 coordinates of the 22 points were derived after applying mean sea level and grid scale factor corrections. These coordinates were considered the true coordinates of the points established at St. Catherine's Oratory. The precision of the targeted points (3 mm) and natural points (5 mm) was assumed equivalent to the coordinated points of the test object at Loughborough University (Section 3.2.2).

Data collection with the recording system was carried out on the second day of field work using DGPS for positioning. Data was collected using the same approach as during the initial recording system tests described in Section 3.6.1. Two data sets with differing camera-to-object distances were collected. The first data set (SCO1) consists of data collected at 12 camera stations. These camera stations were arranged in an arc

a: targeted points b: natural points

Figure 5.2: Coordinated points established at St. Catherine's Oratory.

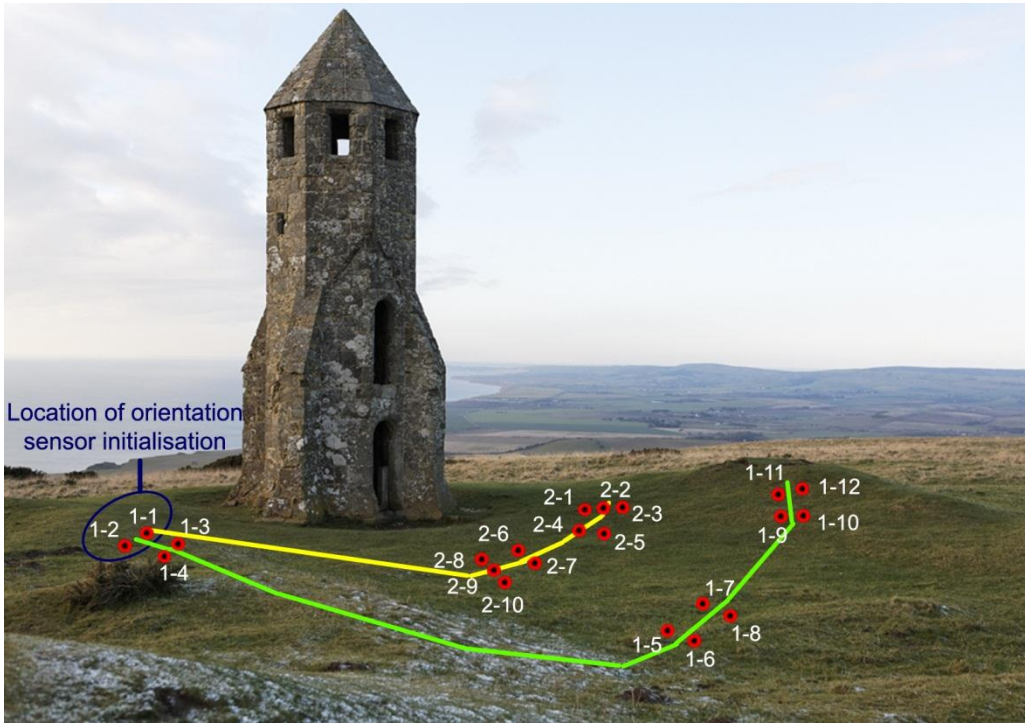

Figure 5.3: Camera station arrangement of data sets SCO1 and SCO2 (background image attribution: WyrdLight.com).

around the eastern side of the tower (Figure 5.3). The approximate camera-to-object distance for camera stations of the SCO1 data set was 10 m. At this distance only targets representing the lower half of the tower could be captured in an image frame. To capture the upper half of the tower at this distance, the mounting frame was pitched up to a maximum of 21°. Images capturing the lower and the upper half of the tower were usually taken from the same location, resulting in some camera stations being in close proximity to each other (Figure 5.3). The second data set (SCO2) consists of data collected at 10 camera stations. These camera stations were arranged in a shallow arc around the eastern side of the tower at an approximate camera-to-object distance of 6 m (Figure 5.3). In order to capture the entire height of the tower at the given camera-to-object distance, up to three images with varying pitch of the mounting frame were acquired from the same location. This resulted in pitch values up to a maximum of 28°.

At the time of data collection, the effect that local magnetic field distortions can have on the orientation sensor heading accuracy was not fully understood. Therefore, sensor initialisation was not repeated at the start of the SCO2 data acquisition phase.

This prevented using the exact data processing and data analysis described in Section 3.6.2 and Section 3.6.3. In order to resolve this issue, a copy of data collected from the two camera stations at the location of orientation sensor initialisation in SCO1 (Figure 5.3) was processed and analysed together with data of SCO2, thus increasing the number of camera stations in SCO2 to 12.

Between collecting data set SCO1 and data set SCO2 the camera initially failed to acquire any more images. To investigate this problem the camera had to be detached from the mounting frame and although the minor camera problem was solved, detaching the camera inevitably compromised the offset calibration stability.

5.1.2 Data processing and analysis

Data collected at St. Catherine's Oratory was processed and analysed using similar methods described in Section 3.6.2 and Section 3.6.3. Rotational and positional offset calibration values and their standard deviation were individually derived from each data set (SCO1 and SCO2). These values are presented in Section 5.1.3. Comparison of the obtained offset calibration values (Section 5.1.3.2) revealed that only the calibration value for positional offsets in z-direction (Δz) changes significantly between SCO1 and SCO2, although the camera was detached from the mounting frame between collecting these two data sets. Changes of similar magnitude also occurred between the initial recording system tests Test6 to Test9, where the camera was not detached from the mounting frame. Therefore, it was decided to use calibration values derived from SCO1 to correct orientation and position measurements of SCO2, and vice versa. From each case study data set, exterior orientation parameters were obtained by applying calibration values independently derived from the other case study data set. These parameters were used as initial exterior orientation in a GAP bundle adjustment, constrained by the standard deviations of their corresponding offset calibration values (Section 3.6.3). All coordinated points established at the tower of St. Catherine's Oratory were used as check points. Using the check point coordinates estimated in the GAP bundle adjustment and comparing them with their true coordinates, indicators for absolute and relative accuracy were calculated using the approach adopted in Section 3.6.3.

These results were achieved using zero control points and are presented in Section 5.1.4.1.

The data sets collected at St. Catherine's Oratory were also used to investigate whether the availability of a single coordinated point at a heritage object can significantly improve the achievable accuracy. Recognising that in real heritage recording projects it might be objectionable to attach survey targets to a heritage object, some other coordinated point could perhaps be established adjacent to the object. Such a point would provide additional control in the bundle adjustment. Furthermore, it could facilitate improvement of independently derived calibration values by compensating for offset changes occurring in the time interval between offset calibration and data collection in the field. For this investigation the approach of data processing and accuracy assessment (Section 3.6.2 and Section 3.6.3) was altered slightly. In order to enhance the comparability of the results achieved using differing data sets, a single coordinated point was available in one image only in this investigation. First, a single coordinated point was used to improve offset calibration values. Independently derived calibration values were used to preliminarily correct direct orientation and position measurements of a data set. This resulted in initial exterior orientation parameters for a "first bundle adjustment", which was performed in order to obtain truth data for offset calibration (Section 3.5). In this bundle adjustment, a single coordinated point was used as a control point with corresponding image point coordinates measured in one image only. Using the truth data obtained from "first bundle adjustment", improved offset calibration values and their standard deviations were determined. After enhancing offset calibration, the effect of a single control point on achievable absolute and relative accuracy was assessed. The improved offset calibration values were applied to the direct orientation and position measurements, resulting in improved initial exterior orientation parameters for a "second bundle adjustment". In this, the same single control point was again used with all remaining coordinated points at the case study site used as check points. The coordinates of these check points estimated in "second bundle adjustment" were finally used to assess achievable absolute and relative accuracy using the methods described in Section 3.6.3.

Accuracy assessment utilising a single control point was conducted using orientation and position measurements of both data sets collected at St. Catherine's Oratory

(SCO1 and SCO2). Calibration values derived from SCO2 were used to obtain improved calibration values for correcting direct measurements of SCO1, and vice versa. In addition, calibration values derived from Test5 of the initial recording system tests (Section 3.6) were also used to obtain improved calibration values for SCO1 and SCO2. Test5 was conducted at the "modern art" test object at Loughborough University (Section 3.2.2), which was considered representative for the type of heritage object found at St. Catherine's Oratory. The offset calibration changes between Test5 and the case study data sets are more significant than the changes between SCO1 and SCO2. The highest changes between calibration values derived from Test5 and the case study data sets occurred for Δh (more than 1.2°) and for Δz (more than 20 mm). This provided the opportunity to investigate whether a single control point can compensate for errors in initial exterior orientation parameters due to inconsistent offset calibration.

5.1.3 Offset calibration at St. Catherine's Oratory

5.1.3.1 Precision achieved

The standard deviations of the offset calibration values are indicators of the calibration precision (Section 3.5.2 and Section 3.5.3). The expected accuracy of orientation sensor and DGPS, respectively, was used as reference for assessing calibration precision (Section 4.1.1). Standard deviations that exceed the expected accuracy of their corresponding measurement device indicate significant offset changes during data collection.

Table 5.1 lists the standard deviations of the heading (s_h), pitch (s_p), and roll (s_r) offset calibration values and the range of heading offset ($s\Delta h$) derived from the data sets collected at St. Catherine's Oratory (SCO1 and SCO2). The first column

Table 5.1: Rotational offset standard deviations and $s\Delta h$ at St. Catherine's Oratory.

Data set	s_h (°)	s_p (°)	s_r (°)	$s\Delta h$ (°)
SCO1	0.10	0.23	0.19	2.15
SCO2	0.01	0.31	0.28	2.45

identifies the data set from where standard deviations and range of heading offset were derived. The subsequent three columns list the standard deviations and range of heading offset. The range of heading offset indicates the suitability of the heading calibration value to correct heading measurements that were not recorded at the location of orientation sensor initialisation. This value was included in the calibration precision assessment, because the standard deviation of the heading calibration value is only of minor significance for heading calibration precision assessment (Section 3.5.2). The range of heading offset also indicates the influence local magnetic field distortions have on the orientation sensor heading measurements. A graphical representation of the standard deviations can be found in Figure 5.4, whilst Figure 5.5 depicts the range of heading offset values.

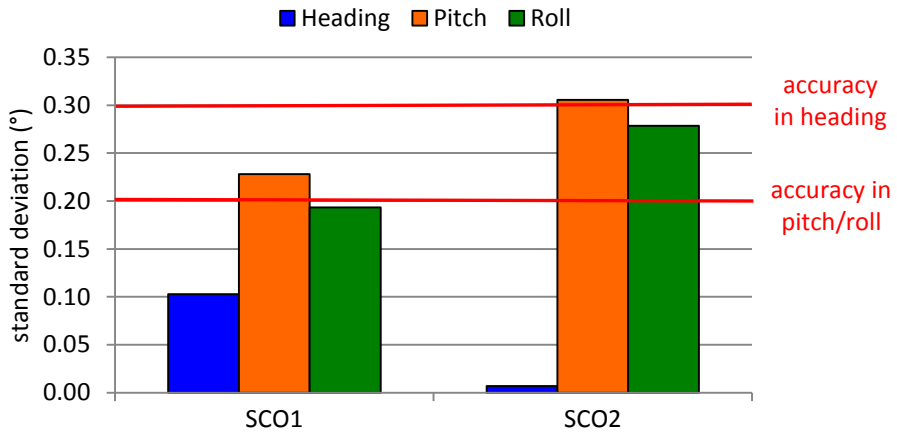

Figure 5.4: Rotational offset standard deviations at St. Catherine's Oratory.

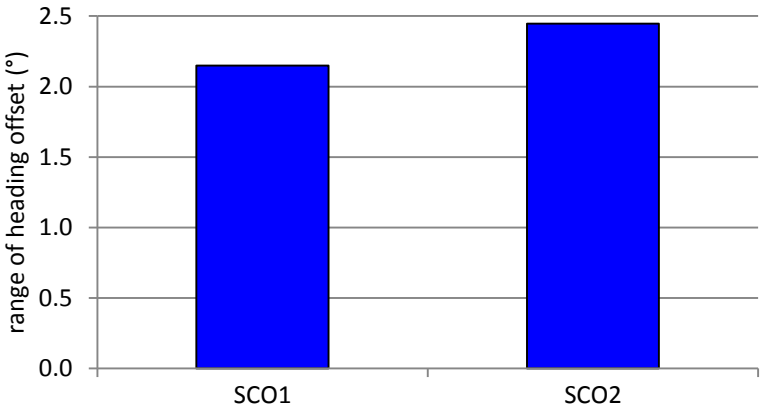

Figure 5.5: Range of heading offset at St. Catherine's Oratory.

Figure 5.4 demonstrates that the rotational calibration values derived from SCO1 are of improved precision compared to the rotational calibration values derived from SCO2. The standard deviation for pitch (s_p) in SCO1 exceeds the expected orientation sensor pitch accuracy of 0.2° (Table 3.2) only slightly by 0.03°. In SCO2 the pitch standard deviation exceeds the expected orientation sensor accuracy by a greater amount (0.11°), indicating significant pitch offset changes during data collection. In the same data set the roll standard deviation also exceeds the expected orientation sensor roll accuracy of 0.2° (Table 3.2) by a magnitude of 0.08°. The decrease in rotational offset calibration precision from SCO1 to SCO2 indicates that the smaller camera-to-object distance in SCO2 and the resulting larger pitch of the mounting frame could cause larger pitch and roll offset changes during data collection. This could suggest that either the camera moves with respect to the orientation sensor when the mounting frame is pitched or the accuracy of orientation sensor measurements decreases with larger pitch values. A more detailed discussion on this issue is provided in Section 6.1.1.

The range of heading offset $s\Delta h$ (Figure 5.5) indicates significant heading offset changes when the recording system is moved away from the location of orientation sensor initialisation. The magnitude of $s\Delta h$ is similar to the corresponding value derived in Test5 (Section 4.1.1.1). These heading offset changes during data collection demonstrate the importance of recognising the influence of local magnetic distortions on magnetometer reading of the orientation sensor.

A decrease in calibration precision from SCO1 to SCO2 is also indicated by the standard deviations of the positional offset calibration values (Table 5.2). The first column of Table 5.2 identifies the data set used to derive the standard deviations of positional offset calibration values. The subsequent three columns list the standard

Table 5.2: Positional standard deviations at St. Catherine's Oratory.

Data set	s_x *(mm)*	s_y *(mm)*	s_z *(mm)*
SCO1	13	15	16
SCO2	25	38	17

deviations in the order: s_x, s_y, and s_z. During data collection the mounting frame was oriented approximately vertical. As a result, the standard deviation for y-offsets (s_y) essentially corresponds to DGPS height measurements and is assessed using the expected DGPS height accuracy of 30 mm. The standard deviations for x-offsets and z-offsets (s_x and s_z) are assessed using the expected planimetric DGPS accuracy of 10 mm (Section 4.1.1.2).

Figure 5.6 is a graphical representation of the values in Table 5.2 and demonstrates the decrease in calibration precision from SCO1 to SCO2. In SCO1 the expected planimetric DGPS accuracy is exceeded by s_x (13 mm) and s_z (16 mm). In SCO2 the expected planimetric DGPS accuracy is exceeded by even greater magnitudes. In this data set the expected planimetric DGPS accuracy is exceeded by 15 mm in s_x and by 7 mm in s_z. These values are too large to be explained by physical offset changes between camera and DGPS antenna. In SCO2 the offset standard deviation s_y also exceeds the expected DGPS accuracy in height by 8 mm. The decrease of positional offset calibration precision from SCO1 to SCO2 could indicate that the larger pitch of the mounting frame decreased the accuracy of DGPS positioning, because it also tilts the DGPS antenna. However, in Test5, even larger pitch values were measured (33°) while the standard deviations of positional offset calibration values did meet the expected DGPS accuracy. This issue will be further discussed in Section 6.1.3.

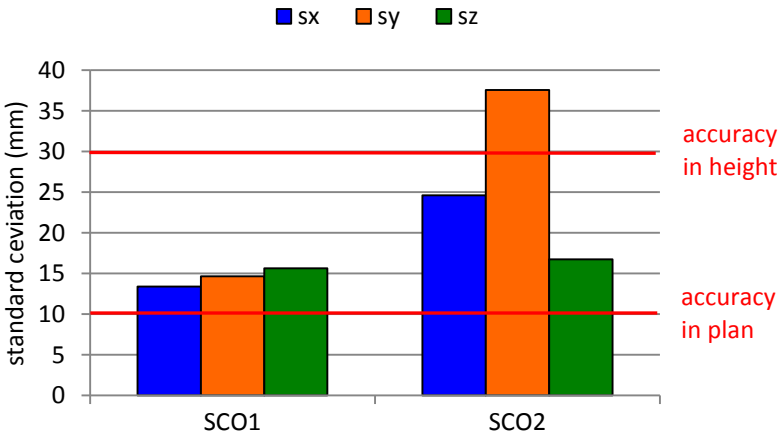

Figure 5.6: Positional standard deviations at St. Catherine's Oratory.

5.1.3.2 Calibration stability between data sets

The offset calibration stability indicates whether calibration values derived from one data set collected at St. Catherine's Oratory can be used to correct orientation and position measurements of the other data set. The calibration is considered stable or consistent when the magnitude of calibration value change does not exceed the expected accuracy of orientation sensor and DGPS, respectively. Table 5.3 lists the offset calibration values derived from data sets collected at St. Catherine's Oratory. The first column defines the data set that was used for offset calibration with subsequent columns displaying offset calibration values in the order: heading (Δh), pitch (Δp), roll (Δr), x (Δx), y (Δy), and z (Δz). Graphical representations of these values are provided in Figure 5.7 (rotational offset calibration values) and Figure 5.8 (positional offset calibration values).

Table 5.3: Offset calibration values at St. Catherine's Oratory.

Data set	*Δh (°)*	*Δp (°)*	*Δr (°)*	*Δx (mm)*	*Δy (mm)*	*Δz (mm)*
SCO1	-2.01	1.74	0.26	-12	-226	-146
SCO2	-2.10	1.68	0.45	-21	-205	-124

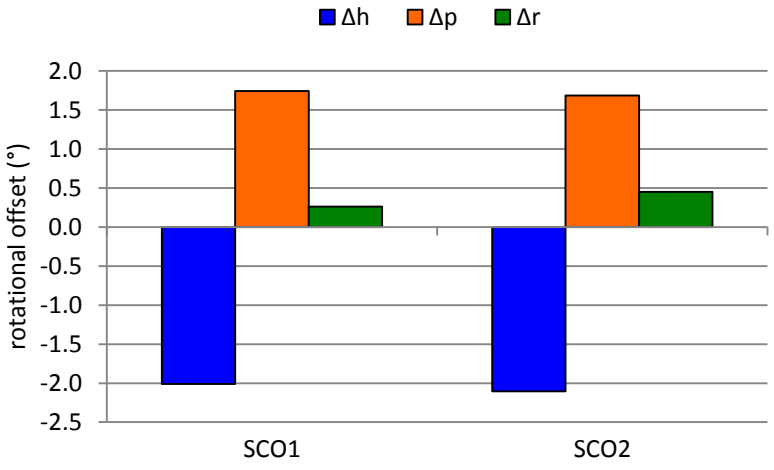

Figure 5.7: Rotational offset calibration values at St. Catherine's Oratory.

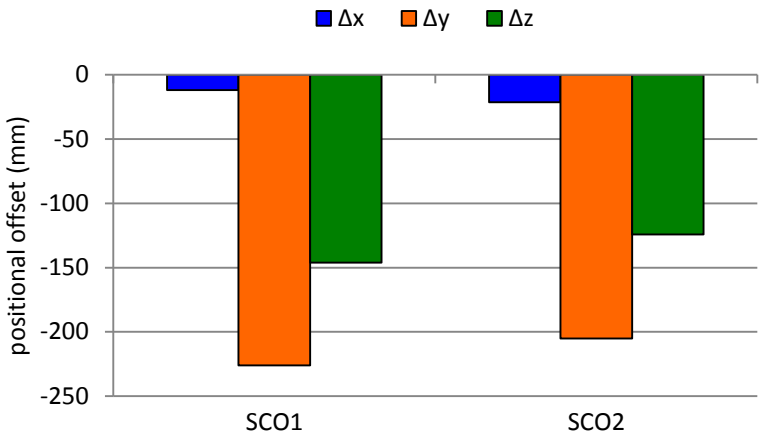

Figure 5.8: Positional offset calibration values at St. Catherine's Oratory.

Table 5.3 and Figure 5.7 demonstrate that the changes in the rotational offset calibration values do not exceed the expected orientation sensor accuracy of 0.3° for heading and 0.2° for pitch and roll. This indicates consistent rotational offset calibration between the two case study data sets, despite the differences in calibration precision (Section 5.1.3.1). However, the heading offset calibration value Δh in both data sets is derived from data of the same camera stations at the location of orientation sensor initialisation (Figure 5.3). Therefore, Δh was expected to be of the same magnitude in both data sets. The difference between the heading calibration values can be explained by using differing images during truth data creation. The images acquired at the location of orientation sensor initialisation were used in two different LPS bundle adjustments, in order to create truth data for each of the case study data sets separately. In these bundle adjustments differing sets of images were used, which resulted in varying estimated exterior orientation parameters for the images at the location of orientation sensor initialisation. This demonstrates the influence the image configuration can have on the results of the offset calibration and will be fully discussed in Section 6.1.4.

The positional offset calibration appears less stable than the rotational offset calibration. It was explained before (Section 5.1.3.1) that the mounting frame was oriented approximately vertical during data collection at St. Catherine's Oratory. Therefore, the y-offset (Δy) changes were assessed using the expected DGPS accuracy in height (30 mm) and the x- and z-offset changes (Δx and Δz) were assessed using the expected DGPS accuracy in plan (10 mm). The changes in Δx and Δy are smaller than

the expected DGPS accuracy in plan and height, respectively. This indicates consistent calibration values for x- and y-offsets. The magnitude of change in Δz is larger (22 mm) and exceeds the expected DGPS accuracy in plan by 12 mm (Table 5.3). This indicates a significant instability of the z-offset calibration. Physical offset changes of this magnitude were considered unlikely to be only caused by detaching the camera from the mounting frame. This issue will be further discussed in Section 6.1.3.

Positional offset calibration instabilities of similar magnitude also occurred between initial recording system tests Test6 to Test9 where the camera was not detached from the mounting frame (Section 4.1.2.2). Therefore, it was decided to use calibration values derived from one data set collected at St. Catherine's Oratory to correct offsets in orientation and position measurements of the other case study data set.

5.1.4 Accuracy achieved at St. Catherine's Oratory

For the St. Catherine's Oratory case study, achievable absolute and relative accuracy was assessed using zero and a single control point, respectively. In this section first the absolute and relative accuracy obtained using zero control points is presented (Section 5.1.4.1). This is followed by absolute and relative accuracy achieved using a single control point in Section 5.1.4.2.

5.1.4.1 Accuracy achieved using zero control points

The accuracy assessment results presented in this section were achieved using the data processing and accuracy assessment approaches described Section 3.6. Therefore, these results should be comparable to the results obtained in the initial recording system tests. This allows an assessment of whether significant accuracy differences occur between the initial tests at Loughborough University and a case study at a real cultural heritage object. Absolute accuracy is indicated by the RMSE calculated from differences between coordinates of check points estimated in a bundle adjustment and the accepted true coordinates of these points. All 22 coordinated points established at St. Catherine's Oratory were used as check points.

Table 5.4: Absolute accuracy at St. Catherine's Oratory using zero control points.

Direct measurements	*Calibration values*	*RMSE (mm)*		
		Easting	*Northing*	*Height*
SCO1	SCO2	10	40	36
SCO2	SCO1	39	24	42

Table 5.4 displays the absolute accuracy achieved at St. Catherine's Oratory without using any control. Offset calibration values for correcting direct orientation and position measurements of each St. Catherine's Oratory case study data set were independently derived from the other case study data set. The first column in Table 5.4 identifies the data set from where the orientation and position measurements originated and the second column identifies the origin of the calibration values used. In the subsequent columns the RMSE achieved for easting, northing, and height is displayed.

Figure 5.9 provides a graphical representation of the values in Table 5.4. The upper labelling on the horizontal axis identifies the data set from where the calibration values originated, analogous to similar representations in Section 4.2. The abbreviation "cSCOX" is used to denote a data set from where calibration value were derived, with "c" being an abbreviation for "calibration", "SCO" being an acronym

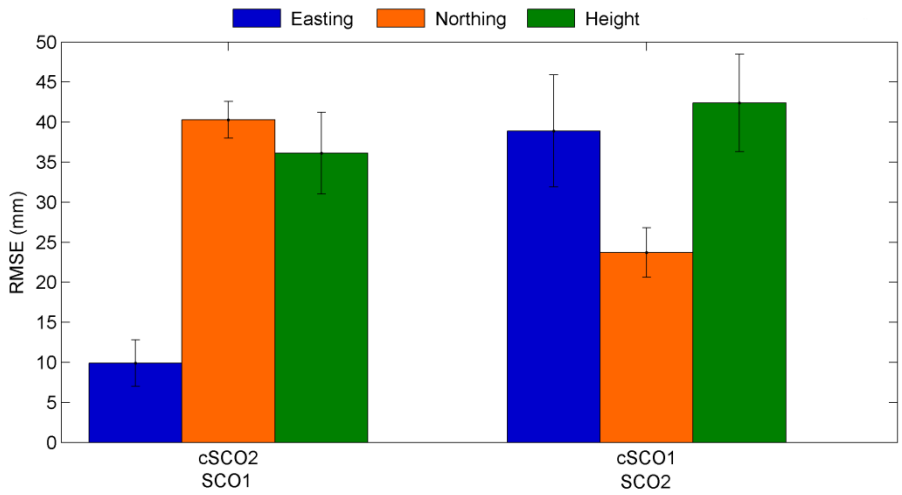

Figure 5.9: Absolute accuracy at St. Catherine's Oratory using zero control points.

for "St. Catherine's Oratory", and "X" being a variable for the data set number (1 – 2). The lower labelling on the horizontal axis in Figure 5.9 identifies the origin of orientation and position measurements used to derive initial exterior orientation parameters.

The largest RMSE obtained in each combination of calibration values and direct measurements are 40 mm (SCO1) and 42 mm (SCO2). Comparing the results depicted in Figure 5.9 to the results of the initial recording system tests at Loughborough University (Section 4.2.1) reveals that the absolute accuracy level obtained in the St. Catherine's Oratory case study is similar to the accuracy level achieved during the initial recording system tests (Section 4.2.1). Also, the RMSE was derived with similar error margins, indicating a similar reliability of these results.

Relative accuracy is indicated by the RMSE derived from distance differences between coordinated points. The RMSE was calculated for easting, northing, and height distances (1D relative accuracy), horizontal distances (2D relative accuracy), and slope distances (3D relative accuracy), similar to the approach described in Section 3.6.3. Table 5.5 presents the relative accuracy achieved with the data sets acquired during the case study at St. Catherine's Oratory. Figure 5.10 provides a graphical representation of the 1D relative accuracy displayed in Table 5.5. As expected, the relative accuracy is higher than the absolute accuracy obtained with the same combination of direct measurements and calibration values. The largest RMSE (23 mm) was achieved for easting in SCO2. The smallest RMSE (7 mm) was achieved for northing in SCO2. The range of achieved RMSE is similar to the RMSE of easting, northing, and height distances achieved in the initial recording system tests (Section 4.2.2).

Table 5.5: Relative accuracy at St. Catherine's Oratory using zero control points.

Direct measurements	*Calibration values*	*RMSE (mm)*				
		Easting	*Northing*	*Height*	*Horizontal*	*Slope*
SCO1	SCO2	9.5	7.7	16.9	6.9	17.1
SCO2	SCO1	22.7	7.3	15.4	12.0	14.5

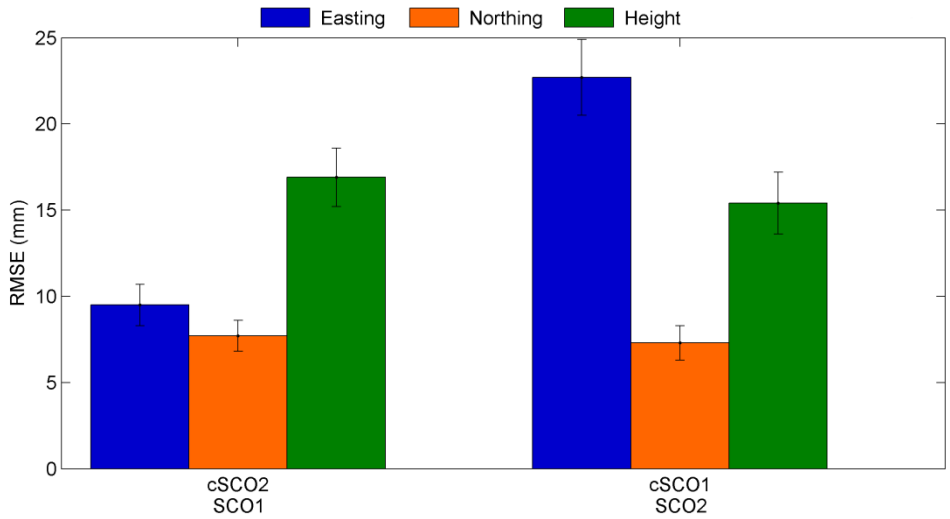

Figure 5.10: 1D relative accuracy at St. Catherine's Oratory using zero control points.

A graphical representation of the RMSE for horizontal and slope relative accuracy can be found in Figure 5.11. The largest RMSE for horizontal distances (12 mm) was achieved in SCO2. The largest RMSE for slope distances (17 mm) was achieved in SCO1. These values are within the range of 2D and 3D relative accuracy values obtained in the initial recording system tests (Section 4.2.2). In each case study data set, the achieved 3D relative accuracy is lower than the achieved 2D relative accuracy. However, 2D and 3D relative accuracy in some cases is higher than easting, northing,

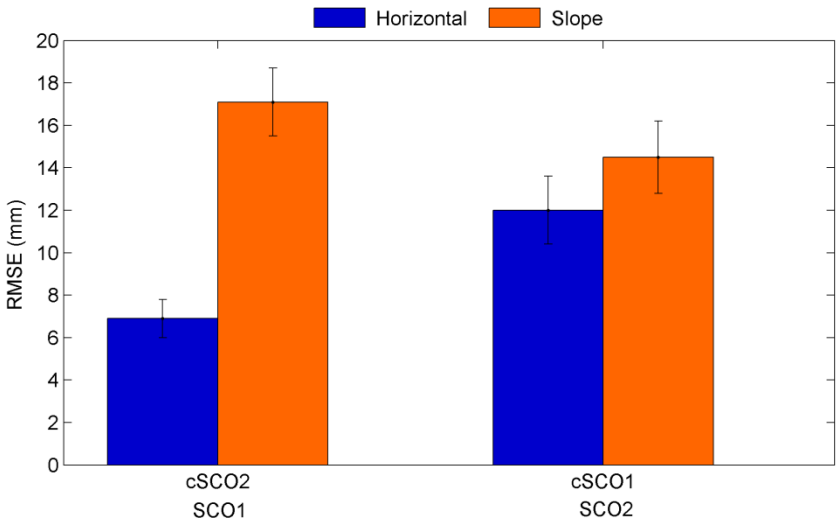

Figure 5.11: 2D and 3D relative accuracy at St. Catherine's Oratory using zero control points.

or height relative accuracy achieved with the same combination. In SCO2 the RMSE of horizontal (12 mm) and slope (15 mm) distances (Figure 5.11) are significantly smaller than the corresponding RMSE of easting distances (23 mm). They are also slightly smaller than or equal to the RMSE of height distances (15 mm) (Table 5.5). It was already explained in Section 4.2.2 that this indicates rotation of the estimated check point coordinates with respect to the national coordinate reference frame used (OSGB36). This will be discussed in more detail in Section 6.2.2.

5.1.4.2 Accuracy achieved using a single control point

The data collected at St. Catherine's Oratory was also used to investigate the absolute and relative accuracy improvements achievable, when a single control point is available for data processing and analysis. The accuracy assessment approach described in Section 3.6.3 was slightly altered, in order to facilitate the utilisation of a single control point for enhancing offset calibration and bundle adjustment result (Section 5.1.2). The accuracy obtained using a single control point is displayed in Table 5.6. The first two columns identify the origin of direct orientation and position measurements and the origin of initial calibration values. Orientation and position measurements of each case study data set were preliminarily corrected using offset calibration values derived independently from the other case study data set and from Test5 (Section 5.1.2). In the subsequent columns the RMSE obtained for easting, northing, and height are displayed. A graphical representation of these values is provided in Figure 5.12, with the upper labelling on the horizontal axis denoting the origin of calibration values and the lower labelling denoting the origin of direct measurements.

Table 5.6: Absolute accuracy at St. Catherine's Oratory using a single control point.

Direct measurements	*Calibration values*	*RMSE (mm)*		
		Easting	*Northing*	*Height*
SCO1	SCO2	11	14	21
	Test5	26	26	30
SCO2	SCO1	23	10	19
	Test5	31	21	32

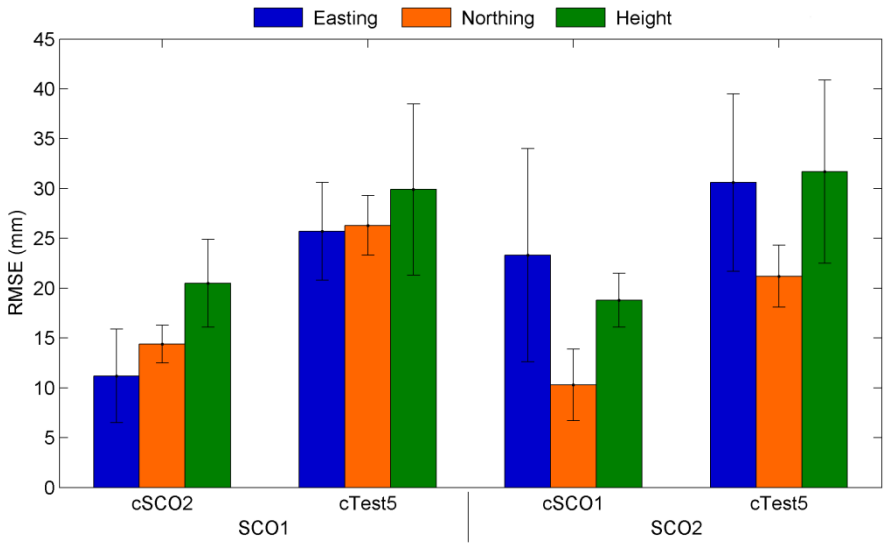

Figure 5.12: Absolute accuracy at St. Catherine's Oratory using a single control point.

Table 5.6 and Figure 5.12 demonstrate that improvements in absolute accuracy can be attained, when a single control point is available with corresponding image point coordinates in one image only. The accuracy achieved using initial offset calibration values derived from case study data sets is 23 mm or higher. The accuracy achieved using calibration values derived from Test5 is lower (38 mm). This indicates that a single control point cannot entirely compensate significant offset calibration value changes. For comparison the achievable absolute accuracy using calibration values of Test5 and zero control points was also investigated, which revealed a RMSE of 59 mm in SCO1 and 79 mm in SCO2. The significant decrease in accuracy does demonstrate the benefit of a single control point. This is further highlighted when the largest RMSE achieved using a single control point (32 mm in Table 5.6) is compared to the largest RMSE achieved using zero control points (42 mm in Table 5.4). These results demonstrate that the availability of a single control point significantly improves the achievable absolute accuracy even when only inconsistent offset calibration values are available. This is certainly due to the additional position information of the coordinated control point constraining the positions of the check points with respect to the OSGB36 reference system. However, using a single control point did slightly increase the error margins of the RMSE in Table 5.6 compared to the values in Table 5.4, indicating decreased reliability of these accuracy values. The increased error margins suggest that the differences between estimated and true check

point coordinates are less homogeneous, which could indicate distortion of the 3D check point positions caused by the additional constraint of the single control point. This will be further discussed in Section 6.2.3.

Table 5.7 contains the relative accuracy obtained with different combinations of preliminary calibration values and orientation and position measurements. Figure 5.13 provides a graphical representation of easting, northing, and height accuracy, while Figure 5.14 graphically represents horizontal and slope relative accuracy.

Figure 5.13 demonstrates that the largest RMSE for 1D distances (34 mm) was achieved for easting in SCO2 using calibration values of SCO1. Surprisingly, this indicates that the relative accuracy is lower than the absolute accuracy obtained with

Table 5.7: Relative accuracy at St. Catherine's Oratory using a single control point.

Measured Parameters	*Calibration values*	*RMSE (mm)*				
		Easting	*Northing*	*Height*	*Horizontal*	*Slope*
SCO1	SCO2	15	6	14	7	14
	Test5	16	10	28	11	28
SCO2	SCO1	34	11	9	19	8
	Test5	28	10	29	14	28

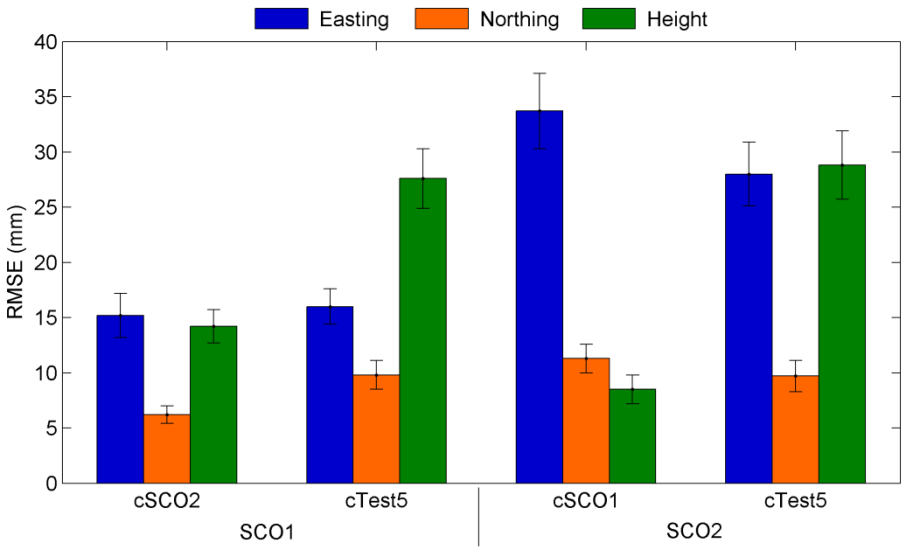

Figure 5.13: 1D relative accuracy at St. Catherine's Oratory using a single control point.

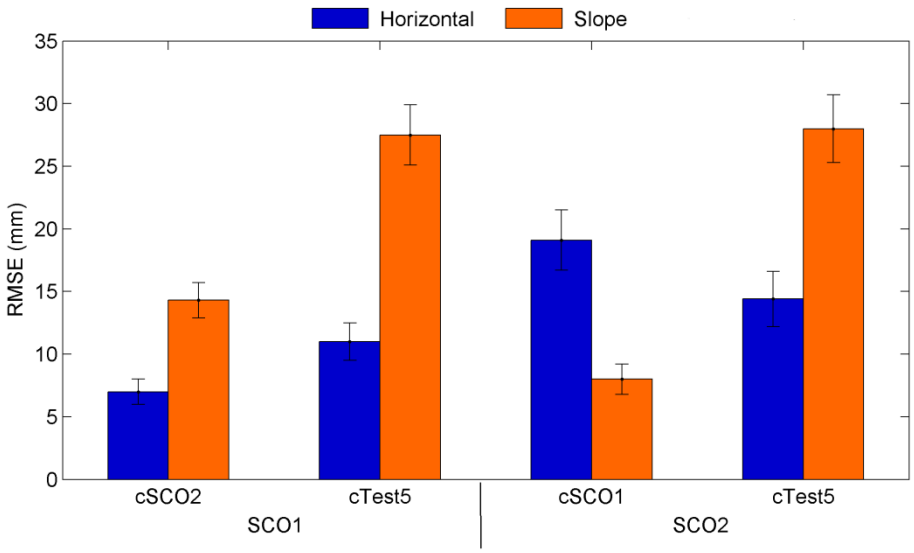

Figure 5.14: 2D and 3D relative accuracy at St. Catherine's Oratory using a single control point.

the same combination using a single control point (23 mm). The relative accuracy obtained with the other combinations is only slightly higher than the corresponding absolute accuracy achieved using a single control point. Furthermore, using a single control point resulted in RMSE of easting, northing and height distances that are larger than the RMSE achieved using zero control points. The RMSE achieved for easting in SCO1 using calibration values derived from SCO2 and a single control point (Table 5.7) is 6 mm larger than the corresponding RMSE achieved not using any control point (Table 5.5). In SCO2 using calibration values derived from SCO1 the RMSE of easting distances achieved using a single control point is even 11 mm larger than the corresponding RMSE obtained without any control point. The RMSE of northing distances achieved with the same combination is also 4 mm larger when a single control point is available. This suggests that the utilisation of a single control point in offset calibration and bundle adjustment can degrade the achievable 1D relative accuracy.

Comparing RMSE of horizontal and slope distances derived using a single control point (Figure 5.14) and RMSE derived without using any control point (Figure 5.11) reveals that 2D relative accuracy can also be degraded when a single control point is used. The RMSE achieved for horizontal distances in SCO2 using calibration values of SCO1 and a single control point is 7 mm larger than the corresponding RMSE

obtained without any control point. The decrease of relative accuracy could be caused by the additional constraint a single control point established during bundle adjustment. This will be fully discussed in Section 6.2.3.

When comparing RMSE of horizontal and slope distances (Figure 5.14) to RMSE of easting, northing, and height distances (Figure 5.13), it is revealed that in some instances 2D and 3D relative accuracy is higher than the corresponding 1D relative accuracy. The RMSE (19 mm) of horizontal distances in SCO2 using calibration values of SCO1 is 15 mm smaller than the corresponding RMSE of easting distances. The RMSE of slope distances in the same combination is even 26 mm smaller. RMSE of horizontal distances that are smaller than corresponding RMSE of easting distances also occur in SCO2 using calibration values of Test5 and in SCO1 using calibration values of SCO2. In both cases, the magnitude of RMSE of horizontal distances is approximately half the magnitude of RMSE of easting distances. This again indicates rotations of the estimated check point coordinates with respect to the national reference system (OSBG36), similar to the relative accuracy results presented in Section 4.2.2 and Section 5.1.4.1.

5.2 Roughting Linn

The second case study in this research project was conducted at Roughting Linn rock-art site in Northumberland. The site is privately owned but is freely accessible to the public. Roughting Linn rock-art site is an elliptical "Fell Sandstone" rock-outcrop (Figure 5.15) measuring approximately 20 m by 15 m and is decorated with prehistoric engraved artwork, known as "petroglyphs". It is considered to be the largest known engraved rock in Northern England (Duffy, 2010). Today Roughting Linn is legally protected as a "Scheduled Monument", similar to St. Catherine's Oratory (Section 5.1). The case study at Roughting Linn rock-art site provided an opportunity to test the performance of the recording system under very different conditions to the initial recording system tests at Loughborough University campus and the case study at St. Catherine's Oratory. The rock-outcrop forms a slightly sloping shape (Figure 5.15). This required pitching the mounting frame, resulting in

Figure 5.15: North-eastern corner of Roughting Linn rock-art site.

data being recorded with negative pitch values between -21° and -51°. Furthermore, the camera to object distance was decreased to approximately 1 to 2 m.

5.2.1 Data collection at Roughting Linn rock-art site

The case study at Roughting Linn was conducted from 23rd to 24th October 2010. The size of the rock-art site and time restrictions required to limit data collection in this case study to two sections of the rock-outcrop. One data collection section was located in the north-eastern corner of the outcrop and was labelled "RL1". The second section was located in the south-eastern corner and labelled "RL2". Four permanent survey stations close to the rock-art site had been already established by English Heritage during an earlier project (Bryan, 2010a). Diagrams of the approximate location of these stations and their OSGB36 coordinates were provided by English Heritage. However, during the site visit only one of the four stations could be found due to the undergrowth. This station was located approximately 45 m north-east of the rock-outcrop under light tree cover next to a road. This location was considered not optimal for DGPS measurements. However, this survey station was the only coordinated point available close to the case study site. The closest active Ordnance Survey GPS Network station, known as "KELS", was located at an approximate distance of 26 km

to Roughting Linn. This distance was considered too long to provide suitable reference data. Therefore, the permanent survey station 45 m north-east of the rock-outcrop was used as DGPS base station for establishing two temporary survey stations closer to the rock-outcrop in a static DGPS survey. The first survey station (RLA) was located north-east of the rock-outcrop and was designated to be used for establishing coordinated points at the first data collection section of the rock (RL1). The second survey station (RLB) was located in the south-east of the rock-outcrop adjacent to the second data collection section (RL2). The DGPS data collected at these two survey stations was post-processed using DGPS base station data and Leica SKI-Pro software. The resulting Cartesian coordinates were converted into OSGB36 coordinates, again using the Grid InQuest transformation software provided by Ordnance survey.

In each data collection section, 19 survey targets were placed on the rock surface to mark the position of coordinated points (Figure 5.16 and Figure 5.17). Targets were placed adjacent to and surrounding rock engravings, focussing data collection on areas of engraved rock, only. This resulted in targets at RL2 being not equally distributed, but perhaps concentrated in two distinct areas (Figure 5.17). In this case study it was desired to avoid attaching targets directly to the rock surface, due to the sensitivity of

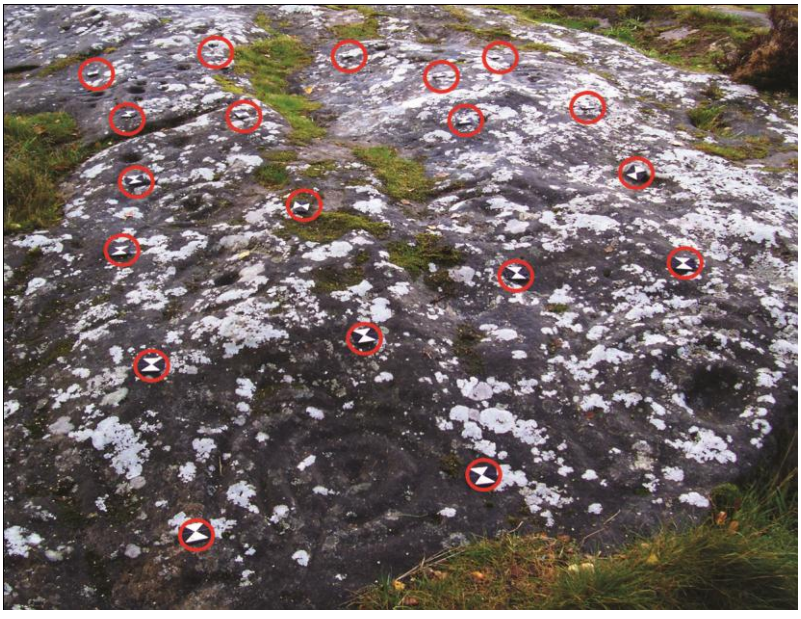

Figure 5.16: Data collection section RL1.

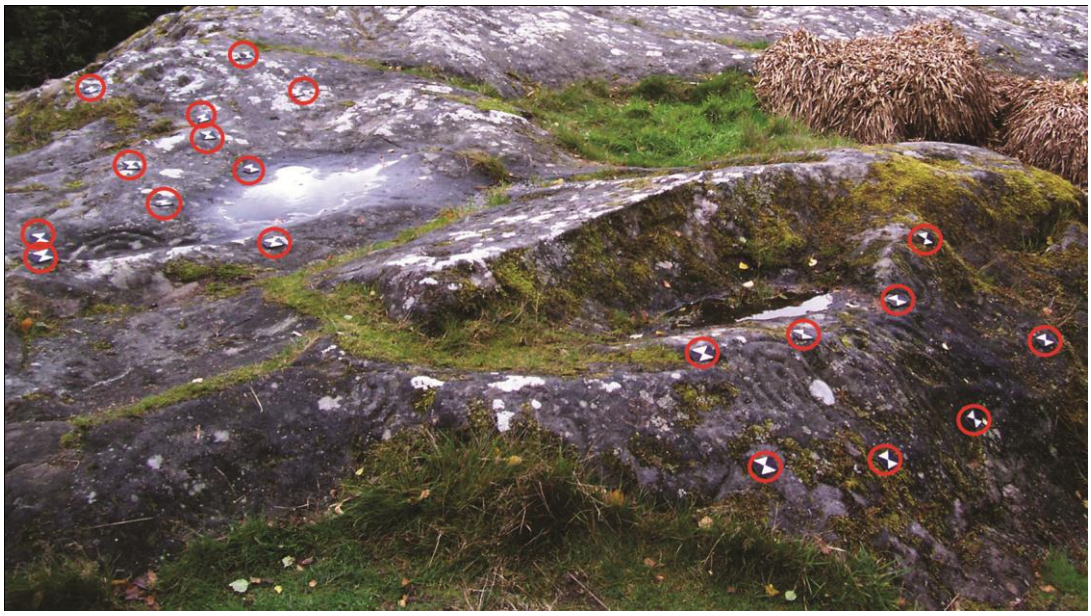

Figure 5.17: Data collection section RL2.

the rock-art site. Instead, the targets were attached to heavy metal washers that were placed on the rock surface in RL1 and RL2. The weight of the washers prevented the targets from moving by wind or rain during data collection. The targets in RL1 and RL2 were coordinated using a Leica TCR 405 Total Station located at survey stations RLA and RLB, respectively. From survey station coordinates and Total Station observations, OSGB36 coordinates for the targeted points in RL1 and RL2 were derived, after applying corrections for mean sea level and grid scale factor. The precision of the coordinates was assumed equivalent to the targeted points of the test object at Loughborough University (3 mm) (Section 3.2.2).

During processing and analysis of the recording system data collected at sections RL1 and RL2, it was noticed that the offset calibration value in y-direction (Δy) derived from the RL2 data set was significantly smaller than Δy derived from the RL1 data set. While investigating reasons for this, a discrepancy in the survey station height coordinates was discovered. During the survey of targets in RL1 the Total Station was located at survey station RLA while the prism was located at survey station RLB. The height distance between RLA and RLB derived from Total Station observations was approximately 56 mm smaller than the height distance calculated from the DGPS coordinates. This difference was reflected in the offset calibration results of data set RL2. Targets in RL2 were surveyed from station RLB, whilst station RLA was used

as DGPS base station during data collection at RL2. To resolve this problem, the height distance difference (56 mm) was subtracted from the DGPS height coordinate of survey station RLB and the coordinates of targeted points at RL2 were corrected accordingly. The height distance difference indicated errors in DGPS positioning of the two survey stations. These errors were probably caused by multipath effects (Section 2.6.3) and decreased DGPS signal reception due to light tree cover during survey station (RLA and RLB) establishment. This certainly affected the determination of horizontal survey station coordinates also, causing shift and rotation of the target point coordinates with respect to the OSGB36 coordinate system. It was not possible to quantify and compensate the error in horizontal positioning during data processing, resulting in this error being reflected in the offset calibration results (Section 5.2.2).

The approach used for data collection was similar to data collection during the initial recording system tests (Section 3.6.1). Previous to the collection of each data set the camera clock was synchronised to the laptop clock and the orientation sensor was initialised at the location of the first camera station. For the entire case study, DGPS was used for positioning with the base station set up at RLA. At the first camera station of RL1 and RL2, respectively, GPS data was acquired for 10 minutes (sampling rate 2 seconds) to enable the resolution of the cycle ambiguity (Section 2.6.2). At all subsequent camera stations GPS data was acquired for 1 minute. Initially, the data set collected at RL1 comprised imagery, orientation and position measurements from 17 camera stations (Figure 5.18) and RL2 comprised data collected at 20 camera stations (Figure 5.19). However, during DGPS post processing of the camera station positions using Leica SKI-Pro and base station data, ambiguities of the carrier phase measurements could not be resolved for all camera stations. This resulted in the positioning accuracy of 9 camera stations of RL1 and 5 camera stations of RL2 dropping to sub-meter level. For this reason, these camera stations were excluded from further data processing and accuracy assessment. Reasons for the problem in solving the carrier phase ambiguity include multipath due to tilt of the DGPS antenna during data collection and will be discussed in more detail in Section 6.1.3.

Initially, camera stations in RL1 were arranged in a semi-circle around the first data

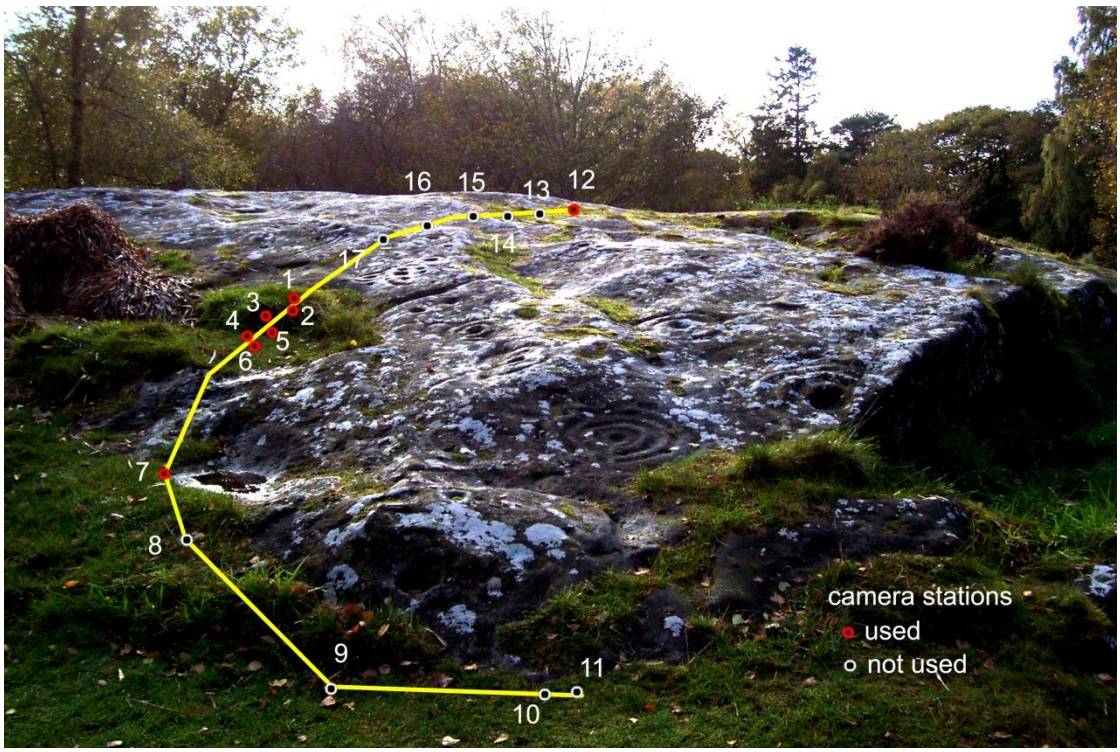

Figure 5.18: Approximate camera station arrangement RL1.

Figure 5.19: Approximate camera station arrangement RL2.

collection section (Figure 5.18), acquiring imagery of this section from differing directions. Only the DGPS positions of camera stations 1-7 and camera station 12 were sufficiently accurate to be used for further data processing and accuracy assessment. Between camera stations the pitch of the mounting frame was varied in order to capture targets directly in front of the camera tripod and those targets further away from the camera tripod.

For RL2 data was initially collected from 20 camera stations. These camera stations were arranged in three lines (Figure 5.19), due to the shape of the section of rock-outcrop that was recorded. The first line approximately aligned to the lower boundary of this section (camera stations 1-10), from which images capturing targets in the lower part of the section were acquired. Furthermore, some of these camera stations (7-10) were arranged to allow capturing all targets of this section in one image frame. The second line was approximately parallel to the first line but crossing the data collection section in the middle. Images acquired at camera stations in the second line (stations 11 to 14) captured targets in the upper part of the data collection section. The third line was aligned to the upper boundary of RL2. Camera stations in this line were also used to acquire images capturing targets in the upper part of the section, but from a different direction. However, in this line DGPS position determined with sufficient accuracy was available for only a single camera station (station 15). Therefore, data collected at the remaining 5 camera stations was not used for further data processing and accuracy assessment.

The two data sets RL1 and RL2 were processed using the approach described for the initial recording system tests (Section 3.6.2). This resulted in rotational and positional offset calibration values and their standard deviations derived from each data set separately.

5.2.2 Offset calibration at Roughting Linn

The case study at Roughting Linn was conducted on 24 October 2010, during the time period between data collection for Test8 and Test9 carried out at Loughborough University. Between Test6 and Test9 of the initial recording system tests, the camera remained attached to the mounting frame. Therefore, the camera also remained attached throughout the Roughting Linn case study. This facilitates comparison of

offset calibration results of the Roughting Linn case study data sets with calibration results of Test6 to Test9 (Section 4.1). Furthermore, the recording system clearly had to be transported to and from the case study site. This enabled assessment of the impact of physically transporting the frame on calibration stability.

5.2.2.1 Calibration precision at Roughting Linn

The standard deviations of offset calibration values are indicators of calibration precision. Table 5.8 contains the rotational offset calibration standard deviations derived from Roughting Linn data sets. As before (Section 5.1.3.1), the first column identifies the case study data set and the subsequent three columns list the standard deviations of the heading (s_h), pitch (s_p), and roll (s_r) calibration values. In the last column the range of heading offset ($s\Delta h$) is displayed, which indicates the suitability of the heading calibration value to correct rotational offsets in heading measurements of camera stations that are not at the location of orientation sensor initialisation. The range of heading offset also indicates the effect of local magnetic field distortions on the heading measurement. A graphical representation of the standard deviations is provided in Figure 5.20. Figure 5.21 depicts the range of heading offset.

The precision of rotational offset calibration was assessed using the expected accuracy of the orientation sensor (Table 3.2) as reference. Standard deviations that exceed the expected accuracy indicate significant rotational offset changes during data collection. The expected accuracy of orientation sensor heading measurements is 0.3°. This was exceeded in RL2 by 0.09°, indicating a slight difficulty in determining the heading offset. This is similar to Test5 of the initial recording system tests (Section 4.1.1.1), where the expected orientation sensor heading accuracy was also exceeded. The significance of the standard deviation of the heading offset calibration value is reduced, because this value is derived using only data from camera stations at the

Table 5.8. Rotational standard deviations and range of heading offset at Roughting Linn.

Data set	s_h (°)	s_p (°)	s_r (°)	$s\Delta h$ (°)
RL1	0.26	0.16	0.78	1.38
RL2	0.39	0.17	0.89	2.86

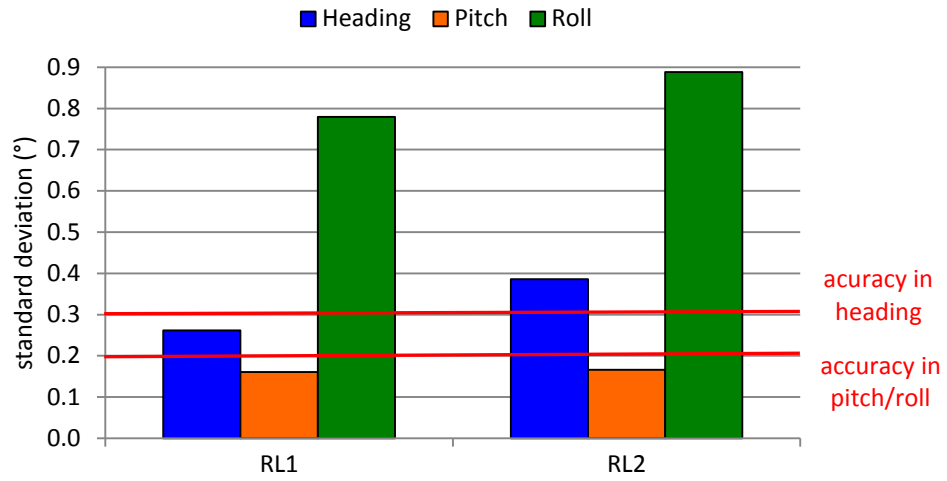

Figure 5.20: Rotational offset calibration precision at Roughting Linn.

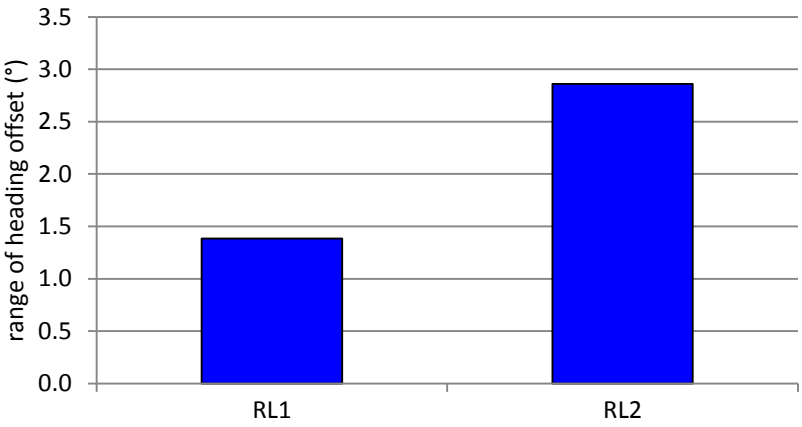

Figure 5.21: Range of heading offset ($s\Delta h$) at Roughting Linn.

location of orientation sensor initialisation. However, this could indicate local magnetic distortions at RL2 that are greater than distortions at RL1. This is further highlighted when the values of $s\Delta h$ derived from the case study data sets (Figure 5.21) are compared to each other. In RL1 the magnitude of $s\Delta h$ is 1.38°. This value increases in RL2 to 2.86°. The larger value indicates greater distortions of the local magnetic field. More detailed discussion on the influence of local magnetic field distortions is provided in Section 6.1.2.

The expected accuracy for pitch and roll measurements is 0.2°. The roll standard deviation derived from RL1 and RL2 is more than three times greater than this value (0.78° and 0.89°, respectively), indicating significant roll offset changes during data

collection (Figure 5.20). These results demonstrate significantly decreased roll calibration precision compared to the results achieved in the initial recording system tests at Loughborough University campus (Section 4.1.1.1). It was considered unlikely that this decrease in calibration precision was caused by physical strain during transport. Recording system tests conducted at Loughborough University before (Test8) and after (Test9) the Roughting Linn case study achieved roll standard deviations that met the expected roll accuracy (Section 4.1.1.1). Further investigation suggested that significant roll offset changes during data collection at Roughting Linn were caused by a slight instability of the camera fixture combined with high mounting frame tilts during data collection. This will be further discussed in Section 6.1.1.

The precision of positional offset calibration at Roughting Linn is indicated by the standard deviations displayed in Table 5.9. The first column denotes the case study data set from where calibration values were derived. The subsequent three columns list the standard deviations for offsets in x- (s_x), y- (s_y), and z-direction (s_z) of the camera coordinate system. A graphical representation of these values is provided in Figure 5.22.

For assessing the precision of positional offset calibration the expected accuracy of DGPS was used as reference. According to Konecny (2003), the expected DGPS accuracy in plan is 10 mm and in height is 30 mm. During data collection at Roughting Linn the mounting frame was pitched between -21° and -51°. Therefore, the mounting frame cannot be considered to be oriented approximately vertical during data collection. However, only two camera stations exceeded absolute pitch values of 45°. The offset calibration value in y-direction (Δy) is mainly influenced by the height measured with DGPS (Figure 3.13). Therefore, the corresponding standard deviation s_y is assessed using the DGPS height accuracy (30 mm) as reference, similar to

Table 5.9: Positional standard deviations at Roughting Linn.

Data set	s_x *(mm)*	s_y *(mm)*	s_z *(mm)*
RL1	18	33	36
RL2	17	26	15

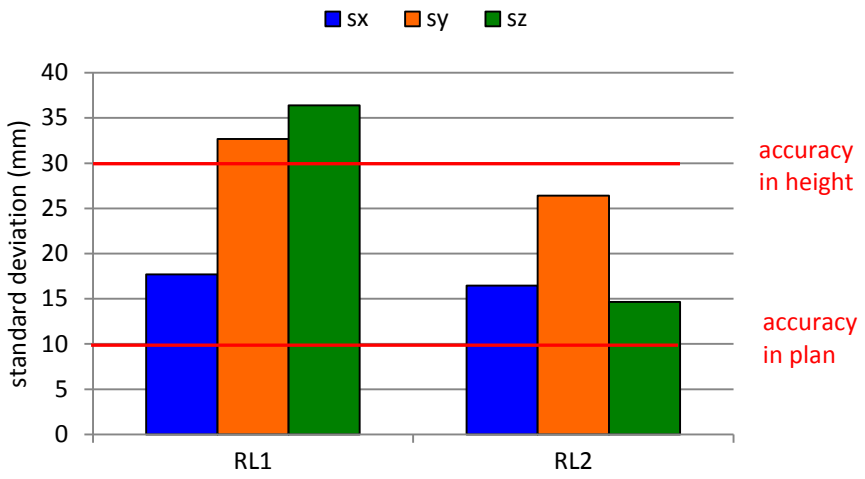

Figure 5.22: Positional offset calibration precision at Roughting Linn

positional calibration precision assessment for the initial recording system tests (Section 4.1.1.2) and for the St. Catherine's Oratory case study (Section 5.1.3.1). For the same reason, the offset calibration value in z-direction (Δz) is essentially influenced by the measured horizontal position (easting and northing). As a result, the corresponding standard deviation s_z is assessed using the expected DGPS accuracy in plan (10 mm) as reference value. The expected DGPS height accuracy is exceeded by s_y in RL1 (33 mm) only. In both data sets the standard deviations s_x and s_z exceed the planimetric DGPS accuracy by magnitudes between 5 mm (s_z in RL2) and 26 mm (s_z in RL1). This indicates significant positional offset changes during data collection that cannot be explained by recording system components moving with respect to each other. These results suggest that the large pitch (-21° to -51°) of the mounting frame during data collection decreased the accuracy of DGPS positioning, because the DGPS antenna is also tilted. This is further emphasised when the standard deviations of positional offset calibration values are compared to standard deviations achieved in initial recording system tests using DGPS and the same camera fixture (Test5 to Test9) (Section 4.1.1.2). The pitch measured during data collection for these tests (0° to 33°) was smaller than the pitch measured during the Roughting Linn case study. Calibration value standard deviations s_y derived from Test5 to Test9 do not exceed the expected DGPS height accuracy. Standard deviations s_x and s_z exceed the expected planimetric accuracy, but only by up to 7 mm. The issue of decreasing DGPS positioning accuracy due to antenna tilt will be further discussed in Section 6.1.3.

5.2.2.2 Calibration stability at Roughting Linn

Calibration stability indicates the suitability of calibration values derived from one data set to correct offsets in orientation and position measurements of other data sets. A calibration value is considered stable or consistent when the magnitude of calibration value change between data sets does not exceed the expected accuracy of orientation sensor and DGPS, respectively. Table 5.10 displays the rotational and positional offset calibration values derived from case study data sets at Roughting Linn. The first column denotes the data set and the subsequent columns list the calibration values in the order: heading (Δh), pitch (Δp), roll (Δr), x-offset (Δx), y-offset (Δy), and z-offset (Δz). The calibration stability of the Roughting Linn data sets was assessed by comparing the offset calibration values derived from RL1 and RL2 to calibration values obtained in Test6 to Test9 of the initial recording system tests. During the entire time period of collecting these data sets, the camera was not detached from the mounting frame. Figure 5.23 provides a graphical representation of the rotational offset calibration values in Table 5.10. In order to enhance comparison, the rotational offset calibration values derived in Test6 to Test9 (Table 4.3) are also displayed in chronological order. The pitch and roll offset calibration values of the case study data sets were considered consistent, because the magnitude of change between the values is smaller than the expected pitch and roll accuracy (0.2°) of the orientation sensor. The magnitude of change in the heading calibration (0.37°) slightly exceeds the expected orientation sensor heading accuracy (0.3°). Heading offset calibration changes of similar magnitude also occurred between the initial recording system tests (Test6 to Test9) (Section 4.1.2.1). These results demonstrate that the rotational offset calibration between the case study data sets is consistently at the same level as the rotational offset calibration between the initial recording system tests

Table 5.10: Offset calibration values at Roughting Linn.

Data set	Δh (°)	Δp (°)	Δr (°)	Δx (mm)	Δy (mm)	Δz (mm)
RL1	-4.85	1.42	-1.06	-10	-201	-51
RL2	-5.22	1.46	-1.14	-13	-205	-49

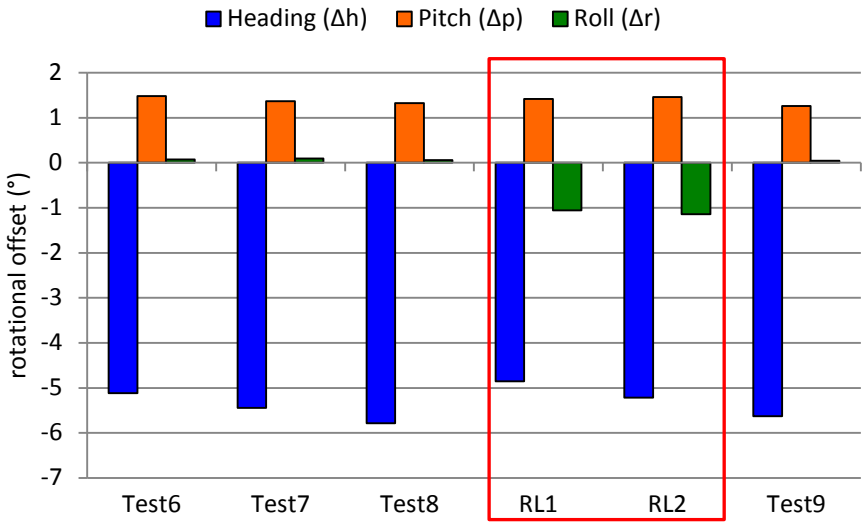

Figure 5.23: Rotational offset calibration values at Roughting Linn and in Test6 to Test9.

(Test6 to Test9). However, comparing calibration results of the Roughting Linn case study to initial test calibration results, reveals significant changes in the roll calibration values. In Test6 to Test9 roll calibration values between 0.04° and 0.1° were obtained. The roll offset calibration values derived from the case study data sets are -1.06° and -1.14°, respectively, indicating roll offset changes greater than 1°. These changes were probably not caused by physical movement during transport to the case study site. The roll offset derived in the recording system test after the case study was conducted (Test9) is similar to the roll offsets derived in the initial tests conducted before the case study (Test6 to Test8). This suggests that transporting the recording system has no significant impact on the rotational offset calibration stability. Therefore, the change in roll offset must be specific to data collection at Roughting Linn. An explanation for the roll calibration value changes could also be the slight instability of the camera fixture in combination with high mounting frame tilts that was already mentioned in Section 5.2.2.1. A detailed discussion of this issue will be provided in Section 6.1.1.

Figure 5.24 provides a graphical representation of the positional offset calibration values listed in Table 5.10. In order to facilitate comparison, the positional offset calibration values derived in Test6 to Test9 (Table 4.4) are also displayed in Figure 5.24. The magnitudes of changes in the positional offset calibration values

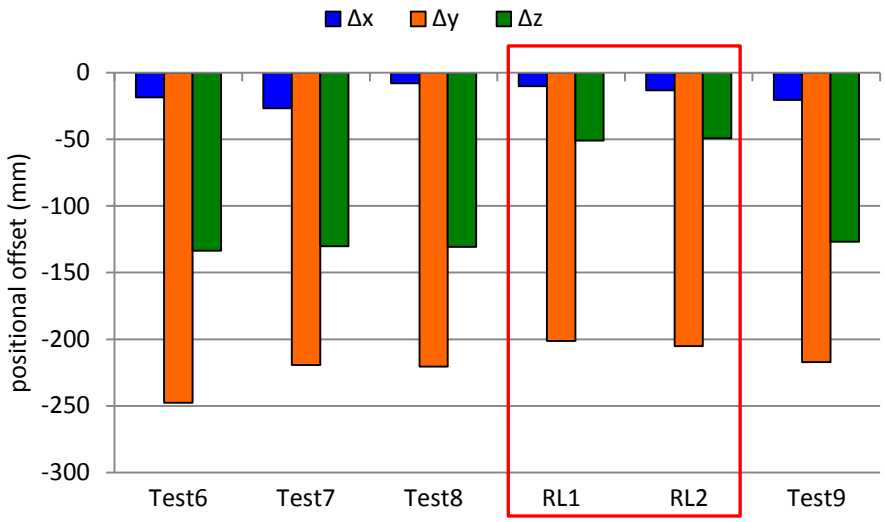

Figure 5.24: Positional offsets derived at Roughting Linn and in Test6 to Test9.

between RL1 and RL2 do not exceed the expected DGPS accuracy (10 mm in plan and 30 mm in height). Therefore, the calibration between these two data sets is considered consistent. However, comparing the positional offset calibration values derived at Roughting Linn with the values derived in Test6 to Test9 reveals significant calibration value changes. The calibration values Δx of RL1 and RL2 are within the range of calibration values derived in Test6 to Test9. However, Δx between Test7 and the case study data sets changes by 17 mm and 14 mm, respectively. This exceeds the expected DGPS accuracy in plan. The y-offset calibration changes were assessed using the expected DGPS accuracy in height as reference, equivalent to the assessment of positional calibration precision (Section 5.2.2.1). The magnitude of the change in Δy from Test6 to RL1 and RL2 is 46 mm and 43 mm, respectively. These values significantly exceed the expected DGPS accuracy in height. An even more significant change occurred for the z-offset calibration values. The z-offset calibration values (Δz) derived in the Roughting Linn case study (Table 5.10) are -51 mm and -49 mm, respectively. Corresponding calibration values derived in Test6 to Test9 range from -127 mm to -134 mm (Table 4.4). This demonstrates z-offset calibration value changes between initial tests and case study of at least 75 mm. The magnitudes of these positional offset changes are certainly too high to be explained by instability of the physical offsets between DGPS antenna and camera. Furthermore, positional offset calibration values derived before (Test8) and after (Test9) demonstrate a return

to the original offset calibration values (Section 4.1.2.2). This indicates that transporting the recording system did not affect the positional offset calibration stability. It was indicated in Section 5.2.1 that errors in DGPS positioning of the survey stations did cause the target point coordinates to shift and rotate with respect to the OSGB36 coordinate system. The error in height could be compensated, but it was not possible to quantify the error in horizontal positioning. When comparing "truth data" derived using these target point coordinates with direct measurements during offset calibration, this positional error is reflected in the calculated x- and z-offsets. This certainly explains the significant changes in Δx and Δz between Roughting Linn data sets and initial test data sets (Test6 to Test9). Another factor that possibly contributed to the positional offset calibration value changes is the decrease in DGPS positioning accuracy due to tilting the DGPS antenna during data collection. This can also explain the significant changes in Δy and will be discussed in Section 6.1.3.

5.2.3 Accuracy achieved at Roughting Linn

Heritage recording projects that do not utilise control points and rely on directly determined exterior orientation only, would require determination of physical offsets between recording system components prior to field work. The lack of control points at the field work site prevents the detection of calibration value changes. The assessment of the calibration stability for the Roughting Linn data sets (Section 5.2.2.2) revealed significant changes in the rotational and positional offset calibration values. Despite these changes, calibration values derived from data sets of Test6 to Test9 were used to correct the direct measurements of the case study data sets for rotational and positional offsets. These corrected measurements were used as initial exterior orientation parameters in a bundle adjustment, in which the coordinated points of RL1 and RL2, respectively, were used as check points. From the check point coordinates estimated in the bundle adjustment and their true coordinates, absolute and relative accuracy were assessed using the approach described in Section 3.6.3. This enabled the evaluation of the accuracy achievable when offset calibration changes occur between offset calibration at a calibration site and data collection during field work. Additionally, the calibration values derived from one Roughting Linn case study data set were also used to independently correct direct measurements

of the other Roughting Linn case study data set. This facilitates comparison of absolute and relative accuracy values obtained using inconsistent calibration values derived at the test field at Loughborough University (Section 3.2.1) and absolute and relative accuracy achieved using more consistent calibration values for offset correction.

5.2.3.1 Absolute accuracy at Roughting Linn

The RMSE of differences between estimated and true check point coordinates is an indicator of achieved absolute accuracy. Table 5.11 lists the RMSE for easting, northing, and height obtained with different combinations of direct measurements (first column) and calibration values (second column). Columns 3 to 5 display the easting, northing, and height RMSE achieved. A graphical representation of the values in Table 5.11 is provided in Figure 5.25. The upper labelling on the horizontal axis denotes the origin of the calibration values and the lower labelling denotes the data set of the direct measurements, similar to graphs in Section 4.2.1.2 and Section 5.1.4.

Figure 5.25 demonstrates that the absolute accuracy achieved using direct measurements of RL2 is significantly degraded when compared to the absolute accuracy obtained using direct measurements of RL1. The largest RMSE in RL2 is

Table 5.11: Absolute accuracy achieved at Roughting Linn.

Direct measurements	*Calibration values*	*RMSE (mm)*		
		Easting	*Northing*	*Height*
RL1	RL2	18	19	5
	Test6	37	38	48
	Test7	39	48	20
	Test8	44	47	20
	Test9	40	44	27
RL2	RL1	7	20	39
	Test6	21	36	122
	Test7	27	55	97
	Test8	30	52	105
	Test9	21	55	113

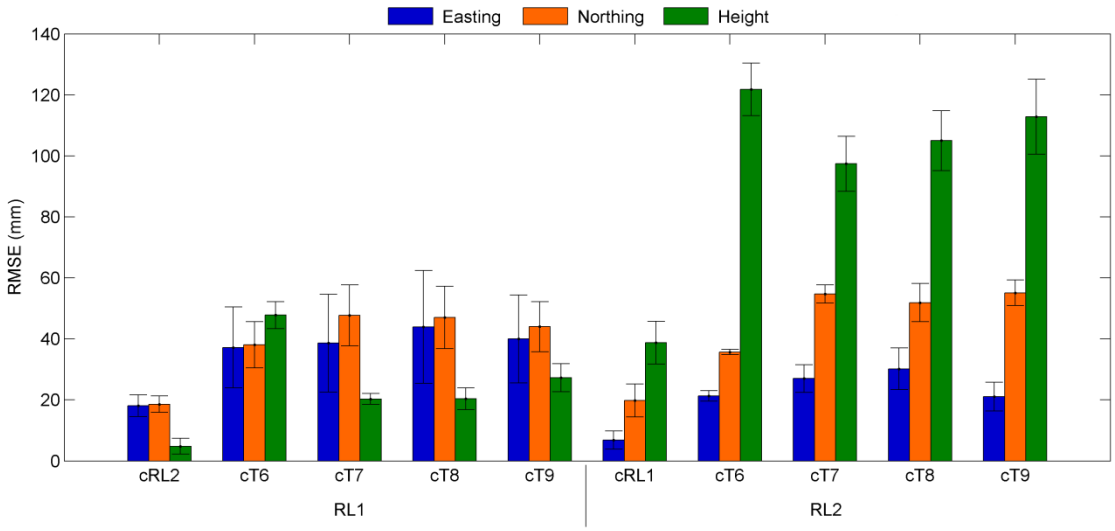

Figure 5.25: Absolute accuracy achieved at Roughting Linn.

122 mm and was achieved for height when calibration values of Test6 are used. RMSE of similar magnitudes (97 mm to 113 mm) were also achieved with combinations of direct measurements originating from RL2 and calibration values originating from initial recording system tests (Test7 to Test9). The largest RMSE in RL1 is 48 mm and was achieved for height using calibration values of Test6. Similar RMSE were also achieved with the other combinations of direct measurements originating from RL1 and calibration values derived from initial recording system tests (Test7 to Test9). These combinations almost achieved the absolute accuracy level of 40 mm in Test6 to Test9 (Section 4.2.1.2). This suggests that the offset calibration value changes between initial test data sets and case study data sets could be compensated during bundle adjustment in RL1 but not in RL2, which will be explained in Section 6.2.1.

As expected, offset calibration values derived from RL1 and RL2 were more consistent and better suited to correct orientation and position measurements recorded during the Roughting Linn case study. Applying calibration values of RL2 to measurements of RL1, and vice versa, resulted in higher absolute accuracy than when using calibration values derived in Test6 to Test9. For RL1 using calibration values of RL2 the largest RMSE achieved was 19 mm (for northing). In RL2 using calibration values of RL1 the largest RMSE achieved was 39 mm (for height). Again, the absolute accuracy in RL2 is lower than in RL1. For each other combination using orientation and position measurements of RL2, the RMSE obtained for height is

significantly larger than the RMSE for easting and northing. The RMSE values of easting and northing in these combinations are closer to corresponding values obtained in RL1. This suggests a source of error in the data of RL2 that in particular influences the absolute height accuracy and could not be compensated during bundle adjustment. This will be further discussed in Section 6.2.1.3.

5.2.3.2 Relative accuracy at Roughting Linn

The RMSE of distance differences between check points (Section 3.6.3) was used as indicator of the achieved relative accuracy. Table 5.12 displays the RMSE of 1D (easting, northing, height), 2D (horizontal), and 3D (slope) distances. This table is structured similar to Table 5.5 in Section 5.1.4.1, with the origins of direct measurements and calibration values in the first two columns followed by the RMSE of 1D, 2D, and 3D distances. Graphical representations of the values in Table 5.12 are provided in Figure 5.26 (1D distances) and in Figure 5.27 (2D and 3D distances).
Figure 5.26 demonstrates that the best 1D relative accuracy in each data set (RL1 and RL2) was achieved when calibration values derived from a case study data set are used to correct rotational and positional offsets. In RL1, using calibration values derived from RL2, RMSE of 1D distances between 7 mm and 10 mm were achieved.

Table 5.12: Relative accuracy achieved at Roughting Linn.

Direct measurements	*Calibration values*	*RMSE (mm)*				
		Easting	*Northing*	*Height*	*Horizontal*	*Slope*
RL1	RL2	10	7	7	7	8
	Test6	36	21	12	39	36
	Test7	43	27	5	48	46
	Test8	50	28	10	49	46
	Test9	39	22	12	41	38
RL2	RL1	9	17	22	16	14
	Test6	5	3	27	4	4
	Test7	14	9	28	6	7
	Test8	22	20	31	4	4
	Test9	15	13	39	4	5

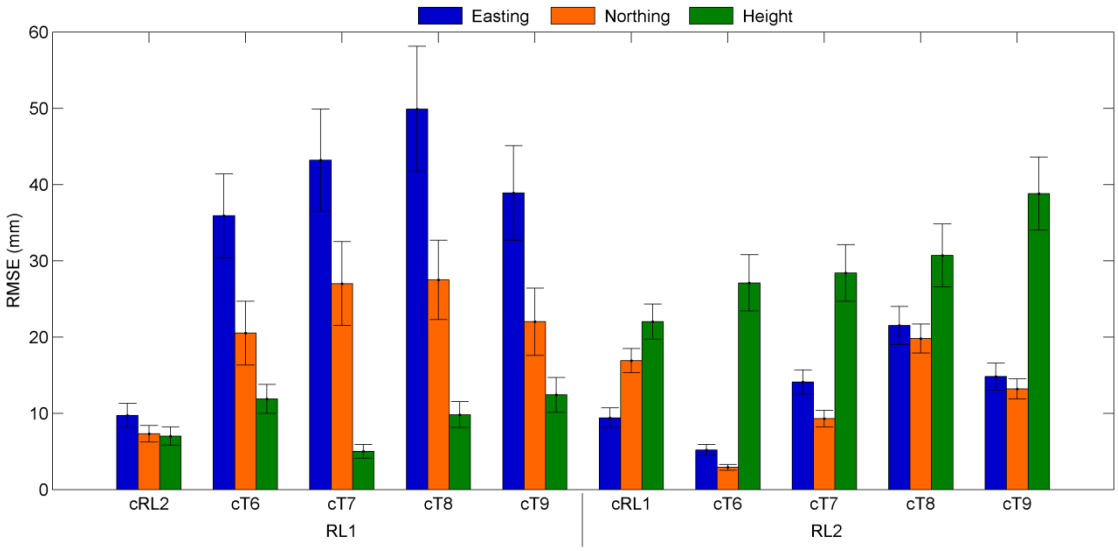

Figure 5.26: RMSE of easting, northing and height distances at Roughting Linn.

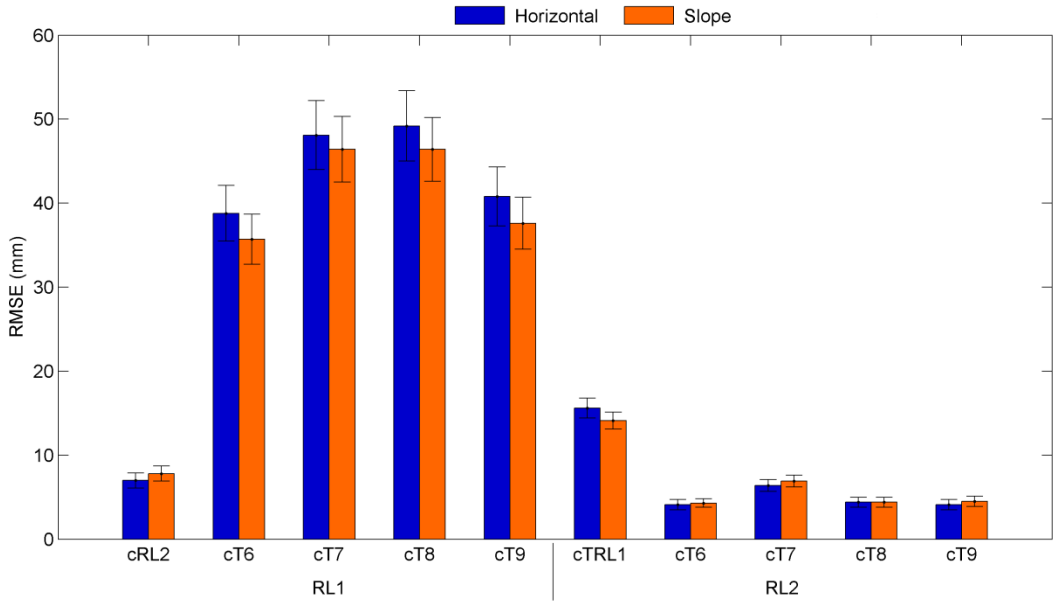

Figure 5.27: RMSE of horizontal and slope distances at Roughting Linn.

In RL2, using calibration values derived from RL1, the RMSE ranges from 9 mm to 22 mm. In both cases this is better than the absolute accuracy obtained with these combinations. When calibration values derived from data sets of Test6 to Test9 were used, the RMSE increases. In this case the RMSE obtained in RL1 is larger than the RMSE obtained in RL2, inverting the results of the absolute accuracy assessment (Section 5.2.3.1). The largest RMSE (50 mm) in RL1 was achieved for easting using calibration values derived in Test8. This is slightly lower than the absolute accuracy

achieved with this combination (47 mm). In RL2 the largest RMSE (39 mm) was achieved for height when calibration values derived from Test9 were used. This value is significantly smaller than the absolute accuracy value obtained with the same combination (113 mm).

The differences in relative accuracy between RL1 and RL2 are highlighted when their RMSE of horizontal and slope distances are compared to each other (Figure 5.27). When calibration values derived from a case study data set (RL1 or RL2) were used for offset correction, the RMSE obtained in RL1 (7 mm and 8 mm, respectively) is smaller than the RMSE obtained in RL2 (16 mm and 14 mm, respectively). However, when calibration values derived from Test6 to Test9 were used, the RMSE for horizontal and slope distances achieved in RL1 (36 mm to 49 mm) is significantly larger than the RMSE achieved in RL2 (4 mm to 7 mm). The results achieved in RL2 using calibration values derived from Test6 to Test9 are even smaller than the 2D and 3D relative accuracy achieved using calibration values derived from RL1. This demonstrates that achievable 2D and 3D relative accuracy is not dependent on the availability of well suited calibration values, but on whether the relation between check point coordinates are maintained during bundle adjustment. This will be further discussed in Section 6.2.2.

Comparing the RMSE of horizontal and slope distances (Figure 5.27) to their corresponding RMSE of easting, northing and height distances (Figure 5.26) reveals that 2D and 3D relative accuracy obtained in RL2 is significantly higher than 1D relative accuracy obtained in RL2. This indicates rotation of the estimated check point coordinates with respect to the OSGB36 coordinate system, similar to relative accuracy results in Section 4.2.2 and Section 5.1.4.1. However, in RL1 horizontal and slope relative accuracy obtained is in the same range as the corresponding easting, northing, and height relative accuracy achieved. This indicates that the estimated check point coordinates are not systematically rotated with respect to the OSGB36 coordinate system but deviate from their true values in differing directions.

The significant differences in absolute and relative accuracy between RL1 and RL2 occur despite their similarities in offset calibration stability and precision. This demonstrates that even small differences between data sets collected using the recording system can result in different levels of achievable absolute and relative accuracy. Further discussion is provided in Section 6.2.

5.2.4 Visualising cultural heritage data in Google Earth

The data collected during the Roughting Linn case study was also used to demonstrate the usability of Google Earth for enhancing accessibility of cultural heritage data. The Google Earth software version used in this research project was Google Earth 6, which was the latest version at the time of writing. Google Earth allows displaying of images in the orientation and position in which they have been acquired, using the "PhotoOverlay" feature of KML (Section 3.7.2). At the same time KML allows imagery to be stored together with corresponding exterior orientation information in one single file. In that way KML can be used to exchange photogrammetric data and images representing cultural heritage objects.

5.2.4.1 Displaying photo overlays

From imagery and exterior orientation parameters of camera stations 1, 3, 5, and 7 of RL1 (Figure 5.18) and camera stations 11 to 14 of RL2 (Figure 5.19), 8 KMZ files were generated using the approach described in Section 3.7. Photo overlays of the 8 images were positioned and oriented using directly determined exterior orientation parameters. For photo overlays of RL1 direct exterior orientation parameters were derived using calibration values of RL2. For photo overlays of RL2 calibration values of RL1 were used to derive exterior orientation parameters. When Google Earth is installed on a computer, opening a KMZ file automatically loads the contents of the file into Google Earth. The content should also be instantly displayed, but uploading the 8 KMZ files generated for this project revealed that this is not always achievable. In order to display the photo overlays the KMZ files had to be manually opened by double-clicking on the photo overlay entry in the Google Earth navigation bar. Similar displaying problems were also observed by other Google Earth users (Google, 2011c) but no solution to this problem has been reported. When the photo overlay is opened, the view of the user is altered to the position and orientation from where the image was acquired, while the image is overlaid on the background imagery of Google Earth (Figure 5.28).

Another displaying issue occurred when more than one KMZ file was loaded into Google Earth. The second and all subsequent photo overlays were displayed with orientation and position values slightly different from the values stored in the KMZ

file. The Google Earth online help (Google, 2011d) suggests clearing the cache of the program in order to solve displaying problems. Clearing the cache after opening each of the KMZ files solved the problem of changing orientation and position value and all 8 KMZ files were subsequently opened In Google Earth.

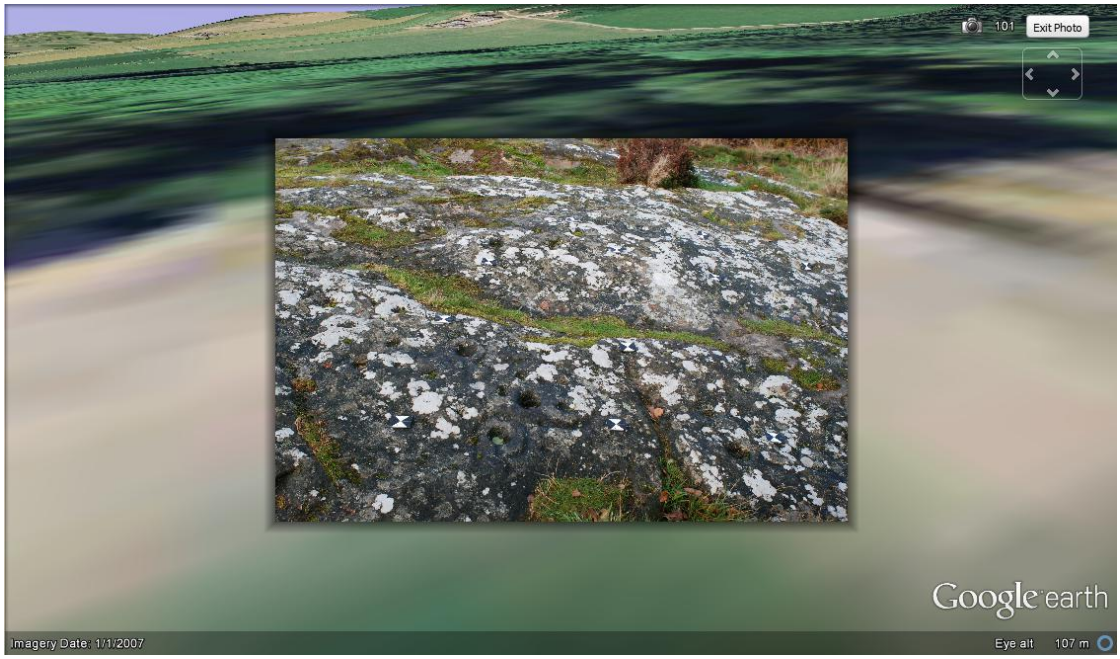

Figure 5.28: Image from camera station 1 of RL1 as photo overlay in Google Earth.

Figure 5.29: Overview of four RL1 images in Google Earth.

Figure 5.30: Overview of four RL2 images in Google Earth.

Figure 5.29 provides an overview of the four images of RL1 after opening in Google Earth. The four images of RL2 are displayed in Figure 5.30. The image icons in these figures indicate the position and orientation of the camera at the time of image acquisition. This demonstrates that KMZ is a practical format for storing exterior orientation information and imagery in a single file and using this information for visualisation of cultural heritage in its geographical context. Further discussion on displaying cultural heritage in Google Earth using KMZ and the benefits to digital heritage data usage and accessibility will be provided in Section 6.5.

5.2.4.2 Photo overlay display evaluation

The aim of photo overlay display evaluation was to investigate the quality of photo overlay positioning and orienting in Google Earth. Figure 5.29 and Figure 5.30 display the orientation and position of the camera at the time of image acquisition from an arbitrary viewpoint. These representations do not allow assessing the quality of the photo overlay display. For assessing the display quality each image was viewed from the position and orientation of the camera at the time of image acquisition. This is achieved by double clicking on the photo overlay entry in Google Earth. In this displaying mode, the photo overlay image can be visually compared to the background image of Google Earth and potential shifts and rotations can be detected.

Figure 3.16 in Section 3.7.2 provides an example how the photo overlay image can be compared to the Google Earth background image. However, the resolution of the Google Earth imagery available for Roughting Linn was not appropriate to provide sufficient detail (Figure 5.28) for evaluating display quality in this project. Furthermore, the accuracy of Google Earth imagery geo-referencing is not known, which might also be a source of error. Therefore, the display quality was visually assessed by comparing the positions of targeted points in the photo overlay image to the assumed true positions of these points in Google Earth. The true positions were displayed in Google Earth using a KML file containing the coordinates of targeted points at RL1 and RL2 and displaying information for these points. This KML file placed a labelled marker at the position of each targeted point in Google Earth. These markers were clamped to the Google Earth terrain and the photo overlays were positioned above the terrain. The resolution of the DEM used as Google Earth terrain is not known, but based on visual assessment it was recognised that it is certainly not sufficient for this process. However, displaying the markers at their height relative to the EGM 96 geoid (Section 3.7.1) would have placed these below the Google Earth terrain, making them undetectable. The alternative approach of clamping the markers to the terrain was considered to be suitable for providing an indicator for general photo overlay displaying quality in Google Earth. In order to facilitate viewing markers and photo overlay at the same time, the transparency of the images was increased. Figure 5.31 and Figure 5.32 depict the semi-transparent photo overlays and the Google Earth markers of the coordinated points for RL1 and RL2, respectively. Targets visible in the photo overlay image corresponding to Google Earth markers were identified and an arrow was drawn between each pair. The arrow indicates the direction and magnitude of the photo overlay target point displacement from the true position of this point. The magnitude of displacement cannot be measured in the photo overlay, but the average distance between subsequently numbered target points in RL1 and RL2 (approximately 0.6 m) can perhaps provide a rudimentary reference for assessing target point displacement. Figure 5.31 demonstrates that the directions of photo overlay point displacements vary within each photo overlay, with the most noticeable variations occurring in Figure 5.31c. Variations also occurred for photo overlays of RL2 (Figure 5.32). The displacements vary not only in direction but also

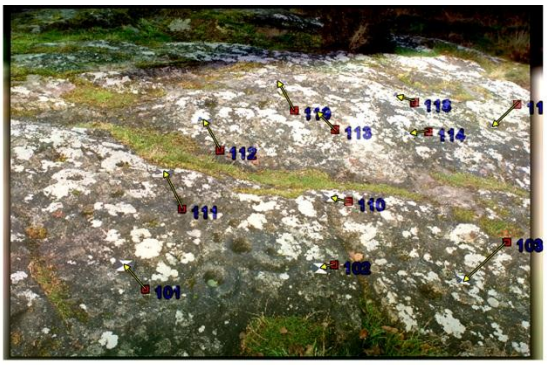

a: camera station 1

b: camera station 3

c: camera station 5

d: camera station 7

Figure 5.31: Displaying correctness RL1 (camera stations 1, 3, 5, and 7).

a: camera station 11

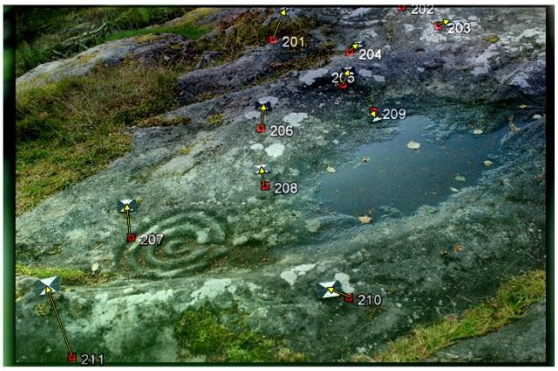

b: camera station 12

c: camera station 13

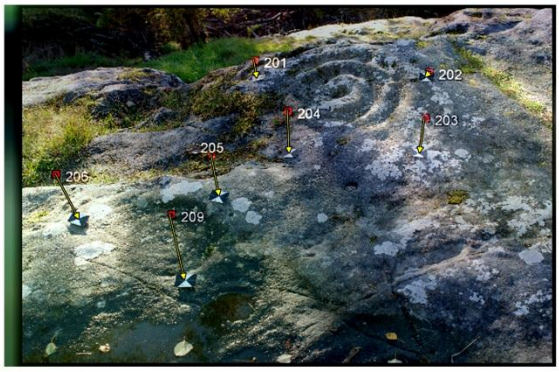

d: camera station 14

Figure 5.32: Displaying correctness RL2 (camera stations 11 to 14).

in their magnitude. Some Google Earth point markers overlap with their corresponding targeted point visible in the photo overlay image. In the same photo overlay, some markers appear closer to non-corresponding targets. In some cases (Figure 5.31a and d) the target points with smaller displacement magnitude appear in parts of the photo overlay that have an approximately similar height in the real world. Displacements of higher magnitudes are clustered in other parts of this photo overlay. The variations appear to be greater in photo overlays created for RL1 (Figure 5.31) than for photo overlays created for RL2 (Figure 5.32). In RL2 (Figure 5.32a, b, and c) most markers are close to the target point representations in the photo overlay. There are several reasons that could have caused the displacements between target points in image and point markers on the Google Earth terrain to vary in their direction and magnitude. Small errors in the exterior orientation can cause rotation and shift of the photo overlay with respect to the true orientation and position at the time of image acquisition. Furthermore, not using orthorectified images distorts the positions of the target points visible in the images with respect to their true position. However, resolving these issues will probably not result in a perfect photo overlay display. It was already noted that the resolution of the DEM used in Google Earth is certainly not sufficient for assessing the displaying quality. The accuracy of the DEM is also not known, which can be another source of error. Finally, the quality of transformation from OSGB36 grid coordinates into WGS 84 geodetic coordinates could also introduce some error. This demonstrates that assessing photo overlay displaying quality in Google Earth is limited by many uncertainties. However, Figure 5.31 and Figure 5.32 indicate that despite these uncertainties images were displayed in their approximate position and orientation at the time of exposure. Therefore, photo overlays in Google Earth are considered sufficient for simple visualisation of cultural heritage in its geographical context. This can benefit cultural heritage conservation projects in several ways, including motivation of volunteers to become involved. These benefits will be discussed in more detail in Section 6.5.2.

5.3 Summary

In this chapter, results of two case studies conducted at heritage sites in the United Kingdom were presented. The offset calibration assessment of the case study conducted at St. Catherine's Oratory suggested that large pitch of the mounting frame during data collection decreases the offset calibration precision. Despite this, the recording system performance assessment revealed achievable absolute accuracy of 42 mm using zero control points. This accuracy level is similar to the absolute accuracy achieved in the initial recording system tests at Loughborough University. The relative accuracy assessment also revealed results similar to those obtained during the initial recording system tests. When a single control point and sufficiently consistent offset calibration values were used, the achievable absolute accuracy could be improved to 23 mm. Even with inconsistent offset calibration values, absolute accuracy of 32 mm could be achieved using a single control point. This demonstrated the benefit that can be obtained from establishing a single coordinated point for recording at a heritage site. Surprisingly, the availability of a single control point decreased the achievable relative accuracy. An explanation could be the constraint imposed by a single control point creates a localised distortion effect during the bundle adjustment.

The second case study was conducted at Roughting Linn rock-art site under significantly different conditions to the initial tests and the first case study. The assessment of the rotational offset calibration precision indicated that large pitch (-21° to -51°) of the mounting frame could cause a decrease in roll offset calibration precision. Furthermore, it was suggested that the large pitch of the mounting frame could also have an effect on the DGPS positioning accuracy as the antenna orientation restricts signal reception and is more susceptible to multipath effects. This was further emphasised by the offset calibration stability assessment. Significant offset changes between initial recording system tests (Test6 to Test9) and Roughting Linn case study data sets were revealed. These changes were partly caused by erroneous target point coordinates used for truth data generation, but also by the large pitch of the mounting frame. When calibration values derived from case study data sets were used, an

absolute accuracy of 39 mm was achieved. Using inconsistent calibration values derived from Test6 to Test9 the achievable absolute accuracy decreased and varied significantly between the two Roughting Linn case study data sets. The best relative accuracy for horizontal and slope distances was obtained using inconsistent calibration values, indicating that 2D and 3D relative accuracy is not dependent upon the consistency of offset calibration values.

The visualisation of cultural heritage data acquired at Roughting Linn in Google Earth revealed some display issues with photo overlays using KMZ file format. These issues could be solved and the visual assessment of display quality suggested that photo overlays can be utilised for simple visualisation of cultural heritage in its geographic context. This also demonstrated the practicability of the KMZ file format for storing exterior orientation parameters and corresponding imagery in a single file.

Further discussion on the results obtained in the two case studies will be provided in Chapter 6.

6 Discussion

In this chapter the results of offset calibration and accuracy assessment that were presented in Chapter 4 and Chapter 5 are discussed. First, influences on offset calibration precision and stability are identified and solutions for enhancing the results of offset calibration are presented. This is followed by discussing achievable absolute and relative accuracy, using zero or one single control point. Some limitations of the recording system used in this project are identified and potentials for enhancing portability and reducing cost of the system are highlighted.

This chapter also includes investigations into the potential of smartphones with an integrated camera, GPS, and orientation sensor as an off-the-shelf system for image-based heritage recording.

Further discussion is provided on the usability of KML to store images and corresponding exterior orientation information in one single file and to visualise cultural heritage in Google Earth. Benefits and problems of this approach are presented before this chapter concludes in a summary.

6.1 Influences on offset calibration precision and stability

Fiani and Pistillo (2004) suggest enhancing the performance of their low-cost mobile mapping system by improving the offset calibration. This demonstrates that stable and precise offset calibration is a crucial factor for the performance of a recording system

capable of direct exterior orientation determination. Offset calibration results in this project demonstrate some difficulties in achieving calibration precision that meets the expected measurement accuracy (in particular positional and roll offsets). Furthermore, some issues with calibration stability, particularly heading offset calibration, became apparent. In this section, influences on offset calibration are investigated and approaches to avoid errors are suggested.

6.1.1 Stability of mounting frame fixtures

Section 3.3.2.2 demonstrated that fixing the camera to the mounting frame was considered the most crucial part of assembling the recording system in this project. While DGPS antenna and TCM5 orientation sensor were obviously designed to be fixed in a system, consumer-grade cameras are usually designed for comfortable handling. This results in difficulties when this kind of camera has to be fixed in orientation and position with respect to other components of a system. The only means of fixture commonly provided with consumer-grade cameras is a 1/4" BSW socket for attachment to a conventional camera tripod. Attaching the camera using this socket does fix it in a position but not in relation to the perspective centre. The camera is not fixed in orientation and can still be rotated, resulting in the perspective centre position being shifted. Recognising this, it is clear that consistent rotational and positional offset calibration values for the recording system can only be achieved when the camera can also be fixed in orientation. This is certainly the most crucial and difficult part of camera fixture. In this research project two differing camera fixture approaches were utilised (Section 3.3.2.2). The initial camera fixture was first believed to be less stable during data collection than the modified camera fixture. It was realised during offset calibration precision assessment (Section 4.1.1) that both camera fixtures can achieve calibration values of similar precision. However, the initial camera fixture did not allow access to imagery saved to the camera memory card without detaching the camera. This compromised the offset calibration stability (Section 4.1.2). Therefore, the modified camera fixture, which allowed access, was considered the better approach of attaching the camera to the mounting frame.

It has been mentioned previously that fixing the orientation of the camera in the mounting frame is the most difficult part of camera fixture. Results of the rotational

calibration precision and stability assessment (Sections 4.1.1.1 and 4.1.2.1) indicated that the modified camera fixture could fix the orientation of the camera to a level sufficient for stable and precise rotational offset calibration. In most cases, the calibration precision of rotational offsets indicated by the calibration value standard deviation met the expected measurement accuracy of the orientation sensor (Section 4.1.1.1). This is theoretically the best rotational calibration precision that can be achieved with the recording system. Also, when the camera remained attached to the mounting frame, the modified camera fixture generally provided consistent or stable rotational offset calibration values (Section 4.1.2.1). Rotational offset calibration values were considered consistent, when the magnitude of change between values derived from differing data sets did not exceed the expected orientation sensor accuracy. However, in some cases changes between rotational calibration values and standard deviations of these values exceeded the expected orientation sensor measurement accuracy. It was suggested that these cases indicate a minor instability of the camera fixture that either allows significant rotational offset changes during data collection or significant changes of the rotational calibration values over time. In this section the effect of the minor camera fixture instability as well as solutions for enhancing the camera fixture are discussed.

The standard deviation that most often exceeded the expected orientation sensor accuracy was the standard deviation of the roll calibration value. Further analysis suggested that roll standard deviations greater than the expected roll accuracy (0.2°) occurred in data sets with a wider range of measured pitch values (range greater than 20°). These data sets are Test5 conducted at the "modern art" test object (Section 4.1.1.1), SCO2 of the St. Catherine's Oratory case study (Section 5.1.3.1), and RL1 and RL2 of the Roughting Linn case study (Section 5.2.2.1). This indicated a dependency of calculated roll offsets on the range of pitch values measured. Figure 6.1 and Figure 6.2 compare calculated roll offsets to measured pitch values for all camera stations of data set SCO2 and Test5, respectively.

With the exception of camera stations 9 and 11 in Test5, a slight correlation between measured pitch and calculated roll offset can be identified in both figures. When measured pitch increases, the calculated roll offset also increases, and vice versa. However, roll offset changes are not always proportional to changes in measured

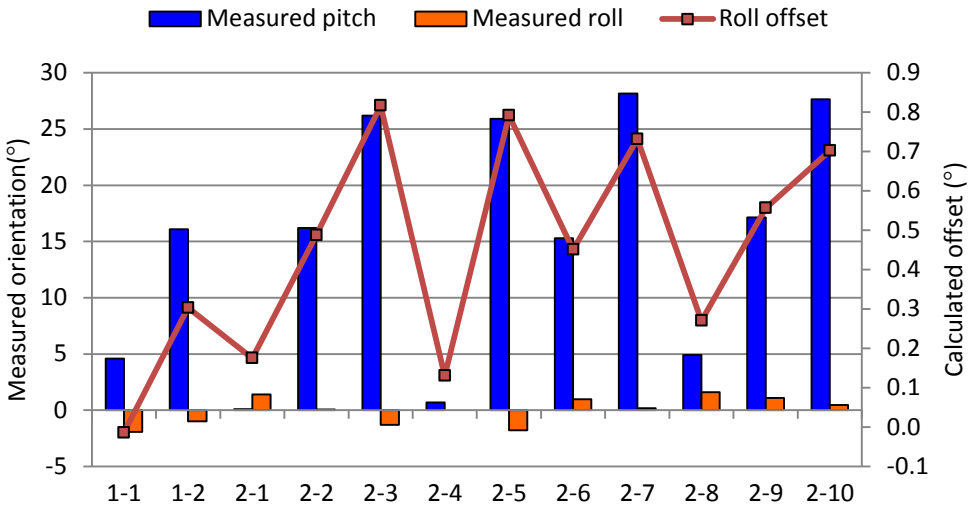

Figure 6.1: Comparison of roll offsets and measured pitch and roll in data set SCO2.

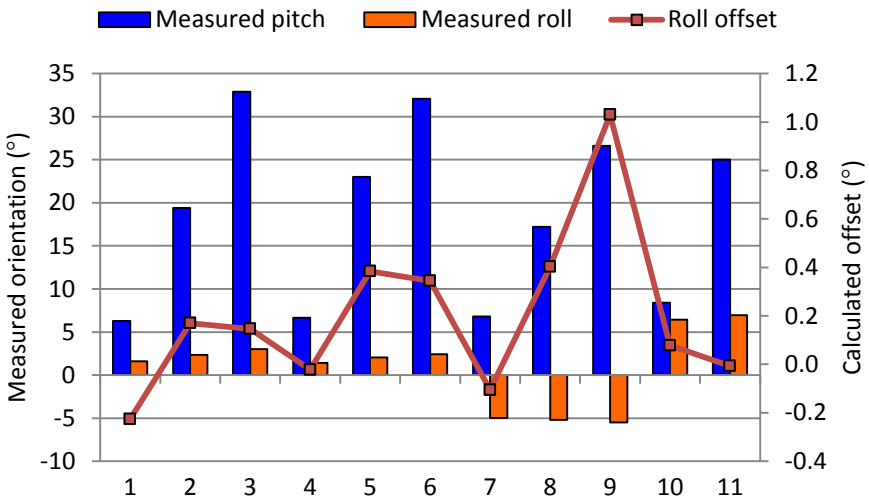

Figure 6.2: Comparison of roll offsets and measured pitch and roll in Test5.

pitch. Camera station 9 and camera station 11 of Test5 (Figure 6.2) have similar measured pitch values (26.6° and 25.0°, respectively), but the calculated roll offsets are significantly different (Figure 6.2). For camera station 9 a roll offset of 1° was calculated while the roll offset calculated for camera station 11 is 0°. Investigation into this issue revealed that the roll of the mounting frame (measured orientation sensor roll) can also cause changes in the magnitude of the calculated roll offset. Camera stations 9 and 11 in Test5 differ significantly in the measured roll, which is -5.5° at camera station 9 and 6.9° at camera station 11. The positive measured roll at

camera station 11 decreased the calculated roll offset, while the negative measured roll at camera station 9 increased the value of roll offset. Comparing camera stations 3 and 6 of the same data set (Test5) a similar but slightly weaker effect can be demonstrated. These correlations between measured pitch and roll and the calculated roll offset was also confirmed in data sets RL1 and RL2 of the Roughting Linn case study.

A further observation was that measured roll only has a significant effect on the calculated offset changes when the magnitude of measured pitch exceeds a certain threshold (approximately 10°). In Test5 camera stations 7 and 10 have measured roll of magnitude similar to camera stations 9 and 11 (approximately 5°), while the magnitude of measured pitch is smaller than 10°. Assessing the roll offsets at these camera stations (7 and 10) reveals that for measured pitch magnitudes smaller than 10°, roll of the mounting frame does not significantly change the calculated roll offset. The correlation between measured pitch and roll and calculated roll offset changes is also observable in data sets where the range of measured pitch is smaller than 20° and the roll calibration value standard deviation does meet the expected roll accuracy. However, the magnitudes of roll offset change are sufficiently small to result in standard deviations that meet the expected roll measurement accuracy. This demonstrates that changes in calculated roll offset are not significant for offset calibration when measured pitch does not exceed 20°. The correlations described above were not observed in data sets using the initial camera fixture. This excludes the orientation sensor as a possible source for roll offset changes during data collection and confirms that even the modified camera fixture is slightly unstable for large measured pitch (magnitude greater than 20°). This can even have an effect on the calibration stability. In RL1 and RL2 of the Roughting Linn case study very low (high negative) pitch values were measured (-20° to -51°). It was noted before that decreasing pitch values decrease the calculated roll offset. Therefore, the negative measured pitch significantly decreased the calculated roll offsets, resulting in negative roll calibration values of approximately -1.1°. This is a roll calibration value change greater than 1° compared to initial recording system tests (Section 4.1.2.1). However, it has to be considered that in the Roughting Linn case study the recording system was tested under extreme pitch conditions. Therefore, these results are certainly not representative for heritage sites where the recording conditions do not require tilting

the mounting frame up to 50°. Furthermore, it is expected that the stability of the camera fixture can easily be improved. In order to identify small weaknesses in the fixing approach the current camera fixture was more closely examined. It was discovered that the aluminium bar and hose clip that fixes the camera in its orientation, slightly elevates the lens. This results in the bottom of the camera body touching the bottom plate of the mounting frame only at the back of the camera. Towards the front of the camera there is a small, visually hardly recognisable gap between camera body and mounting frame. Due to this gap, rotations of the camera in roll direction are not sufficiently restricted by the camera body completely touching the mounting frame plate. Furthermore, the currently used aluminium bar and hose clip in the front that fix the camera in its orientation are comparatively thin. When the mounting frame is pitched and rolled during data collection, it is probable that the weight of the camera physically strains the camera fixture. Depending on the magnitude of pitch and roll the aluminium bar and hose clip could be temporarily deformed, allowing the camera to rotate in roll direction. This issue could be easily solved by lowering the aluminium bar at the front of the mounting frame, which would close the gap between camera body and mounting frame and more rigidly restrict the camera in rotations in roll direction.

The investigation of significant roll offset changes during data collection revealed a minor instability of the camera fixture that affects the calculated roll offsets, depending on measured pitch and roll. This raises the question whether the slight camera fixture instability could also have influenced calibration value determination for pitch or heading. The pitch calibration value standard deviation significantly exceeded the expected orientation sensor pitch accuracy of 0.2° (Table 3.2) in data set SCO2 of the St. Catherine's Oratory case study only (Section 5.1.3.1). The results of investigating this issue suggested that this was probably caused by reattaching the camera to the mounting frame between data collection of SCO1 and data collection of SCO2 (Section 5.1.1) not sufficiently tightly. Therefore the slight camera fixture instability has no significant effect on the pitch calibration value determination.

A further enhancement could be exchanging the currently used aluminium bar and hose clip for parts that are less likely to deform when these are physically strained during data collection. This might not only enhance the offset calibration precision but also the offset calibration stability. While the camera remained attached to the

mounting frame, the most significant calibration value offset changes occurred for heading. Heading calibration values range from -4.85° in data set RL1 (Section 5.2.2.2) to -5.78° in Test8 (Section 4.1.2.1). The calibration value change of approximately 1° significantly exceeds the expected orientation sensor heading accuracy (0.3°). This change is not detectable visually and its main source is most probably slight deformations of the camera fixture. These can be caused by unavoidable handling the mounting frame during data collection and transportation. Using more rigid materials for camera fixture would certainly reduce heading calibration value changes.

6.1.2 Heading determination using magnetometers

The utilisation of magnetometers and accelerometers allows orientation determination independent of any data that has to be provided by external sources. Due to MEMS technology these sensors are also available at low-cost and in small-size (Section 2.5.2). This is certainly the reason why orientation sensors comprising magnetometers and accelerometers are utilised when solutions for mobile and low-cost orientation determination is required (Fiani and Pistillo, 2004; Coppa et al., 2007). The drawback of utilising magnetometers is the influence of local distortions to the magnetic field on heading measurements. In Coppa et al. (2007) an orientation sensor comparable to the TCM5 used in this project (Section 3.3.1.2) was integrated in a small-size mobile mapping system. The authors noted that the sensitivity of the magnetometers to magnetic disturbances could have affected heading measurements and resulted in a decrease of the achievable accuracy of the whole system. They further remarked that it was not possible to determine the magnitude of the influence of magnetic distortions on the orientation sensor measurement. The TCM5 orientation sensor provides software that is capable of determining the local magnetic field distortions during an initialisation process and adjusting heading measurements accordingly (Section 3.3.1.2). In this way the orientation sensor can adjust the heading measurements according to the actual magnetic distortion at any location where the magnetic field distortions are constant (PNI, 2009). However, a change in the spatial relation between sensor and nearby objects potentially distorts the local magnetic field and invalidates the values used for adjusting the heading measurements. As a result,

the most accurate heading measurements would be achieved when the orientation sensor is re-initialised every time the tripod carrying the recording system mounting frame is moved. This would prevent heading offset changes of magnitudes depicted in Figure 6.3. However, a drawback to this approach is the increased amount of time required for data collection. This would also complicate the utilisation of the recording system, which compromises the aim of this research project to develop an easy-to-use and low-cost system suitable for heritage recording (Section 1.1). Therefore, in this project this problem was solved successfully by conducting orientation sensor initialisation once at the location of the first camera station for data collection (Section 3.6.1). Only data collected at this location was used for heading offset calibration and the exterior orientation parameter φ of images acquired at this location were constrained differently to images of other camera stations during the bundle adjustment (Section 3.6.3).

Figure 6.3 demonstrates the effect local magnetic field distortions can have on heading measurements. It depicts the calculated heading offsets for all camera stations of the St. Catherine's Oratory case study data sets (SCO1 and SCO2) (Section 5.1.1). The upper labelling on the horizontal axis identifies the camera station and the lower labelling identifies the data set. The orientation sensor was initialised at the location of camera station 1-1 and 1-2 in SCO1. With increasing station number in SCO1 the distance between camera station and location of orientation sensor initialisation increases. In SCO2 camera stations with a small number (2-1 to 2-3) are further away from the location of orientation sensor initialisation than camera stations with a larger number (2-8 to 2-10). In order to enhance comprehension, this camera station arrangement is sketched in Figure 6.4. Figure 6.3 demonstrates that the greater the distance between camera station and location of orientation sensor initialisation the more the calculated heading offset deviates from the heading offsets at the initialisation location used for calibration value determination. A second effect of increased distance to the location of orientation sensor initialisation is that pitching the mounting frame also influences the calculated heading offset (Figure 6.3). At camera stations 1-1 to 1-4 that were at or close (maximum distance approximately 1 m) to the sensor initialisation location no significant influence of mounting frame pitch is apparent. At camera stations 1-5 and 1-6 that were located at an approximate distance

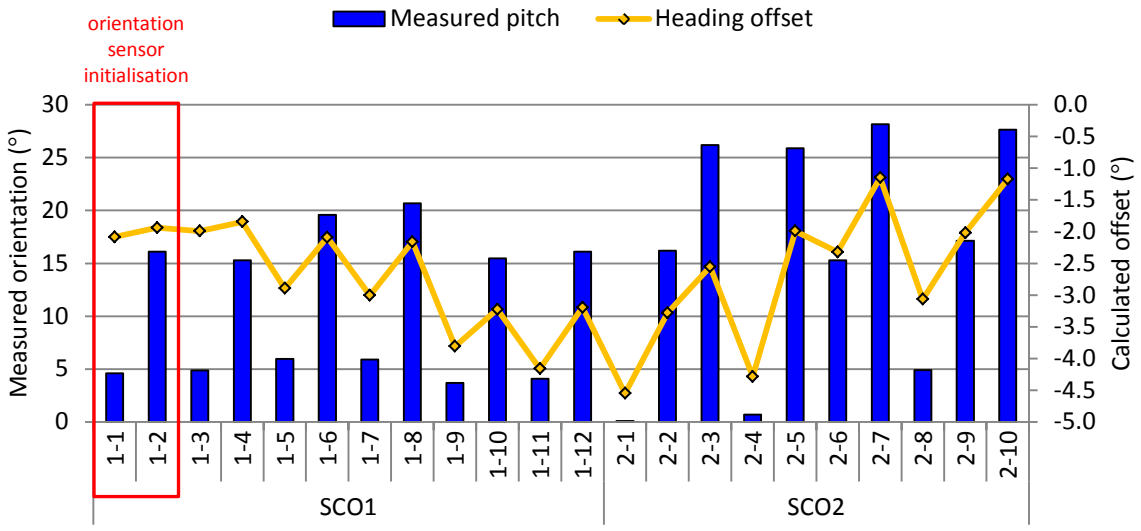

Figure 6.3: Calculated heading offset and measured pitch in data sets SCO1 and SCO2.

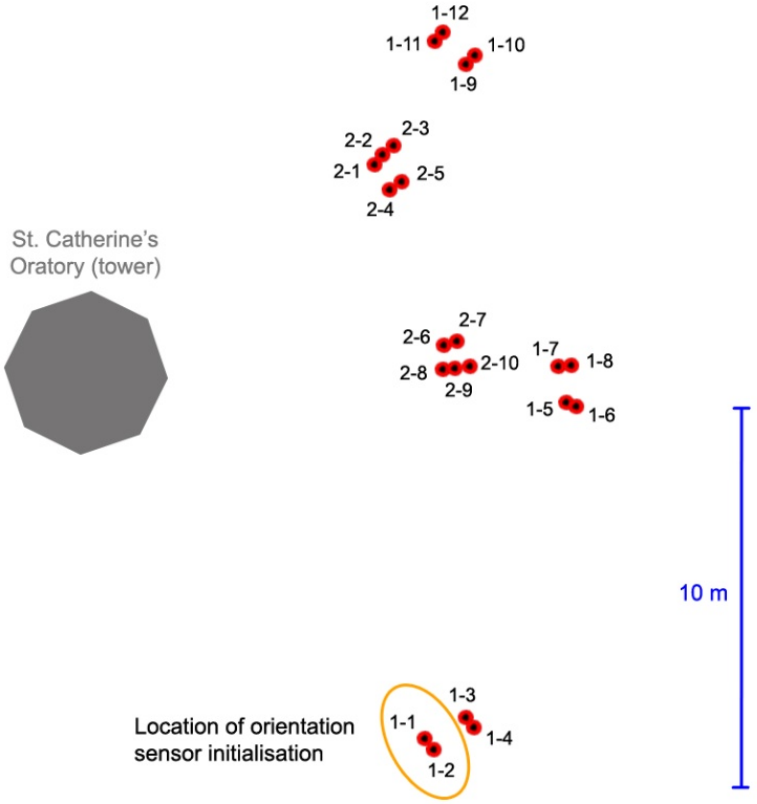

Figure 6.4: Camera station distribution at St. Catherine's Oratory.

of 10 m to the initialisation location (Figure 6.4), a pitch difference of 13.6° caused a heading offset difference of 0.8°. This demonstrates the importance of orientation sensor initialisation prior to data collection and of restricting heading calibration value determination to data acquired at the location of orientation sensor initialisation. The importance of orientation sensor initialisation prior to data collection is further highlighted in Figure 6.5, which depicts the range of heading offset ($s\Delta h$) derived in all data sets of this research project. The range of heading offset was introduced because the heading calibration value standard deviation was derived from camera stations at the location of orientation sensor initialisation only and was considered not suitable to indicate heading offset calibration precision (Section 3.5.2). The range of heading offsets is the maximum difference between the heading offset calibration value and heading offsets calculated at camera stations not at the orientation sensor initialisation location. It indicates the suitability of the heading calibration value to correct heading offsets at camera stations not at the location of orientation sensor initialisation. The range of heading offsets also indicates the intensity of local magnetic field distortions and their effect on the orientation sensor heading measurement. Figure 6.5 demonstrates that the intensity of magnetic field distortions can vary significantly between data collection sites, even when they are only a short distance apart. The least distortions occur at the test field, indicating that local magnetic field distortions at this site are either smaller or more homogeneous than

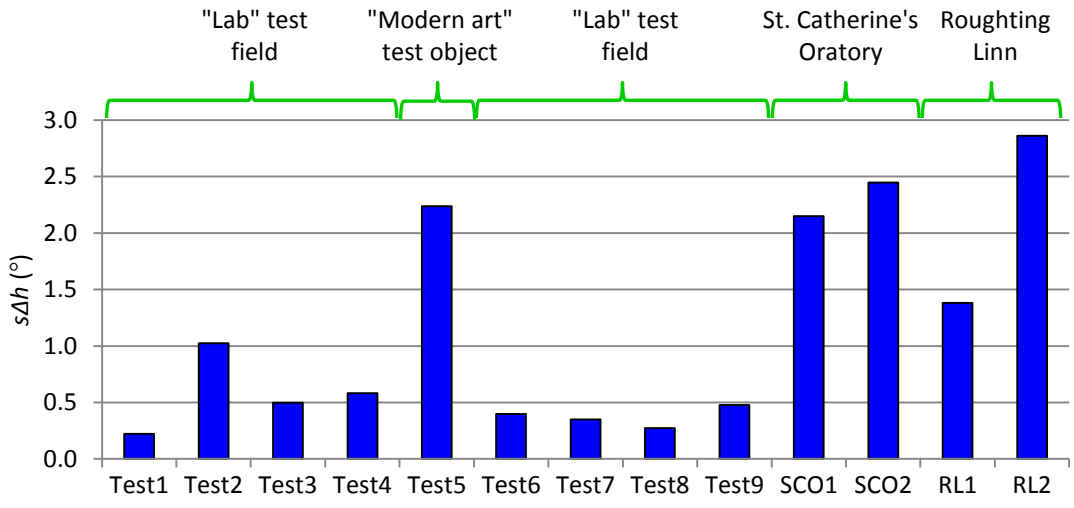

Figure 6.5: Range of heading offset ($s\Delta h$) for all data sets.

distortions at the other sites. At the Roughting Linn case study site (Section 5.2.1) the distance between the two data collection sections, RL1 and RL2, is approximately 7 m. Nevertheless, the range of heading offsets changes from 1.4° in RL1 to 2.9° in RL2. In Test5 $s\Delta h$ is higher than in the other initial recording system tests (Test1 to Test4 and Test6 to Test9). This is not surprising because the "modern art" test object (Section 3.2.2) used for data collection is made of iron. It is well known that ferrous metals have a great influence on the local magnetic field, which in Test5 even affected the heading offset calibration. The standard deviation derived from measurements at the two camera stations at the location of orientation sensor initialisation is 0.45° and exceeds the expected orientation sensor heading accuracy by 0.15° (Section 4.1.1.1). A similar effect of local magnetic field distortions on the heading calibration determination was observed in RL2 (Section 5.2.2.1). Despite the heading standard deviation being not significant as an indicator for calibration precision, this demonstrates that high local magnetic field distortions can cause difficulties in determining the heading offset, even when the orientation sensor was initialised. Therefore, the usability of the TCM5 orientation sensor for heading determination is limited at sites of high local magnetic field distortions. This is also noted in the TCM5 user manual (PNI, 2009), which mentions large masses of ferrous metal and large electric currents as source for high local magnetic distortions. Before using the recording system for recording cultural heritage data it is therefore recommended to check whether high magnetic field distortions due to large masses of ferrous metal and large electric currents can be expected at the heritage site. When high distortions can be expected the utilisation of additional control (for example a single control point) should be considered in order to compensate errors caused by insufficiently adjusted heading measurements. For the case study at Roughting Linn the high local magnetic field distortions would not have been predictable without measurements of the magnetic field on site. Despite a significant change of magnetic distortions intensity between RL1 and RL2 (Figure 6.5), the heading offset calibration value change only slightly exceeded the expected orientation sensor heading accuracy and was comparable to heading offset changes between the initial recording system tests (Section 5.2.2.2). This demonstrates that without obvious signs for high local magnetic distortions, comparatively stable heading offset calibration might still be possible.

6.1.3 Influence of DGPS antenna tilt

In most initial recording system tests and in both case studies the standard deviation of the positional offset calibration values exceeded the expected DGPS positioning accuracy. It has been noted before that this could have been caused by a decrease in DGPS positioning accuracy due to tilt of the antenna (Section 4.1.1.2), which was rigidly fixed to the mounting frame. During data collection the recording system mounting frame was pitched at differing angles in order to capture all coordinated points at a test site. In most cases this resulted in measured pitch values ranging from approximately 0° to 33°, but during the Roughting Linn case study pitch values between -20° and -51° were measured (Section 5.2.1). Additionally, small variations in mounting frame roll were unintentionally introduced during data collection of the data sets used in this research project. Pitching and rolling the mounting frame also causes tilt (roll and pitch) of the DGPS antenna fixed on the top of the mounting frame. Kirk (2010) has examined this issue and mentions two main reasons for a decrease in DGPS positioning accuracy due to antenna tilt: influence of antenna modelling and increased multipath effects. Antennas are modelled or designed to optimise the reception of satellite signals arriving from differing elevations while aiming to attenuate multipath effects. Incoming satellite signals from different elevations introduce consistent biases in phase measurement that are depending on satellite elevation. These biases are compensated using antenna specific filter masks. Furthermore, antennas are usually designed to have low reception for signals arriving from elevations less than 10° to 15° above the horizon. This aims to reduce the effect of multipath from the ground and satellite signals with high signal-to-noise ratio, but also requires the antenna to be level (Kirk, 2010). When a DGPS antenna is tilted, the error compensating effects of antenna design are reduced. For example, the satellite elevation angle relative to a tilted antenna is different to the elevation angle expected at a levelled antenna. Therefore, elevation dependant biases are not correctly compensated by the antenna filter mask. According to Kirk (2010) this can cause ranging errors between satellite and antenna of up to 2 mm for a 5° tilt, up to 7 mm for a 20° tilt, and up to 10 mm for 45° tilt (Figure 6.6). The magnitude of error that can be caused by tilting the DGPS antenna could explain the exceeding of the expected

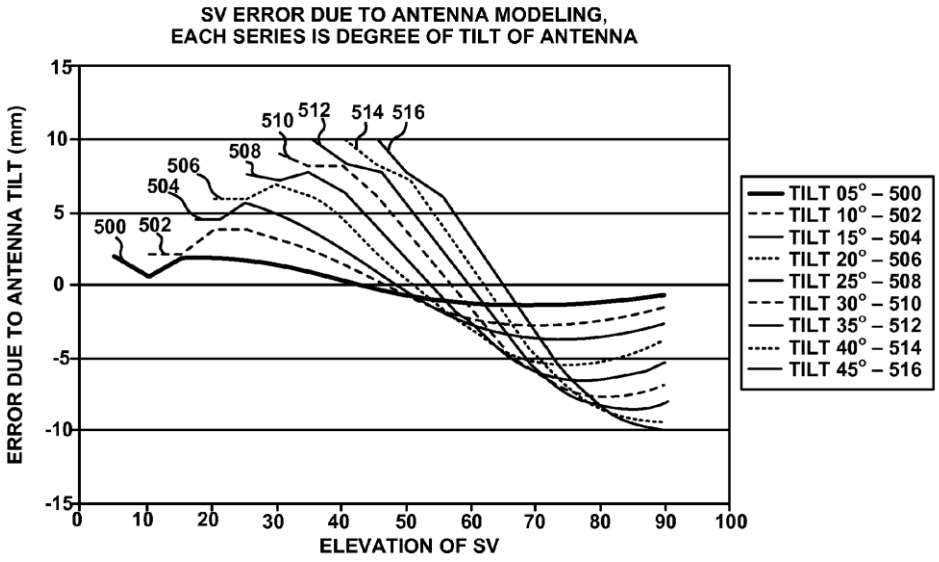

Figure 6.6: GNSS ranging error depending on antenna tilt and effective satellite elevation (from Kirk, 2010).

DGPS positioning accuracy (10 mm for plan and 30 mm for height) in the initial recording system tests at Loughborough University campus. With the exception of Test2, the standard deviations of positional offset calibration values derived in initial recording system tests at Loughborough University campus do not exceed the expected DGPS accuracy by more than 7 mm (Section 4.1.1.2). The measured pitch in the initial recording system tests at Loughborough University campus ranged from approximately 0° to 33°, which could result in ranging errors between 2 mm and 8 mm (Figure 6.6). Curiously, in Test5, where the highest pitch values were measured, positional offset standard deviations did not exceed the expected DGPS positioning accuracy. However, the DGPS ranging error due to antenna tilt is also dependent on satellite elevation. Figure 6.6 depicts the expected error for some combinations of antenna tilt and effective satellite elevation. The effective satellite elevation is the elevation of the satellite relative to the DGPS antenna. Assuming that the antenna is tilted (pitched or rolled) exactly towards the position of the satellite or away from it, the effective satellite elevation can be calculated by adding the tilt to the actual satellite elevation relative to the horizon or subtracting it, respectively. Generally, antenna tilt does not occur exactly to or from the satellite but in some angle to the satellite. Furthermore the actual positioning error is a combination of the ranging

errors of each satellite-antenna distance. Predicting the positional error due to antenna tilt is therefore not possible using measured pitch and roll values only. However, the values graphically displayed in Figure 6.6 are suitable indicators for ranging errors that can be expected. These errors cannot completely explain all cases where positional offset calibration value standard deviations exceeded the expected DGPS accuracy. In data set SCO2 of the St. Catherine's Oratory case study, the expected DGPS accuracy was exceeded by 15 mm (Section 5.1.3.1) and in data set RL1 of the Roughting Linn case study the expected DGPS accuracy was exceeded by 27 mm (Section 5.2.2.1).

It was mentioned above that tilting a DGPS antenna can increase the significance of multipath. Multipath is caused by satellite signals arriving at the antenna not only from the direct line of sight, but also as signals reflected from surrounding objects (El-Rabbany, 2006). This extends the measured range and is a major source of error in DGPS positioning, even when antennas are not tilted (Braasch, 1996; Grewal et al., 2001). In the case of positioning using carrier phase measurement the maximum error can be as large as a quarter of a cycle (approximately 48 mm for the L1 carrier phase) (El-Rabbany, 2006). Antennas are designed to reduce the effect of multipath, particularly from the ground. The DGPS antenna used in this project is a Leica AT502 antenna with built-in metallic groundplane disk. This groundplane disk shields the antenna from below, usually attenuating multipath signals from the ground. When the antenna is tilted the groundplane disk cannot longer effectively shield the antenna from signals arriving from the ground. In contrast, for increasing tilt of the antenna the groundplane disk is more likely to shield direct satellite signals, resulting in only multipath signals being received by the antenna. This can cause significant errors in positioning (Kirk, 2010). Blockage of the direct signal of a satellite while the antenna increasingly received multipath signals of this satellite certainly occurred during data collection at Roughting Linn. The highest absolute pitch (-51°) in this case study was measured at camera station 15 in the RL2 data set. At this camera station the measured heading of the orientation sensor was 0.8°. This indicates that the DGPS antenna was tilted approximately towards grid north. For simplification reasons measured roll at this camera station is not taken into account, because the roll influence is considered insignificant for this example. When the antenna is tilted by -51° to north its groundplane disk shields all signals from satellites in the south that are at an actual

elevation angle below 51°. Figure 6.7 and Figure 6.8 depict satellite elevation and satellite azimuth, respectively, at Roughting Linn at the time of data collection for data set RL2. These figures demonstrate that GPS satellite 16 (SV16) at the time of data collection at camera station 15 was located in the south at an approximate elevation angle of 35°. Therefore, only reflected signals from this satellite could be received by the antenna. This certainly caused the significant change between positional offsets calculated for camera station 15 in RL2 and offsets calculated for other camera stations in RL2 (Figure 6.9). Similar effects of the antenna tilt were observed for other camera stations in RL1 and RL2. Even when a tilted antenna receives direct signals from all satellites theoretically visible from a camera station, the antenna tilt still increases the amount of received multipath signals reflected from the ground.

Another effect of multipath is that it can significantly corrupt ambiguity resolution for carrier phase measurements (Braasch, 1996; Grewal et al., 2001). This explains why for some camera stations in RL1 and RL2 carrier phase ambiguities could not be solved (Section 5.2.1).

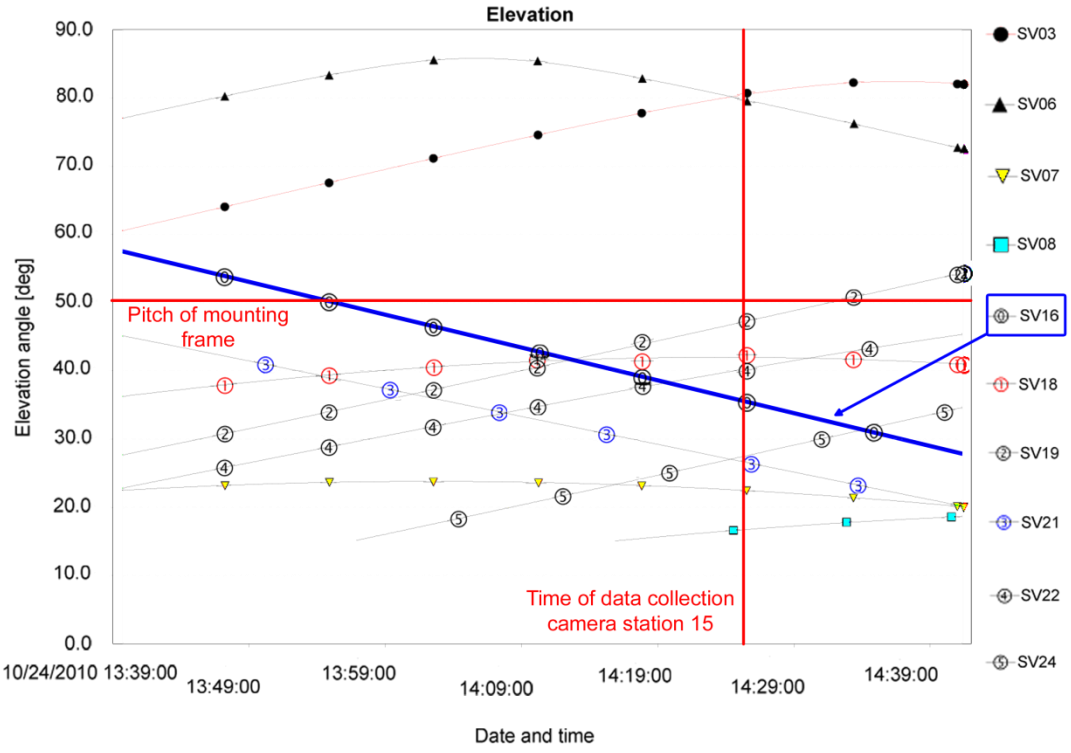

Figure 6.7: Satellite elevation at Roughting Linn during collection of data set RL2.

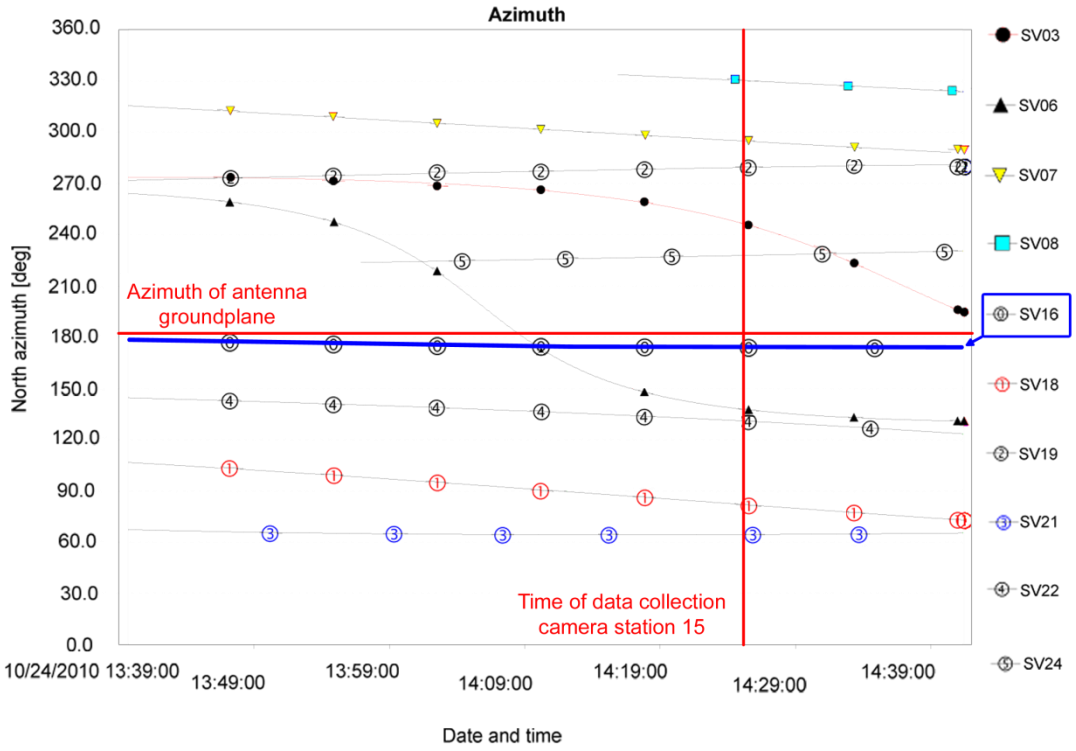

Figure 6.8: Satellite azimuth at Roughting Linn during collection of data set RL2.

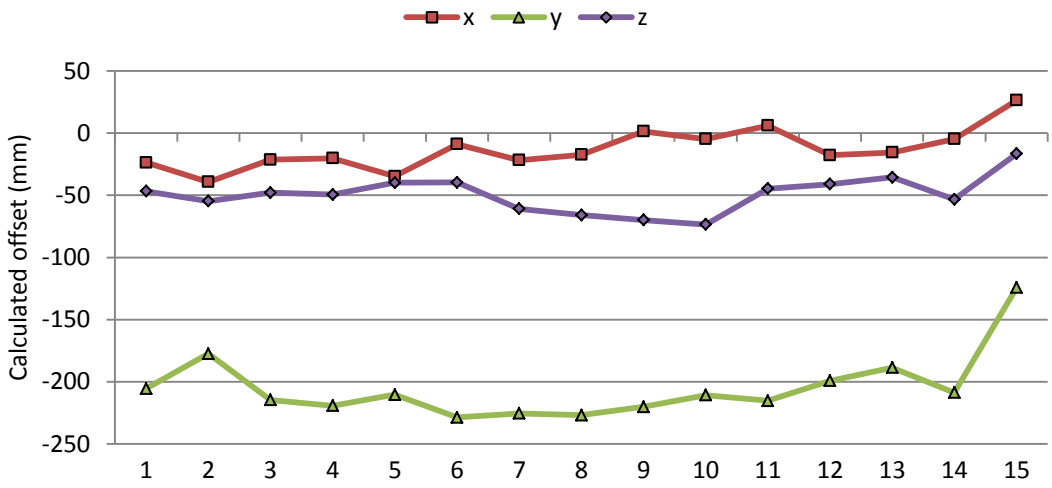

Figure 6.9: Changes in calculated positional offsets in data set RL2.

It is practically impossible to exactly define the contribution of multipath on positional offset calibration value changes, because the exact reflectance pattern at each location is unknown. However, the results of the Roughting Linn case study demonstrated that precise positional offset calibration using DGPS for positioning cannot be achieved

when the recording system mounting frame is constantly tilted by more than 20°. This is due to the way the recording system is currently assembled. A solution could be to fix another spigot to the mounting frame that allows recording objects at low elevation angles from the ground without subjecting the antenna to very high tilts (greater than 20°). In this case positional offset calibration can be conducted according to the kind of heritage object to be recorded. This flexibility would certainly improve the usability of the recording system.

6.1.4 Truth data accuracy

Another factor influencing offset calibration precision and stability is the accuracy of truth data used in the offset calibration process. In this research project, exterior orientation parameters derived indirectly in a bundle adjustment using coordinated control points were used as truth data for offset calibration. This truth data was assumed to represent the true orientation and position of the camera at the time of exposure. When assessing offset calibration precision and stability the accuracy of the truth data has to be considered. The results of the offset calibration stability assessment in the St. Catherine's Oratory case study (Section 5.1.3.2) demonstrated that the truth data can change slightly when the image configuration changes (Section 5.1.3.2). Data of the two camera stations at the location of orientation sensor initialisation were used in data set SCO1 and in data set SCO2. The heading calibration value in both data sets was derived from offsets calculated at these two camera stations only. However, a heading calibration value change of 0.1° between data sets SCO1 and SCO2 occurred (Table 5.3). This could only be caused by using differing sets of images in the bundle adjustment and demonstrates a well-known issue of the bundle adjustment technique. A bundle adjustment is based on least-squares estimation and simply minimises the sum of squares of residuals of observations (Cooper and Robson, 2001). Using a different set of images changes the set of observations during adjustment. As a result, parameters estimated during bundle adjustment will also vary slightly, demonstrating that in general no unique solution for these parameters exist (Cooper and Robson, 2001). Being dependent on the observations used in the bundle adjustment, slightly different exterior orientation parameters will be determined using different image sets. Therefore, the accuracy of

truth data used for offset calibration will inevitably influence the stability of offset calibration.

Generally the variations in exterior orientation parameters used as truth data caused by differing image configurations are smaller than the expected measurement accuracy of orientation sensor and DGPS. The magnitude of the heading offset change between SCO1 and SCO2 (0.1°) is smaller than the expected orientation sensor heading accuracy (0.3°). Testing the variation of exterior orientation parameters depending on the images used, suggested that the impact of the camera configuration on the offset calibration is less significant than the expected measurement accuracy of orientation sensor and DGPS. However, small changes in truth data due to image configuration can add to other sources for offset calibration value changes (Sections 6.1.1 to 6.1.3). This can cause offset calibration value changes that slightly exceed the expected orientation sensor and DGPS accuracy (Section 4.1.2).

6.2 Practicability of the recording system for cultural heritage recording

6.2.1 Achievable absolute accuracy

The accuracy assessment of the initial recording system tests (Section 4.2.1) and the case studies (Section 5.1.4 and Section 5.2.3) demonstrated practicability of the recording system for heritage recording projects that require data for measurements in relation to a 3D national coordinate system of medium accuracy. The recording system can achieve absolute accuracies better than 43 mm without any control. In most cases the absolute accuracy is even better than 25 mm. These accuracies were achieved with error margins normally between 1.5 mm and 3.5 mm. When relating the absolute accuracy results to the extents of the test field in easting (8.5 m), northing (6.5 m), and height (6.3 m), ratios between 1:150 and 1:3130 were achieved. The huge potential of a similar system for direct exterior orientation determination was already mentioned in Fiani and Pistillo (2004). However, the authors noted that the differences between directly and photogrammetrically determined exterior orientation parameters

were comparatively high and indicated that the system was not practicable at that time. Coppa et al. (2007) also used a similar system for mobile mapping and noted that the displacements between the surveyed path and the corresponding route on a map varied between 0.6 m and 1.5 m. Other low-cost approaches to image-base recording found in literature (Section 2.8) either only enabled scaled measurements (Chandler and Fryer, 2005; Ordóñez et al., 2008; Bryan and Chandler, 2008) or relied on the availability of control points (Bosch et al., 2005; Boochs et al., 2007). Therefore, the results achieved in this research project demonstrate that this recording system (Section 3.3) improves low-cost cultural heritage recording by enabling direct exterior orientation determination in close-range photogrammetry. The accuracy achieved in this study is certainly higher than the achievable accuracy indicated by others (Fiani and Pistillo, 2004; Coppa et al., 2007), but further improvements are certainly possible. Potential enhancements could include ensuring stable offset calibration and robust image configuration (Section 6.2.1.1) and altering the exterior orientation parameter constraints during bundle adjustment (Section 6.2.1.2).

6.2.1.1 Influence of offset calibration stability and image configuration

Comparing the accuracies achieved using different combinations of direct measurements and calibration values demonstrated variations in absolute accuracy. This inconsistency was already noted in Section 4.2.1.2 with relation to Figure 4.7, where the achieved absolute accuracy varied from 5 mm to 40 mm. This figure demonstrated that the absolute accuracy level of 25 mm was significantly exceeded only when calibration values derived in Test6 were applied to direct measurements of Test8 and Test9, respectively. An investigation into this issue revealed that the heading calibration value between Test6 and Test8 changed by 0.7° while the heading calibration value between Test6 and Test9 changed by 0.5°. Both changes exceeded the expected orientation sensor heading accuracy (0.3°) and indicated unstable heading offset calibration, while other offset calibration values between these tests were considered stable (Section 4.1.2). This suggested that the large RMSE (40 mm and 34 mm, respectively) achieved in Test8 and Test9 using calibration values of Test6 was mainly caused by heading offset calibration values that were perhaps not suitable for correcting heading offsets in the direct measurements. Proof of this was provided by further data analysis, which is now described.

In order to investigate the effect of offset calibration value changes on the achievable accuracy, calibration values derived in Test6 were combined with calibration values that were considered better suited to correct offsets in direct measurements of Test8. The best absolute accuracy in Test8 was achieved when calibration values of Test7 were used to derive initial exterior orientation parameters. The magnitude of heading calibration value change between Test7 and Test8 is 0.33° and only slightly exceeds the expected heading measurement accuracy (0.3°). Therefore, the calibration values of Test6 were combined with calibration values derived in Test7 in six different ways. In each combination, a single calibration value of Test6 was exchanged with the corresponding calibration value of Test7, while the other calibration values remained unchanged. This resulted in 6 differing sets of calibration values, each containing a single value derived in Test7 and 5 values derived in Test6. These calibration values were subsequently applied to the direct measurements of Test8. The resulting initial exterior orientation parameters were utilised in a bundle adjustment, equivalent to the accuracy assessment process described in Section 3.6.3. The RMSE of check point coordinate differences achieved with the 6 different calibration value combinations is displayed in Figure 6.10. The only significant improvement of the absolute accuracy occurs when the heading calibration value derived from Test7 is used instead of the

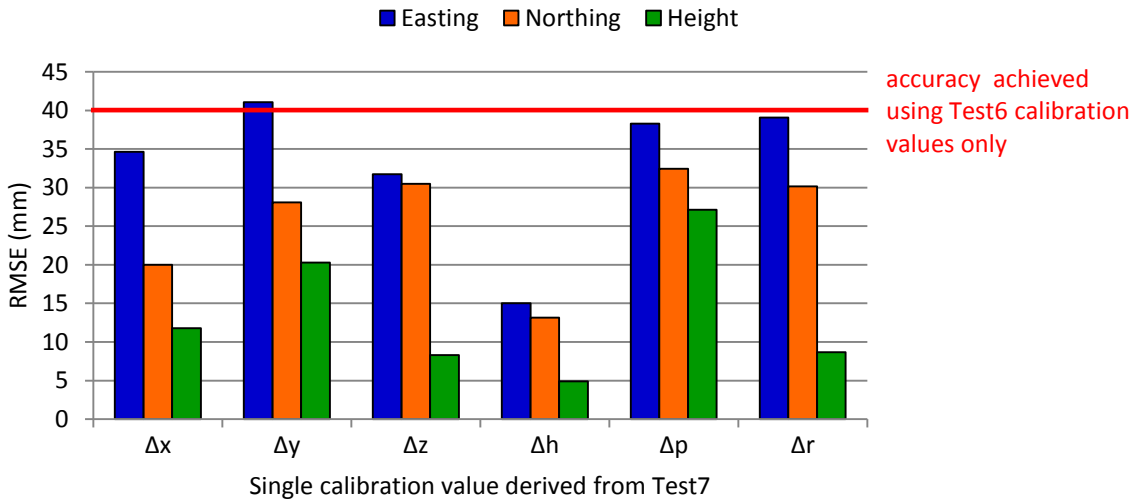

Figure 6.10: Absolute accuracy in Test8 using varying combinations of Test6 and Test7 calibration values.

heading calibration value derived in Test6. In this combination absolute accuracy of 15 mm is achieved while the absolute accuracy achieved with other combinations is close to the accuracy achieved using only calibration values derived from Test6 (40 mm). A similar result was also obtained when conducting the same test using direct measurements of Test9. This proves the importance of enhancing the camera fixture (Section 6.1.1) in order to achieve more consistent heading offset calibration values. When heading calibration stability of the recording system can be maintained, absolute accuracy better than 20 mm to 25 mm could be expected. This significantly improves the practicability of the recording system for cultural heritage recording.

However, the absolute accuracy achieved in Test6 to Test9 (Figure 4.7) also demonstrates that in some cases absolute accuracy better than 20 mm can be obtained, despite inconsistent heading calibration values. This is possible when the offset error can be compensated during bundle adjustment. The effect of the heading calibration value change between Test6 and Test8 on the achievable absolute accuracy was discussed above. This would suggest that a similar effect can be observed when calibration values derived from Test8 are applied to direct measurements of Test6. However, the actual absolute accuracy achieved in this combination was 15 mm (Section 4.2.1.2). A similar observation could be made when calibration values of Test9 were applied to direct measurements of Test6. This demonstrates that the error introduced by the heading calibration value change could be compensated during bundle adjustment in Test6 but not during bundle adjustment in Test8 and Test9, respectively. It was already discussed in Section 6.1.4 that bundle adjustment is based on least-squares estimation and minimises residuals of observations. Therefore, errors in the initial exterior orientation parameters are also minimised. The compensation of measurement errors during bundle adjustment was already demonstrated in Section 4.2.1.1. It also has been noted that the values of parameters estimated in a bundle adjustment can change when the image configuration changes (Section 6.1.4). Fraser (1996) describes the significance of image configuration for accuracy and precision of bundle adjustment. Generally, a more convergent image configuration results in better bundle adjustment results than a less convergent image configuration (Mason, 1995; Fraser, 1996). During the initial recording system tests at Loughborough University campus, images were generally acquired only with mild convergence due to the flatness of the “lab” test field (Section 3.2.1). However, in

Test6 some images were acquired with greater convergence, initially in order to test the offset calibration algorithm on data with a greater variation in measured heading. This resulted in a more convergent image configuration that probably enabled compensation of the effect of less suited heading calibration values during bundle adjustment in Test6. Figure 6.11 displays representations of the image configurations in Test6 and Test8. The image configurations in these tests only differed significantly in their arrangement in the horizontal plane. For simplification Figure 6.11 only displays the image configuration in the horizontal plane. The ability of Test6 to compensate heading errors during bundle adjustment better than Test8 is further demonstrated by testing the sensitivity of both data sets to errors caused by unstable heading offset calibration. For all images in both data sets, exterior orientation parameters were estimated in a LPS bundle adjustment using every other coordinated point of the "lab" test field as a control point. For testing, these exterior orientation parameters were considered to be free of error and are referred to as reference parameters. In order to simulate a heading error in the exterior orientation parameters caused by unstable heading offset calibration, 0.5° were added to the parameter φ for all images in both data sets. The other parameters remained unchanged. The resulting sets of exterior orientation parameters are referred to as simulated parameters. Subsequently reference and simulated exterior orientation parameters were used in a GAP bundle adjustment, generally constrained by their accuracy stated in the LPS

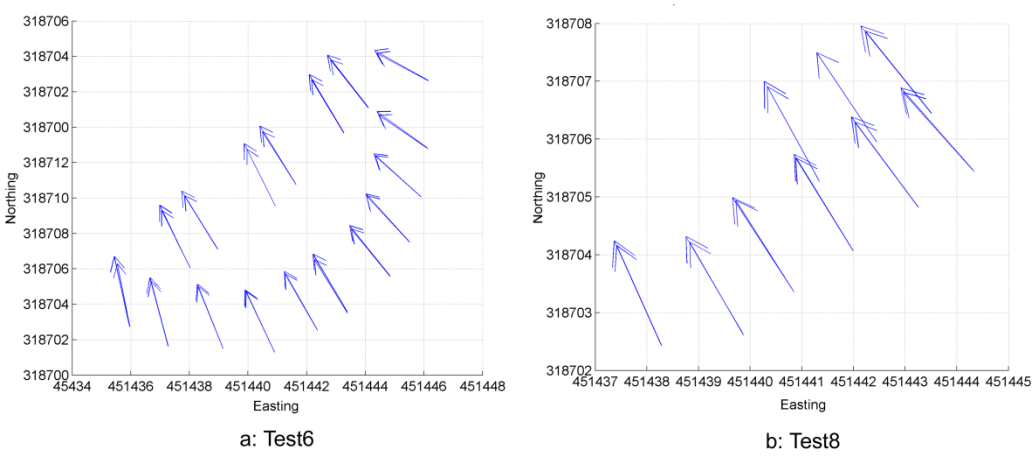

Figure 6.11: Comparison of image configurations in Test6 and Test8.

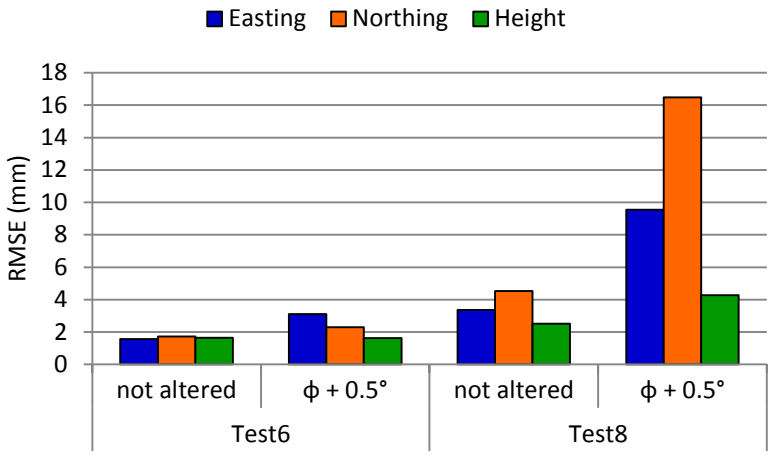

Figure 6.12: Testing error compensation capability of Test6 and Test8.

bundle adjustment report. For the simulated parameters, φ was constrained by 0.25°, which is obviously too tight considering the actual error introduced in φ. This reflects that in reality the magnitude of heading calibration value change is unknown and is therefore not considered when constraining φ. No control points were used in the GAP bundle adjustment and the remaining coordinated points of the test field were used as check points. The estimated check point coordinates were compared to their true value and the RMSE of the check point coordinates differences was calculated (Figure 6.12). Comparing the RMSE (absolute accuracy) achieved using the simulated exterior orientation parameters to the results achieved using the reference parameters reveals that the simulated error degrades the absolute accuracy in Test8 by up to 12 mm while the change in RMSE in Test6 is smaller than 1.5 mm. This demonstrates that even with an offset calibration error, an acceptable level of absolute accuracy is achievable, because calibration errors can be compensated when convergent imagery is used in the bundle adjustment. When possible, convergent imagery should be acquired in order to enable compensation of potential exterior orientation errors caused by unstable heading offset calibration values.

6.2.1.2 Selection of exterior orientation parameter constraints

Another factor that can help to improve absolute accuracy is the selection of an appropriate stochastic model through appropriate constraints during the bundle adjustment. In this project the standard deviations of offset calibration values were used to constrain directly determined exterior orientation parameters (Section 3.6.3).

This approach was initially chosen because the standard deviations were expected to be of the same magnitude or even slightly exceed the expected measurement accuracy of orientation sensor and DGPS, respectively. The expected measurement accuracy of the orientation sensor was specified by the manufacturer PNI with 0.3° for heading and 0.2° for pitch and roll (Table 3.2). For DGPS the expected measurement accuracy (10 mm in plan and 30 mm in height) stated in Konecny (2003) was used (Section 4.1.1.2). The results of offset calibration precision assessment (Sections 4.1.1, 5.1.3.1, and 5.2.2.1) demonstrated that in many cases the calibration value standard deviations were significantly tighter than the expected measurement accuracy. The standard deviations in these cases indicate an actual accuracy that was better than the expected accuracy. Bundle adjustment constraints based on these values could be considered too tight, when used on exterior orientation parameters derived from another data set where the actual offset standard deviation equals the expected accuracy. A better approach would be to use the expected measurement accuracy of orientation sensor and DGPS as constraints during the bundle adjustment, when calibration standard deviations indicate an actual accuracy that is better than the expected accuracy. Replacing all standard deviations by their corresponding expected measurement accuracy value, when they were smaller than this value resulted in improvements in achieved absolute accuracy for some combinations. Figure 6.13 provides a comparison of absolute accuracy achieved in Test8 using the initial approach of selecting constraints (standard deviations only) and using the modified

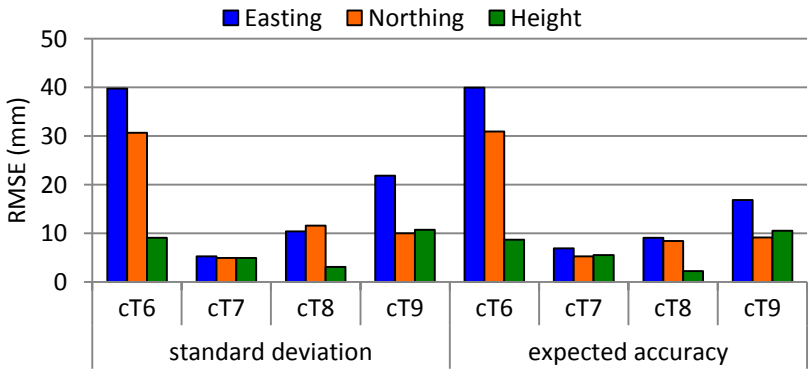

Figure 6.13: Influence of exterior orientation parameter constraints on absolute accuracy in Test8.

approach (expected measurement accuracy when necessary). The upper labelling indicates the origin of the calibration values and the lower labelling indicates the approach used for selecting constraints. Using the expected accuracy as constraint for some parameters resulted in minor improvements in the accuracy achieved using calibration values of Test8 (3 mm) and calibration values of Test9 (5 mm). Similar results were obtained in other combinations of direct measurements and calibration values. This approach does not always result in an improvement of absolute accuracy and can even slightly decrease the absolute accuracy (calibration values of Test6 and Test7 in Figure 6.13). However, the potential improvement of absolute accuracy outweighs the slight decrease in accuracy that might occur in some cases. Therefore, the expected measurement accuracy of orientation sensor and DGPS should be used as exterior orientation parameter constraint during bundle adjustment whenever the offset calibration value standard deviation is smaller than the corresponding expected measurement accuracy.

6.2.1.3 Other influences on achievable accuracy

Besides the factors discussed in Section 6.2.1.1 (consistency of offset calibration values and image configuration) and Section 6.2.1.2 (stochastic model used in the bundle adjustment), the achievable absolute accuracy is also influenced by the accuracy of direct measurements and how the bundle adjustment minimises residuals.
In Section 6.1.4 it was already noted that no unique bundle adjustment solution exists and that the solution is dependent on the observations used in the bundle adjustment. Small changes to these observations can cause residuals being minimised differently, resulting in slightly differing estimated parameters. Slightly differing initial exterior orientation parameters used in the bundle adjustment can therefore result in varying estimates for check point coordinates. This influences the result of accuracy assessment, because check point coordinates estimated in a bundle adjustment relying only on direct exterior orientation parameters, were used to derive indicators for achievable absolute accuracy (Section 3.6.3). The absolute accuracy of the Roughting Linn data sets (Section 5.2.3.1) demonstrated this effect. When calibration values of initial recording system tests were used for offset correction, errors degrading the height accuracy could be compensated in RL1 but not in RL2. The fact that differing initial exterior orientation parameters will affect the bundle adjustment results

differently can explain why combinations, where offset calibration values and direct measurements are derived from the same data set, do not always achieve the best accuracy for this data set (Section 4.2.1.2). Offset calibration values derived from the same data set as the direct orientation and position measurements were considered to be best suited for correcting rotational and positional offsets in these measurements. However, only in Test7 of the initial recording system tests this combination also achieved the best absolute accuracy (Section 4.2.1.2). The influence of how residuals are minimised during bundle adjustment also contributes to the inconsistency of achieved absolute accuracy within and between data sets, but the achievable relative accuracy is influenced even more significantly (Section 6.2.2).

Another factor that affects the achievable accuracy is the expected measurement accuracy of orientation sensor and DGPS. With the improvements discussed in Section 6.2.1.1 and Section 6.2.1.2 the absolute accuracy achievable with the recording system can get close to the expected DGPS positioning accuracy (10 mm in plan and 30 mm in height). Not considering potential errors introduced by the orientation sensor, the centimetre positioning accuracy of DGPS limits the currently achievable absolute accuracy. For higher accuracy positioning, longer observation times would be required for each camera station, which would significantly increase the time require for data collection and decrease the efficiency of the recording system.

6.2.2 Achievable relative accuracy

In the area of heritage recording the provision of data for measurements that are accurate in relation to each other is considered an important objective of data acquisition (Bryan, 2010b). It provides opportunity to relate features of an object, or several small objects of one site, more accurately to each other. In many cases when data collection for accurate positioning in a 3D national coordinate system is not possible due to restrictions in cost and expertise, scaled measurements are considered a suitable alternative (Bryan and Chandler, 2008; Ordóñez et al., 2008). It therefore seems sensible to reappraise the accuracy of data collected in a relative way, as well as absolute conducted so far. The relative accuracy achieved in the initial recording system tests and in the case studies is generally better than the absolute accuracy

achieved. The achieved relative accuracy varies between 3 mm to 26 mm for easting, northing, and height distances. The ratios achieved when relating these results to the average distances measured between check points range from 1:90 to 1:870. The upper limit of achieved relative accuracy is perhaps too large for some cultural heritage documentation projects but when horizontal (2D) and slope (3D) distances are considered, relative accuracy in most cases improves significantly. The most recent test results (Test6 to Test9) demonstrated achievable horizontal and slope relative accuracy between 3 mm and 12 mm (accuracy-distance-ratio ranging from 1:370 to 1:1750). The error margins for these results were smaller than 1 mm, indicating small changes in calculated check point distances. It has been noted before (Section 4.2.2) that the improvement in relative accuracy from easting, northing, and height distances to horizontal and slope distance indicate rotation of the estimated check point coordinates, with respect to the national coordinate system (OSGB36). Figure 6.14 depicts the horizontal differences between estimated and true check point coordinates for Test8 using calibration values of Test6. With this combination the worst RMSE for easting, northing, and height distances of the initial recording system tests was achieved. The arrows originate at the true check point coordinates and point in the direction of the estimated check point coordinates. The length of the arrows indicates the magnitude of the horizontal distance between true and estimated coordinates. For visualisation purposes the original magnitude was multiplied by 50, resulting in the length of the arrows appearing exaggerated compared to the values of the coordinate axes. The arrows in Figure 6.14 indicate a counter-clockwise rotation of the estimated check point coordinates with respect to the OSGB36 coordinate system. In Section 4.2.2 it was suggested that this rotation is caused by insufficiently stable rotational offset calibration. Significant coordinate rotations appear in the horizontal plane only, which indicates a correlation to heading offset calibration value changes. In fact, the largest heading calibration value change (0.7°) occurred between Test6 and Test8, resulting in the check point coordinate rotation depicted in Figure 6.14. Exchanging the heading calibration value of Test6 with the heading calibration value of Test7 (Section 6.2.1) the achieved 1D relative accuracy was improved and the check point coordinate rotation significantly reduced. A similar 1D relative accuracy result is achieved in Test9 using calibration values of Test6.

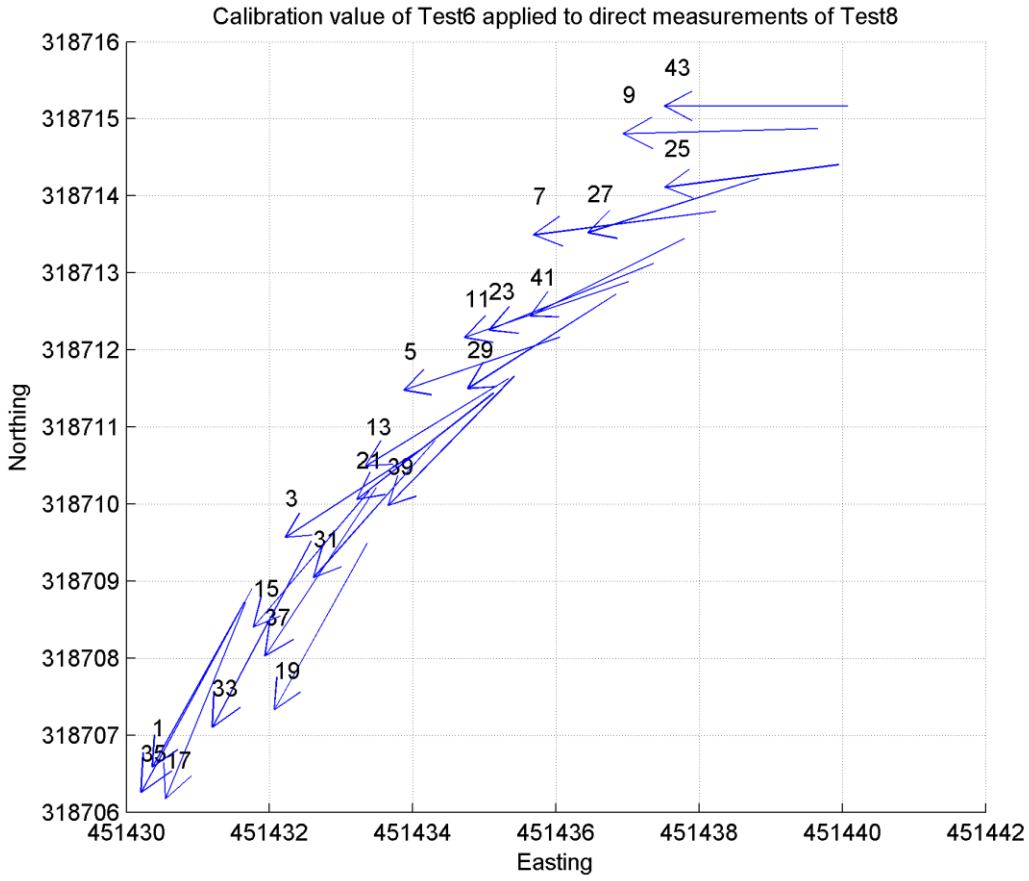

Figure 6.14: Direction of horizontal check point coordinate differences.

Between these two tests the heading calibration value change was the second largest (0.5°). This demonstrates that stable offset calibration is crucial for easting, northing, and height relative accuracy, similar to the achievable absolute accuracy discussed in Section 6.2.1. The similarity between achievable absolute and achievable 1D relative accuracy was already identified in Section 4.2.2. Therefore, the image configuration also influences the achievable relative accuracy for easting, northing, and height distances. This explains why in some data sets errors due to heading calibration value changes, could be better compensated than in others.

The rotation of the check point coordinates in the horizontal plane reduces the significance of the achievable 1D relative accuracy. When using horizontal (2D) distances the effect of the rotation is cancelled out, resulting in significantly better relative accuracy (Table 4.11). Therefore, RMSE derived from horizontal distances is considered a better indicator of the relative recording system performance. The 2D

relative accuracy results of the most recent tests (Test6 to Test9) are very encouraging, because most of them (12 out of 16 combinations) are smaller than 8 mm (Figure 4.11). The RMSE derived from slope (3D) distances is only slightly larger, indicating that the relation in height between the check points could be better maintained during bundle adjustment than the relation in easting and northing.

In Section 5.2.3.2 it was indicated that the achievable horizontal and slope relative accuracy is not dependent on the availability of well suited calibration values, but on whether the bundle adjustment can maintain the relation between check points. The significant positional calibration value changes between initial recording system tests and data sets of the Roughting Linn case study of up to 85 mm (Section 5.2.2.2) are not correlated to the offset calibration stability of the recording system (Section 5.2.2.2). However, the results of the Roughting Linn case study demonstrated that small differences between data sets such as image configuration and offset calibration can result in the bundle adjustment minimising residuals differently and significantly different levels of relative accuracy achievable. The horizontal and slope relative accuracy achieved in data set RL2 using calibration values of the initial tests was better than 7 mm. At the same time corresponding RMSE in data set RL1 ranged from 35 mm to 50 mm. An explanation could be that small differences in the characteristics of a data set cause residuals of observations being minimised differently during bundle adjustment. The significant positional offset calibration value changes from initial test data sets and Roughting Linn data sets certainly amplify this effect by providing erroneous initial exterior orientation parameters that are too tightly constrained during bundle adjustment. When better suited calibration values are used, the achieved horizontal and slope relative accuracy ranges from 7 mm to 16 mm, which is comparable to the results of the initial recording system tests.

6.2.3 Improvement by availability of a single control point

In some heritage recording projects it might be possible to establish a single control point at or adjacent to the heritage object. This usually does not significantly increase the total cost and time for heritage recording. Even when no experts are available for surveying this control point using a Total Station, coordinated control points can be obtained using DGPS. This can even be achieved using the equipment already

available with the recording system. The DGPS receiver of the recording system could be used to derive coordinates for at least one single point prior to data collection. This point would normally be positioned on the ground, which is only practical for low-rising, horizontal objects, for example Roughting Linn (Section 5.2). For vertical structures, such as St. Catherine's Oratory (Section 5.1), a surveying target could be attached to a cane that is positioned in the ground adjacent to the heritage object. Coordinates of this control point could be determined by positioning the DGPS antenna exactly above the target and measuring the height distance between antenna and target centre.

In Section 5.1.4.2 it was demonstrated that the availability of a single control point can significantly improve the achievable absolute accuracy. Using the data processing approach described in Section 5.1.2, the absolute accuracy obtained in the St. Catherine's Oratory case study changed from 42 mm using no control points to 23 mm using a single control point (Section 5.1.4). A single control point also allows to achieve an acceptable level of absolute accuracy (32 mm) even when the offset calibration values used for initial exterior orientation determination are inaccurate (Section 5.1.2). Using the same inaccurate offset calibration value without any control point achieved an absolute accuracy of 79 mm only. Therefore, whenever establishing a single control point at a heritage site is feasible, this opportunity should be used to improve the achievable absolute accuracy.

The effect of utilising a single control point is different for the achievable relative accuracy, as a single control point actually decreased the achieved relative accuracy. It was noted in Section 5.1.4.2 that this could have been caused by the bundle adjustment being over constrained, creating localised distortion. This effect can be explained by comparing the deviations of estimated check points from their true coordinates when either a single or no control point is used. Figure 6.15 displays deviations of estimated check point coordinates from their true values for data sets SCO1 using calibration values derived from SCO2 (a to c) and SCO2 using calibration values derived from SCO1 (d to f). For simplification only the deviation in the horizontal plane are displayed. Graphs "a" and "d" depict the direction of check point deviations when no control points were used during bundle adjustment. Graphs "b" and "e" display the result achieved when coordinated point 10 was used as control

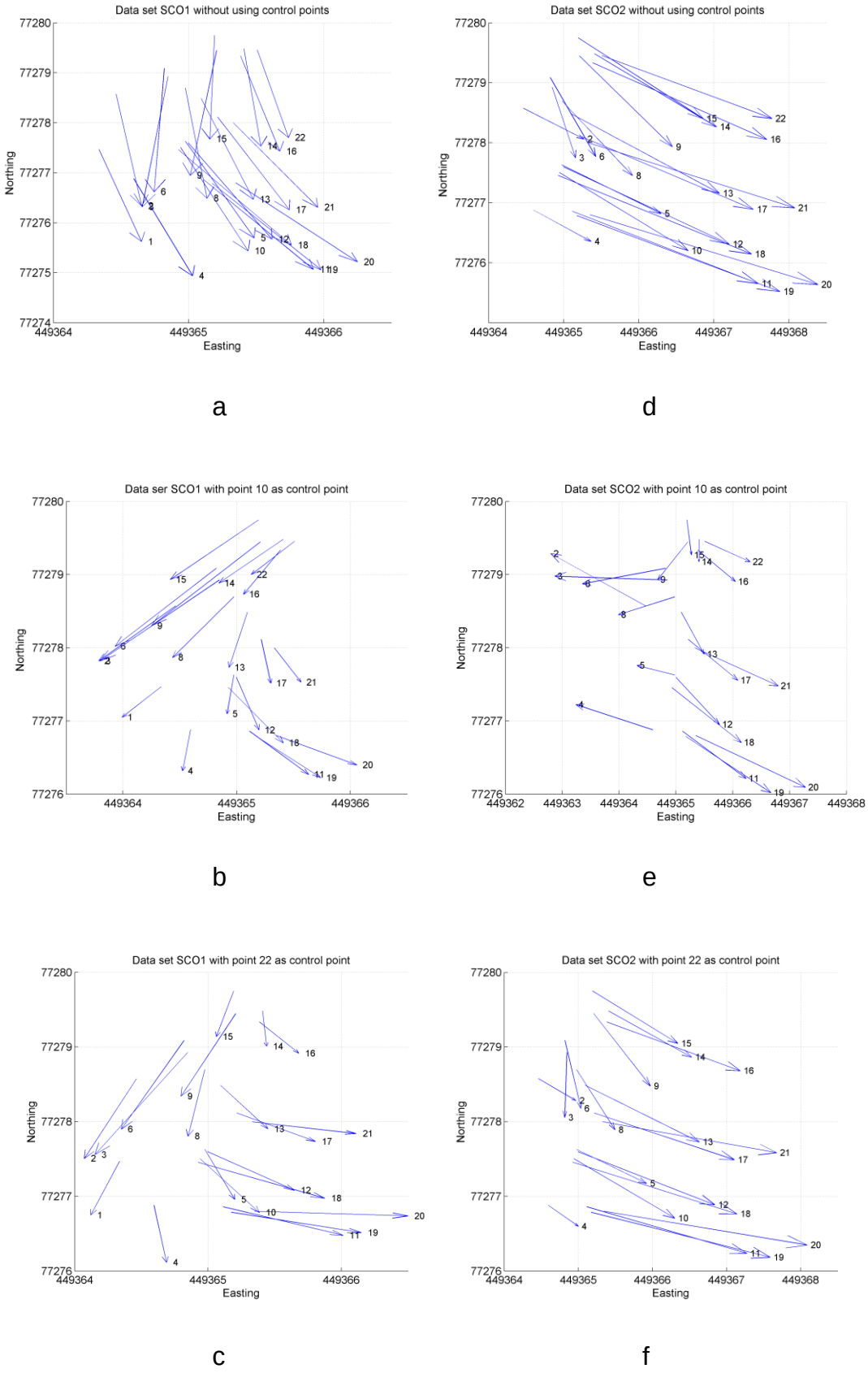

Figure 6.15: Comparison of check point coordinate changes using no (a, d) or a single (b, e, c, f) control point in data sets SCO1 and SCO2.

point. These results are the same as the results presented in Section 5.1.4.2. Graphs "c" and "f" display the result achieved using a different coordinated point (point 22) as single control point. These results were produced in order to test the influence of control point location on the achievable relative accuracy. For enhancing visualisation, the arrow length indicating the magnitude of deviation in the horizontal plane was amplified by multiplying the original length by 50. Figure 6.15 demonstrates that when no control points are used during bundle adjustment the estimated check point coordinates are slightly rotated with respect to the OSGB36 coordinate system. This rotation is comparable to the rotations discovered in the initial recording system tests (Section 6.2.2). When coordinated point 10 is used as control point, the arrows of the graph do not describe a slight rotation but point in differing directions. This indicates distortion of the check point coordinates positions, which was also indicated by the slight increase of absolute accuracy error margins when a single control point was used (Section 5.1.4.2). The effect of distortions is more prominent in data set SCO2 (Figure 6.15e), where points located at greater elevation than point 10 (points 1 to 9) divert from their true coordinates in a westerly direction and points located at smaller elevation (points 11 to 22) divert in an easterly direction. A similar, but less prominent effect can be observed for SCO1 (Figure 6.15b). This is also reflected in the degradation of the relative accuracy from SCO1 to SCO2 (Section 5.1.4.2). The impact of using a single control point on the direction of check point coordinate deviation apparently varies for different data sets. This is certainly caused by slight differences in image configuration between the data sets. The kind of check point coordinate deviation (random direction or rotation) is also dependent on the location of the control point used in the bundle adjustment. Point 10 was located approximately in the centre of the tower of St. Catherine's Oratory. Point 22 was located at the bottom of the tower. Figure 6.15 demonstrates that using a different control point in SCO1 did not change the results significantly. Using point 22 as control point in data set SCO2, resulted in a significant change in the directions of estimated check point coordinates (Figure 6.15f). The arrangement of arrows is similar to the case when no control points are used and indicates a slight rotation. This resulted in the easting relative accuracy improving from 34 mm (point 10) to 23 mm (point 22) and the northing relative accuracy improving from 11 mm to 6 mm. The horizontal relative accuracy also improved from 19 mm to 11 mm.

Figure 6.15 displays check point coordinate deviations in the horizontal plane only, but utilising a single control point during bundle adjustment also had an effect in height. The relative accuracy in height and slope distances degraded from 9 mm (point 10) to 14 mm (point 22) and from 8 mm to 13 mm, respectively. However, these values are similar to the relative accuracy achieved in SCO2 using no control points. This demonstrates that using a single control point during bundle adjustment does not improve the achievable relative accuracy. Depending on image configuration and location of the control point, relative accuracy can even degrade. Therefore, it is better not to use a single control point measured in a single image during bundle adjustment, when measurements that are accurate in relation to each other are required. Nevertheless, when establishing a control point at a heritage site is feasible, it is advisable to carry out this additional work and to acquire at least one image in which the control point is visible. In case measurements in a 3D national coordinate system are required at a later stage, a single control point can enable measurements of significantly improved absolute accuracy.

In this project the effect of a single control point was tested with the point measured in a single image only. In reality, a coordinated point established at a cultural heritage site would be chosen to be visible in more than one image. This certainly will further improve the achievable absolute accuracy. Measuring a control point in several images might even reduce the negative effect on the relative accuracy.

6.3 Limitations and potential for enhancements

6.3.1 Portability

The portability of the recording system is an important factor for its usability in cultural heritage recording. Heritage sites are often not directly accessible by car and it might be necessary to carry recording equipment a certain distance in a pathless area. For the case study at St. Catherine's Oratory the recording system was carried about 700 m in pathless terrain up a hill. Even for the Roughting Linn case study the

recording system was carried for about 50 m. This demonstrates that the recording system is portable, even in rough terrain. For transportation the recording system can be separated into four parts: Laptop, mounting frame, tripod, and DGPS receiver. These parts can be carried by one person, but their combined weight makes transportation more difficult, particularly in rough terrain. The DGPS receiver is certainly the heaviest and bulkiest part of the recording system. Portability could be greatly improved when the currently used survey-grade DGPS receiver could be exchanged with a smaller and lighter receiver that is capable of also providing centimetre accuracy. The SXBlue III GPS receiver of Geneq that was announced in 2010 (Geneq, 2010b) is smaller and significantly lighter than the Leica System 500 receiver currently used for positioning. Table 6.1 provides a comparison of receiver and antenna dimensions and weight specified for the Leica System 500 (Leica Geosystems, 1999) and the Geneq SXBlue III (Geneq, 2010b) DGPS receivers. Assuming the SXBlue III achieves centimetre accuracy in positioning, which is claimed by the manufacturer (Geneq, 2010b), it would be a suitable replacement for the Leica System 500 receiver and help to improve portability of the recording system. Another aspect of portability is the ease of moving the recording system at the heritage site during data collection. Figure 3.6 in Section 3.3 reveals that currently some of the recording system components are connected via cable (orientation sensor to laptop and DGPS antenna to receiver, respectively). This complicates moving the recording system between camera stations. Tripod with mounting frame, DGPS receiver, and laptop establish three entities that are connected via cable and cannot be

Table 6.1: Dimension and weight of System 500 and SXBlue III GNSS receivers.

	Feature	*Leica System 500*	*Geneq SXBlue III*
Receiver	Dimension (mm)	205 x 165 x 72	141 x 80 x 56
	Weight (g)	1250	517
Antenna	Dimension (mm)	160 x 50	19.8 x 55.4
	Weight (g)	400	79.4
Combined weight (g)		1650	596.4

moved at the same time. The distance any of the three entities can be moved at any one time depends on the length of the cables between them. This significantly reduces portability and flexibility during data collection. Using a DGPS that is comparable to the SXBlue III in size and weight can allow attaching the DGPS receiver to the mounting frame or the tripod. The same would be possible when the laptop is exchanged with a smaller size and lower weight computer, for example a tablet computer. This would allow moving the recording system as one entity. Another approach to overcome the slightly awkward moving of the recording system during data collection is establishing wireless data transfer between the recording system components. This could be achieved by using technologies such as Bluetooth. As long as the maximum data transfer distance is not exceeded the tripod with the mounting frame can be freely moved around during data collection. For example, the maximum transfer distance using Bluetooth technology is approximately 100 m (Bluetooth SIG, 2011), which would at many cultural heritage sites enable moving the mounting frame without moving laptop and DGPS receiver.

The possible enhancements suggested above do not influence the performance of the recording system (calibration precision and stability, achievable accuracy) but improve transportation and handling of the system. Thus, improving its ease-of-use for non-specialists, particularly when cultural heritage located in remote, less accessible areas is recorded.

6.3.2 Utilisation of DGPS

Utilising DGPS for positioning provided independence from the availability of known points at a cultural heritage site. On the other hand, reference data for differential positioning is necessary to achieve centimetre accuracy. In Great Britain reference data can be obtained from the Ordnance Survey Active GPS Network free of charge. In 2011 this network comprised over 100 continuously operating reference stations throughout Great Britain (Ordnance Survey, 2011d). However, these stations are not evenly distributed and depending on the location of the heritage site, distances to the closest station can vary significantly. At St. Catherine's Oratory the distance to the closest reference station was only approximately 9 km while at Roughting Linn the distance was approximately 26 km. The latter distance was considered too long to

assure stable atmospheric corrections. This can be considered a limitation of utilising DGPS. Positioning is still possible, but the further the reference station is away from the rover the less accurate the positioning will be. A solution to this problem could be acquiring atmospheric corrections from a virtual reference station. A virtual reference station is always fictitiously located close to the rover position and its observations are interpolated from surrounding real reference stations (Wanninger, 1999). There is currently no freely available service from Ordnance Survey for creating virtual reference stations. Virtual reference station services are provided by manufacturers of GNSS equipment, such as Trimble (Trimble Navigation, 2010). However, such a service is not free of charge and using the GNSS equipment supplied by these manufacturers is encouraged.

The main limitation in usability of the recording system is the requirement to have a line of sight from the DGPS antenna to at least four satellites at the same time (Section 2.6.1). This limits the application of the recording system to the outdoors, when DGPS is used for positioning. Furthermore, when cultural heritage is recorded in an outdoor environment, obstruction from trees and other high objects such walls close to the recording system, can hinder accurate DGPS positioning. To enable positioning in areas difficult for DGPS, the position of the recording system can also be determined using Total Station and a prism attached to the mounting frame (Section 3.3.1.5). The practicability of this approach was proven in Test4 of the initial recording system tests (Section 4.2.1.1). Bryan and Chandler (2008) noted that volunteers in the "Northumberland and Durham Rock Art Pilot Project" did find the operation of a Total Station for target points surveys difficult. Therefore, it has to be expected that the usability of the recording system by non-specialists in surveying would be limited. Even in that case, the recording system still provides the benefit of exterior orientation determination without attaching targets to heritage objects. This is particularly important when objects with sensitive surfaces need recording.

Even when utilisation of DGPS for positioning is feasible, it is not known whether non-specialists feel comfortable with operating survey-grade DGPS receivers. At the time of writing no examples could be identified in literature where non-specialists used survey-grade DGPS for positioning. However, many people can be expected to have been in contact with GPS at least in form of car navigation systems or even consumer-grade, hand-held GPS receivers. A basic understanding of GPS could be an

advantage when non-specialists are introduced to survey-grade DGPS, helping them to gain sufficient knowledge for operating such a system. This needs to be confirmed in field tests where non-specialists acquire heritage data using the recording system and DGPS for positioning.

Another limitation of utilising DGPS is the currently still high cost for survey-grade DGPS receivers. This prevented the development of a real low-cost system for cultural heritage recording at this time. Recent developments (SXBlue III of Geneq) indicate a trend towards smaller-size, and lower-cost DGPS receivers, that provide centimetre accuracy in positioning. In 2010 the cost for an SXBlue III rover was quoted to be £ 3,150 (Stevens, 2010). This is still more expensive than consumer-grade, hand-held receivers, which were quoted in 2005 at maximum € 500 (approximately £ 440) by Schwieger and Gläser (2005). More recent pricing quotes indicate a similar price range with a considerable number of devices available for less than £ 200 (Garmin, 2012). However, the cost for the SXBlue III is less than half the cost for a conventional survey-grade DGPS receiver (approximately £ 8,000 in 2006). Other manufacturers might follow this trend and future advances in mobile phone technology (Section 6.4) might even enable them to offer their products at lower cost. This is encouraging for the development of a real low-cost recording system for cultural heritage recording.

6.4 Recording using a system based upon a smartphone

In the previous section the trend towards smaller-size and lower-cost DGPS receivers was indicated. Similar trends can also be observed with other technologies. The most interesting developments for image-based heritage recording are certainly in the areas of digital consumer-grade cameras and mobile phones. Several authors reported on the feasibility of calibrating consumer-grade cameras (Bosch et al., 2005; Wackrow et al., 2007) and small-size cameras integrated in mobile phones (Akca and Gruen, 2009; Chikatsu and Takahashi, 2009) sufficiently accurate for close-range photogrammetry. Mobile phone cameras have already been used in many applications for data

acquisition. The images acquired were used to automatically recognise faces (Al-Baker et al., 2005), characters (Rohs, 2004), and even heritage objects (Pittore et al., 2005) for retrieving online information about a person or an object. In recent years small-size GPS was integrated into consumer-grade cameras and some mobile phones ("smartphones") to provide automatic geotagging functionality and other services (Section 2.4.2). Often a magnetic compass and MEMS-based tilt sensors are also integrated to determine the orientation of the photograph. The integration of camera, GPS, and orientation sensors into mobile phones can provide benefits for their applicability in photogrammetry, which was already recognised by Akca and Gruen (2009). The integration of GPS, compass, and tilt sensor in a consumer-grade camera or a smartphone with integrated camera can basically provide the same data as the recording system developed in this research project. When this data can be extracted from the camera and smartphone, respectively, direct exterior orientation determination would be possible. Therefore, these devices can be considered off-the-shelf systems that facilitate image-based recording (Kirchhöfer et al., 2011). In order to assess the accuracy currently achievable with such a system, a performance test was conducted using an "htc desire" smartphone (Figure 6.16). The "htc desire" integrates a 5 mega pixel camera, a digital compass, accelerometers, and GPS (HTC, 2011). For calibrating the camera of the smartphone, 9 images were acquired at the "lab" test field at Loughborough University (Section 3.2.1) in March 2011. Camera calibration was conducted using the approach described for calibrating the Nikon D80 SLR camera of the recording system (Section 3.3.1.1).

Also in March two sets of images for accuracy assessment were acquired at the "lab" test field. Each set consisted of four images. 3D orientation and position data at the time of exposure was extracted from the smartphone using an application known as "Imageotag" (Silva, 2011). At the time of image exposure, Imageotag extracts geodetic coordinates from the GPS, magnetic north from the compass, and pitch and roll from the accelerometers and prints this information on a copy of the original image. From these copies direct orientation and position information was manually extracted. The geodetic coordinates from the GPS were converted into OSGB36 grid coordinates using Grid InQuest software and Grid North was derived from the Magnetic North measurements of the compass using the approach described in

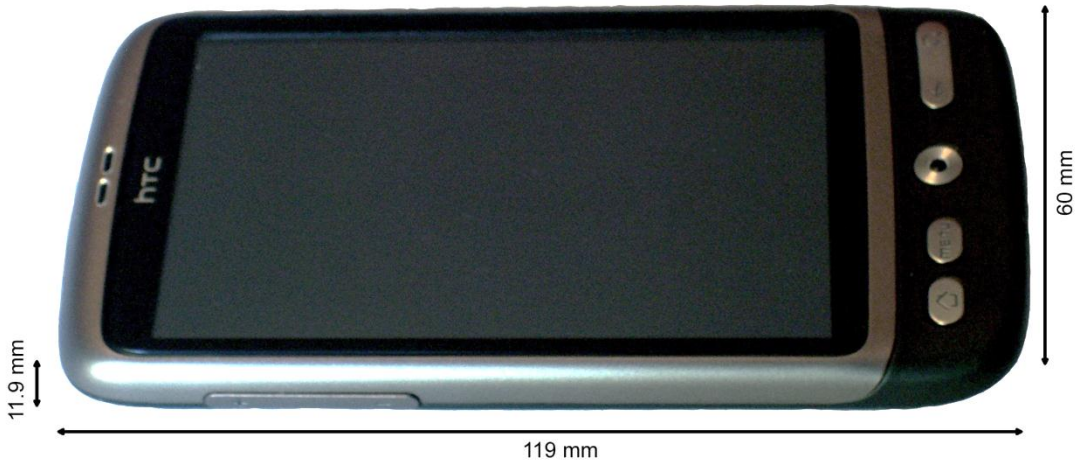

Figure 6.16: Dimensions of smartphone "htc desire".

Section 3.6.2. The two sets of images and their corresponding positions and orientations at the time of exposure establish two data sets (data set A and data set B, respectively) comparable to the data sets collected during the initial recording system tests and the case studies of this project. For both data sets rotational and positional offset calibration was conducted based on the calibration process described in Section 3.5, but the approach of determining the heading offset calibration value and its standard deviation was slightly altered. For the smartphone performance test, heading measurements at all camera stations of a data set were used in the calibration process, instead of only camera stations at the location of orientation sensor initialisation. The reason for this was that the smartphone offers no functionality to compensate errors in heading (compass) measurements due to local magnetic field distortions. Therefore, heading measured at all camera stations was considered to be of equal accuracy and equally suited to be used for offset calibration. Figure 6.17 and Figure 6.18 depict the offset calibration precision and stability achieved. The positional offset calibration precision and stability is presented using the unit meters (m) instead of the unit millimetres (mm) used for the recording system calibration results. No information about the expected accuracy of compass and accelerometers could be found in the smartphone specifications (HTC, 2011) that could be used as reference for calibration precision assessment. However, the measurement accuracy is certainly worse than the expected accuracy of the orientation sensor. This is also

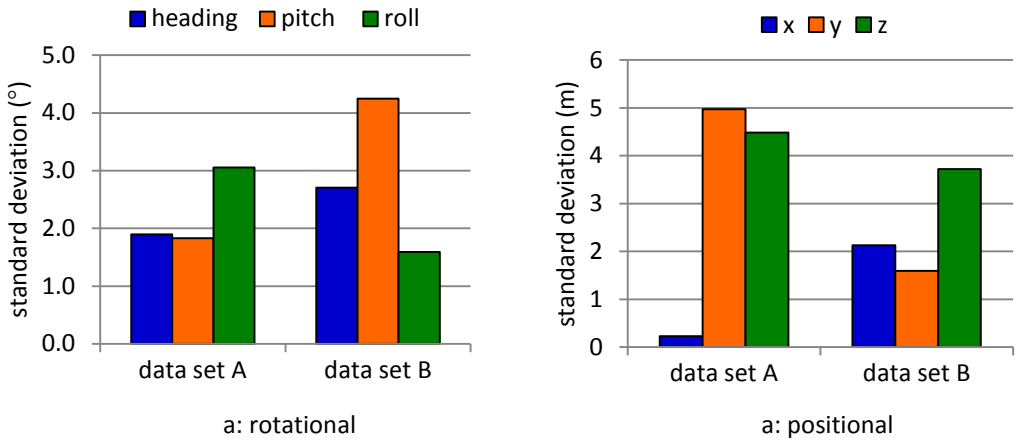

Figure 6.17: Precision of rotational and positional offset calibration using smartphone.

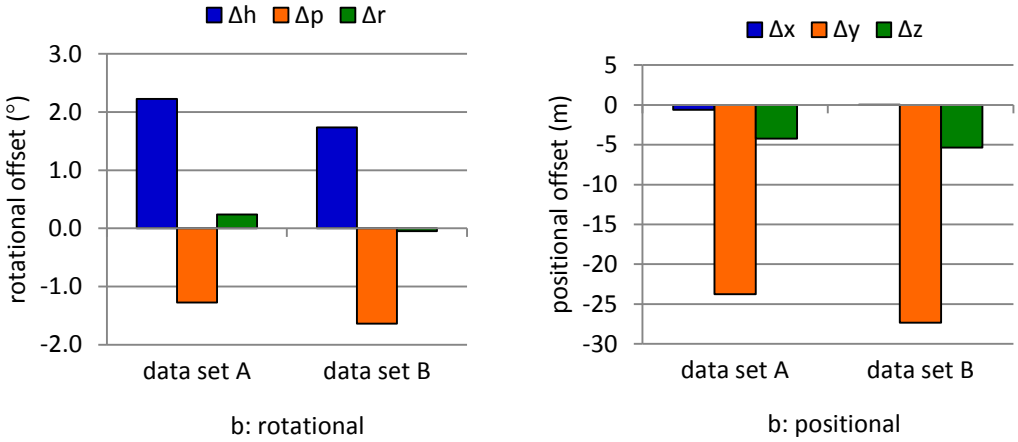

Figure 6.18: Stability of rotational and positional offset calibration using smartphone.

indicated by the rotational offset calibration standard deviation (Figure 6.17a), which is significantly larger than rotational calibration standard deviations derived for the recording system (Section 4.1.1.1). For the smartphone, standard deviation for heading, pitch and roll between 1.5° and 4.5° were achieved. These values can be used as indicators of the expected compass and accelerometer accuracy of the smartphone. The GPS positioning accuracy cannot be expected to be better than the theoretical positioning accuracy of code-based GPS, which is 10 m in plan and 19 m in height (El-Rabbany, 2006). This explains why the standard deviation of positional offset calibration derived for the smartphone (Figure 6.17b) is significantly larger than the positional standard deviations derived for the recording system developed in this project (Section 4.1.1.2).

The lower measurement accuracy of the smartphone GPS, compass, and accelerometers also influences the offset calibration stability (Figure 6.18). The rotational offset calibration values change by up to 0.5° (Figure 6.18a). The positional offset calibration value changes by up to 4.6 m (Figure 6.18b). Naturally, the positional offset calibration values displayed in Figure 6.18b do not represent the actual positional offset between GPS antenna and camera integrated in the smartphone, which cannot be greater than the dimension of the smartphone (Figure 6.16). The comparatively large positional offset calibration value is caused by the low positioning accuracy of the smartphone. Figure 6.18b indicates that in case of data set A and data set B offset calibration partly compensates this positional error, because positional offset calibration values derived in both data sets are comparatively similar.

For assessing the achievable absolute and relative accuracy, offset calibration values derived in data set A were applied to direct measurements of data set B, and vice versa. The resulting orientation and position values were used as initial exterior orientation parameters in a bundle adjustment using no control points. With the exception of φ, the parameters were constrained according to the description in Section 3.6.3. It was explained above that heading measurements at all camera stations were considered to be of equal accuracy. Therefore, φ at all camera stations was constrained by the standard deviation of the heading calibration value and not by heading measurement accuracy and range of heading offset (Section 3.6.3). Indicators for absolute and relative accuracy were derived from the estimated check point coordinates and their true values, equivalent to the approach described in Section 3.6.3. Additionally, achievable absolute and relative accuracy was also assessed for the case of a single control point being available in a single image, according to the description in Section 5.1.2. Figure 6.19 displays the absolute accuracy achieved for the smartphone data sets A and B. The displaying unit is meter (m). The absolute accuracy achieved without any control is 18.6 m (data set A) and 4.7 m (data set B). As expected, the availability of a single control point can significantly improve the achievable absolute accuracy (10.4 m and 2.9 m, respectively).

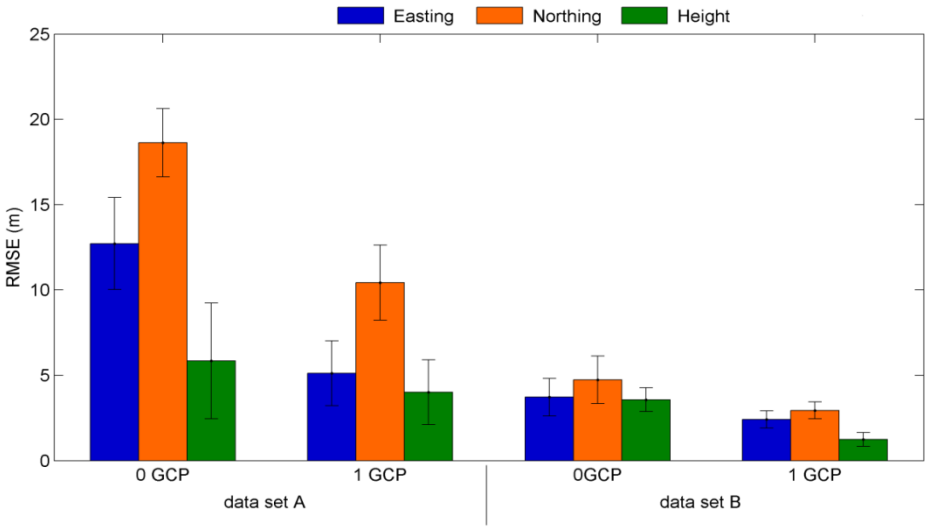

Figure 6.19: Absolute accuracy achieved using “htc desire” smartphone.

Figure 6.20 depicts the relative accuracy achieved using the smartphone with no and one single control point, respectively, during bundle adjustment. The unit for the RMSE of distance differences is also meter (m). As expected, the achievable relative accuracy is better than the absolute accuracy. Relative accuracy for easting northing and height distances (Figure 6.20a) vary between 2.2 m and 8.4 m when no control points were used. Using a single control point significantly improved the results (RMSE between 0.8 m and 4.8 m). The relative accuracy derived for horizontal and slope distances (Figure 6.20b) was also improved by using a single control point. This is probably due to the control point compensating some of the positional errors caused by the low accuracy of the smartphone GPS. This indicates that with low-accuracy GPS a single control point can improve the achievable relative accuracy. In Section 5.1.4.2 it was demonstrated that this is not the case when a recording system utilising survey-grade DGPS is used for data collection. The assessment of achievable absolute and relative accuracy did reveal significant variations between data set A and data set B. These variations are probably a result of differing data set characteristics (image configuration, offset calibration, direct measurement accuracy). The effect of variations in image configuration and initial exterior orientation parameters on how the bundle adjustment minimises residuals and achievable accuracy was already discussed in Section 6.2. It was also noted that large offset calibration value changes between data sets can amplify this effect (Section 6.2.2). The offset calibration value

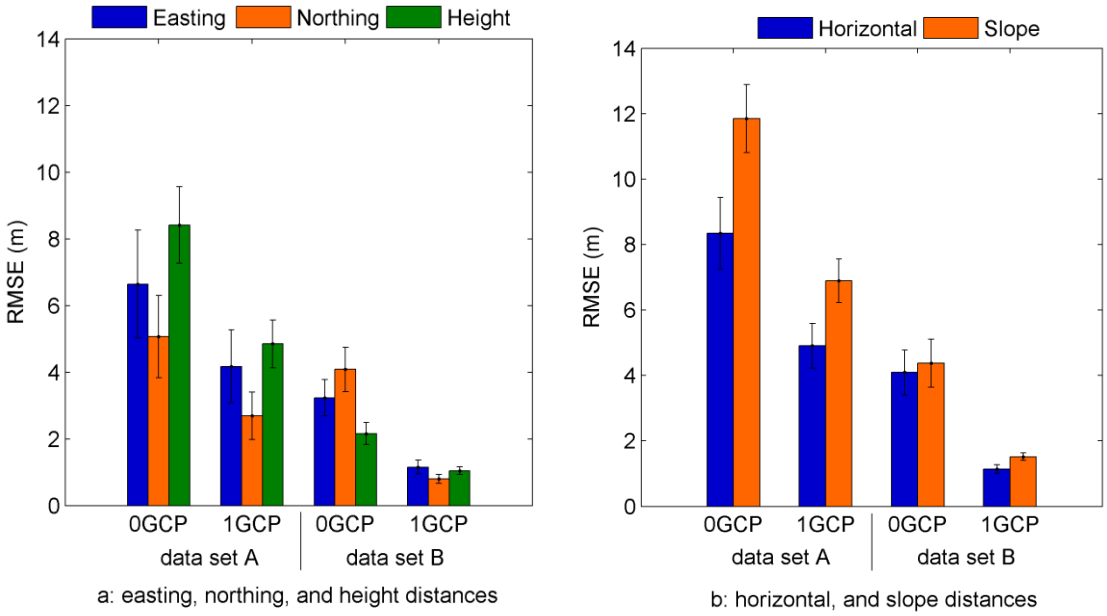

Figure 6.20: Relative accuracy achieved using "htc desire" smartphone.

changes between the two smartphone data sets are comparatively large, despite meeting the expected rotational and positional measurement accuracy (Figure 6.18). This can explain why the achievable accuracy variations between the smartphone data sets are significantly larger than the variations between data sets acquired using the recording system developed in this research project.

The absolute and relative accuracy currently achievable using a system based upon a smartphone is certainly not sufficient for accurate cultural heritage recording. It also does not comply with demands to use the best available technique for heritage recording (ICOMOS, 1964; UNESCO, 1972; Moullou and Mavromati, 2007). However, these results demonstrate the potential smartphones could have for cultural heritage recording in the future. Their greatest advantage is their low-cost and ease-of-use that would enable basically everybody to record cultural heritage. This could be of high interest in cultural heritage recording projects that aim to involve volunteers of the local community in the recording process, for example Bryan and Chandler (2008). It can be deduced from the calibration precision results in Figure 6.17 and the expected accuracy of the smartphone GPS that the smartphone GPS accuracy is the limiting factor on the currently achievable absolute accuracy. The accuracy of smartphone orientation measurement can be assumed to be approximately 5° (Figure 6.17a). The displacement that would result from a rotational error of 5° in the

exterior orientation rotation parameters at a camera-to-object distance of 10 m is smaller than the expected accuracy for code-based GPS. The limitation of application caused by the GPS accuracy becomes even more apparent, when the possibility of positional offset calibration value changes greater than the changes depicted in Figure 6.19 are considered. It has been noted before that positional errors due to code-based GPS accuracy were mainly compensated by the positional offset calibration values. This was possible because the calibration values derived in data set A and data set B were comparatively similar. Both data sets were collected at the same day in temporally close proximity, which provided similar GPS conditions for positioning in both data sets. This cannot be expected when data collection for offset calibration and data collection during field work are conducted at differing times and in different places. As a result positional offset calibration values might differ significantly from each other, indicating that they are less suited to compensate the positional error.

To investigate the effect of positional offset calibration values less suited for compensating the positional error, a short test was conducted using data of data sets A and B. The positional offset calibration values derived from data set A were altered twice in order to simulate more significant calibration value changes. These might be possible when the calibration and recording data set are not acquired under similar GPS conditions. In the first alteration each calibration value Δx, Δy, and Δz of data set A was changed by +3 m. In the second, the original positional offset calibration values were changed by +5 m. These altered calibration values were applied to the directly measured positions in data set B, resulting in two differing sets of initial exterior orientation parameters. For both sets of exterior orientation parameters the bundle adjustment process could not provide a solution. When a single control point was used during bundle adjustment, a solution could be provided for the case when positional offset calibration values were changed by +3 m. The achieved absolute accuracy in this case was 6.2 m, demonstrating that the control point could partly compensate for the badly suited initial exterior orientation parameters. However, even when using a single control point, a change of positional offset calibration values by +5 m did cause the bundle adjustment to terminate without solution. This demonstrates that calibration values that partly compensate the positional error are required to achieve absolute and relative accuracy comparable to the values displayed in Figure 6.19.

Developments on the mobile phone market in recent years indicate a trend towards smaller devices with increased performance. Akca and Gruen (2009) expect the cameras of mobile phones to improve in their quality and performance. When these developments continue and expand to also involve positioning and orientation devices integrated into smartphones, smartphones could in future be used as low-cost and easy-to-use systems for heritage recording, in particular when a single control point is available during data acquisition. It might be argued whether GPS devices that are capable of differential positioning and carrier phase measurement and, thus, provide centimetre positioning accuracy, will be integrated into smartphones in the future. However, recent research suggests that current smartphone GPS positioning accuracy can be enhanced by integrating inertial orientation data and wireless positioning techniques using systems such as Wi-Fi or Global System for Mobile Communications (GSM) into the positioning process (Constandache et al., 2010). The utilisation of smartphones is certainly an interesting field for further research in image-based recording and direct exterior orientation determination for close-range photogrammetry.

6.5 Photogrammetric heritage data usage and accessibility

6.5.1 Exterior orientation storage

One intention of this project was to investigate the practicability of combined storage of images and corresponding exterior orientation parameters in a single file using already existing standards of digital data storage. Probably the best known standard that provides the opportunity to store non-image data within an image file is Exif. The most recent Exif standard at the time of writing allows storage of additional information about an image, including 3D positions and 1D orientation, within the JPEG image header (Camera & Imaging Product Association, 2010). Therefore Exif is currently not suitable for storing exterior orientation parameters of an image, which would require storing 3D orientation. When the Exif standard is extended in the future

to also include storing 3D orientation, the practicability of storing exterior orientation information in the Exif image header should be re-assessed.

For this project the current version of the KML standard (Open Geospatial Consortium, 2008) was found to provide a suitable alternative to the Exif image header standard. Using data of the Roughting Linn case study, it was successfully demonstrated that imagery and corresponding exterior orientation can be saved in one single file (Section 5.2.4). The data stored in this file was further used to display images in a virtual globe (Google Earth) in their position and orientation during exposure. Visualisation of the images was achieved without manually loading images and assigning corresponding exterior orientation parameters. This demonstrates the practicability of storing exterior orientation and images in a single file and the opportunities this approach provides for automation in data utilisation. An advantage of using the KML standard instead of the Exif standard is that the exterior orientation information is stored in ASCII text file format. Using the Exif JPEG image header for data storage would require to save exterior orientation in a binary file format. This is not as easily accessible using simple word processing software commonly available on consumer-grade computers, such as Microsoft Notepad and WordPad. Furthermore, the KML standard also allows to save a theoretically unlimited number of images and their corresponding exterior orientation information within one single file. Exterior orientation of either a single image or multiple images is stored within a single KML file that is contained in a KMZ (compressed KML) file. This KMZ file also contains the corresponding images and appears to the user as a single file. In fact, a KMZ file is equivalent to a compressed folder ("zip-file") (Google, 2011b). Direct access to the contents of a KMZ file is easily possible by decompressing the KMZ using standard software such as the commercial "WinZip" (WinZip Computing, 2011) or the free open source "7-Zip" (Pavlov, 2011). This also demonstrates easy data accessibility when the KML approach is used.

KMZ files in this project were generated using purposely coded software in the programming language C# (Section 3.7.1). The main reason for this was to increase efficiency in producing KMZ files. Generating KMZ files is also possible for people who have no programming knowledge and without the need to buy specialised software. KMZ files can be created from scratch using a blank text file in a data folder and examples and information provided by Google (Google, 2011e). The KML

approach of storing images and exterior orientation in one file is therefore well suited for heritage recording projects that aim to involve volunteers for data recording and processing. In Bryan and Chandler (2008) it was reported that volunteers after some training became adept in processing images using photogrammetric software. This certainly is also achievable for the generation of KMZ files when some basic training is provided.

6.5.2 Online accessibility and visualisation

In Section 2.1.5 the benefits of making cultural heritage data accessible online were noted. One approach of improving online accessibility and visualisation was successfully tested in Section 5.2.4. In this test the KML feature "PhotoOverlay" was utilised for displaying images acquired in the case study at Roughting Linn in their position and orientation at the time of exposure in Google Earth. The displaying quality was visually evaluated by comparing the positions of targeted points visible in the photo overlay images with their position in Google Earth identified by markers on the terrain (Section 5.2.4.2). The results demonstrated that the "PhotoOverlay" feature of KML is sufficient for basic visualisation tasks. The displacements between targeted points visible in the photo overlay image and their corresponding markers on the Google Earth terrain are influenced by differing factors. Some displacement can be expected due to small errors in the exterior orientation of images used to generate the photo overlays. Some variations in direction and magnitude of the displacement could be explained by distortions due to not using orthorectified images for the photo overlays. However, using orthorectified images might not significantly improve the displaying quality, because Google Earth itself could be a source of error. The quality of the background data used in Google Earth (DEM, georeferencing of imagery, quality of orthophotos) is generally not known. Eugster and Nebiker (2008) already noted that virtual globes often use out-of-date geodata and unknown models of the Earth. Goodchild (2007a) discovered miss-registered background imagery in Google Earth. A similar issue was found during data analysis of the St. Catherine's Oratory case study in this research project. When camera station and target point coordinates were displayed in Google Earth for visualisation purposes, the point markers appeared shifted southwards from their real position by approximately 11 m. This demonstrates

that the correctness of Google Earth background data cannot be guaranteed and that results derived using this data will inherit the potential inaccuracy of the data (Goodchild, 2007a). Furthermore, even when the underlying DEM of Google Earth is accurate, its resolution can be expected to be comparatively low. This results in the surface of the rock-outcrop at Roughting Linn not being appropriately reflected for close-range photogrammetry. Even with orthorectified images used for the photo overlay, displacements between image targets and corresponding markers can be expected. Another source of error could be the transformation of the target point coordinates from OSGB36 grid coordinates into geodetic coordinates, required for displaying their position in Google Earth. Therefore, the evaluation of the photo overlay displaying quality is indeed difficult and it cannot be recommended to conduct large scale and detailed data analysis or measurements based on photo overlays displayed in Google Earth.

The advantage of utilising the KML "PhotoOverlay" feature in Google Earth is that it provides an inexpensive and easy-to-use tool for visualising cultural heritage data online. The displaying quality is certainly sufficient for providing an overview of the heritage data that is already available, thus avoiding repeated recording work. This benefit was already noted by Çayırezmez (2007). Furthermore, visualisation in Google Earth could aide early stage planning and decision making in heritage recording and conservation projects. The displaying facilities offered by Google Earth also provide an interactive environment for accessing cultural heritage online. This is of particular interest for lay people who like to experience cultural heritage in its geographic context, but are not able to access the heritage site in the real world. Providing an online environment to access heritage interactively can also raise awareness (Sheppard and Cizek, 2009) of cultural heritage and the need to protect it.

Finally, the displaying facilities in Google Earth can add a benefit to cultural heritage recording that is not directly related to accurate visualisation. Goodchild (2007a) remarked that the opportunity to share ones work online is an important factor that motivates people to produce and freely share data on the internet. The main reason behind this behaviour was identified as taking pride in one's own work and wishing to share it with other people. Many online platforms where people contribute data in form of images, maps, and even 3D models (for example Google Earth, Flickr, PhotoSynth, and OpenStreetMap) prove that there is a huge interest of lay people to

provide free online data. Providing an opportunity to display cultural heritage data on an online platform, could also motivate members of local communities to voluntarily join projects that aim to record local cultural heritage. For this kind of project the KML “PhotoOverlay” feature could be used as simple tool to achieve heritage data visualisation and sharing on the internet.

6.6 Summary

In this chapter the performance of the recording system, recommendations for data collection, and possibilities for enhancements were discussed.

In the first section the influences on offset calibration results were highlighted. A slight instability of the camera fixture, utilisation of magnetometers for heading determination, and tilting the DGPS antenna during data collection were identified as the main sources for small inaccuracies in the rotational and positional offset calibration. It was noted that small alterations to the camera fixture could significantly improve rotational offset calibration. However, heading is also influenced by local magnetic field distortions. Areas of high magnetic distortions can limit the usability of the orientation sensor for heading determination, which should be considered during the field work planning process. Changes to the camera fixture have no effect on positional offset calibration precision and stability. Positional offset calibration is mainly influenced by the decrease of DGPS positioning accuracy due to antenna tilt. It was demonstrated that increasing tilt of the antenna (and the mounting frame), increases the potential for positioning errors due to antenna design and multipath. As a result the recording system in its current assembling was considered not well suited for recording heritage objects with low elevation angle from the ground. Fixing another spigot to the mounting frame that allows to record objects at low elevation without tilting the DGPS antenna by more than 20° could be a solution to this problem and would increase the flexibility of the recording system significantly.

Despite these limitations it was stated that the recording system can achieve absolute accuracy of better than 43 mm, which is suitable for medium accurate cultural heritage recording. Potential to further enhance this result were discussed in Section 6.2.1 and it was concluded that with these enhancements, absolute accuracy of 25 mm is

possible. Furthermore, evidence for the suspected rotation of check point coordinates with respect to the OSGB36 coordinate system was presented. This rotation was mainly caused by unstable heading offset calibration and reduced the significance of easting, northing, and height relative accuracy. Measures of horizontal and slope relative accuracy were considered better indicators for the recording system performance. The influence of using a single control point on achievable absolute and relative accuracy was also discussed. When feasible, a single control point should be established prior to data collection. This can significantly improve absolute accuracy without notably increasing cost for heritage recording, in particular when it appears on more than one image.

The following section (Section 6.3) focussed on the limitations of the current recording system and potential for enhancements. The currently awkward handling during data collection could be eliminated by either establishing wireless data transfer or using small-size, low-cost DGPS receivers capable of providing centimetre positioning accuracy. The latter would also decrease the cost and enable the development of a real low-cost recording system. Furthermore, it was noted that the ease-of-use of survey-grade DGPS receivers by non-specialists should be investigated in field tests.

This chapter also provided an opportunity to test and discuss the practicability of smartphones for image-based heritage recording (Section 6.4). Smartphones with integrated camera, GPS, and orientation sensors could eventually provide data similar to the recording system developed in this project. The currently achievable accuracy is mainly limited by the positioning accuracy of the built-in GPS and is not considered sufficient for cultural heritage recording. However, the potential of smartphones for image-based heritage recording was demonstrated. It is expected that smartphone cameras, GPS, and orientation sensors will improve in their performance, providing an interesting field for future research in direct exterior orientation determination for close-range photogrammetry.

The penultimate section in this chapter (Section 6.5) was concerned with successfully storing image and corresponding exterior orientation parameters in a single KMZ file and visualisation in Google Earth. This approach is particularly beneficial for heritage recording projects that involve volunteers and low-cost equipment and software. The main advantages of utilising features of the KML standard for data storage and

visualisation were identified as low-cost, ease of accessing stored data, and simplicity in generating data files.

7 Conclusion

The aim identified for this research project was to *"demonstrate the practicability of direct exterior orientation determination in close-range photogrammetry for reducing cost and enhancing and widening cultural heritage data recording, usage, and accessibility"*. This can help to attenuate the risk of losing cultural heritage by reducing costs for recording and enabling non-specialists to become involved. This was considered particularly advantageous for smaller heritage sites of local or regional significance that might not be recorded due to lack of money and labour. During this study a recording system was assembled, consisting of a consumer-grade, digital SLR camera, a small-size orientation sensor, a survey-grade DGPS receiver and antenna, and an off-the-shelf laptop. Similar systems have already been tested for mobile mapping applications but reports found during the literature review suggested that their achievable accuracy is insufficient for heritage recording. However, results achieved in this research project demonstrated the recording systems usability for many cultural heritage recording requirements. This was seen in both a series of system tests conducted at Loughborough University and two case studies at real heritage sites.

The aim above reflects that the scope of this research extends beyond data collection to also include cultural heritage data utilisation. Images of cultural heritage and their corresponding exterior orientation were stored in a single file, utilising features provided by the KML standard. It was demonstrated that this improves data handling and enables automatic display of image-based heritage data in Google Earth. The benefits cultural heritage recording projects could gain from this include improving

planning processes, raising awareness of the need to record, and motivating volunteers to become involved.

The accomplishment the aim provided comprehensive understanding of the benefit low-cost solutions for data recording and utilisation can provide in the field of cultural heritage recording and conservation. While working on accomplishing this aim, various achievements were gained. These are summarised in the following section.

7.1 Achievements of this research project

The following paragraphs provide a summary of the achievements of this research project:

- *Investigation of the usability of low-cost sensors for enhancing cultural heritage data recording.*

In an extensive literature review it was established that using an image-based recording system comprised of off-the-shelf sensors and capable of direct exterior orientation determination can enhance cultural heritage recording by avoiding expensive control point surveys and enable non-specialists to become involved. It was found that consumer-grade digital cameras have already proven to be suitable for cultural heritage recording using close-range photogrammetry. It was further established that low-cost MEMS-based orientation sensors can provide measurement accuracy sufficient for close-range photogrammetry, while positioning using low-cost GPS receivers is not yet sufficiently accurate. The recording system developed in this PhD research utilised the low-cost TCM5 orientation sensor for determination of the exterior orientation angles, achieving medium accuracy (25 mm – 40 mm). This indicates that this sensor is usable for direct exterior orientation determination in close-range photogrammetry, when measurements of medium accuracy are acceptable. This and its comparatively low cost (£ 1,600) and small size demonstrates the suitability of this sensor to substitute the bigger-size and more expensive IMUs in close-range photogrammetry applications. The utilisation of magnetometers for heading determination was identified as the main limitation of the TCM5 orientation

sensor. Local magnetic field distortions can be compensated in an initialisation process, but moving the mounting frame would require re-initialisation. In order to avoid the resulting increase in data collection time and decrease in ease-of-use, a method was developed that only required orientation sensor initialisation once at the location of the first camera station prior to data collection (Section 3.5.2 and Section 3.6.3). This stochastic method proved to be suitable to minimise the effect of local magnetic field distortions on heading calibration and achievable accuracy and to enhance usability of the orientation sensor.

Unfortunately, no low-cost and small-size GPS receiver that provides centimetre positioning accuracy was available when this recording system was assembled. GPS receivers of the low-cost segment usually only use code-based GPS with an expected accuracy of 10 m for plan and 19 m for height. This was considered not sufficiently accurate to be used for direct exterior orientation determination in this project. Tests conducted using smartphone data confirmed this by demonstrating that the accuracy of code-based GPS is the limiting factor in the achievable accuracy. Therefore, a survey-grade DGPS receiver was used in order to prove the principle of direct exterior orientation determination in close-range photogrammetry. Recent developments suggest that there is potential for low-cost, centimetre accuracy GPS receivers being available in future. Such a low-cost receiver could substitute the more expensive survey-grade DGPS receiver and facilitate the assembling of a real low-cost and transportable recording system.

It can be concluded that currently available low-cost orientation sensors are usable for direct exterior orientation determination in close-range photogrammetry, while low-cost GPS receivers currently do not provide positioning accuracy suitable for medium accurate measurement. It could be expected that improved low-cost GPS receivers of acceptable accuracy could be available in future.

- *Construction of an image-based recording system that is capable of direct exterior orientation determination in close-range photogrammetry for cultural heritage recording.*

The recording system that was assembled at Loughborough University comprises a Nikon D80 digital SLR camera, a PNI TCM5 orientation sensor, a Leica System 500 DGPS receiver, and an off-the-shelf laptop. During data collection the orientation

sensor provided 3D orientation measurements and the DGPS receiver provided 3D position measurements at the time of image exposure. Camera, orientation sensor, and DGPS antenna were attached to a mounting frame that was designed to fix these components in their orientation and position with respect to each other. This enabled calibration of rotational and positional offsets between mounting frame components. Using calibration values derived in an offset calibration process, the exterior orientation of each image at the time of exposure could be derived from the direct orientation sensor and DGPS measurements. The practicability of the recording system for cultural heritage recording was demonstrated in two case studies at real heritage sites that differed in the type of heritage object that was recorded. The case studies allowed assessing the portability of the system, which is significant for its usability. The system can be transported even in pathless terrain, enabling recording of heritage sites that are not easily accessible. The case studies further revealed that the current assembling of the recording system is only suitable for recording objects that are mainly vertically structured. Heritage objects that are mainly horizontally structured require significant tilts of the mounting frame during data collection, resulting in a decrease in DGPS positioning accuracy due to antenna tilt. It was concluded that the type of heritage object that will be recorded has to be considered when the recording system is assembled.

- *Assessment of offset calibration precision and stability.*

Precise and stable offset calibration was found to be crucial to the achievable absolute accuracy. In order to achieve the third objective (Section 1.1) precision and stability of offset calibration were assessed using the expected measurement accuracy of orientation sensor and DGPS as reference (Section 4.1). The assessment of calibration results of differing data sets demonstrated that an acceptable level of offset calibration precision could generally be maintained. However, calibration precision decreased when data was collected with high tilts of the mounting frame (greater than 20°). Investigations revealed that this was caused by a slight instability of the camera fixture and particularly, decreasing DGPS positioning accuracy due to antenna tilt. Possibilities for enhancing calibration precision by modifying the camera fixture and antenna attachment were identified (Section 6.1.1 and Section 6.1.3). These modifications could also help to enhance offset calibration stability. Generally, stable

offset calibration was achieved in most cases. Some inconsistency in offset calibration values was revealed for heading. It has been noted that this might be solved by using more rigid materials for fixing the camera to the mounting frame (Section 6.1.1).

- *Assessment of accuracy achievable with the recording system using direct exterior orientation determination.*

In this research project, the assessment of achievable accuracy was divided into assessment of absolute accuracy and assessment of relative accuracy. Absolute accuracy was indicated by the RMSE of differences between the true coordinates of check points and corresponding coordinates estimated in a bundle adjustment that relied on direct exterior orientation parameters only. It was demonstrated that the recording system can achieve absolute positional accuracy in the object space of 43 mm without using additional control information, which was considered sufficient for medium accurate heritage recording. Furthermore, improving the heading offset calibration stability and collecting convergent imagery can increase the achievable absolute accuracy to 25 mm (Section 6.2.1.1).

The achieved relative accuracy was better than the achieved absolute accuracy. Relative accuracy was indicated by the RMSE of differences between check point distances calculated using true check point coordinates and distances calculated using check point coordinates estimated in a bundle adjustment that relied on direct exterior orientation values only. RMSE was calculated for 1D (easting, northing, and height), 2D (horizontal), and 3D (slope) distances. Horizontal and slope relative accuracy was generally better than 12 mm. However, the results of easting, northing, and height relative accuracy assessment were often worse than 12 mm. This was caused by the estimated check point coordinates being slightly rotated with respect to the OSGB36 grid coordinate system, which was identified as a result of not sufficiently corrected heading offsets.

These results were achieved during recording system tests at Loughborough University and were confirmed in two case studies at real cultural heritage sites. Obtaining these results without using control points demonstrated that medium accurate cultural heritage data recording can be achieved without affecting the heritage object.

The influence of the availability of a single control point on the achievable accuracy was also investigated. The results demonstrated that a single control point can significantly improve the achievable absolute accuracy. However, it can also degrade the achievable relative accuracy, due to the bundle adjustment being additionally constrained in one point only. A single control point can be easily established using the DGPS receiver that is already comprised in the recording system. It was recommended to always establish a single control point as an integrated part of data collection when possible. Depending on whether achievable relative accuracy is considered more important than achievable absolute accuracy, this control point might or might not be used during data processing.

- *Development of a MatLab routine based on simple methods for calibrating rotational and positional offsets between recording system components.*

For partly achieving the fifth objective (Section 1.1) the MatLab routine presented in Appendix A was developed. This routine consists of two principal steps: determination of calibration values and their precision and application of these values to direct measurements. Calibration values for rotational and positional offsets were determined by comparing photogrammetrically estimated exterior orientation parameters to direct orientation and position measurements. This required converting photogrammetric rotation angles ω, φ, and κ into the orientation sensor angles heading, pitch and roll, which was achieved by devising a subroutine ("wpk2hpr") that is also presented in Appendix A.3.1. The arithmetic mean of calculated offsets between estimated and measured 3D orientations and 3D positions represent offset calibration values, while the standard deviation indicates their precision. By applying these offset calibration values to direct measurements, directly derived exterior orientation parameters were obtained. To enable utilisation of these parameters for photogrammetric processing, the exterior orientation angles were converted from heading, pitch, and roll into ω, φ, and κ. This was achieved by another subroutine ("hpr2dcm"), which is presented in Appendix A.3.3. The approach for offset calibration used in this project does not determine calibration values using a specialised bundle adjustment, which is the conventional approach for direct exterior orientation determination in aerial photogrammetry. This would require users either developing or gaining access to such a specialised software package and developing

the necessary expertise for its operation. Instead, simpler methods were chosen that can be more easily implemented by non-specialists using off-the-shelf software.
After completion of this study, a more straightforward and easier to implement approach for converting ω, φ, and κ into heading, pitch, and roll, and vice versa, was found. This approach was not explained in the methodology chapter (Chapter 3) of this thesis, but the MatLab code that implements this approach was included in the Appendix. The subroutine "wpk2hpr" Version 2.0 (Appendix A.3.2) replaces the original version of subroutine "wpk2hpr" (Version 1.0) (Appendix A.3.1). Appendix A.3.4 comprises the subroutine "hpr2wpk" that transforms heading, pitch, and roll angles into ω, φ, and κ angles. This subroutine replaces the subroutine "hpr2dcm" (Appendix A.3.3).

- *Using a low-cost approach for improving photogrammetric heritage data storage and usability and assessing the benefits for heritage recording projects.*

This achievement also corresponds to the fifth objective (Section 1.1). Photogrammetric data storage can be improved when exterior orientation information is stored in the same file as the corresponding image (Section 3.7.1 and Section 6.5.1). This was achieved using features provided in the current KML standard. Images acquired at the case study at Roughting Linn were stored in a compressed KML (KMZ) file. The same file comprises an ASCII text-based KML file that contains corresponding exterior orientation information. The KMZ file appears to users as a single file, improving data handling. This approach demonstrated that photogrammetric data storage in a single file is possible. It further provided an opportunity to examine enhancement in data utilisation. Using the "PhotoOverlay" feature of the KML standard enabled visualisation of the data stored in the KMZ file in Google Earth, where each image can be displayed according to its position and orientation. This was achieved by opening the KMZ file in Google Earth, demonstrating the level of automation that can be achieved when image and exterior orientation are stored in a single file.
Visualising cultural heritage data in Google Earth is also a means of providing online and hence wider access to cultural heritage data. In this project the benefits of this approach were investigated by evaluating the displaying quality and identifying potential uses for low-cost online heritage data visualisation. However, current

limitations associated with Google Earth visualisations demonstrated that accuracies are insufficient for accurate measurement and detailed data analysis. Nevertheless, Google Earth was identified as suitable tool for providing quick and easy online access to cultural heritage data, which can aid decision making and planning in cultural heritage conservation projects and enhance data sharing. Other benefits were identified as raising awareness of the importance of heritage protection and serving as motivator for volunteers getting involved in heritage recording projects.

The KML and KMZ files used for visualisation can easily be generated utilising freely available software. Google Earth can be used as free tool for displaying the data stored in these files. This makes this approach well suited for cultural heritage recording projects that involve volunteers and that seek to reduce cost for heritage recording and data utilisation.

7.2 Recommendations for future work

The previous section listed the achievements of this research project. During the course of this study, some areas of further work were identified:

- **Validating usability by non-specialists:** In this project the recording system and data processing methods were designed aiming at usability by non-specialists and easy implementation using off-the-shelf hardware and software. Experiences during field work suggested that the recording system could indeed be used by non-specialists. This needs to be validated in further tests where non-specialists use the system for heritage recording after some introductory training. From their experiences, indicators for the current level of usability and possibilities for enhancements can be derived. It was already indicated in Section 6.3.2 that the non-specialists' ease in operating a survey-grade DGPS receiver should be a major part of this investigation. In the same way the project participants could be trained in data processing (offset calibration, bundle adjustment, data storage in KMZ files, and visualisation in Google Earth) in order to also assess the usability of the data processing methods devised in this research project.

- **Enhancing the recording system:** The potential of further improving the performance of the recording system in terms of calibration precision, calibration stability and achievable accuracy by modifying the camera and antenna fixture of the mounting frame was already identified in Section 6.1. Modifying the camera fixture should aim at removing the slight instability that was discussed in Section 6.1.1, enabling precise and stable roll offset calibration even when the mounting frame is pitched by more than 20°. Using more rigid materials for the camera fixture might help to improve heading offset calibration stability, which enhances achievable absolute accuracy (Section 6.2.1.1). Modification of the antenna fixture is also recommended, in order to increase the range of heritage objects that can be recorded using the recording system. By adding another spigot for DGPS antenna fixture to the back of the mounting frame (opposite the viewing direction of the camera) recording objects on or close to the ground without introducing extreme tilts of the DGPS antenna would be possible.

- **Improving the portability of the recording system:** Portability is an important factor of usability, because it directly influences time and labour that is required for data acquisition. It has been noted that this can be achieved by introducing wireless data transfer between recording system components and by decreasing the size and weight of the DGPS receiver and antenna (Section 6.3.1). It is recommended to test alternative GPS receivers that are smaller than conventional survey-grade DGPS receivers and are specified to provide centimetre positioning accuracy, such as the SXBlue III of Geneq. Such a GPS receiver could substitute the currently used Leica System 500.

- **Constructing a real low-cost recording system:** Equipment cost could be reduced by constructing a system that is completely based on low-cost components. The current system uses a survey-grade DGPS receiver (approximately £ 8,000 in 2008), which is certainly not low-cost. Using the SXBlue III (£ 3,150 in 2010) could already significantly decrease costs and future improvements in positioning accuracy of real low-cost GPS receivers (approximately £ 450) can be expected.

- **Enhancing performance of system based upon a smartphone:** In Section 6.4 the potential of smartphones with integrated camera, orientation sensor, and GPS for low-cost heritage recording was demonstrated. It was suggested that the expected accuracy of GPS integrated into smartphones currently is the limiting factor in achievable accuracy. However, smartphone GPS might improve similar to smartphone cameras and provide more accurate positioning in future. Another possibility is enhancing GPS positioning accuracy by integrating inertial orientation data and position information derived from wireless positioning techniques (for example Wi-Fi and GSM) (Constandache et al., 2010). Further tests should investigate possibilities for enhancing the performance of direct exterior orientation determination utilising smartphones.

References

ACHILLE, C., MONTI, C., MONTI, C.C. AND SAVI, C. (2005): Survey and representation of the Villa Reale di Monza to support of the International Design Competition. *CIPA XX International Symposium 2005*, Torino, Italy, pp. 43-48.

AGOSTO, E., ARDISSONE, P. AND BORNAZ, L. (2005): The Castle of Graines: Different survey methodologies for the documentation of historical buildings. *CIPA XX International Symposium 2005*, Torino, Italy, pp. 55-58.

AKCA, D. AND GRUEN, A. (2009): Comparative geometric and radiometric evaluation of mobile phone and still video cameras. *Photogrammetric Record,* 24(127). pp. 217-245.

AL-BAKER, O., BENLAMRI, R. AND AL-QAYEDI, A. (2005): A GPRS-based remote human face identification system for handheld devices. *Second IFIP International Conference on Wireless and Optical Communications Networks,* Dubai, United Arab Emirates, pp. 367-371.

ALBERTZ, J. AND WIEDEMANN, A. (1996): From analogue to digital close-range photogrammetry. *First Turkish-German Joint Geodetic Days 1995*, Istanbul, Turkey, pp. 245-253.

ALDRIDGE, D. (1989): How the ship of interpretation was blown off course in the tempest: Some philosophical thoughts. In: *Heritage Interpretation, Vol. 1, The Natural and Build Environment*, (Ed. Uzzell, D.L.), Pinter, London, pp. 64-87.

ALSPAUGH, D. (2004): A brief history of photogrammetry. In: *Manual of Photogrammetry*, (Eds. McGlone, J.C.; Mikhail, E.M.; Bethel, J.S.), 5th edition, American Society for Photogrammetry and Remote Sensing, pp. 1-12.

ALVES, J., LOBO, J. AND DIAS, J. (2003): Camera-inertial sensor modelling and alignment for visual navigation. *Machine Intelligence & Robotic Control*, 5(3), pp. 103-111.

ANDREWS, D.P., BECKETT, N.J., CLOWES, M. AND TOVEY, S.M. (2005): A comparison of rectified photography and orthophotography as applied to historic floors – with particular reference to Croughton Roman Villa. *CIPA XX International Symposium 2005*, Torino, Italy, pp. 77-81.

ANDREWS, D.P., BEDFORD, J., BLAKE, W.H., CLOWES, M., CRISPE, A., PAPWORTH, H.E. AND QUINTERO, M.E.S. (2007): Partnership in learning: English Heritage and the Raymond Lemaire International Centre for Conservation. *CIPA XXI International Symposium 2007*, Athens, Greece, pp. 67-72.

ARDISSONE, P., BORNAZ, L., LO TURCO, M. AND VITALI, M. (2005): The relief of the Porta Palatina: A comparison between different survey methodologies and representations. *CIPA XX International Symposium 2005*, Torino, Italy, pp. 86-90.

ARIAS, P., HERRÁEZ, J., LORENZO, H. AND ORDÓÑEZ, C. (2005): Control of structural problems in cultural heritage monuments using close-range photogrammetry and computer methods. *Computers and Structures*, 83(21-22), pp. 1754-1766.

Askey, P. (2006): Nikon D80 Review: Digital Photography Review. [online] Available at: <http://www.dpreview.com/reviews/NikonD80/> [Accessed 20 March 2009].

AVŞAR, E.Ö., DURAN, Z., AKYOL, O. AND TOZ, G. (2008): Modeling of the Temple of Apollo Smintheus using photogrammetry and virtual reality. *International Archives of the Photogrammetry, Remote Sensing and Spatial Information Sciences*, 37(B5), pp. 357-360.

BARBER, D., MILS, J. AND BRYAN, P. (2003): Towards a standard specification for terrestrial laser scanning of cultural heritage. *CIPA XIX International Symposium 2003,* Antalya, Turkey, pp. 171-176.

BECK, A. (2006): Google Earth and World Wind: remote sensing for the masses? [online] Available at: <http://www.antiquity.ac.uk/projgall/beck308/> [Accessed 05 January 2011].

BELL, D.G., KUEHNEL, F., MAXWELL, C., KIM, R., KASRAIE, K., GASKINS, T., HOGAN, P. AND COUGHLAN, J. (2007): NASA World Wind: Opensource GIS for mission operations. *IEEE Aerospace Conference 2007*, Big Sky, USA, pp. 1-9.

BLAKE, B (2007): Metric survey techniques for historic buildings. In: *Structures & Construction in Historic Building Conservation,* (Ed. Forsyth, M.), WileyBlackwell, Oxford, pp. 41-63.

BLOWER, J., GEMMELL, A., HAINES, K., KIRSCH, P., CUNNINGHAM, N., FLEMING, A. AND LOWRY, R. (2007): Sharing and visualizing environmental data using Virtual Globes. *UK e-Science All Hands Meeting 2007*, Nottingham, UK, pp. 102-109.

BLUETOOTH SIG (2011): Bluetooth basics. [online] Available at: <http://www.bluetooth.com/Pages/Basics.aspx> [Accessed 06 September 2011].

BÖHLER, W. AND MARBS, A. (2004): 3D scanning and photogrammetry for heritage recording: A comparison. *12th International Conference on Geoinformatics 2004*, Gävle, Sweden, pp. 291-298.

BONFIGLI, M.E., CABRI, G., LEONARDI, L. AND ZAMBONELLI, F. (2004): Virtual visits to cultural heritage supported by web-agents. *Information and Software Technology,* 46(3), pp. 173-184.

BOOCHS, F., HEINZ, G., HUXHAGEN, U. AND MÜLLER, H. (2007): Low-cost image based system for non-technical experts in cultural heritage documentation and analysis. *CIPA XXI International Symposium 2007,* Athens, Greece, pp. 165-170.

BOSCH, R., KÜLÜR, S. AND GÜLCH, E. (2005): Non-metric camera calibration and documentation of historical buildings. *CIPA XX International Symposium 2005*, Torino, Italy, pp. 142-147.

BOSCHETTI, L., ROY, D.P. AND JUSTICE, C.O. (2008): Using NASA's World Wind virtual globe for interactive internet visualization of the global MODIS burned area product. *International Journal of Remote Sensing*, 29(11), 3067- 3072.

BRAASCH, M.S. (1996): Multipath effects. In: *Global Positioning System: Theory and Applications. Volume 1* (Ed. Parkinson, B. W. and Spilker Jr., J. J.), American Institute of Aeronautics and Astronautics, Washington DC, pp. 547-568.

BRODIE, M.A., WALMSLEY, A. AND PAGE, W. (2008): The static accuracy and calibration of inertial measurement units for 3D orientation. *Computer Methods in Biomechanics and Biomedical Engineering*, 11(6), pp. 641-648.

BRYAN, P. (2010a): RE: Visit at Loughborough and rock-art site. [email] (Personal communication, 13 September 2010).

BRYAN, P. (2010b): Research project progress and case study planning. (Personal communication, meeting at Loughborough University 29 September 2010).

BRYAN, P. AND CHANDLER, J.H. (2008): Cost-effective rock-art recording within a non-specialist environment. *International Archives of the Photogrammetry, Remote Sensing and Spatial Information Sciences*, 37(B5), pp. 259-264.

BUHAGIAR, C.M., BAILEY, T., GOVE, M. (2006): CHIMS: The Cultural Heritage Inventory Management System for the Maltese Islands. *The 7th International Symposium on Virtual Reality, Archaeology and Cultural Heritage 2006*, Nicosia, Cyprus, pp. 43-48.

BUTLER, D. (2006): Virtual globes: the web-wide world. *Nature*, 439, pp. 776-778.

CAMERA AND IMAGING PRODUCT ASSOCIATION (2010): *CIPA DC-008-Translation-2010, Exchangeable image file format for digital still cameras: Exif Version 2.3.* Camera & Imaging Product Association, Tokyo, Japan, 190 pages.

CAMPANELLA, C., TESSONI, M., BORTOLOTTO, S., CIOCCHINI, E. AND ZANGHERI, F. (2005): Basilica of Saint Peter Martyr from Verona in S. Anastasia (Verona): Structures geometric survey and photographic campaign for the preservation project. *CIPA XX International Symposium 2005*, Torino, Italy, pp. 171-176.

CASIO AMERICA (2010): Casio releases compact EXILIM® camera with Hybrid-GPS. [online] Available at: <http://www.casio.com/news/content/1B060E9E-E4B0-4211-80EA-A04348021519/> [Accessed 10 January 2011]

ÇAYIREZMEZ, N.A. (2007): Cultural heritage inventory system of Turkey on the web. *CIPA XXI International Symposium 2007*, Athens, Greece, pp. 207-209.

CHANDLER, J.H. AND CLARK, J.S. (1992) The archival photogrammetric technique. Further applications and development. *Photogrammetric Record*, 14(80), pp 241-247.

CHANDLER, J.H. AND FRYER, J.G. (2005): Recording Aboriginal rock art using cheap digital cameras and digital photogrammetry. *CIPA XX International Symposium 2005*, Torino, Italy, pp. 193-198.

CHANDLER, J.H. AND FRYER, J.G. AND Jack, A. (2005): Metric capabilities of low-cost digital cameras for close range surface measurement. *Photogrammetric Record*, 20(109), pp. 12-26.

CHANDLER, J.H., BRYAN, P. AND FRYER, J.G. (2007): The development and application of a simple methodology for recording rock art using consumer-grade digital cameras. *Photogrammetric Record*, 22(117), pp. 10-21.

CHEN, A., LEPTOUKH, G.G., KEMPLER, S.J. AND DI, L. (2009): Visualization of Earth science data using Google Earth™. *International Archives of the Photogrammetry, Remote Sensing and Spatial Information Sciences*, 38(4/W10), 6 pages [on CD-ROM].

CHIANG, K.-W., HUANG, Y.-S., TSAI, M.-L. AND CHEN, K.-H. (2010): The perspective from Asia concerning the impact of Compass/Beidou-2 on future GNSS. *Survey Review*, 42(315), pp. 3-9.

CHIKATSU, H. AND TAKAHASHI, Y. (2009): Comparative evaluation between consumer grade cameras and mobile phone cameras for close range photogrammetry. *Proceedings of SPIE Vol. 7447: Videometrics, Range Imaging, and Applications X*, pp. 74470H-1-74470H-12.

CIPA (2010): CIPA Web Site – Objectives. [online] Available at, http://cipa.icomos.org/OBJECTIVES.HTML> [Accessed 4th April 2011].

CLOWES, M (2002): Digital photogrammetry at English Heritage: a pictorial review of projects to date. *Photogrammetric Record*, 17(99), pp. 441-452.

CONSTANDACHE, I.; CHOUDHURY, R.R. AND RHEE, I. (2010): Towards mobile phone localization without war-driving. *IEEE 29th Conference on Computer Communications*, San Diego, California, USA, 9 pages.

COOPER, M.A.R. AND ROBSON, S. (2001): Theory of close range photogrammetry. In: *Close range photogrammetry and machine vision* (Ed. Atkinson, K. B.), Whittles Publishing, Caithness, pp. 9-51.

COPPA, U., GUARNIERI, A., PIROTTI, F. AND VETTORE, A. (2007): A backpack MMS application. *5th International Symposium on Mobile Mapping Technology*, Padua, Italy, 7 pages.

CORKE, P., LOBO, J. AND DIAS, J. (2007): An introduction to inertial and visual sensing. *International Journal of Robotics Research*, 26(6), pp. 519-535.

CRAGLIA, M., GOODCHILD, M.F., ANNONI, A., CAMARA, G., GOULD, M., KUHN, W., MARK, D., MASSER, I., MAGUIRE, D., LIANG, S. AND PARSONS, E. (2008): Next-Generation Digital Earth. A position paper from the Vespucci Initiative for the Advancement of Geographic Information Science. *International Journal of Spatial Data Infrastructures Research*, 3, pp. 146-167.

CRAMER, M. AND STALLMANN, D. (2002): On the use of GPS/inertial exterior orientation parameters in airborne photogrammetry. In: *OEEPE Integrated Sensor Orientation Test Report and Workshop* (Eds. Heipke, C., Jacobsen, K., and Wegmann, H.), Bundesamt für Kartographie und Geodäsie, Frankfurt a.M., pp. 109-121.

CURRIE, C.K. (2001): *An archaeological and historical survey of the Knowles Farm & St. Catherine's Hill and Downs estates, Isle of Wight: Volume 2*. Report to the National Trust (Southern Region), CKC Archaeology, Eastleigh, 89 pages.

CYARK (n.d.): About CyArk. [online] Available at: <http://archive.cyark.org/about> [Accessed 29 November 2010].

DAY, N. (2010): Terrestrial photogrammetry as an alternative to laser scanning. *Geomatics World*, 18(2), pp. 36-38.

DUFFY, S.M. (2010): Polynomial texture mapping at Roughting Linn rock art site. *International Archives of the Photogrammetry, Remote Sensing and Spatial Information Sciences*, 38(5), pp. 213-217.

EL-RABBANY, A. (2006): *Introduction to GPS: the global positioning system.* Artech House, Boston and London, 210 pages.

ELVIDGE, C.D. AND TUTTLE, B.T. (2008): How Virtual Globes are Revolutionizing Earth Observation Data Access and Integration. *International Archives of the Photogrammetry, Remote Sensing and Spatial Information Sciences*, 37(B6a), pp. 137-140.

ENGINEERING SURVEYING RESEARCH CENTRE (1994): *General Adjustment Program user manual*. Department of Civil Engineering, City University, London, 12 pages.

ENGLISH HERITAGE (2000): *Metric Survey Specifications for English Heritage*. English Heritage, Swindon, 111 pages.

ENGLISH HERITAGE (2005): English Heritage Research Agenda: An introduction to English Heritage's research themes and programmes. [online] Available at: <http://www.english-heritage.org.uk/content/imported-docs/a-e/researchagenda.pdf> [Accessed 12 January 2011].

ENGLISH HERITAGE (2007a): English Heritage Images of England: a searchable photographic archive of the historic buildings of England. [online] Available at: <http://www.imagesofengland.org.uk/> [Accesses 12 January 2011].

ENGLISH HERITAGE (2007b): *3D laser scanning for heritage.* English Heritage, London, 43 pages.

ENGLISH HERITAGE (2008): *Heritage at Risk*. English Heritage, London, 36 pages.

ENGLISH HERITAGE (2009): *Metric Survey Specifications for Cultural Heritage*. 2nd ed., English Heritage, Swindon, 126 pages.

ENGLISH HERITAGE (n.d.): St. Catherine's Oratory | English Heritage. [online] Available at: <http://www.english-heritage.org.uk/daysout/properties/st-catherines-oratory/> [Accessed 11 May 2011].

ERDAS (2008): *LPS Project Manager User's Guide*. ERDAS, Norcross, 416 pages.

ESRI (2009): ArcGIS® Explorer—Deliver Your GIS to Everyone. [online] Available at: <http://www.esri.com/library/fliers/pdfs/arcgis-explorer.pdf> [Accessed 5 January 2011].

EUGSTER, H. AND NEBIKER, S. (2008): UAV-based augmented monitoring–real-time georeferencing and integration of video imagery with virtual globes. *International Archives of the Photogrammetry, Remote Sensing and Spatial Information Sciences*, 37(B1), 1229-1236.

EUROPEAN COMMUNITIES (2008): NET-HERITAGE fact sheet. [online] Available at: <http://www.netheritage.eu/download/213_K_EN_Text02_layout02_25nov2008(03)~(02)_commentsJB.PDF> [Accessed 22 November 2010].

FAWCETT, J. (1998): *Historic Floors: Their History and Conversation.* Butterworth Heinemann, Oxford, 250 pages.

FIANI, M. AND PISTILLO, P. (2004): A low-coast MMS integrating GPS, digital compass and a camera to the direct georeferencing of digital images. *International Archives of Photogrammetry, Remote Sensing and Spatial Information Sciences*, 35(5), pp. 747-752.

FLICKR (2011): Flickr: Explore everyone's photos on a Map. [online] Available at: <http://www.flickr.com/map/> [Accessed 6 January 2011].

FORLANI, G. AND PINTO, L. (2002): Integrated INS/DGPS systems: calibration and combined block adjustment. In: *OEEPE Integrated Sensor Orientation Test Report and Workshop* (Eds. Heipke, C., Jacobsen, K., and Wegmann, H.), Bundesamt für Kartographie und Geodäsie, Frankfurt a.M., pp. 85-96.

FRASER, C.S. (1996): Network design. In: *Close range photogrammetry and machine vision* (Ed. Atkinson, K. B.), Whittles Publishing, Caithness, pp. 256-281.

FRYER, J.G., MITCHELL, H. AND CHANDLER, J.H. (2007): *Applications of 3D measurement from images*. Whittles Publishing, Dunbeath – Caithness, 304 pages.

GABELLONE, F. AND MONTE, A. (2005): A virtual thematic Museum of the Terra d'Otranto Lighthouses based on a low cost methodology. *CIPA XX International Symposium 2005*, Torino, Italy, pp. 813-818.

GARMIN (2012): On the Trail. [online] Available at: <https://buy.garmin.com/shop/shop.do?cID=143> [Accessed 13 March 2012].

GENEQ (2010a): SXBlue III. Rugged, Bluetooth high accuracy L1/L2 RTK-Mapping receiver. [online] Available at: <http://www.sxbluegps.com/SXBlue-III-version 1.1.pdf> [Accessed 12 January 2011].

GENEQ (2010b): SXBlue III GPS. Technical specifications. [online] Available at <http://www.sxbluegps.com/SXBlue-III.pdf> [Accessed 26 August 2011].

GIRELLI, V.A., TINI, M.A. AND ZANUTTA, A. (2005): Traditional and unconventional photogrammetric techniques for metrical documentation of cultural heritage: The example of the "Rolandino Dei Passaggieri" Tomb (St. Domenico Square) survey in Bologna. *CIPA XX International Symposium 2005*, Torino, Italy, pp. 310-315.

GOODCHILD, M.F. (2007a): Citizens as sensors: the world of volunteered geography. *GeoJournal*, 69(4), pp. 211-221.

GOODCHILD, M.F. (2007b): Citizens as sensors: web 2.0 and the volunteering of geographic information. *GeoFocus (Editorial)*, 7, pp. 8-10.

GOOGLE (2010): KML FAQ - KML - Google Code. [online] Available at: <http:// code.google.com/apis/kml/faq.html#whatiskml> [Accessed 04 January 2011].

GOOGLE (2011a): Google Earth: Desktop. [online] Available at: <http://www. google. co.uk/intl/en_uk/earth/explore/products/desktop.html> [Accessed 04 January 2011].

GOOGLE (2011b): KMZ Files – KML – Google code. [online] Available at: <http://code.google.com/apis/kml/documentation/kmzarchives.html> [Accessed 08 September 2011].

GOOGLE (2011c): The jpeg associated with a Photo Overlay does not appear unless I click its Properties and OK. - Google Earth Help. [online] Available at: <http://www.google.com/support/forum/p/earth/thread?tid=734cde329f5b66a2&hl =en> [Accessed 05 July 2011].

GOOGLE (2011d): Delete your cache : Fix a Problem - Google Earth Help. [online] Available at: <http://earth.google.com/support/bin/answer.py?hl=en&answer= 207 12> [Accessed 02 July 2011].

GOOGLE (2011e): Developer's guide – KML – Google code. [online] Available at: <http://code.google.com/apis/kml/documentation/topicsinkml.html> [Accessed 08 September 2011].

GREWAL, M.S., WEILL, L.R. AND ANDREWS, A.P. (2001): *Global positioning systems, inertial navigation, and integration*. Wiley, New York and Chichester, 392 pages.

GRUEN, A. AND AKCA, D. (2008): Evaluation of metric performance of mobile phone cameras. *International Calibration and Orientation Workshop EuroCOW 2008*, Castelldefels, Spain, 10 pages.

GRUSSENMEYER, P., LANDES, T., VOEGTLE, T. AND RINGLE, K. (2008): Comparison methods of terrestrial laser scanning, photogrammetry and tacheometry data for recording of cultural heritage buildings. *International Archives of Photogrammetry, Remote Sensing and Spatial Information Sciences*, 37(B5), pp. 213-218.

GUARNIERI, A., MENIN, A., PIROTTI, F. AND VETTORE, A. (2008): Low cost system: GPS/MEMS for Positioning. *FIG Working Week 2008*, Stockholm, Sweden, 10 pages.

HADDAD, N. AND AKASHEH, T. (2005): Documentation of archaeological sites and monuments: Ancient theatres in Jerash. *CIPA XX International Symposium 2005*, Torino, Italy, pp. 350-355.

HEIPKE, C., JACOBSEN, K., WEGMANN, H., ANDERSEN, Ø. AND NILSEN, B. (2002): Test Goals and Test Set Up for the OEEPE Test "Integrated Sensor Orientation". In: *OEEPE Integrated Sensor Orientation Test Report and Workshop* (Eds. Heipke, C., Jacobsen, K., and Wegmann, H.), Bundesamt für Kartographie und Geodäsie, Frankfurt a.M., pp. 11-18.

HERBERT, D.T. (1995a): Preface. In: *Heritage, Tourism and Society*. (Ed. Herbert, D.T.), Pinter, London, pp. xi-xii.

HERBERT, D.T. (1995b): Heritage Places, Leisure and Tourism. In: *Heritage, Tourism and Society*. (Ed. Herbert, D.T.), Pinter, London, pp. 1-20.

HERITAGE3D (n.d.): Home Panel | Heritage3D. [online] Available at: <www.heritage3d.org> [Accessed 09 March 2012].

HEWISON, R. (1989): Heritage: An Interpretation. In: *Heritage Interpretation, Volume 1, The Natural and Built Environment*, (Ed. Uzzell, D.L.), Pinter, London, pp. 15-23.

HTC (2011): HTC – Products – HTC Desire – Specification. [online] Available at: <http://www.htc.com/uk/product/desire/specification.html> [Accessed 29 August 2011].

HUNTER, M. (1996): Introduction: the fitful rise of British preservation. In: *Preserving the Past: The Rise of Heritage in modern Britain*, (Ed. Hunter, M.), Alan Sutton, Stroud, pp. 1-16.

ICOMOS (1964): International Charter for the Conservation and Restoration of Monuments and Sites. [online] Available at: <http://www.international.icomos.org/charters/charters.pdf> [Accessed 05 May 2009].

ICOMOS (1996): Principles for the Recording of Monuments, Groups of Buildings and Sites. [online] Available at: <http://www.international.icomos.org/charters/charters.pdf> [Accessed 05 May 2009].

IKEUCHI, K., NAKAZAWA, A., HASEGAWA, K. AND OHISHI, T. (2003): The Great Buddha Project: modeling cultural heritage for VR systems through observation. *2nd IEEE/ACM International Symposium on Mixed and Augmented Reality*, Tokyo, Japan, 10 pages.

JOHNSON, P. AND THOMAS, B. (1995): Heritage as Business. In: *Heritage, Tourism and Society*, (Ed. Herbert, D.T.), Pinter, London, pp. 170-190.

KARARA, H.M. (1979): *Handbook of non-topographic photogrammetry*. American Society of Photogrammetry, Falls Church, VA, 206 pages.

KELLY, J. AND SUKHATME, G.S. (2008): Fast relative pose calibration for visual and inertial sensors. *11th International Symposium on Experimental Robotics*, Athens, Greece, pp. 515-524.

KEMP, B., JANSSEN, A.J. AND VAN DER KAMP, B. (1998): Body position can be monitored in 3D using miniature accelerometers and earth-magnetic field sensors. *Electroencephalography and clinical Neurophysiology*, 109, pp. 484-488.

KIRCHHÖFER, M., CHANDLER, J., AND WACKROW, R. (2011): Cultural heritage recording utilising low-cost close-range photogrammetry. *CIPA XXIII International Symposium 2011*, Prague, Czech Republic, 8 pages [on CD-ROM].

KIRK, G.R. (2010): *Tilt compensation for GNSS antenna*. United States Patent 20100283674, published application, 16 pages.

KONECNY, G. (2003): *Geoinformation. Remote sensing, photogrammetry and geographic information systems*. Taylor & Francis, Tokyo, London, 248 pages.

KOREC (n.d.): Ricoh G700SE Digital Camera. [online] Available at: <http://www.korecgroup.com/measured-solutions/gis-data-collection/digital-cameras-with-gps/ricoh-g700se-digital-camera.php> [Accessed 10 January 2011]

KRAUS, K. (1993): *Photogrammetry Vol.1: Fundamentals and Standard Processes*. Dümmler, Bonn, 397 pages.

LAEFER, D. AND LENNON, D. (2008): Viability assessment of terrestrial LiDAR for retaining wall monitoring. *GeoCongress 2008*, New Orleans, Louisiana, USA, pp. 247-254.

LAENEN, M. (1989): Looking for the future through the past. *Heritage Interpretation, Vol. 1, The Natural and Built Environment*, (Ed. Uzzell, D.L.), Pinter, London, pp. 88-95.

LAUTURE, J.-Y. (2010): RE: TR: Quotation Query: SXBlue II-L GPS (NS). [email] (Personal communication, 30 September 2010).

LEICA CAMERA (n.d.): Leica Camera AG - Photography - V-LUX 20. [online] Available at: <http://en.leica-camera.com/photography/compact_cameras/v-lux_20/> [Accessed 10 January 2011].

LEICA GEOSYSTEMS (1999): GPS surveying – System 500. Technical Specifications. [online] Available at: <http://www.leica-geosystems.com/downloads123/zz/gps/gps_system500/brochures-datasheet/711759-SR530_Techn_Spec_en%5B1%5D.pdf> [Accessed 26 August 2011].

LEICA GEOSYSTEMS (2006): *Leica TPS400 Series. User Manual Version 4.0*. Leica Geosystems AG, Heerbrugg, 154 pages.

LENZ, J. AND EDELSTEIN, A.S. (2006): Magnetic sensors and their applications. *IEEE Sensors Journal*, 6(3), pp. 631-649.

LERMA, J.L., NAVARRO, S., CABRELLES, M. AND VILLAVERDE, V. (2010): Terrestrial laser scanning and close range photogrammetry for 3D archaeological documentation: the Upper Palaeolithic Cave of Parpalló as a case study. *Journal of Archaeological Science*, 37(3), pp. 499-507.

LEROY, T. (2005): Saving Voskopoja, complete photogrammetric coverage of three Albanian painted churches. *CIPA XX International Symposium 2005*, Torino, Italy, pp. 414-419.

LINSINGER, S. (2005): ”3D laser” versus “stereo photogrammetry“ for documentation and diagnosis of buildings and monuments (pro and contra). *CIPA XX International Symposium 2005*, Torino, Italy, pp. 425-426.

LOBO, J. AND DIAS, J. (2007): Relative pose calibration between visual and inertial sensors. *International Journal of Robotics Research*, 26(6), pp. 561-575.

LUHMANN, T., ROBSON, S., KYLE, S. AND HARLEY, I. (2006): *Close range photogrammetry: principles, techniques and applications*. Whittles Publishing, Dunbeath – Caithness, 510 pages.

LUINGE, H. AND VELTINK, P.H. (2004): Inclination measurement of human movement using a 3-D accelerometer with autocalibration. *IEEE Transactions on Neural Systems and Rehabilitation Engineering*, 12(1), pp. 112-121.

MANZONI, G., RIZZO, R.G. AND ROBIGLIO, C. (2005): Mobile mapping systems in cultural heritages survey. *CIPA XX International Symposium 2005*, Torino, Italy, pp. 437-440.

MASCI, M.E., BUONAZIA, I., MERLITTI, D. (2007): The project of the Italian Culture Portal. A standard based model for interoperability amongst cultural heritage data sources. *CIPA XXI International Symposium 2007*, Athens, Greece, pp. 481-486.

MASON, S. (1995): Expert system-based design of close-range photogrammetric networks. *ISPRS Journal of Photogrammetry and Remote Sensing*, 50(5), pp. 13-24.

MICHAEL (n.d.): MICHAEL: Explore the European digital cultural heritage. [online] Available at: <http://www.michael-culture.org/en/home> [Accessed 12 January 2011].

MICROSOFT (n.d. a): Background – Photosynth. [online] Available at: <http://photosynth.net/Background.aspx> [Accessed 12th October 2011].

MICROSOFT (n.d. b): FAQ – Photosynth. [online] Available at: <http://photosynth.net/faq.aspx> [Accessed 12th October 2011].

MIKHAIL, E.M., BETHEL, J.S. AND MCGLONE, J.C. (2001): *Introduction to modern photogrammetry*. Wiley, New York and Chichester, 279 pages.

MIRI, M. AND VARSHOSAZ, M. (2005): Standardization of geomatics applications in cultural heritage. Map Middle East 2005. [online] Available at: <http://www.gisdevelopment.net/application/archaeology/general/me05_022.pdf> [Accessed 7 January 2011].

MIRZAEI, F.M. AND ROUMELIOTIS, S.I. (2008): A Kalman filter-based algorithm for IMU-camera calibration. *IEEE Transactions on Robotics*, 24(5), pp. 1143 – 1156.

MOULLOU, D. AND MAVROMATI, D. (2007): Topographic and photogrammetric recording of the Acropolis of Athens. *CIPA XXI International Symposium 2007*, Athens, Greece, pp. 515-520.

MUDGE, M., ASHLEY, M. AND SCHROER, C. (2007): A digital future for cultural heritage. *CIPA XXI International Symposium 2007*, Athens, Greece, pp. 521-526.

MUGGAH, J. AND MIOC, D. (2010): Arctic basemaps in Google Maps. *International Archives of the Photogrammetry, Remote Sensing and Spatial Information Sciences*, 38(4/W13), 5 pages.

NATIONAL GEOSPATIAL-INTELLIGENCE AGENCY (n.d.): NGA: (U) NGA EGM96 Geoid Calculator (UNCLASSIFIED). [online] Available at: <http://earth-info.nga.mil/GandG/wgs84/gravitymod/egm96/intpt.html> [Accessed 14 October 2011].

NISHUMURA, S. AND KIMOTO, K. (2009): System for assisting in the restoration of stone walls, using 3D modeling. *CIPA XXII International Symposium 2009*, Kyoto, Japan, 63-67.

NIU, X., HASSAN, T., ELLUM, C. AND EL-SHEIMY, N. (2006): Directly georeferencing terrestrial imagery using MEMS-based INS/GNSS integrated systems. *XXIII FIG Congress*, Munich, Germany, 16 pages.

NOAA (2011): NOAA's Geophysical Data Center - Geomagnetic Data [online] Available at: <http://www.ngdc.noaa.gov/geomagmodels/struts/CalcDeclination> [Accessed 15 February 2011]

OPEN GEOSPATIAL CONSORTIUM (2008): *OGC KML. OGC Standard, OGC 07-147r2, Version 2.2.0*, (Ed. Wilson, T.), 251 pages.

Ordnance Survey (2007): ProjectionandTransformationCalculations.xls v3.35 [online] Available at: <http://www.ordnancesurvey.co.uk/oswebsite/gps/docs/ProjectionandTransformationCalculations.xls> [Accessed 15 February 2011]

ORDNANCE SURVEY (2011a): National GPS Network - Station Name and Number. [online] Available at: <http://gps.ordnancesurvey.co.uk/viewpassiverec1.asp?recnumber=C1SK5014> [Accessed 10 June 2011].

ORDNANCE SURVEY (2011b): Welcome to OS Net - Quest Software. [online] Available at: <http://www.ordnancesurvey.co.uk/oswebsite/gps/osnetfreeservices/furtherinfo/questsoftware.html> [Accessed 22 March 2011].

ORDNANCE SURVEY (2011c): Active Station RINEX Data. [online] Available at: <http://gps.ordnancesurvey.co.uk/active.asp> [Accessed 11 June 2011].

ORDNANCE SURVEY (2011d): Overview of the OS Net free services. [online] Available at: <http://www.ordnancesurvey.co.uk/oswebsite/gps/osnetfreeservices/> [Accessed 06 September 2011].

ORDÓÑEZ, C., ARIAS, P., HERRÁEZ, J., RODRÍGUEZ, J. AND MARTÍN, M.T. (2008): A combined single range and single image device for low-cost measurement of building façade features. *Photogrammetric Record*, 23(122). pp. 228-240.

PALUMBO, G. AND OGLEBY, C.L. (2004): Heritage at risk and CIPA today: a report on the status of heritage documentation. *International Archives of the Photogrammetry, Remote Sensing and Spatial Information Sciences*, 35(B5), pp. 239-842.

PAVLOV, I. (2011): 7-Zip. [online] Available at: <http://www.7-zip.org/> [Accessed 08 September 2011].

PETRIE, G., BETHEL, J.S. AND WALKER S. (2004): Classical photogrammetric equipment. In: *Manual of Photogrammetry*, (Eds. McGlone, J.C.; Mikhail, E.M.; Bethel, J.S.), 5th edition, American Society for Photogrammetry and Remote Sensing, pp. 731-761.

PIETRONI, E. AND FORTE, M. (2007): A virtual collaborative environment for archaeology through multi-user domain in the web. *CIPA XXI International Symposium 2007*, Athens, Greece, pp. 585-589.

PITTORE, M., CAPPELLO, M., ANCONA, M. AND SCAGLIOLA, N. (2005): Role of image recognition in defining the user's focus of attention in 3G phone applications: the AGAMEMNON experience. *IEEE International Conference on Image Processing*, Genova, Italy, Vol. 3, pp. 1012-1015.

PNI (2009): *User guide. TCM3 & TCM5*. PNI Corporation, Santa Rosa, 58 pages.

POPOVIC, R.S., FLANAGAN, J.A. AND BESSE, P.A. (1996): The future of magnetic sensors. *Sensors and Actuators A*, 56, pp. 39-55.

POWER OF PLACE OFFICE AND ENGLISH HERITAGE (2000): *Power of Place: The Future of the Historic Environment*. Power of Place Office, 50 pages.

REULKE, R., WEHR, A. AND GRIESBACH, D. (2004): High resolution mapping using CCD-line camera and laser scanner with integrated position and orientation system. *International Archives of Photogrammetry, Remote Sensing and Spatial Information Sciences*, 35(B3), pp. 322-327.

RICOH (2010): Ricoh announces the G700SE digital camera featuring Bluethooth® and wireless LAN support. [online] Available at: <http://www.ricoh.com/r_dc/press/release/nr_g700se.html> [Accessed 10 January 2011].

ROBERTS, P. (2004): *Draft. Conservation Statement: St Catherine's oratory and tower, Isle of Wight.* Not published, internal document of English Heritage. 11 pages.

ROHS, M. (2004): Real-world interaction with camera phones. *Second International Symposium on Ubiquitous Computing Systems*, Tokyo, Japan, pp. 74–-89.

SCHÖNING, J., RAUBAL, M., MARSH, M., HECHT, B., KRÜGER, A. AND ROHS, M. (2008): Improving interaction with virtual globes through spatial thinking: Helping users Ask "Why?". *IUI 2008 Proceedings of the 13th International Conference on Intelligent User Interfaces*, Canary Islands, Spain, pp. 129–138.

SCHWIDEFSKY, K. (1970): Precision photogrammetry at close ranges with simple cameras. *Photogrammetric Record*, 6(36), pp. 567-589.

SCHWIEGER, V. AND GLÄSER, A. (2005): Possibilities of low cost GPS technology for precise geodetic applications. *FIG Working Week 2005*, Cairo, Egypt, 16 pages.

SETO, T, MATSUMOTO, A., IIZUKA, T. AND YANO, K. (2009): Public participation GIS of historical landscapes: A case study of "Kyo-Machiya Community-Building Survey" in Kyoto City. CIPA XXII International Symposium 2009, Kyoto, Japan, pp. 47-51.

SHARPE, K. AND BARNETT, T. (2008): Recording England's rock art. A handbook for project officers. [online] Available at: <http://archaeologydataservice.ac.uk/catalogue/adsdata/arch-836-1/dissemination/pdf/ERA_Recording_Handbook.pdf> [Accessed 12 January 2011].

SHARPE, K., BARNETT, T., RUSHTON, S., BRYAN, P., LEE, G. AND MAZEL, A. (2008): *England's Rock Art. The prehistoric rock art of England: recording, managing and enjoying our carved heritage*. English Heritage and Northumberland County Council, 28 pages.

SHEPPARD, S.R.J. AND CIZEK, P. (2009): The ethics of Google Earth: Crossing thresholds from spatial data to landscape visualisation. *Journal of Environmental Management*, 90(6), pp. 2102-2117.

SILVA, G.J. (2011): Imageotag. [online] Available at: <http://imageotag.appspot.com> [Accessed 07 September 2011].

SPELLER, K.E. AND YU, D. (2004): A low-noise MEMS accelerometer for unattended ground sensor applications. *Unattended/Unmanned Ground, Ocean, and Air Sensor Technologies and Applications VI, Proceedings of SPIE, 5417*, pp. 63-72.

STENSGAARD, A.-S., SAARNAK, C.F.L., UTZINGER, J., VOUNATSOU, P., SIMOONGA, C., MUSHINGE, G., RAHBEK, C., MØHLENBERG, F. AND KRISTENSEN, T.K. (2009): Virtual globes and geospatial health: the potential of new tools in the management and control of Vector-borne diseases. *Geospatial Health*, 3(2), pp. 127-141.

STEVENS, A. (2010): FW: TR: Quotation Query: SXBlue II-L GPS (NS). [email] (Personal communication, 1 October 2010).

SYNTHETICS TECHNICAL CONSULTING (2011): Online coordinate reprojection system - Synectics Technical Consulting. [online] Available at: <http:// www.synectics-tc.com/resources/downloads/coordinate-reprojection.html> [21 October 2011].

TACK, F., DEBIE, J., GOOSSENS, R., DE MEULEMEESTER, J. AND DEVRIENDT, D. (2005): A feasible methodology for the use of close range photogrammetry for the recording of archaeological excavations. *CIPA XX International Symposium 2005*, Torino, Italy, 561-565.

TRIMBLE NAVIGATION (2010): Trimble VRS Now. [online] Available at: <http://trl.trimble.com/docushare/dsweb/Get/Document-511749/022506-132B_VRS_Now_General_BRO_0710_LR_pbp.pdf> [Accessed 08 September 2011].

UNESCO (1954): Hague convention for the protection of cultural property in the event of armed conflict. [online] Available at: <http://unesdoc.unesco.org/images/0008/000824/082464mb.pdf> [Accessed 19 May 2009].

UNESCO (1972): Convention concerning the protection of the world cultural and natural heritage. [online] Available at: <http://whc.unesco.org/archive/convention-en.pdf> [Accessed 5 May 2009].

UNESCO (2003): Convention for the safeguarding of the intangible cultural heritage. [online] Available at: <http://unesdoc.unesco.org/images/0013/001325/132540e.pdf> [Accessed 9 May 2009].

UZZELL, D.L. (1989): Introduction: The Natural and Built Environment. In: *Heritage Interpretation, Vol. 1, The Natural and Built Environment* (Ed. Uzzell, D.L.), Pinter, London, pp. 1-14.

VANDEPORTAELE, B., DEHAIS, C., CATTOEN, M. AND MARTHON, P. (2006): ORIENT-CAM, a camera that knows its orientation and some applications. *Lecture Notes in Computer Science*, 4225, pp. 267-276.

VAN SICKLE, J. (2008): *GPS for Land Surveyors*. 3rd edition, CRC Press Taylor & Francis Group, Boca Raton and London and New York, 338 pages.

WACKROW, R. (2008): *Spatial measurement with consumer grade digital cameras*. Ph.D. thesis, Loughborough University, 196 pages.

WACKROW, R., CHANDLER, J.H. AND BRYAN, P. (2007): Geometric consistency and stability of consumer-grade digital cameras for accurate spatial measurement. *Photogrammetric Record*, Vol. 22 (118), pp. 121-134.

WACKROW, R. AND CHANDLER, J.H. (2008): A convergent image configuration for DEM extraction that minimises the systematic effects caused by an inaccurate lens model. *Photogrammetric Record*, 23(121), pp. 6-18.

WACKROW, R. AND CHANDLER, J.H. (2011): Minimising systematic error surfaces in digital elevation models using oblique convergent imagery. *Photogrammetric Record*, 26(133), pp. 16-31.

WANNINGER, L. (1999): The performance of virtual reference stations in active geodetic GPS-networks und solar maximum conditions. *ION GPS 99*, Nashville, USA, pp. 1419 – 1427.

WIKIMAPIA (2010): Wikimapia Guidelines. [online] Available at: <http://wikimapia.org/special_pages/guidelines/> [Accessed 6 January 2011].

WING, M.G., EKLUND, A. AND KELLOGG, L.D. (2005): Consumer-grade global positioning system (GPS) accuracy and reliability. *Journal of Forestry*, 103(4), pp. 169-173.

WINZIP COMPUTING (2011): WinZip - Windows Zip Utility - Zip Files, Unzip Files. [online] Available at: <http://www.winzip.com/win/en/index.htm> [Accessed 08 September 2011].

WORLD WIND CENTRAL (2010a): Google Earth comparison - World Wind Wiki. [online] Available at: <http://worldwindcentral.com/wiki/Google_Earth_comparison> [Accessed 5 January 2011]

WORLD WIND CENTRAL (2010b): World Wind - World Wind Wiki. [online] Available at: <http://worldwindcentral.com/wiki/World_Wind> [Accessed 5 January 2011]

Yahoo! (2011): Yahoo! Maps Web Services – YDN. [online] Available at: <http://developer.yahoo.com/maps/> [Accessed 6 January 2011]

Xsens Technologies (2009): MTi-G. Miniature AHRS with integrated GPS. [online] Available at: <http://www.xsens.com/images/stories/products/PDF_Brochures/mti-g%20leaflet%2009.pdf> [Accessed 30 June 2009]

Yilmaz, H.M., Yakar, M., Gulec, S.A. and Dulgerler, O.N. (2007): Importance of digital close-range photogrammetry in documentation of cultural heritage. *Journal of Cultural Heritage*. 8(4), pp. 428-433.

Appendix A:

Matlab code

A.1 Offset calibration code

```
%*********************************************************************
% This code calibrates the rotational offset between orientation
% sensor (TCM5) and perspective centre of the camera and positional
% offsets between DGPS antenna or prism and perspective centre of the
% camera.
% Author: Melanie Kirchhoefer
% Version 2.0
%*********************************************************************


clear all
clc


%--------------------------------------------------------------------
% Read truth data and direct measurements
%--------------------------------------------------------------------

%--- Truth data (tab delimited, no headings):
% ID,Easting, Northing, Height, Omega, Phi, Kappa
LPS_eo = dlmread('LPS_eo.txt','\t',0,0);


%--- Direct orientation (tab delimited, no headings):
% Heading (Magnetic North), Heading (Grid North), Pitch, Roll
TCM_orientation = dlmread('orientation.txt','\t',0,0);


%--- Direct position (tab delimited, no headings):
% ID, Easting, Northing, Height
GPSTS_position = dlmread('position.txt','\t',0,0);
```

```
%=========================================================================
% Rotational offset calibration
%=========================================================================

%-------------------------------------------------------------------------
%Conversion omega, phi, kappa into heading, pitch, roll and offset
% calculation
%-------------------------------------------------------------------------

lg = length(TCM_orientation(:,1));
hpr_data = zeros(lg,3);
heading = zeros(3,lg);
pitch = zeros(3,lg);
roll = zeros(3,lg);

% f = focal length from camera calibration only used for wpk2hpr
% Version 1.0
f = 24.46;

for i = 1:lg
    % use code in wpk2hpr.m Version 1.0 for rotation angles
    %conversion
    %% [h,p,r] = wpk2hpr(LPS_eo(i,5),LPS_eo(i,6),LPS_eo(i,7),f);
    % use code in wpk2hpr Version 2.0 for rotation angles conversion
    [h,p,r] = wpk2hpr(LPS_eo(i,5),LPS_eo(i,6),LPS_eo(i,7));
    hpr_data(i,:) = [h,p,r];

    %compare heading values from TCM to values from LPS
    heading(1,i) = TCM_orientation(i,2);
    heading(2,i) = h;
    heading(3,i) = heading(2,i)-heading(1,i);
    % only necessary for wpk2hpr Version 1.0
    %% th = heading(3,i);
    %% if th > 180
    %%     heading(3,i) = (360 - heading(2,i) + heading(1,i))*(-1);
    %% elseif th < -180
    %%     heading(3,i) = 360 - heading(1,i) + heading(2,i);
    %% end
    %compare pitch values from TCM to converted values from LPS
    pitch(1,i) = TCM_orientation(i,3);
    pitch(2,i) = p;
    pitch(3,i) = pitch(2,i)-pitch(1,i);
    %compare roll values from TCM to converted values from LPS
    roll(1,i) = TCM_orientation(i,4);
    roll(2,i) = r;
    roll(3,i) = roll(2,i)-roll(1,i);
end

%-------------------------------------------------------------------------
% Calculation of rotational offset calibration values and
% standard deviations
%-------------------------------------------------------------------------

%--- Heading
% Calibration value only derived from measurements at orientation
% sensor initialisation location
ini_img = 2; %number of images at initialisation location

h_offset = mean(heading(3,1:ini_img)); % calibration value
h_std_ini = std(heading(3,1:ini_img)); % standard deviation
```

```
maxdiff = 0; % indicates range of heading offsets

for i = ini_img+1:lg
    diff = heading(3,i)-h_offset;
    if abs(diff) > maxdiff
        maxdiff = abs(diff);
    end
end

%--- Pitch
pitch_stat = [0,0];
pitch_stat(1) = mean(pitch(3,:)); % calibration value
pitch_stat(2) = std(pitch(3,:)); % standard deviation

%--- Roll
roll_stat = [0,0];
roll_stat(1) = mean(roll(3,:));  % calibration value
roll_stat(2) = std(roll(3,:)); % standard deviation


%--- Rotate heading, pitch roll standard deviation into standard
% deviations for omega, phi, kappa
% approach using code in hpr2dcm for conversion between types of
% angles (alternatively an approach utilising hpr2wpk.m (see below)
% can be used, which more straightforward)

% rotation matrix rotating from terrestrial to normal case of
% photogrammetry
%% Rsc = [1,0,0;
%%     0,0,-1;
%%     0,1,0];
% use code in hpr2dcm.m for conversion
%% R = hpr2dcm(0.3,pitch_stat(2),roll_stat(2)) * Rsc; % 0.3 is
            % expected heading accuracy of orientation sensor
%% std_w = abs(rad2deg(atan2(-R(2,3),R(3,3))) - 90);
%% std_p = abs(rad2deg(asin(R(1,3))));
%% std_k = abs(rad2deg(atan2(-R(1,2),R(1,1))));


% alternative code, more straightforward
[std_w,std_p,std_k] = hpr2wpk(0.3,pitch_stat(2),roll_stat(2));
std_w = std_w -90;


%=========================================================================
% Positional offset calibration
%=========================================================================

%-------------------------------------------------------------------------
% Calculate absolute offsets between GPS/TS and camera
%-------------------------------------------------------------------------

dist_vect = zeros(3,lg);
for i = 1:lg
    dist_vect(1,i) = LPS_eo(i,2)-GPSTS_position(i,2); % Easting
    dist_vect(2,i) = LPS_eo(i,3)-GPSTS_position(i,3); %Northing
    dist_vect(3,i) = LPS_eo(i,4)-GPSTS_position(i,4); % Height
end
```

```
%-------------------------------------------------------------------
% Normalise offsets
%-------------------------------------------------------------------

% Apply inverse rotation matrix to each offset vector, using
% photogrammetric angles derived in LPS

dist_norm = zeros(3,lg);


for i = 1:lg
    % use code in rotmatrix.m for creating the rotation matrix
    A = rotmatrix(LPS_eo(i,5),LPS_eo(i,6),LPS_eo(i,7),1);
    dist_norm(:,i) = A*dist_vect(:,i);
end

%-------------------------------------------------------------------
% Calculation of positional offset calibration values and
% standard deviations
%-------------------------------------------------------------------

stats_pos = [mean(dist_norm(1,:)),std(dist_norm(1,:)); % x
                                                       % calibration
    mean(dist_norm(2,:)),std(dist_norm(2,:)); % y calibration
    mean(dist_norm(3,:)),std(dist_norm(3,:))]; % z calibration

offset_calibr = [stats_pos(1,1); stats_pos(2,1); stats_pos(3,1)];
offset = offset_calibr;


%===================================================================
% Create calibration output files
%===================================================================

% write rotational calibration values
dlmwrite('hpr_corr.txt',[h_offset;mean(pitch(3,:));
mean(roll(3,:))],'\t');

% write rotational standard deviations (omega, phi, kappa) and
% range of heading offsets for constraining exterior
% orientation parameters in bundle adjustment
dlmwrite('orientation_std_wpk.txt',[std_w;std_p;std_k;
                                                  maxdiff],'\t');

% write rotational standard deviations in heading, pitch, roll
dlmwrite('orientation_stats_hpr.txt',[h_std_ini;pitch_stat(2);
                                        roll_stat(2)],'\t');

% write positional calibration values
dlmwrite('pos_corr.txt',offset,'\t');

% write positional standard deviations
dlmwrite('position_stats.txt',[stats_pos(1,2);stats_pos(2,2);
                                        stats_pos(3,2)],'\t');
```

A.2 Exterior orientation determination code

```
%*********************************************************************
% This code applies rotational and positional offset calibration
% values to direct measurements of orientation sensor and DGPS (or
% Prism). The results are direct exterior orientation parameters for
% each image.
% Author: Melanie Kirchhoefer
% Version 2.0
%*********************************************************************


clc

lg = length(TCM_orientation);


%---------------------------------------------------------------------
% Read files
%---------------------------------------------------------------------

%--- Direct orientation (tab delimited, no headings):
% Heading (Magnetic North), Heading (Grid North), Pitch, Roll
TCM_orientation = dlmread('orientation.txt','\t',0,0);

%--- Direct position (tab delimited, no headings):
% ID, Easting, Northing, Height
GPSTS_position = dlmread('position.txt','\t',0,0);

%--- Rotational calibration values:
% Heading, Pitch, Roll
ori_correction = dlmread('hpr_corr.txt','\t',0,0);

%--- Positional calibration values:
% X, Y, Z
pos_correction = dlmread('pos_corr.txt','\t',0,0);



%=====================================================================
% Determine rotational exterior orientation parameters (omega, phi,
% kappa)
%=====================================================================

%---------------------------------------------------------------------
% Apply calibration values
%---------------------------------------------------------------------

TCM_corr = zeros(lg,3); % corrected angles in heading, pitch, roll


for i = 1:lg
    % heading
    TCM_corr(i,1) = TCM_orientation(i,2) + ori_correction(1);
    th = TCM_corr(i,1);
```

```
    if th < 0
        TCM_corr(i,1) = 360 + th;
    elseif th > 360
        TCM_corr(i,1) = th - 360;
    End
    % pitch
    TCM_corr(i,2) = TCM_orientation(i,3) + ori_correction(2);
    % roll
    TCM_corr(i,3) = TCM_orientation(i,4) + ori_correction(3);
end

%-------------------------------------------------------------------------
% Conversion into omega, phi, kappa
%-------------------------------------------------------------------------

%--- Approach using code in hpr2dcm.m; there is a more
% straightforward approach using code in hpr2wpk.m (see below)
% rotation matrix rotating from terrestrial to normal case of
% photogrammetry
%% Rsc = [1,0,0;
%%     0,0,-1;
%%     0,1,0];

%% omega_tcm = zeros(lg,1);
%% phi_tcm = zeros(lg,1);
%% kappa_tcm = zeros(lg,1);

%% for i = 1:lg
%%     % use code in hpr2dcm.m for conversion
%%     R1 = hpr2dcm(TCM_corr(i,1),TCM_corr(i,2),TCM_corr(i,3));
%%     R2 = R1 * Rsc;
%%     % extract angle from rotation matrix
%%     omega_tcm(i,1) = rad2deg(atan2(-R2(2,3),R2(3,3)));
%%     phi_tcm(i,1) = rad2deg(asin(R2(1,3)));
%%     kappa_tcm(i,1) = rad2deg(atan2(-R2(1,2),R2(1,1)));
%% end

%% direct_ori = [omega_tcm,phi_tcm,kappa_tcm];


%--- Approach using hpr2wpk.m

direct_ori = zeros(lg,3);

for i = 1:lg
    [omega,phi,kappa] =
            hpr2wpk(TCM_corr(i,1),TCM_corr(i,2),TCM_corr(i,3));
    direct_ori(i,:) = [omega,phi,kappa];
end


%=========================================================================
% Determine positional exterior orientation parameters (easting
% (X), northing (Y), height (Z))
%=========================================================================


format long
```

```
%-----------------------------------------------------------------------
% Rotate positional calibration values
%-----------------------------------------------------------------------

% For each image positional calibration values are rotated in the
% rotated camera coordinate system at the time of exposure.
% This results in absolute corrections for each image

offsets = zeros(3,lg); % absolute corrections
for i = 1:lg
    %use TCM data corrected and converted to omega, phi, kappa
    A = rotmatrix(direct_ori(i,1),direct_ori(i,2),
                                          direct_ori(i,3),1);
    offsets(:,i) = A'*pos_correction(:,1);
end


%-----------------------------------------------------------------------
% Apply absolute corrections to direct position measurements
%-----------------------------------------------------------------------

% This results in direct positional exterior orientation
% parameters

direct_pos = zeros(lg,3);
for i = 1:lg
    direct_pos(i,1) = GPSTS_position(i,2)+offsets(1,i);
    direct_pos(i,2) = GPSTS_position(i,3)+offsets(2,i);
    direct_pos(i,3) = GPSTS_position(i,4)+offsets(3,i);
end
%=======================================================================
% Create exterior orientation parameters output files
%=======================================================================

%--- Direct rotational exterior orientation parameters
dlmwrite('direct_orientations.txt',direct_ori,'\t',0,0);

%--- Direct positional exterior orientation parameters
dlmwrite('direct_positions.txt',direct_pos,'delimiter','\t',
'precision','%.6f');
```

A.3 Sub-routines

A.3.1 wpk2hpr.m Version 1.0

```
%*****************************************************************
% This function converts photogrammetric angles omega, phi, kappa
% into orientation sensor (TCM5) angles heading (h), pitch (p), roll
% (r).
% Author: Melanie Kirchhoefer
% Version 1.0
%*****************************************************************
```

```
 function [h,p,r] = wpk2hpr(w,p,k,f)

%--------------------------------------------------------------------
% Define camera axis vector and perpendicular
%--------------------------------------------------------------------

%--- Camera axis (pos + neg)
c1 = [0;0;f];
c2 = [0;0;-f];

%--- Perpendicular to camera axis
c3 = [1;0;0];
%--------------------------------------------------------------------
% Calculate heading, pitch, and roll angles
%--------------------------------------------------------------------

%--- Create rotation matrix from omega, phi, kappa
R = rotmatrix(w,p,k,1);

%--- Rotate camera axis and perpendicular
C1 = R' * c1;
C2 = R' * c2;
C3 = R' * c3;
%--- Calculate distances
dX = C2(1)-C1(1);
dY = C2(2)-C1(2);
dZ = C2(3)-C1(3);
dL = sqrt(dX^2 + dY^2);

%--- Calculate heading
h_1 = rad2deg(atan2(dX,dY));
if h_1 < 0
    h = 360 + h_1;
else
    h = h_1;
end

%--- Calculate pitch
p = rad2deg(atan2(dZ,dL));

%--- Calculate roll
dR3 = sqrt(C3(1)^2 + C3(2)^2);
dZ3 = 0 - C3(3);
r = rad2deg(atan2(dZ3,dR3));
```

A.3.2 wpk2hpr.m Version 2.0

```
%*********************************************************************
% This function converts photogrammetric angles omega, phi, kappa
% into orientation sensor (TCM5) angles heading (h), pitch (p), roll
% (r).
% Author: Melanie Kirchhoefer
% Version 2.0
%*********************************************************************
```

```
function [h,p,r] = wpk2hpr(w,p,k)

%--- Matrix rotating system from terrestrial case to normal case of
%    photogrammetry

RTN = [1,0,0;
    0,0,-1;
    0,1,0];

%-------------------------------------------------------------------
% derive rotation matrix from omega, phi, kappa
%-------------------------------------------------------------------

R = rotmatrix(w,p,k,1)'*RTN';

%-------------------------------------------------------------------
% Calculate heading, pitch, and roll angles
%-------------------------------------------------------------------

h = 360-rad2deg(atan2(-R(1,2),R(2,2)));
p = asind(R(3,2));
r = rad2deg(atan2(-R(3,1),R(3,3)));
```

A.3.3 hpr2dcm.m

```
%*******************************************************************
% This function derives a rotation matrix from heading, pitch, roll
% of the TCM5 orientation sensor. This matrix can be used to extract
% other types of rotation angles, for example omega, phi, and kappa.
% Author: Melanie Kirchhoefer
% Version 1.0
%*******************************************************************


function [dcm] = hpr2dcm(h,p,r)

%===================================================================
% Function to derive a rotation matrix from independent
% heading, pitch and roll angles.
%===================================================================

H = 360-h;
P = p;
R = r;

Xo = [1;0;0];
Yo = [0;1;0];


%-------------------------------------------------------------------
% Rotation matrices
%-------------------------------------------------------------------

% rotation matrix about x-axis
rotX = [1,0,0;
    0,cosd(P),-sind(P);
    0,sind(P),cosd(P)];
```

```
% rotation matrix about y-axis
rotY = [cosd(R),0,sind(R);
    0,1,0;
    -sind(R),0,cosd(R)];
% rotation matrix about z-axis
rotZ = [cosd(H),-sind(H),0;
    sind(H),cosd(H),0;
    0,0,1];


%---------------------------------------------------------------------
% Derive new coordinates of x-axis
%---------------------------------------------------------------------

%--- Background: The angle between the new x-axis (x-axis of
% the rotated system) and the original xy-plane (non-tilted
% sensor) is roll measure by the sensor. At the same time the
% new x-axis has to be rectangular to the new y-axis. The
% following calculations find a vector representing the new x-
% axis where both requirements are true.

%--- Rotate Xo about Yo (roll)
X1 = rotY * Xo;

%--- Calculate the additional rotation a of X about Zo caused
% by pitch
% y-distance (n) depending on pitch and correct z-value for
% roll
n = X1(3)/tand(90-P);
m = cosd(R); % magnitude of vector x projected on x-y-plane
a = asindd(n/m) * (-1); % angle to be added to heading

% rotation about Zo considering pitch (rotate by heading+a)
rotZ2 = [cosd(H+a),-sind(H+a),0;
    sind(H+a),cosd(H+a),0;
    0,0,1];

%--- Rotate X1 about Zo (new x-axis points in right direction
% (right angle to heading)
X2 = rotZ2 * X1;

%---------------------------------------------------------------------
% Derive new coordinates of y-axis
%---------------------------------------------------------------------

%--- Rotate Yo about Xo
Y1 = rotX * Yo;

%--- Rotation around Zo (heading)
Y2 = rotZ * Y1;

%---------------------------------------------------------------------
% Derive new coordinates of z-axis
%---------------------------------------------------------------------

%--- Using vector cross product to calculate a vector
% perpendicular to the X2-Y2-plane -> new Z-axis
Z1 = cross(X2,Y2);
```

```
%-----------------------------------------------------------------------
% Rotation matrix (direction cosine matrix)
%-----------------------------------------------------------------------

dcm=[X2,Y2,Z1];
```

A.3.4 hpr2wpk.m

```
%*********************************************************************
% This function derives a rotation matrix from heading, pitch, roll
% of the TCM5 orientation sensor. This matrix can be used to extract
% other types of rotation angles, for example omega, phi, and kappa.
% This function substitutes hpr2dcm.m
% Author: Melanie Kirchhoefer
% Version 1.0
%*********************************************************************


function [w,phi,k] = hpr2wpk(h,p,r)

%--- Matrix rotating system from terrestrial case to normal case of
%    photogrammetry

RTN = [1,0,0;
    0,0,-1;
    0,1,0];

%-----------------------------------------------------------------------
% Derive a rotation matrix from heading, pitch and roll angles.
%-----------------------------------------------------------------------

R = rotmatrix(360-h,p,r,2)*RTN;

%-----------------------------------------------------------------------
% Calculate omega, phi, and kappa.
%-----------------------------------------------------------------------

w = rad2deg(atan2(-R(2,3),R(3,3)));
phi = asind(R(1,3));
k = rad2deg(atan2(-R(1,2),R(1,1)));
```

A.3.5 rotmatrix.m

```
%*********************************************************************
% This function creates a rotation matrix from rotation angles. The
% order of argument input is: angle of first rotation, angle of
% second rotation, angle of third rotation, and rotation sequence. If
% the rotation sequence is "1" then the rotation matrix rotates about
% rotated axes of the reference system in the sequence XYZ
% (photogrammetric angles; Rkpw). If the rotation sequence is "2",
% then the matrix rotates about fixed axes of the reference system in
% the sequence ZXY (orientation sensor angles; Rzxy).
% Author: Melanie Kirchhoefer
% Version 2.0
%*********************************************************************
```

```
function [R] = rotmatrix(w,p,k,order)

Rkpw =
[cosd(p)*cosd(k),cosd(w)*sind(k)+sind(w)*sind(p)*cosd(k),
      sind(w)*sind(k)-cosd(w)*sind(p)*cosd(k);
-cosd(p)*sind(k),cosd(w)*cosd(k)-sind(w)*sind(p)*sind(k),
      sind(w)*cosd(k)+cosd(w)*sind(p)*sind(k);
sind(p),-sind(w)*cosd(p),cosd(w)*cosd(p)];



Rzxy =
[cosd(w)*cosd(k)-sind(w)*sind(p)*sind(k), -sind(w)*cosd(p),
      cosd(w)*sind(k)+sind(w)*sind(p)*cosd(k);
sind(w)*cosd(k)+cosd(w)*sind(p)*sind(k), cosd(w)*cosd(p),
      sind(w)*sind(k)-cosd(w)*sind(p)*cosd(k);
-cosd(p)*sind(k), sind(p), cosd(p)*cosd(k)];


if order == 1
    R = Rkpw;
elseif order == 2
    R = Rzxy;
end
```

Appendix B:
Conference contributions

CIPA Symposium Prague, 12th – 16th September 2011:

KIRCHHÖFER, M., CHANDLER, J. AND WACKROW, R. (2011): Cultural heritage recording utilising low-cost close-range photogrammetry. *Proceeding of CIPA XXIIIth International Symposium*, Prague, Czech Republic, 8 pages [on CD-ROM].

ISPRS WG V/2 Conference York, 17th – 19th August 2011:

KIRCHHÖFER, M., CHANDLER, J. WACKROW, R., BRYAN, P., TOVEY, S. (in press): A low-cost photogrammetric recording system for cultural heritage recording: calibration and testing. *International Archives of the Photogrammetry, Remote Sensing and Spatial Information Sciences*, (Accepted June 2011).

CULTURAL HERITAGE RECORDING UTILISING LOW-COST CLOSE-RANGE PHOTOGRAMMETRY

Melanie KIRCHHÖFER[1], Jim CHANDLER[1], Rene WACKROW[1]

[1]Loughborough University, School of Civil and Building Engineering
Loughborough, LE11 3TU, United Kingdom

m.k.kirchhoefer@lboro.ac.uk, j.h.chandler@lboro.ac.uk, r.wackrow@lboro.ac.uk

Keywords: close-range photogrammetry, heritage recording, orientation sensor, low-cost, smartphones

Abstract: *Cultural heritage is under a constant threat of damage or even destruction and comprehensive and accurate recording is necessary to attenuate the risk of losing heritage or serve as basis for reconstruction. Cost effective and easy to use methods are required to record cultural heritage, particularly during a world recession, and close-range photogrammetry has proven potential in this area. Off-the-shelf digital cameras can be used to rapidly acquire data at low cost, allowing non-experts to become involved. Exterior orientation of the camera during exposure ideally needs to be established for every image, traditionally requiring known coordinated target points. Establishing these points is time consuming and costly and using targets can be often undesirable on sensitive sites. MEMS-based sensors can assist in overcoming this problem by providing small-size and low-cost means to directly determine exterior orientation for close-range photogrammetry. This paper describes development of an image-based recording system, comprising an off-the-shelf digital SLR camera, a MEMS-based 3D orientation sensor and a GPS antenna. All system components were assembled in a compact and rigid frame that allows calibration of rotational and positional offsets between the components. The project involves collaboration between English Heritage and Loughborough University and the intention is to assess the system's achievable accuracy and practicability in a heritage recording environment. Tests were conducted at Loughborough University and a case study at St. Catherine's Oratory on the Isle of Wight, UK. These demonstrate that the data recorded by the system can indeed meet the accuracy requirements for heritage recording at medium accuracy (1-4cm), with either a single or even no control points. As the recording system has been configured with a focus on low-cost and easy-to-use components, it is believed to be suitable for heritage recording by non-specialists. This offers the opportunity for lay people to become more involved in their local heritage, an important aspiration identified by English Heritage. Recently, mobile phones (smartphones) with integrated camera and MEMS-based orientation and positioning sensors have become available. When orientation and position during camera exposure is extracted, these phones establish off-the-shelf systems that can facilitate image-based recording with direct exterior orientation determination. Due to their small size and low-cost they have potential to further enhance the involvement of lay-people in heritage recording. The accuracy currently achievable will be presented also.*

1. INTRODUCTION

Cultural heritage plays a vital role in education about the past, in creating cultural or individual identity, and even in providing economical support for local communities [1,2,3]. Despite these widely acknowledged benefits, cultural heritage is at a constant risk by neglect and decay, deliberate destruction and damage due to social and economic progress, disasters, and armed conflict [3,4,5]. From this risk, an increased need to record spatially can be recognised. Comprehensive and accurate documentation can attenuate the risk of losing heritage and in the worst case serve as a basis for reconstruction [5]. The suitability of properly calibrated consumer-grade cameras for many heritage recording tasks has been demonstrated in [6,7,8]. Recognising the desirability to record within a three-dimensional (3D) national reference system, establishing known coordinated target points for exterior orientation estimation remains time consuming and costly and requires surveying expertise. Direct exterior orientation estimation for close-range applications

could overcome this problem by avoiding expensive target point surveys and enabling non-experts to record cultural heritage within an appropriate national reference system. In that way the cost is reduced even further by the possibility to employ volunteers [9]. Direct exterior orientation estimation in close-range photogrammetry can be achieved using orientation sensors based on Micro Electro Mechanical Systems (MEMS) technology that have emerged on the market in recent years. Although their accuracy is lower than that of their large-size counterparts, results of utilising them for mobile mapping projects and photogrammetry look promising [10,11]. Direct positioning can be achieved using Global Positioning System (GPS) devices. Although positioning with current low-cost, handheld GPS devices does not meet the requirements for some applications of close-range photogrammetry, there is potential for improvements in the future [12]. One example is the announcement of GENEQ Inc. to release a small-size, high accuracy GPS receiver (SXBlue III) that is available for much lower cost than conventional survey-grade GPS receivers [13].

This paper presents the development and testing of a low-cost recording system for cultural heritage recording that utilises a low-cost orientation sensor and GPS for direct exterior orientation determination. Furthermore, the potential of utilising smartphones with integrated camera, orientation and position sensors for low-cost cultural heritage recording is investigated. First the recording system and its components are presented and the data collection and analysis process is explained. This is followed by a description of a recording system performance test at Loughborough University and of a case study on the Isle of Wight, UK. The results of these tests are presented in Section 4. In Section 5 the methodology of the smartphone test is described and the results of this test are presented. After discussing the results of the recording system and smartphone tests, this paper finishes in a conclusion.

2. METHODOLOGY

2.1 Recording System

The recording system presented here comprises a calibrated consumer-grade digital camera (Nikon D80) for image acquisition, a small-size 3D orientation sensor (PNI TCM5) for orientation measurement, a survey-grade differential GPS (DGPS) (Leica System 500) for 3D positioning, and a laptop for operating the orientation sensor (Figure 1a).

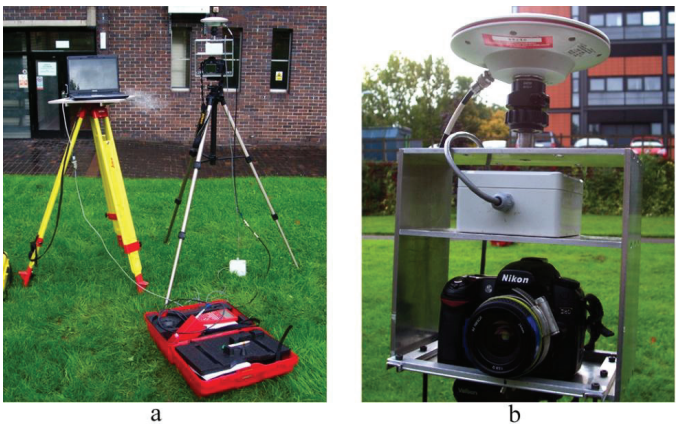

Figure 1: Full recording system (a) and mounting frame (b).

Camera, orientation sensor, and DGPS antenna were attached to a purposely built mounting frame that constrains the components in their orientation and position (Figure 1b). This enables a reliable calibration of the rotational and positional offsets between components.

When the recording system was assembled in early 2010, no low-cost, small-size DGPS receivers were available on the market to provide centimetre accuracy required in this project. Therefore, it was decided to use a survey-grade DGPS receiver, enabling positioning with centimetre accuracy. Although this is certainly not a low-cost component, it facilitates the testing of the principles of direct exterior orientation determination for close-range photogrammetry.

The TCM5 orientation sensor is capable of measuring heading, pitch and roll using magnetometers and accelerometers. The expected accuracy of the measured angles is 0.3° in heading and 0.2° in pitch and roll [14].

2.2 Offset calibration

In order to achieve accurate exterior orientation parameters of the camera, the rotational offset between camera and orientation sensor and the positional offset between camera and DGPS antenna need to be calibrated. Exterior orientation parameters for a set of images acquired using the recording system were derived indirectly in a Leica Photogrammetric Suite (LPS) bundle adjustment. These parameters were used as truth data and compared to orientation sensor and DGPS measurements acquired at the time of exposure. For this purpose a routine was coded in MathWorks' Matrix Laboratory (MatLab) that used truth and measured data to estimate offset calibration values and their precision. Calibration values are defined by the arithmetic mean of the offsets calculated for each image and precision is indicated by the standard deviation. The calibration values were applied to the directly measured orientation and position values in order to derive direct exterior orientation parameters for each image. The MatLab routine also included an algorithm to convert the true omega, phi, and kappa values into equivalent heading, pitch and roll values, in order to enable comparison between indirectly derived (omega, phi, kappa) and directly measured (heading, pitch, roll) orientation angles. Another algorithm was needed to convert the corrected heading, pitch, and roll values into omega, phi, and kappa that were suitable for utilisation in a bundle adjustment. A detailed description of the offset calibration process will be presented in a future publication.

2.3 Data collection and analysis

For testing the performance of the recording system, data was recorded from a varying number of camera stations adjacent to a test object which included coordinated points. A camera station here is defined as the position and orientation of the mounting frame at the time of image acquisition. For each acquired image, orientation and position at the time of exposure was measured by the orientation sensor and the DGPS receiver, respectively. Imagery, orientation and position data of all camera stations acquired on a particular date establish a data set. Calibration values were derived from the collected data and applied to the measurements of the same data set. Because the camera had been detached from the mounting frame between collection of differing data sets, no independently derived offset calibration values that were considered suitable to correct orientation and position measurements were available. Assuming that the best suitable calibration values are derived from the same data set, the results of accuracy assessment indicate the theoretically highest accuracy achievable. The corrected orientation sensor and DGPS measurements were used to provide initial exterior orientation parameters, constrained by the estimated calibration precision, in a bundle adjustment software known as GAP [15]. For each data set the GAP bundle adjustment was run twice. For the first run no control points were used, relying on the exterior orientation parameters derived from orientation sensor and DGPS only. The coordinated points of the test object were used as check points and their coordinates were estimated in the bundle adjustment. In the second run one coordinated point was used as control point with corresponding image point coordinates in only one image. In this bundle adjustment coordinates for the remaining check points were estimated. For both runs the estimated coordinates were compared to the known coordinates of the points, so allowing the calculation of the Root Mean Square Error (RMSE) for easting, northing, and height to quantify absolute accuracy. Relative accuracy was assessed also. 3D distances between all possible pairs of coordinated points were calculated from the check point coordinates estimated in the bundle adjustment. These distances were compared to corresponding distances calculated from the original check point coordinates. The RMSE of the distance differences indicates the 3D relative accuracy.

3. TESTING

3.1 Initial test

The recording system was initially tested at Loughborough University. A metal piece of art located on Loughborough University campus was chosen as test object (Figure 2a). The test object is a vertical structure with a small diameter on the ground and is accessible from all sides. It was considered representative for the type of heritage object that was also found at the case study site (Section 3.2). On the southern side of the test

object 17 points with known Ordnance Survey National Grid (OSGB36) coordinates were established. In the lower part that could be reached without auxiliary means (approximately up to 2m) survey targets were used to mark the points. In the upper part of the test object natural points defined by distinctive features, such as corners and intersections of steelwork, were selected. Imagery, orientation and position data was collected at 11 camera stations arranged in an arc around the southern side of the test object with an approximate camera-to-object distance of 6m. At this distance some images were acquired with the mounting frame tilted up to 33°, in order to cover the entire height of the test object (approximately 6m). The data collected was processed and analysed using the methods described in Section 2.3 and the results can be found in Section 4.

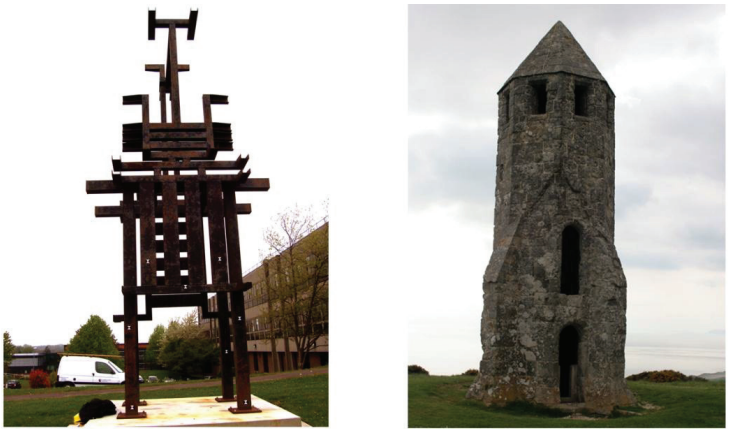

a b

Figure 2: Test object at Loughborough University (a) and case study site St. Catherine's Oratory, Isle of Wight, UK (b).

3.2 Case study

The aim of the case study was to test the performance of the recording system at a real heritage site. St. Catherine's Oratory (Figure 2b) on the Isle of Wight, UK, was chosen as case study test site. St. Catherine's Oratory is an approximately 11m high, octagonal tower built in 1328. It is located in the south of the Isle of Wight on one of the highest parts of the Island [16]. On the eastern side of the tower 22 points with known OSGB36 coordinates were established. Analogous to the test object at Loughborough University, targeted points were used in the lower part and natural points were used in the upper part of the tower. Two data sets were collected during the case study. The first data set (DS1) consists of data collected from 12 camera stations arranged in an arc around the eastern side of the tower with an approximate camera-to-object distance of 10m. The second data set (DS2) consists of data collected from 12 camera stations arranged in an arc around the eastern side of the tower with an approximate camera-to-object distance of 6m. Due to the camera-to-object distance and the height of the tower, the mounting frame was tilted up to 21° in DS1 and 28° in DS2 in order to cover the entire height of the tower. Each data set was processed and analysed separately using the methods described in Section 2.3. The results of the analysis can be found in Section 4.

4. RESULTS

4.1 Absolute accuracy

Absolute accuracy quantifies the recording systems capability to provide data for measurements that are accurate in relation to a national coordinate reference system. It is indicated by the RMSE of the differences between object coordinates of check points estimated in a GAP bundle adjustment and their original coordinates. Figure 3 depicts the absolute accuracy achieved in the initial recording system test and in the case study using zero or just one single control point (CP).

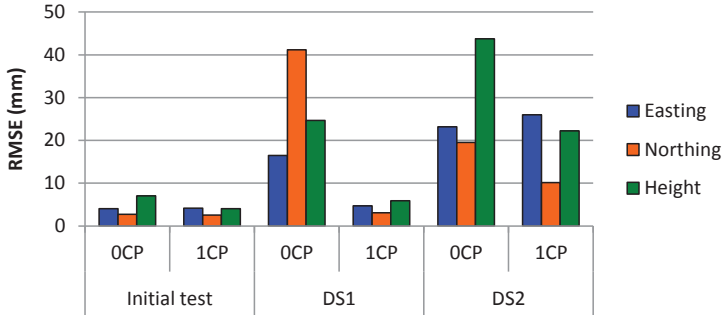

Figure 3: Absolute accuracy achieved in recording system test.

The best accuracy is achieved in the initial test with values not exceeding 7.0mm. There is no significant difference between using zero or a single control point. The RMSE achieved in the case study using no control points is significantly higher than the RMSE of the initial test, with values up to 41.2mm in DS1 and 43.7mm in DS2. The accuracy in DS1 and DS2 is enhanced by using a single control point in the GAP bundle adjustment. However, the RMSE in DS2 (26.0mm) is significantly higher than the RMSE in DS1 (5.9mm). The accuracy variations between the three data sets indicate that their direct exterior orientation parameters used in the GAP bundle adjustment are of different accuracy.

4.2 Relative accuracy

The relative or inner accuracy quantifies the recording system capability to provide data for measurements that are accurate in relation to each other. This was assessed by comparing 3D distances between check point coordinates estimated in a GAP bundle adjustment with equivalent distances derived from the original coordinates. The RMSE of the distance differences indicates the relative accuracy. Figure 4 depicts the relative accuracy achieved in the initial recording system test and in the case study using zero or a single control point.

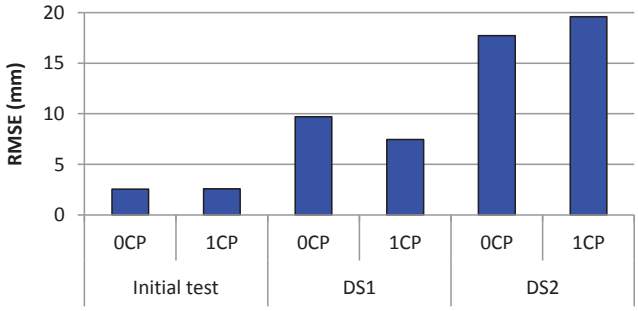

Figure 4: Relative accuracy achieved in recording system tests.

The best relative accuracy is achieved for the initial test, with 2.5 mm when zero control points were used. Similar to the absolute accuracy, the relative accuracy achieved in the case study is worse than the relative accuracy achieved in the initial test. The relative accuracy achieved is also significantly different between the case study data sets, DS1 and DS2. When zero control points are used, the RMSE increased from DS1 (9.7mm) to DS2 (17.7mm) by 8mm. Similar to the results of the absolute accuracy assessment, this indicates accuracy differences between the exterior orientation parameters derived from the three data sets. The utilisation of one single control point seems to have no significant effect on the achievable relative accuracy.

5. SMARTPHONE TEST

Smartphones with integrated camera and MEMS-based orientation and positioning sensors have potential to facilitate image-based recording with direct exterior orientation determination. When orientation and

position during exposure can be extracted these phones establish off-the-shelf systems that are in principle similar to the recording system presented in this paper. The usability of smartphones for image-based heritage recording was tested using the "htc desire" smartphone. This smartphone integrates a 5 mega pixel camera, a GPS antenna, a digital compass and accelerometers [17]. In March 2011 the camera of the smartphone was calibrated and the smartphone used to acquire imagery at a test field established on an outside wall at Loughborough University using 22 coordinated points. Orientation and position at the time of exposure were extracted using a smartphone application ("Imageotag") that prints the data derived from GPS, compass, and accelerometers on a copy of the original image. Imagery, orientation and position data was processed and analysed using the methods described in Section 2.3. This resulted in indicators for absolute (Figure 5a) and relative (Figure 5b) accuracy achievable when zero or one single control point is used. The results of the smartphone test are presented using the unit meters (m) instead of the unit millimetres (mm) used for the recording system test results.

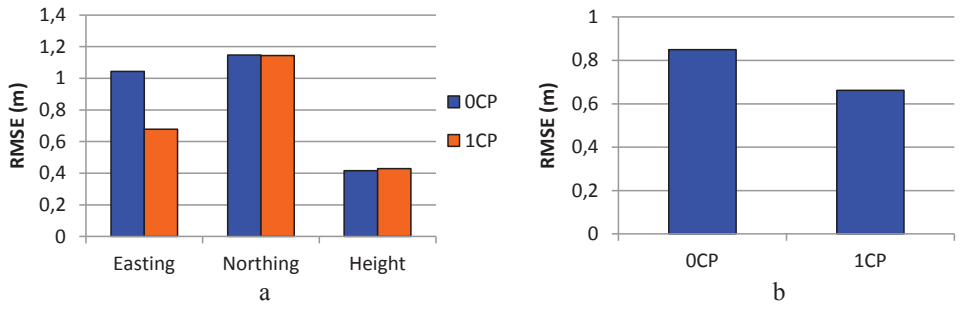

Figure 5: Absolute (a) and relative (b) accuracy achieved using a smartphone.

Figure 5a demonstrates that the smartphone can achieve an absolute accuracy of 1.15m without using control points in the bundle adjustment. When a single control point is used in the bundle adjustment a significant increase in accuracy is only achieved for Easting where the RMSE drops from 1.04m to 0.68m. Using a single control points also improves the relative accuracy (Figure 5b). The RMSE of the relative accuracy changes from 0.85m achieved when no control point was used to 0.66m when a single control point was used in the GAP bundle adjustment.

6. DISCUSSION

6.1 Performance of the original recording system

The results of the absolute accuracy assessment demonstrated that an accuracy level of 44mm can be achieved without control points when suitable exterior orientation parameters are available. With the utilisation of a single control point the absolute accuracy level can be improved to 26mm. As expected, the relative accuracy is better than the absolute accuracy, achieving 18mm without using any control points.

The accuracy assessment also revealed significant differences in absolute and relative accuracy between the three data sets. This could be caused by variations in the accuracy of the direct exterior orientation parameters used in the GAP bundle adjustment. Because the calibration values and exterior orientation parameters were derived from the same data set, the standard deviations of the calibration values are also indicators of the accuracy of the directly measured values from where the exterior orientation parameters were derived. Investigating this issue, it was revealed that the standard deviations of the positional offset calibration values varied significantly between the three data sets (Table 1).

Table 1: Standard deviations of positional offset calibration values.

	Easting (mm)	*Northing (mm)*	*Height (mm)*
Initial test	7.86	9.21	9.35
DS1	13.40	14.65	15.64
DS2	24.62	37.57	16.74

The standard deviations increase from the initial test data set to DS1 and also from DS1 to DS2, demonstrating the decrease in accuracy of the directly measured positions from the initial test to DS2. Because the case study standard deviations exceed the expected accuracy of DGPS, which is 10mm in plan and 30mm in height [18], the decrease in positioning accuracy is either caused by instability of the recording system components fixture to the mounting frame or by a decrease in DGPS accuracy. A decrease in DGPS accuracy during data collection at St. Catherine's Oratory could have been caused by tilting the mounting frame for some images, which also tilts the DGPS antenna. However, in the initial test, data was collected under similar conditions. Further investigations will be conducted in order to identify the reason for the decrease in positioning accuracy.

The results of the absolute and relative accuracy assessment were achieved by correcting direct orientation and position measurements using offset calibration values derived from the same data set. Therefore, the calibration values are not independently derived and the results indicate only the theoretical accuracy achievable when well suited calibration values are available. After analysis of the data sets presented here, further test data sets were collected that enabled accuracy assessment using independently derived calibration values. Preliminary results suggest that the level of accuracy achieved in the tests presented here can also be achieved with independently derived calibration values, when stable offset calibration is maintained. These results will be presented in a future publication.

6.2 Performance of a system based upon a smartphone

As expected, the accuracy achieved using the "htc desire" smartphone is substantially worse than the accuracy achieved using the developed recording system. The smartphone achieved 1.15m absolute and 0.68m relative accuracy without using control points. This significant difference to the results achieved with the recording system is caused by the smartphone sensor accuracy. The accuracy of the smartphone orientation and position sensors is expected to be lower than the accuracy of the recording system DGPS and orientation sensor. No information could be found about the compass and accelerometer accuracy, but the standard deviations derived during offset calibration can be used as indicators for orientation accuracy. Here standard deviations for heading, pitch, and roll between 2° and 3° were achieved. The accuracy of the integrated GPS can be expected to be no better than the theoretical positioning accuracy of code-based GPS, which is 6-10m [18]. This is higher than the displacement that would result from a rotational error of 3° in the exterior orientation rotation parameters at a camera-to-object distance of 10m. Therefore, at close-range, the positioning accuracy of the smartphone is probably the limiting factor on the currently achievable absolute accuracy. However, the absolute accuracy achieved in this smartphone test is better than the expected GPS positioning accuracy. This can be explained by the offset calibration partly compensating the positional error. Similar to the processing and analysis of the recording system data, calibration values and exterior orientation parameters were derived from the same data set. In order to test how well independently derived calibration values can compensate positioning errors, further data collection and analysis will be carried out.

7. CONCLUSION

The results presented in this paper demonstrate that an absolute accuracy of 44mm can be achieved with an image-based recording system combined with direct exterior orientation determination. When a single control point is available for data processing the accuracy can be improved to 26mm. The recording system also achieves relative accuracy levels of 20mm and below. Preliminary results derived from further tests have indicated that this accuracy level can also be achieved when independently derived offset calibration values are used. The recording system is therefore believed to be suitable for many cultural heritage recording tasks. When the survey-grade DGPS receiver is replaced by a low-cost device for positioning with centimetre accuracy, the recording system will be a proper low-cost system that is suitable for heritage recording by non-specialists. The results of the smartphone test (1.2m absolute and 0.8m relative accuracy) demonstrate that even with well suited calibration values the currently achievable accuracy of the GPS positioning does not meet requirements for most cultural heritage recording tasks. However, the usability of smartphones for image-based recording was demonstrated and with in future potentially more accurate integrated orientation and position sensors, smartphones could be used for low-cost heritage recording by non-specialists.

8. ACKNOWLEDGEMENT

The authors wish to acknowledge the investment in a TCM5 orientation sensor by English Heritage, which made this project possible. Thanks are due to the National Trust for granting permission to conduct the case study at St. Catherine's Oratory. In addition the authors wish to thank the Remote Sensing and Photogrammetry Society (RSPSoc) for partly funding the first authors attendance at the CIPA 2011 conference in Prague.

9. REFERENCES

[1] Uzzell, D.L.: *Introduction: The Natural and Built Environment*. In: Heritage Interpretation, Vol. 1, The Natural and Built Environment, London, Pinter, 1-14, 1989.
[2] Herbert, D.T.: *Preface*. In: Heritage, Tourism and Society, London, Pinter, xi-xii, 1995.
[3] Power of Place Office, English Heritage: *Power of Place: The Future of the Historic Environment*, London, Power of Place Office, 50 pages, 2000.
[4] UNESCO: *Convention concerning the protection of the world cultural and natural heritage*, http://whc.unesco.org/archive/convention-en.pdf, 2009-05-05.
[5] Palumbo, G., Ogleby, C.L.: *Heritage at risk and CIPA today: a report on the status of heritage documentation*, International Archives of the Photogrammetry, Remote Sensing and Spatial Information Sciences 2004, 35(2004)B5, 239-842.
[6] Bosch, R.et al.: *Non-metric camera calibration and documentation of historical buildings*. Proceedings of CIPA 2005, Torino, September 2005, 142-147.
[7] Chandler, J.H., Fryer, J.G.: *Recording Aboriginal rock art using cheap digital cameras and digital photogrammetry*, Proceedings of CIPA 2005, Torino, September 2005, 193-198.
[8] Wackrow, R et al. *Geometric consistency and stability of consumer-grade digital cameras for accurate spatial measurement*. The Photogrammetric Record 2007, 22(2007)118, 121-134.
[9] Bryan, P., Chandler, J.H.: *Cost-effective rock-art recording within a non-specialist environment,* International Archives of the Photogrammetry, Remote Sensing and Spatial Information Sciences 2008, 37(2008)B5, 259-264.
[10] Niu, X. et al.: *Directly georeferencing terrestrial imagery using MEMS-based INS/GNSS integrated systems*, Proceedings of XXIII FIG Congress 2006, Munich, October 2006, 16 pages
[11] Guarnieri, A. et al.: *Low cost system: GPS/MEMS for Positioning*. Proceedings of FIG Working Week 2008, Stockholm, June 2008, 10 pages.
[12] Schwieger, V., Gläser, A.: *Possibilities of low cost GPS technology for precise geodetic applications*. Proceedings of FIG Working Week 2005, Cairo, April 2005, 16 pages.
[13] GENEQ Inc.: *SXBlue III. Rugged, Bluetooth high accuracy L1/L2 RTK-Mapping receiver*. http://www.sxbluegps.com/SXBlue-III-version1.1.pdf, 2011-01-12.
[14] PNI Corporation: *TCM 5. Tilt compensated 3-axis compass module*, http://www.pnicorp.com/files/TCM5%20Datasheet_05-14-2009.pdf, 2009-05-30.
[15] Chandler, J. H., Clark, J. S.: *The archival photogrammetric technique. Further applications and development*, The Photogrammetric Record 1992, 14(1992)80, 241-247.
[16] English Heritage: *St. Catherine's Oratory | English Heritage*, http://www.english-heritage.org.uk/daysout/properties/st-catherines-oratory/, 2011-05-11.
[17] HTC Corporation: *HTC - Products - HTC Desire – Specification*, http://www.htc.com/www/product desire/specification.html, 2011-05-12.
[18] Konecny, G.: *Geoinformation. Remote sensing, photogrammetry and geographic information systems*. London, Taylor & Francis, 248 pages, 2003.

A LOW-COST PHOTOGRAMMETRIC RECORDING SYSTEM FOR CULTURAL HERITAGE RECORDING: CALIBRATION AND TESTING

M. K. Kirchhöfer [a,*], J. H. Chandler [a], R. Wackrow [a], P. Bryan [b], S. Tovey [b]

[a] Department of Civil and Building Engineering, Loughborough University, Loughborough, LE11 3TU UK – (m.k.kirchhoefer, j.h.chandler, r.wackrow)@lboro.ac.uk

[b] English Heritage Photogrammetry Team, Tanner Row, York, Y01 6WP, UK – (paul.bryan, stephen.tovey)@english-heritage.org.uk

Commission V, WG V/2

KEY WORDS: Cultural Heritage, Recording, Non-Metric, Photogrammetry, Close Range

ABSTRACT:

Close-range photogrammetry utilising consumer-grade digital cameras has proved successful as a cost effective and easy to use method for cultural heritage recording. The traditional way of obtaining exterior orientation parameters during exposure requires known coordinated target points. To overcome the cost of establishing these points, a recording system has been developed that is capable of deriving the exterior orientation directly and cheaply. The system comprises a digital camera, an orientation sensor and a DGPS receiver.
The project involves collaboration between English Heritage and Loughborough University and the intention is to assess the performance and practicability of the system. Offset calibration stability and achievable accuracy were investigated using data collected at a test field at Loughborough University. The results indicate that the system can meet the accuracy requirements for heritage recording, even with slightly unstable offset calibration values.

1. INTRODUCTION

1.1 Motivation

Cultural heritage is at a constant risk by man-made and natural threats (UNESCO, 1972; Palumbo and Ogleby, 2004). Comprehensive and accurate documentation can attenuate the risk of losing heritage and serve as a basis for reconstruction (Palumbo and Ogleby, 2004). The aim of this project is to develop and test a low-cost and easy-to-use recording system that is capable of direct exterior orientation estimation. Such a system would reduce costs by avoiding expensive control point surveys and enabling non-specialists to become involved.

1.2 Related work

Chandler and Fryer (2005) and Bryan and Chandler (2008) reduced recording costs by using only scale bars as reference. In the latter non-specialist volunteers were successfully trained in applying photogrammetry in rock-art recording.
A recording system similar to the one presented here was developed and tested by Fiani and Pistillo (2004). The authors report high differences between direct and indirect exterior orientation parameters. They considered the system not practicable at that time and suggested enhancing the calibration procedure.

2. METHODOLOGY

2.1 Recording System

The recording system presented here comprises a Nikon D80 consumer-grade camera, a small-size 3D orientation sensor (PNI TCM5), and a Leica System 500 DGPS receiver (Figure 1a). Camera, orientation sensor, and DGPS antenna were assembled in a rigid frame that allows calibration of the rotational and positional offsets between the components (Figure 1b).

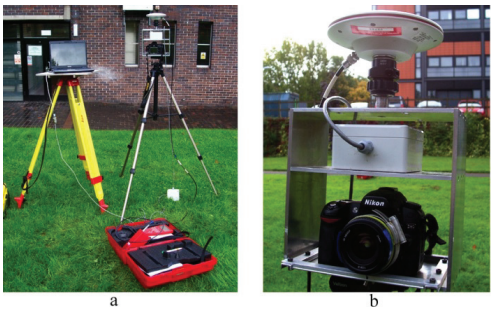

a b

Figure 1. Recording system.

2.2 Testing

For testing the recording system, three test data sets were collected at a test field consisting of coordinated target points on an outside wall at Loughborough University (Figure 1). A data set comprises imagery, orientation sensor and DGPS measurements.

* Corresponding author

Figure 2. Test field at Loughborough University

In order to derive exterior orientation parameters from orientation sensor and DGPS measurements, the rotational and positional offsets between the components were calibrated. This was achieved by comparing exterior orientation parameters derived indirectly from the images in a bundle adjustment to orientation sensor and DGPS measurements.
Offset calibration was carried out for each test data set and the resulting calibration values were applied to the two other data sets. The corrected orientation sensor and DGPS measurements were used as initial exterior orientation parameters in a bundle adjustment. In this, object coordinates of the test field points were estimated without using additional control. For assessing the absolute accuracy, the RMSE of the differences between the estimated coordinates and the known true coordinates was calculated. From the estimated coordinates ten distances between target points were calculated and compared to corresponding distances calculated from the known true coordinates. The RMSE of the distance differences is an indicator for relative accuracy.

3. RESULTS

3.1 Calibration

Figure 3 shows rotational and positional offset calibration values derived for the three test data sets. The heading offset varies by 0.7º, while pitch and roll offsets are more stable. The highest changes in the positional calibration values occur for Northing with 28.3mm between Test1 and Test3.

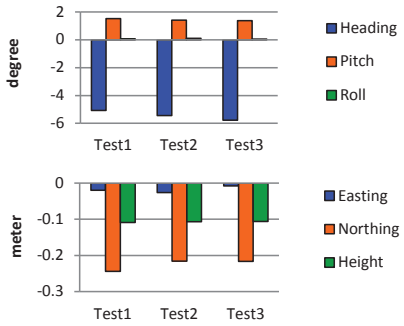

Figure 3. Rotational and positional offset calibration values.

3.2 Accuracy

Figure 4 shows that for all combinations of calibration values and test data the RMSE of the check point comparison does not exceed 30mm. In the cases when calibration values were derived in Test2 and Test3 the RMSE is smaller than 20mm.

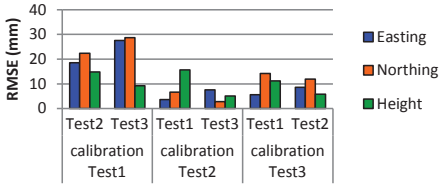

Figure 4. Absolute accuracy achieved for all combinations of calibration values and test data sets.

Figure 5 depicts the relative accuracy for all combinations of calibration values and test data sets. The values range from 2.2mm to 3.9mm. They are significantly lower than their corresponding absolute accuracy values.

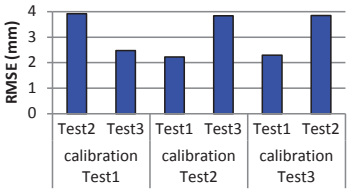

Figure 5. Relative accuracy achieved for all combinations of calibration values and test data sets.

4. DISCUSSION

Stable calibration is a prerequisite for accurate exterior orientation determination. The changes between the calibration values are higher than the expected accuracy of the orientation sensor and DGPS, and indicate movements of components with respect to each other. However, a RMSE below 30mm was achieved for all test data sets. This indicates that erroneous offset corrections due to unstable calibration can be compensated through the bundle adjustment. These results indicate that the system presented is capable of direct exterior orientation determination. It is suitable for recording cultural heritage of similar shape and extent as the test field to an absolute accuracy of 30mm. The practicability of the system for recording heritage objects of different type has to be assessed in further tests. Importantly, relative or internal accuracy within any derived data is better than the 30mm implies.

5. CONCLUSION

The results showed that the recording system presented is suitable for recording cultural heritage. Due to the focus on low-cost and easy-to-use components, the system is believed to be suitable for heritage recording by non-specialists. This offers

the opportunity for lay people to become involved in their local heritage, an important aspiration identified by English Heritage.

REFERENCES

Bryan, P. and Chandler, J.H. 2008. Cost-effective rock-art recording within a non-specialist environment. *International Archives of the Photogrammetry, Remote Sensing and Spatial Information Sciences*, Beijing, China, Vol. XXXVII, Part B5, pp. 259-264

Chandler, J.H. and Fryer, J.G. 2005. Recording Aboriginal rock art using cheap digital cameras and digital photogrammetry. *CIPA 2005 XX international Symposium*, Torino, Italy, pp. 193-198

Fiani, M. and Pistillo, P. 2004. A low-coast MMS integrating GPS, digital compass and a camera to the direct georeferencing of digital images. *International Archives of Photogrammetry, Remote Sensing and Spatial Information Sciences*, Istanbul, Turkey, Vol. XXXV, Part B5, pp. 747-752

Palumbo, G. and Ogleby, C.L. 2004. Heritage at risk and CIPA today: a report on the status of heritage documentation. *International Archives of Photogrammetry, Remote Sensing and Spatial Information Sciences*, Istanbul, Turkey, Vol. XXXV, Part B5, pp. 839-841

UNESCO 1972. Convention concerning the protection of the world cultural and natural heritage. UNESCO, Paris, 16 pages

ACKNOWLEDGEMENTS

The authors wish to acknowledge the investment in a TCM5 orientation sensor by English Heritage that made this project possible.